CHARACTERIZATION OF CPI AND CPII [FEFE]-HYDROGENASES REVEALS

PROPERTIES CONTRIBUTING TO CATALYTIC BIAS

by

Jacob Hansen Artz

A dissertation submitted in partial fulfillment
of the requirements for the degree

of

Doctor of Philosophy

in

Biochemistry

MONTANA STATE UNIVERSITY
Bozeman, Montana

November 2016

ACKNOWLEDGEMENTS

TABLE OF CONTENTS

TABLE OF CONTENTS – CONTINUED

TABLE OF CONTENTS – CONTINUED

TABLE OF CONTENTS – CONTINUED

vii

LIST OF TABLES

LIST OF FIGURES

LIST OF FIGURES – CONTINUED

LIST OF FIGURES – CONTINUED

LIST OF FIGURES – CONTINUED

ABSTRACT

The need for food, fuel, and pharmaceuticals has been increasing at a growing rate as the world's population increases and lifestyles improve. All of these needs are highly energy dependent, and, to a significant degree, rely on an inefficient use of fossil fuels. In order to break free of this dependence, new understanding is required for how to efficiently generate the products humanity needs. Here, a model system of two closely related [FeFe]-hydrogenases, CpI and CpII, is employed in order to understand how biology is able to efficiently control the formation of reduced products, in order to further delineate the limits of control, and the extent to which biology may be co-opted for technological needs. CpI, one of nature's best catalysts for reducing protons to hydrogen gas, is compared to CpII, which functions catalytically to oxidize hydrogen to protons and electrons. Oxygen sensitivity, midpoint potentials, catalytic mechanisms, and catalytic bias are explored in-depth using electron paramagnetic resonance, Fourier Transform Infrared spectroscopy, and protein film voltammetry. CpI and CpII have been found to function under different metabolic conditions, and key amino acids influencing their distinct behavior have been identified. The conduit arrays of hydrogenases, which direct electrons to or from the active site, have been found to have distinct midpoint potentials in CpII compared to CpI, effectively reversing the favored electron flow through CpII in comparison to CpI. In order to probe the contributions of the protein framework on catalysis, analysis of site-specific amino acid substituted variants have been used to identify several determinants that affect the H-cluster environment, which contributes to the observed differences between CpI and CpII. This has resulted in a deeper understanding of the hydrogenase model system and the ability to directly influence catalytic bias. Thus, the work presented here represents key progress towards developing unidirectional catalysts, and demonstrates the possibility of targeted, rational design and implementation of unidirectional catalysts.

CHAPTER 1

INTRODUCTION

Introduction to Hydrogenases

Hydrogenases, which catalyze the reversible reduction of protons to hydrogen (H2), are ancient enzymes that play a critical role in metabolism[1]. Hydrogenases are categorized according to the type of metal found in their active site, and there are several distinct types of hydrogenases: the [FeFe]-hydrogenases, which are the subject of this chapter, the well-known [NiFe]-hydrogenases, which are phyologenetically and mechanistically distinct from the [FeFe]-hydrogenases, and the [Fe]-only hydrogenases, which are only found in a subset of methoanogenic archaea, and rely on an additional cofactor, methenyltetrahydromethanopterin[2]. [FeFe]-hydrogenases are widely distributed among fermentative anaerobic microorganisms, and likely evolved in order to recycle excess reducing equivalents that accumulated during the fermentative metabolism[3].

[FeFe]-hydrogenases have, to date, been extensively studied by a combination of biochemical, structural, and spectroscopic techniques[4]. A key finding has been the composition of the strictly conserved active site organometallic cluster, termed the H-cluster, which is comprised of a [4Fe-4S] cubane with a cysteine thiolate linkage to a unique [2Fe-2S] cluster, termed the 2Fe subcluster, which is decorated by the diatomic carbon monoxide (CO) and cyanide (CN-) ligands bound to the iron atoms, with further coordination to a bridging dithiomethylamine (DTMA) bridge[5].   The CO and CN-ligands are both strong π-acceptor ligands, which serve to poise the Fe atoms of the 2Fe

subcluster in a low spin state that is capable as functioning catalytically between the II/I

oxidation states[1].
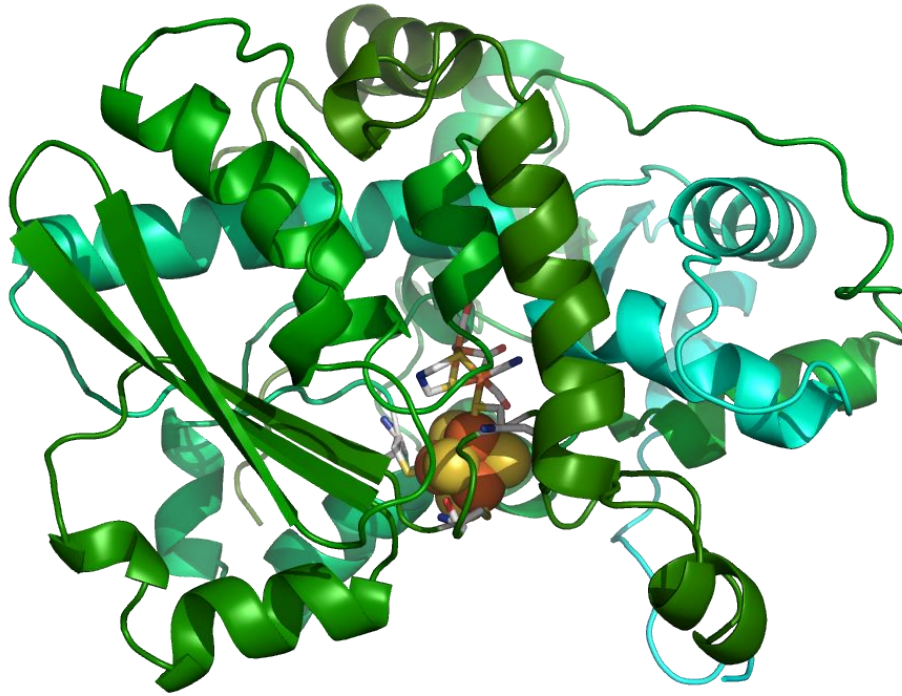
Figure 1.1 [FeFe]-hydrogenase from *Chlamydomonas reinhardtii*
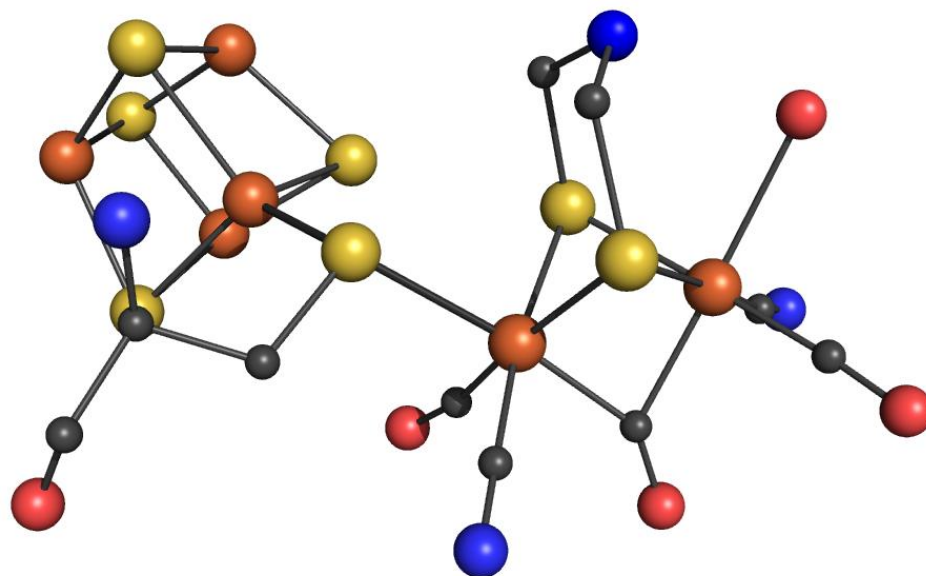
Figure 1.2 Ball-and-stick depiction of the H-cluster, the catalytic site common to [FeFe]-hydrogenases

In order to facilitate fast turnover rates ranging from $10^3 - 10^4$ s^{-1} [6] the active site requires rapid proton transfer (PT)[7] as well as electron transfer (ET), or, in some cases, these processes occur simultaneously as proton-coupled electron transfer (PCET)[8-9]. The structure of the hydrogenase supports this through a proton-transfer channel and through a distinct electron transfer pathway, or conduit array. The protein environment around the H-cluster is critical for binding the cubane of the H-cluster[5, 10], as in the strictly conserved first coordination sphere amino acids, however, there are a variety of other amino acids in the secondary coordination sphere that function collectively to tune the catalytic properties of the enzyme, using conserved residues that may transfer protons[11-13]. Additional residues use hydrogen bonding networks to stabilize the H-cluster. The electronic properties of these secondary coordination sphere amino acids are of particular importance for catalysis. The H-cluster, primary, and secondary coordination spheres all

participate to lower the kinetic barriers of hydrogen activation, resulting in a spectacularly active catalyst. Proton availability and midpoint potentials (E_m's) of [FeS] clusters serve as further control points for hydrogen catalysis.

Electron transfer, as stated above, is critical for fast catalysis, and is typically (though not always) achieved through additional [FeS] clusters that form a conduit array for electrons to travel to and/or from the active site[14]. These [FeS] clusters are generally [4Fe-4S] clusters or [2Fe-2S] clusters, and may be site-differentiated with non-cysteinyl ligands, including histidine, aspartic acid, and glutamic acid. The various clusters that are present serve to relate the hydrogenase to particular physiological electron donor/acceptors, which are matched, in part, by E_m. Of interest is the fact that bifurcating enzymes, which oxidize hydrogen and send one electron to a high-potential acceptor, and one electron to a low-potential acceptor, often have particularly complicated conduit arrays, which encompass perhaps ten [FeS] cluster sites. Different microorganisms often display multiple copies of hydrogenases in their genomes, often for structurally and functionally distinct enzymes.

In addition to being found in anaerobic fermentative bacteria, such as the Firmicutes, they are found in the lower Eukarya, particularly the algae and protists, typically involved in proton reduction, rather than hydrogen oxidation. It is intriguing that to date no [FeFe]-hydrogenases have been found in the archaea, suggesting that [FeFe]-hydrogenases were not found among the last universal common ancestor (LUCA)[5].

The algae represent an excellent model system for the study of hydrogenases, as they have found a way to couple energy from sunlight to the reduction of protons[15],

which overcomes several of the key technical barriers to implementation of similar

technology, namely, efficient direction of electrons through metabolism, synthesis of a

hydrogen catalyst using earth-abundant elements, and overcoming oxygen intolerance

through spatial and temporal separation of the hydrogenases from oxygen[16].

<u>Taxonomic and Functional Diversity of Hyd</u>

[FeFe]-hydrogenases (Hyd) comprise at a minimum the catalytic subunit, HydA, which

contains a conserved ~350 residue H-cluster domain where a unique iron-sulfur (Fe-S)

cluster is bound forming the site of reversible proton reduction. The active site Fe-S

cluster consists of a [4Fe-4S] cluster bridged to a 2Fe subcluster via a cysteine thiol [5, 17-

19]. Three conserved cysteine-containing motifs coordinate the active site H-cluster:

TSCCPxW (L1), MPCxxKxxE (L2) and ExMxCxxGCxxG (L3)[20]. The presence of these

three conserved ligands is a defining feature of HydA and one which differentiates them

from closely related, but non-catalytic, paralogs identified in eukaryotes, e.g., Nar1, as

well as other closely related paralogs found in bacteria, e.g., HydS, which will be

discussed more below. In addition to the H-cluster domain, HydA often include N-

terminal (F-cluster) and C-terminal (C-cluster) domains with motifs predicted [14, 20-21] or

shown [5, 22] to ligate additional Fe-S clusters that are believed to add flexibility to facilitate

electron transfer to and/or from the active site H-cluster. The simplest form of HydA

includes those identified in green algae, such as *Chlamydomonas reinhardtii*, which

generally only contains the H-cluster domain [4, 15, 23-26]. More complex forms of HydA are

more common and possess several additional Fe-S clusters, including those with both the

F- and C-clusters [5, 18, 27]. In addition to F- and C-cluster mediated functional variation,

HydA can exist in multiple forms with different quaternary structures, including those that are monomeric as well as those that are multimeric [1, 14, 20, 28-29]. Multiple HydAs of variable quaternary structure can be present in a single genome [14, 21, 30-33] where they have been shown to form complexes with paralogs of the large and small subunits of NADH dehydrogenase (referred to as HydB and HydC, respectively) [30-31, 34-37]. Genome sequencing efforts continue to reveal novel Hyd diversity at the level of H cluster ligand variation, F- and C-cluster variation, and variation in the proteins that partner with HydA (e.g., see refs [14, 33, 37]).

Efforts to catalog the diversity of Hyds, which begin ~ 15 years ago with the pioneering work of Vignais et al. 2001[29], have recently been updated and refined using evolutionary methods[20]. Building on these reports, Calusinska et al., 2010[14] developed a classification scheme for clostridial Hyd that was based on the composition of F- and C-clusters as well as subunit composition. More recently, a comprehensive screening of Hyd in 2919 publically available archaeal and bacterial genomes was conducted[21]. Using informatics methods, this study identified Hyd in 265 (9.1%) of the complete genomes publically available in July 2014[21]. Among these genomes, a total of 714 hydA homologs were identified that spanned members representing 17 of the 30 bacterial phyla. No hydA homologs were identified among archaeal genomes representing 5 archaeal phyla. Greater than 90% of the 714 HydA homologs are encoded by members of the bacterial phyla Firmicutes, Proteobacteria, Spirochaetes, Thermotogae and which encoded on average ~ 2 HydA isoforms per HydA encoding genome[21]. This taxonomic distribution is similar to that reported in earlier publications [3, 20, 29]. Using informatics tools, the proteins encoded in the flanking regions of HydA in the genomes of these organisms was

determined and protein homology and network approaches were used to identify co-occurring genes. Through this work, a new classification scheme was developed that unified Hyd into one of three structural and functional groups (Fig 1.2)[21]. These groupings were driven largely by the composition of proteins in the gene neighborhoods of HydA that were predicted to form a complex with HydA or that were predicted to be involved in regulation of Hyd activity, as discussed below. Variation in F- and C-cluster composition or HydA active site ligand composition was not found to vary by group type[21].

Group 1 (G1) enzymes were predicted to be monomeric while those in Group 2 (G2) and Group 3 (G3) were predicted to be multimeric forming complexes with HydB, HydC subunits and in the case of G3, also a ferredoxin-like protein termed HydD. G1 Hyd are the most abundant form of Hyd representing 68% of the total Hyds identified[21]. G1 Hyd are also the best characterized and are ferredoxin (Fd)-dependent enzymes[29]. Examples include the Hyd from eukaryotic algae, such as *Chlamydomonas reinhardtii*[10], as well as HydA1 from the anaerobic bacteria *Clostridium pasteurianum*[5] and Desulfovibrio desulfuricans[22]. The [FeFe]-hydrogenase from *C. reinhardtii* comprises only the H-cluster domain, with no additional F or C clusters no additional iron-sulfur clusters[20]. Hyd consisting of only the H-cluster domain is common among algae, however, recent genome sequencing efforts reveal the presence of G1 Hyd in a Chlorella strain that have complex F-clusters[26]. G1 Hyd, in particular those from *C. reinhardtii*, have become models for biochemical studies due to the simplicity of their structure (i.e., lack of F- and C-clusters) relative to G2 and G3 Hyd [10, 38-39]. *C. pasteurianum* encodes for three different Hyd[40], all of which are classified as G1. These enzymes vary,

however, in their F-cluster compositions suggesting that they have different functional roles within the cells[41]. Biochemical studies also suggest that these enzymes have distinct functional roles with one of the enzymes (termed CpI) exhibiting a bias towards H_2 production and one of the other enzymes (termed CpII) exhibiting a bias toward H_2 oxidation.

G2 (22% of total homologs) and G3 (11% of total homologs) Hyd are common among anaerobic bacteria, in particular in the phylum Firmicutes[3, 14]. Representatives of these multimeric Hyd have been shown to bifurcate electrons, or the coupling of the simultaneous reduction or oxidation of two electron acceptors or donors in an enzyme complex whereby a thermodynamically favorable exergonic reaction drives a thermodynamically unfavorable endergonic reaction [30-31, 33-35, 37, 42]. Examples of G2 and G3 Hyd that have been biochemically characterized include those from *Acetobacterium woodii*[36], *Clostridium autoethanogenum*[37], *Moorella thermoacetica*[33] and *Thermotoga maritima*[30]. The trimeric G2 Hyd from *T. maritima* (i.e. HydABC complex) couples the simultaneous oxidation of NADH and Fd to the production of $H2$[30] while the tetrameric G3 Hyd from *A. woodii* (i.e. HydABCD complex) couples the oxidation of H_2 to the simultaneous reduction of NAD^+ and Fd[36]. Interestingly, a trimeric G2 Hyd from the acetogen *M. thermoacetica* functions physiologically as a reversible enzyme, catalyzing either the oxidation or production of H_2 contingent on cultivation conditions[43]. Like the above examples, the oxidation or production of H_2 is coupled to Fd and NAD+/NADH reduction/oxidation[43]. When *M. thermoacetica* cells are grown under autotrophic conditions they oxidize H2 by simultaneously reducing both Fd and NAD+. In contrast,

glucose-grown *M. thermoacetica* cells used the same enzyme complex to reduce protons to produce H2 by coupling with the oxidation of Fd and NADH.

Informatics analysis of the 2919 genomes available in 2014 revealed that the HydA copy number per genome, when broken out by group designation, varied substantially. Multiple copies (isoforms) of G1 Hyd's in the same genome was common among Hyd-encoding genomes (117 of 287 genomes). Interestingly, several genomes contained three or more copies of HydA, with a maximum copy number/genome of seven HydA's (*Desulfotomaculum carboxydivorans* CO-1-SRB, DSM 14880). Fifty-two percent of the HydA-encoding genomes encoded for at least two different types of Hyd with 77 genomes found to encode for G1 and G2 Hyds, 44 found to encode for G2 and G3 Hyds, and 17 genomes found to encode for all three groups of Hyds. The co-existence of multiple isoforms of Hyd suggests they have different functional roles within the organisms and suggests the need to differentially regulate these enzymes. Indeed, previous studies have identified other genes in the gene neighborhoods of bifurcating G2 and G3 enzymes. These include HydS, which is homologous to HydA and which has been proposed as a H2 sensor based on the presence of a Per-ARNT-Sim (PAS) domain[31, 44]. In addition, proteins hypothesized to be involved in signal transduction (e.g. serine-threonine kinases/phosphatases and histidine kinases) were identified in the flanking gene environment of hydA in C. thermocellum and T. maritima[31]. The recent informatics analysis of the proteins encoded in available gene neighborhood of hydA[21] also revealed a high level of correlation between G2 and G3 enzymes and specific regulatory proteins, including HydS as well as proteins putatively involved in post-translational modification (PTM) including serine phosphatase (Sp), HydS, histidine

kinase-like (Hkl) proteins, and serine threonine kinase (Stk). Sp and HydS were enriched in the gene neighborhoods of G2 Hyds while Hkl, and Stk were enriched in the gene neighborhood of G3 Hyds. The difference in regulatory gene association between the two groups indicates that G2 and G3 Hyds may be subject to different modes of PTM and/or that these PTM enzymes exhibit specificity for target Hyd proteins allowing for their differential regulation if both types of protein are present in the same organism.

Biochemical and mass spectral methods applied to purified Hyd protein complexes from Thermotoga maritima (G2 Hyd) and Caldicellulosiruptor bescii (G3) revealed evidence that is consistent with PTM of HydAB and HydC in T. maritima as well as HydAB and HydD from C. bescii[21].
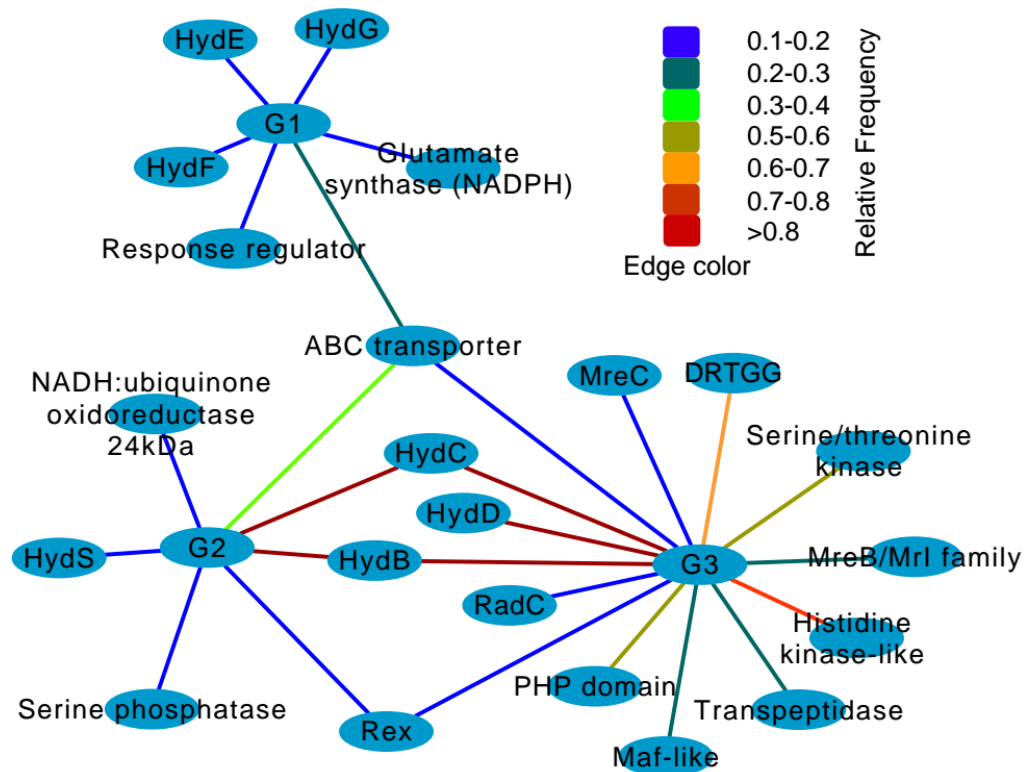
Figure 1.3. Network analysis of proteins encoded by genes flanking (+/− 10 genes) hydA. Only proteins (n = 22) encoded in the flanking regions of > 10% of the each HydA group (i.e. relative frequency of > 10%) were considered in this analysis. Here, edge color represents the relative frequency of each protein in each group. The force directed organic layout was used to visualize the correlation in the network using Cytoscape[45]. The average pattern associated with each of the 3 defined Hyd groups was included in this analysis [indicated by Group 1 (G1), Group 2 (G2), and Group 3 (G3)].

Hydrogenase Mechanism

The exact mechanism of the [FeFe]-hydrogenases is still the subject of intense scrutiny[1-2], although there are multiple features that have been clearly identified. The H-cluster sits in a hydrophobic pocket[5]. A proton relay functions to deliver protons from the solvent to the active site[7, 13], and, hydrogenases often have a conduit array of additional [FeS] clusters that serves to deliver electrons to or from the active site[20].

Finally, two different gas channels have been demonstrated computationally that function to transport H_2, and sometimes O_2, to or from the active site[46-47].

Within the H-cluster, the 2Fe subcluster contains two irons, proximal (Fe_p) and distal (Fe_d) to the cubane, each of which transitions between Fe^I or Fe^{II} state[1-2]. The Fe_d has an open coordination site[19], and is therefore thought to be the site of proton reduction/H2 activation during the catalytic cycle. The bridging atom of the 2Fe subcluster, now identified as nitrogen[48], is positioned at the base of the proton transfer channel and is thought to serve as part of the relay of protons to the Fe_d[13]. The presence of CO and CN− ligands further serve to stabilize the iron atoms of the 2Fe subcluster in a low-spin state that is conducive to enzymatic turnover[49-50]. Emerging evidence suggests that the presence of the cubane is critical for turnover[51-52]. The cubane is strongly coupled to the 2Fe subcluster[53-54], and may serve as an electron reservoir[55-57], allowing for the efficient reduction of substrate at the Fe_d.
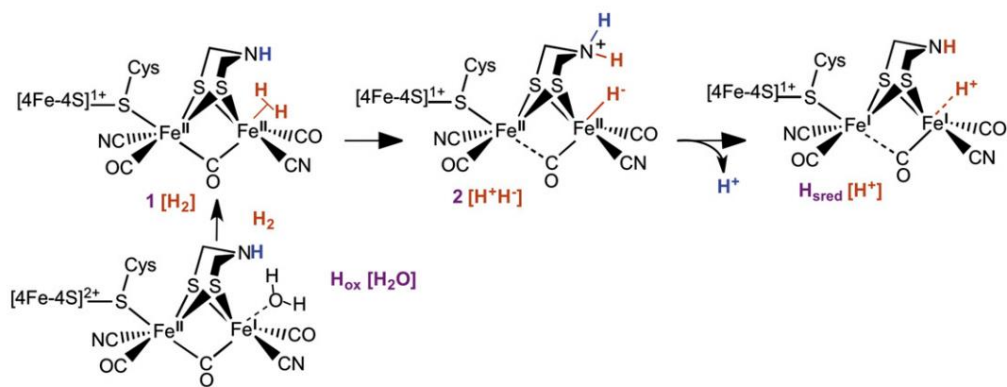
Figure 1.4 Proposed hydrogenase mechanism.

The protein framework is critical for tuning the function of [FeFe]-hydrogenases[12]. Beyond the strictly conserved first coordination sphere of cysteines that

directly bind the H-cluster, there is a wide variety of natural variation representing

differences in the second coordination sphere. These amino acids, while critical for

turnover, are poorly understood thus far, though they clearly influence the diatomic

ligands of the H-cluster[2], thereby impacting catalysis. Amino acids in the secondary

coordination sphere are further likely to influence the midpoint potential, the

hydrophobicity, and the sterics of the H-cluster, although the extent to which each of

these features contributes to the observed catalytic profile has yet to be parsed. Clearly,

observed natural variation among these sites would represent an evolutionary strategy for

optimally tuning a hydrogenase to a particular cellular function[28], and predicting how to

influence hydrogen turnover through alteration of the first/second coordination spheres

will be a fruitful area of research.

<u>Hydrogenase Maturation</u>

The complex nature of the hydrogenase cofactors necessitates a variety of other enzymes

to function as maturation machinery[58]. The conduit array [FeS] clusters as well as the

cubane of the active site are formed readily in E. coli as well as other biological systems,

suggesting that the typical [FeS] machinery of the isc or suf systems is used for the

maturation of these more standard [FeS] cofactors. The cubane of the H-cluster is

obligatorily formed prior to 2Fe subcluster insertion[10]. By comparing the crystal

structures of the fully-maturated CpI enzyme to the 'apo' form of the CrHydA enzyme[10],

it appears that two loop regions are in an open confirmation in the apo form, allowing for

2Fe subcluster insertion, whereupon the loops close again. The 2Fe Subcluster, in

contrast to the other cofactors, requires several unique proteins, HydE, HydF, and HydG,

to form the fully active H-cluster[59], where HydE and HydG are radical s-

adenysylmethionine (SAM) enzymes, and HydF is a GTPase. The maturation process

requires careful steps given the typically toxic nature of CO and CN- ligands to the cell.

All three maturases are required for the formation of the H-cluster, though no additional

proteins are needed. The formation of the H-cluster is likely dependent on small,

common, exogenous molecules to complete activation. Recently, the development of a

synthetic process to create the 2Fe subcluster without the maturases has led to a new

innovations and insights in the field[48].

Role of HydF

HydF, the [FeS] cluster binding GTPase, most probably functions as a scaffold

and transferase of the fully formed 2Fe subcluster to HydA. Only HydF formed in the

background of HydE and HydG (HydFEG) is capable of activating HydA[59]. HydF is

known to have a complex interplay between dimeric and tetrameric states, where the

interfaces are implicated in the possible binding of the 2Fe subcluster precursor[60]. Two

distinct [FeS] clusters have been found in HydF, and [4Fe-4S] cubane that is typically

ligated by three cysteine residues, and a [2Fe-2S] cluster that is potentially involved as

the scaffold for 2Fe subcluster formation[61]. A variety of spectroscopic evidence is highly

suggestive of the role of HydFEG in harboring a fully-formed 2Fe subcluster[62]. Fourier

Transform Infrared (FTIR) spectroscopy reveals the presence of Fe-CO, Fe-CO-Fe, and

Fe-CN stretching modes[63], while electron paramagnetic resonance (EPR) shows signals

that bear strong resemblance to the maturated HydA. HydF has been shown to interact

with both HydE and HydG, though not simultaneously, as HydE and HydG are thought to

use the same binding site on HydF[64]. Experiments demonstrate that the binding affinity

of HydE to HydF is around an order of magnitude greater that the affinity of HydG for

HydF. The hydrolysis of GTP to GDP is thought to be associated with the HydE/HydF

and HydG/HydF interactions, wherein the GTPase activity may be involved in regulating

interactions between the maturases[62]. GTPase activity is not strictly necessary for HydA

activation, which suggests that the GTP hydrolysis does not directly contribute to the

formation of the 2Fe subcluster[62].

Role of HydG

The monomeric 55 Kda HydG is a member of the radical SAM family[65], and has

been shown to form the diatomic ligands and to interact with HydF[66]. HydG harbors two

[4Fe-4S] clusters, one found in the CX3CX2C N-terminal motif that is conserved among

radical SAM enzymes, and one cluster found in a CX2CX22C motif[67]. Like its homolog

ThiH, HydG has been shown to perform the radical cleavage of tyrosine to para-cresol

and dehydroglycine (DHG), which may undergo a further decarbonylation step to

simultaneously produce both CO and CN ligands[68]. All five of the diatomic ligands have

been assigned as originating in tyrosine, suggesting that multiple HydG catalysis steps

may be required for proper maturation of HydF[69]. The diatomic ligands likely bind to the

C-terminal cluster, and have been observed via FTIR to exhibit characteristic Fe-CO and

Fe-CN stretching bands[70]. Experiments with 57Fe reveal that iron from HydG becomes

incorporated in HydA, so HydG likely transfers the Fe-diatomic ligands to the HydF

scaffold, which may then incorporate the 2Fe subcluster into HydA[70]. Further

characterization of each of these steps will be critical for full understanding of hydrogenase maturation.

Role of HydE

HydE, a 42 Kda radical SAM enzyme[71], currently has little in the way of direct biochemical evidence to support its role in H-cluster formation, though it is essential for HydA activation. While it has been hypothesized to participate in chaperoning HydF to HydA[72], HydF is capable of maturating HydA without the presence of HydE, suggesting that a chaperoning activity is not necessary. Rather, in light of the chemistries of HydF and HydG, HydE is more likely involved in the formation of the dithiomethylamine bridge[73]. Further support for this comes from one of HydE's nearest homologs, PylB, which is a methylornithine synthase[74]. This suggests possible mechanistic parallels between HydE and PylB, where HydE is also likely to use difficult radical chemistry in the breaking and formation of chemical bonds. Despite a search for the small molecule substrate of HydE, to date the substrate remains unresolved. Possible clues may be derived from several solved crystal structures[75-76], which depict S-adenosyl methionine bound inside an electropositive cavity that features three anion binding sites within the TIM barrel fold. Additional work will be necessary in order to conclusively elucidate both the role of HydE in H-cluster biosynthesis, as well as the enzyme's substrate.
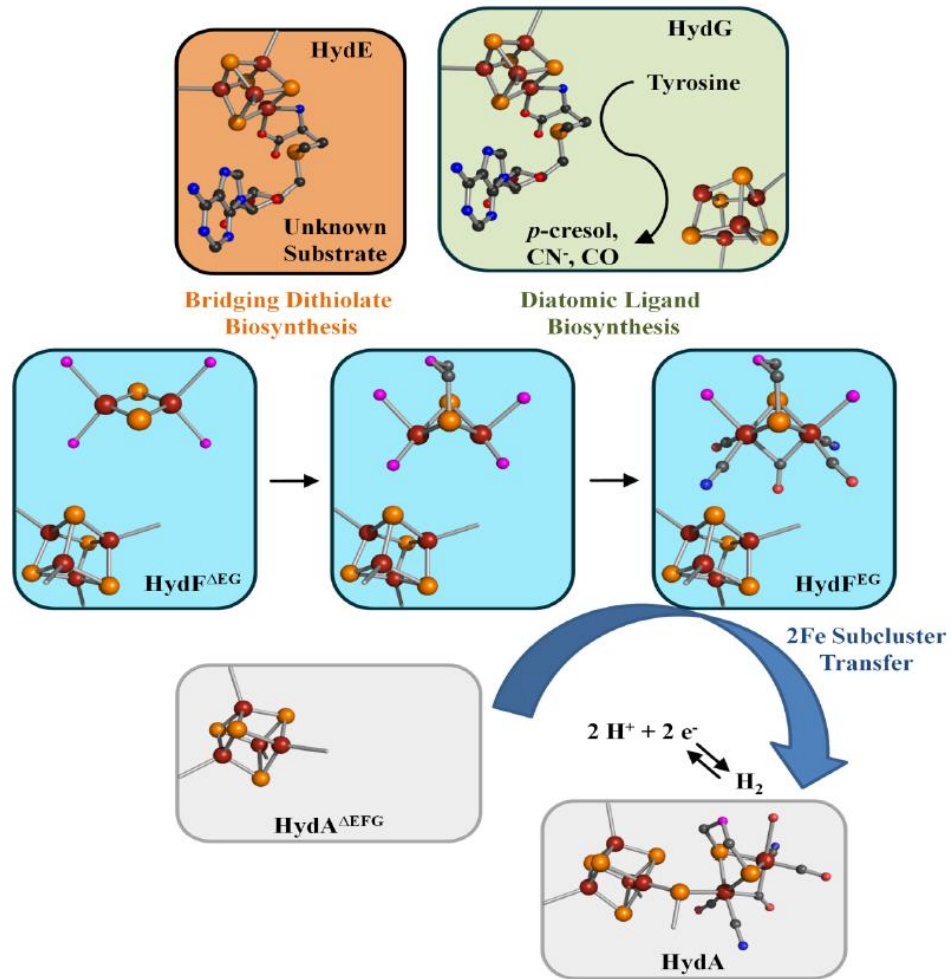
Figure 1.5 Schematic of the activation process of the [FeFe]-hydrogenase. HydF acts as a scaffold and HydE and HydG build a 2Fe subcluster. The 2Fe subcluster is transferred to HydA creating a fully mature enzyme that is capable of catalysis.

Future Directions

While much has been learned about hydrogenases thus far, many frontiers still need to be explored. The full breadth of hydrogenase activities that naturally occur have yet to be identified, particularly among the bifurcating hydrogenases, which have only recently begun to be characterized. Much remains to be learned about the metabolic

contexts of bifurcation, as well as the nature of the bifurcating sites themselves. In regards to hydrogenase maturation, there is as of yet much unknown about the interactions of HydE, HydG, and HydF with HydA to fully activate HydA. Chief among these questions are the nature of the substrate of HydE, and the composition of the 2Fe subcluster precursor that HydF transfers to HydA. The phylogeny of hydrogenases also opens the door to several lines of inquiry. How does the natural variation among sequences influence activity? What are limits of hydrogenases in different metabolic contexts? Discerning these answers will require a concentrated effort that will surely reveal many novel features of hydrogenases.

Despite the remaining challenges, combining the insights gained from structure-function studies of hydrogenase and its maturases will allow for the creation and utilization of new technologies, where electron flow may be directed through systems to reversibly produce hydrogen gas, and will be paramount for the formation of biofuels.

References

1.   Peters, J. W.; Schut, G. J.; Boyd, E. S.; Mulder, D. W.; Shepard, E. M.; Broderick, J. B.; King, P. W.; Adams, M. W. W., [FeFe]- and [NiFe]-hydrogenase diversity, mechanism, and maturation. *Biochimica et Biophysica Acta (BBA) - Molecular Cell Research* **2015,** *1853* (6), 1350-1369.

2.   Lubitz, W.; Ogata, H.; Rüdiger, O.; Reijerse, E., Hydrogenases. *Chemical reviews* **2014,** *114* (8), 4081-4148.

3.   Vignais, P. M.; Billoud, B., Occurrence, classification, and biological function of hydrogenases: an overview. *Chemical reviews* **2007,** *107* (10), 4206-72.

4.   Mulder, D. W.; Shepard, E. M.; Meuser, J. E.; Joshi, N.; King, P. W.; Posewitz, M. C.; Broderick, J. B.; Peters, J. W., Insights into FeFe -Hydrogenase Structure, Mechanism, and Maturation. *Structure* **2011,** *19* (8), 1038-1052.

5.   Peters, J. W.; Lanzilotta, W. N.; Lemon, B. J.; Seefeldt, L. C., X-ray crystal structure of the Fe-only hydrogenase (CpI) from Clostridium pasteurianum to 1.8 angstrom resolution. *Science (New York, N.Y.)* **1998,** *282* (5395), 1853-8.

6.   Madden, C.; Vaughn, M. D.; Díez-Pérez, I.; Brown, K. A.; King, P. W.; Gust, D.; Moore, A. L.; Moore, T. A., Catalytic Turnover of [FeFe]-Hydrogenase Based on Single-Molecule Imaging. *Journal of the American Chemical Society* **2012,** *134* (3), 1577-1582.

7.   Cornish, A. J.; Gartner, K.; Yang, H.; Peters, J. W.; Hegg, E. L., Mechanism of proton transfer in [FeFe]-hydrogenase from Clostridium pasteurianum. *The Journal of biological chemistry* **2011,** *286* (44), 38341-7.

8.   Bourrez, M.; Steinmetz, R.; Ott, S.; Gloaguen, F.; Hammarström, L., Concerted proton-coupled electron transfer from a metal-hydride complex. *Nat Chem* **2015,** *7* (2), 140-145.

9.   Mulder, D. W.; Ratzloff, M. W.; Bruschi, M.; Greco, C.; Koonce, E.; Peters, J. W.; King, P. W., Investigations on the role of proton-coupled electron transfer in hydrogen activation by [FeFe]-hydrogenase. *J Am Chem Soc* **2014,** *136* (43), 15394-402.

10.   Mulder, D. W.; Boyd, E. S.; Sarma, R.; Lange, R. K.; Endrizzi, J. A.; Broderick, J. B.; Peters, J. W., Stepwise [lsqb]FeFe[rsqb]-hydrogenase H-cluster assembly revealed in the structure of HydA[Dgr]EFG. *Nature* **2010,** *465* (7295), 248-251.

11.   Ginovska-Pangovska, B.; Dutta, A.; Reback, M. L.; Linehan, J. C.; Shaw, W. J., Beyond the Active Site: The Impact of the Outer Coordination Sphere on Electrocatalysts for Hydrogen Production and Oxidation. *Accounts of Chemical Research* **2014,** *47* (8), 2621-2630.

12.   Knörzer, P.; Silakov, A.; Foster, C. E.; Armstrong, F. A.; Lubitz, W.; Happe, T., Importance of the Protein Framework for Catalytic Activity of [FeFe]-Hydrogenases. *Journal of Biological Chemistry* **2012,** *287* (2), 1489-1499.

13.   Morra, S.; Maurelli, S.; Chiesa, M.; Mulder, D. W.; Ratzloff, M. W.; Giamello, E.; King, P. W.; Gilardi, G.; Valetti, F., The effect of a C298D mutation in CaHydA [FeFe]-hydrogenase: Insights into the protein-metal cluster interaction by EPR and FTIR spectroscopic investigation. *Biochimica et Biophysica Acta (BBA) - Bioenergetics*.

14. Calusinska, M.; Happe, T.; Joris, B.; Wilmotte, A., The surprising diversity of clostridial hydrogenases: a comparative genomic perspective. *Microbiology (Reading, England)* **2010,** *156* (Pt 6), 1575-88.

15. Ghirardi, M. L.; Posewitz, M. C.; Maness, P. C.; Dubini, A.; Yu, J.; Seibert, M., Hydrogenases and hydrogen photoproduction in oxygenic photosynthetic organisms. *Annual review of plant biology* **2007,** *58*, 71-91.

16. Ghirardi, M. L., Implementation of photobiological H2 production: the O 2 sensitivity of hydrogenases. *Photosynthesis research* **2015,** *125* (3), 383-93.

17. Mulder, D. W.; Ortillo, D. O.; Gardenghi, D. J.; Naumov, A. V.; Ruebush, S. S.; Szilagyi, R. K.; Huynh, B.; Broderick, J. B.; Peters, J. W., Activation of HydA(DeltaEFG) requires a preformed [4Fe-4S] cluster. *Biochemistry* **2009,** *48* (26), 6240-8.

18. Adams, M. W., The structure and mechanism of iron-hydrogenases. *Biochimica et biophysica acta* **1990,** *1020* (2), 115-45.

19. Nicolet, Y.; Lemon, B. J.; Fontecilla-Camps, J. C.; Peters, J. W., A novel FeS cluster in Fe-only hydrogenases. *Trends Biochem Sci* **2000,** *25* (3), 138-43.

20. Meyer, J., [FeFe] hydrogenases and their evolution: a genomic perspective. *Cell. Mol. Life Sci.* **2007,** *64* (9), 1063-1084.

21. Poudel, S.; Tokmina-Lukaszewska, M.; Colman, D. R.; Refai, M.; Schut, G. J.; King, P. W.; Maness, P. C.; Adams, M. W.; Peters, J. W.; Bothner, B.; Boyd, E. S., Unification of [FeFe]-hydrogenases into three structural and functional groups. *Biochimica et biophysica acta* **2016,** *1860* (9), 1910-21.

22. Nicolet, Y.; Piras, C.; Legrand, P.; Hatchikian, C. E.; Fontecilla-Camps, J. C., Desulfovibrio desulfuricans iron hydrogenase: the structure shows unusual coordination to an active site Fe binuclear center. *Structure* **1999,** *7* (1), 13-23.

23. Forestier, M.; King, P.; Zhang, L.; Posewitz, M.; Schwarzer, S.; Happe, T.; Ghirardi, M. L.; Seibert, M., Expression of two [Fe]-hydrogenases in Chlamydomonas reinhardtii under anaerobic conditions. *European journal of biochemistry / FEBS* **2003,** *270* (13), 2750-8.

24. Happe, T.; Kaminski, A., Differential regulation of the Fe-hydrogenase during anaerobic adaptation in the green alga Chlamydomonas reinhardtii. *European journal of biochemistry / FEBS* **2002,** *269* (3), 1022-32.

25. Happe, T.; Mosler, B.; Naber, J. D., Induction, localization and metal content of hydrogenase in the green alga Chlamydomonas reinhardtii. *European journal of biochemistry / FEBS* **1994,** *222* (3), 769-74.

26. Meuser, J. E.; Boyd, E. S.; Ananyev, G.; Karns, D.; Radakovits, R.; Narayana Murthy, U. M.; Ghirardi, M. L.; Dismukes, G. C.; Peters, J. W.; Posewitz, M. C., Evolutionary significance of an algal gene encoding an [FeFe]-hydrogenase with F-domain homology and hydrogenase activity in Chlorella variabilis NC64A. *Planta* **2011,** *234* (4), 829-43.

27. Chen, J.-S.; Mortenson, L. E., Purification and properties of hydrogenase from Clostridium pasteurianum W5. *Biochimica et Biophysica Acta (BBA) - Protein Structure* **1974,** *371* (2), 283-298.

28. Boyd, E. S.; Hamilton, T. L.; Swanson, K. D.; Howells, A. E.; Baxter, B. K.; Meuser, J. E.; Posewitz, M. C.; Peters, J. W., [FeFe]-hydrogenase abundance and diversity along a vertical redox gradient in Great Salt Lake, USA. *International journal of molecular sciences* **2014,** *15* (12), 21947-66.

29. Vignais, P. M.; Billoud, B.; Meyer, J., Classification and phylogeny of hydrogenases. *FEMS microbiology reviews* **2001,** *25* (4), 455-501.

30. Schut, G. J.; Adams, M. W. W., The Iron-Hydrogenase of Thermotoga maritima Utilizes Ferredoxin and NADH Synergistically: a New Perspective on Anaerobic Hydrogen Production. *Journal of bacteriology* **2009,** *191* (13), 4451-4457.

31. Zheng, Y.; Kahnt, J.; Kwon, I. H.; Mackie, R. I.; Thauer, R. K., Hydrogen Formation and Its Regulation in Ruminococcus albus: Involvement of an Electron-Bifurcating [FeFe]-Hydrogenase, of a Non-Electron-Bifurcating [FeFe]-Hydrogenase, and of a Putative Hydrogen-Sensing [FeFe]-Hydrogenase. *Journal of bacteriology* **2014,** *196* (22), 3840-3852.

32. Verhagen, M. F.; O'Rourke, T. W.; Menon, A. L.; Adams, M. W., Heterologous expression and properties of the gamma-subunit of the Fe-only hydrogenase from Thermotoga maritima. *Biochimica et biophysica acta* **2001,** *1505* (2-3), 209-19.

33. Wang, S.; Huang, H.; Kahnt, J.; Thauer, R. K., A Reversible Electron-Bifurcating Ferredoxin- and NAD-Dependent [FeFe]-Hydrogenase (HydABC) in Moorella thermoacetica. *Journal of bacteriology* **2013,** *195* (6), 1267-1275.

34. Herrmann, G.; Jayamani, E.; Mai, G.; Buckel, W., Energy Conservation via Electron-Transferring Flavoprotein in Anaerobic Bacteria. *Journal of bacteriology* **2008,** *190* (3), 784-791.

35. Li, F.; Hinderberger, J.; Seedorf, H.; Zhang, J.; Buckel, W.; Thauer, R. K., Coupled Ferredoxin and Crotonyl Coenzyme A (CoA) Reduction with NADH Catalyzed by the Butyryl-CoA Dehydrogenase/Etf Complex from Clostridium kluyveri. *Journal of bacteriology* **2008,** *190* (3), 843-850.

36. Schuchmann, K.; Muller, V., A bacterial electron-bifurcating hydrogenase. *The Journal of biological chemistry* **2012,** *287* (37), 31165-71.

37. Wang, S.; Huang, H.; Kahnt, J.; Mueller, A. P.; Kopke, M.; Thauer, R. K., NADP-specific electron-bifurcating [FeFe]-hydrogenase in a functional complex with formate dehydrogenase in Clostridium autoethanogenum grown on CO. *Journal of bacteriology* **2013,** *195* (19), 4373-86.

38. English, C. M.; Eckert, C.; Brown, K.; Seibert, M.; King, P. W., Recombinant and in vitro expression systems for hydrogenases: new frontiers in basic and applied studies for biological and synthetic H2 production. *Dalton transactions (Cambridge, England : 2003)* **2009,** (45), 9970-8.

39. Posewitz, M. C.; Mulder, D. W.; Peters, J. W., New Frontiers in Hydrogenase Structure and Biosynthesis. *Current Chemical Biology* **2008,** *2* (2), 178-199.

40. Pyne, M. E.; Utturkar, S.; Brown, S. D.; Moo-Young, M.; Chung, D. A.; Chou, C. P., Improved Draft Genome Sequence of Clostridium pasteurianum Strain ATCC 6013 (DSM 525) Using a Hybrid Next-Generation Sequencing Approach. *Genome Announcements* **2014,** *2* (4).

41.   Bruno-Barcena, J. M.; Chinn, M. S.; Grunden, A. M., Genome Sequence of the Autotrophic Acetogen Clostridium autoethanogenum JA1-1 Strain DSM 10061, a Producer of Ethanol from Carbon Monoxide. *Genome Announcements* **2013,** *1* (4).

42.   Buckel, W.; Thauer, R. K., Energy conservation via electron bifurcating ferredoxin reduction and proton/Na+ translocating ferredoxin oxidation. *Biochimica et Biophysica Acta (BBA) - Bioenergetics* **2013,** *1827* (2), 94-113.

43.   Huang, H.; Wang, S.; Moll, J.; Thauer, R. K., Electron bifurcation involved in the energy metabolism of the acetogenic bacterium Moorella thermoacetica growing on glucose or H2 plus CO2. *Journal of bacteriology* **2012,** *194* (14), 3689-99.

44.   Henry, J. T.; Crosson, S., Ligand-binding PAS domains in a genomic, cellular, and structural context. *Annual review of microbiology* **2011,** *65*, 261-86.

45.   Shannon, P.; Markiel, A.; Ozier, O.; Baliga, N. S.; Wang, J. T.; Ramage, D.; Amin, N.; Schwikowski, B.; Ideker, T., Cytoscape: a software environment for integrated models of biomolecular interaction networks. *Genome research* **2003,** *13* (11), 2498-504.

46.   Goldet, G.; Brandmayr, C.; Stripp, S. T.; Happe, T.; Cavazza, C.; Fontecilla-Camps, J. C.; Armstrong, F. A., Electrochemical kinetic investigations of the reactions of [FeFe]-hydrogenases with carbon monoxide and oxygen: comparing the importance of gas tunnels and active-site electronic/redox effects. *J Am Chem Soc* **2009,** *131* (41), 14979-89.

47.   Lautier, T.; Ezanno, P.; Baffert, C.; Fourmond, V.; Cournac, L.; Fontecilla-Camps, J. C.; Soucaille, P.; Bertrand, P.; Meynial-Salles, I.; Leger, C., The quest for a functional substrate access tunnel in FeFe hydrogenase. *Faraday discussions* **2011,** *148*, 385-407; discussion 421-41.

48.   Berggren, G.; Adamska, A.; Lambertz, C.; Simmons, T. R.; Esselborn, J.; Atta, M.; Gambarelli, S.; Mouesca, J. M.; Reijerse, E.; Lubitz, W.; Happe, T.; Artero, V.; Fontecave, M., Biomimetic assembly and activation of [FeFe]-hydrogenases. *Nature* **2013,** *499* (7456), 66-69.

49.   Pierik, A. J.; Hulstein, M.; Hagen, W. R.; Albracht, S. P., A low-spin iron with CN and CO as intrinsic ligands forms the core of the active site in [Fe]-hydrogenases. *European journal of biochemistry / FEBS* **1998,** *258* (2), 572-8.

50.   Kubas, A.; De Sancho, D.; Best, R. B.; Blumberger, J., Aerobic damage to [FeFe]-hydrogenases: activation barriers for the chemical attachment of O2. *Angewandte Chemie (International ed. in English)* **2014,** *53* (16), 4081-4.

51.   Roseboom, W.; De Lacey, A. L.; Fernandez, V. M.; Hatchikian, E. C.; Albracht, S. P., The active site of the [FeFe]-hydrogenase from Desulfovibrio desulfuricans. II. Redox properties, light sensitivity and CO-ligand exchange as observed by infrared spectroscopy. *Journal of biological inorganic chemistry : JBIC : a publication of the Society of Biological Inorganic Chemistry* **2006,** *11* (1), 102-18.

52.   Adamska, A.; Silakov, A.; Lambertz, C.; Rudiger, O.; Happe, T.; Reijerse, E.; Lubitz, W., Identification and characterization of the "super-reduced" state of the H-cluster in [FeFe] hydrogenase: a new building block for the catalytic cycle? *Angewandte Chemie (International ed. in English)* **2012,** *51* (46), 11458-62.

53.   Silakov, A.; Reijerse, E. J.; Albracht, S. P. J.; Hatchikian, E. C.; Lubitz, W., The Electronic Structure of the H-Cluster in the [FeFe]-Hydrogenase from Desulfovibrio desulfuricans: A Q-band 57Fe-ENDOR and HYSCORE Study. *Journal of the American Chemical Society* **2007,** *129* (37), 11447-11458.

54.   Popescu, C. V.; Münck, E., Electronic Structure of the H Cluster in [Fe]-Hydrogenases. *Journal of the American Chemical Society* **1999,** *121* (34), 7877-7884.

55.   Keita, Bineta, Ulrich Kortz, Luis Roberto Brudna Holzle, Spencer Brown, and Louis Nadjo. 2007. 'Efficient Hydrogen-Evolving Cathodes Based on Proton and Electron Reservoir Behaviors of the Phosphotungstate $[H_7P_8W_{48}O_{184}]_{33}$- and the Co(II)-Containing Silicotungstates $[Co_6(H_2O)_{30}\{Co_9Cl_2(OH)_3(H2O)_9(\beta\text{-}SiW_8O_{31})_3\}]_5$- and $[\{Co_3(B\text{-}\beta\text{-}SiW_9O_{33}(OH))(B\text{-}\beta\text{-}SiW_8O_{29}OH)_2\}_2]_{22}$', *Langmuir*, 23: 9531-34.

56.   Kortz, A.; Chen, B.; Naresh, S.; Dalal, A.; Zhao, Y.; Keita, B., Enhanced proton and electron reservoir abilities of polyoxometalate grafted on graphene for high-performance hydrogen evolution. *Energy Environ. Sci.* **2016**.

57.   Becker, R.; Amirjalayer, S.; Li, P.; Woutersen, S.; Reek, J. N. H., An iron-iron hydrogenase mimic with appended electron reservoir for efficient proton reduction in aqueous media. *Science Advances* **2016,** *2* (1).

58.   King, P. W.; Posewitz, M. C.; Ghirardi, M. L.; Seibert, M., Functional Studies of [FeFe] Hydrogenase Maturation in an Escherichia coli Biosynthetic System. *Journal of bacteriology* **2006,** *188* (6), 2163-2172.

59.   McGlynn, S. E.; Shepard, E. M.; Winslow, M. A.; Naumov, A. V.; Duschene, K. S.; Posewitz, M. C.; Broderick, W. E.; Broderick, J. B.; Peters, J. W., HydF as a scaffold protein in [FeFe] hydrogenase H-cluster biosynthesis. *FEBS Letters* **2008,** *582* (15), 2183-2187.

60.   Cendron, L.; Berto, P.; D'Adamo, S.; Vallese, F.; Govoni, C.; Posewitz, M. C.; Giacometti, G. M.; Costantini, P.; Zanotti, G., Crystal Structure of HydF Scaffold Protein Provides Insights into [FeFe]-Hydrogenase Maturation. *Journal of Biological Chemistry* **2011,** *286* (51), 43944-43950.

61.   Czech, I.; Stripp, S.; Sanganas, O.; Leidel, N.; Happe, T.; Haumann, M., The [FeFe]-hydrogenase maturation protein HydF contains a H-cluster like [4Fe4S]–2Fe site. *FEBS Letters* **2011,** *585* (1), 225-230.

62.   Shepard, E. M.; McGlynn, S. E.; Bueling, A. L.; Grady-Smith, C. S.; George, S. J.; Winslow, M. A.; Cramer, S. P.; Peters, J. W.; Broderick, J. B., Synthesis of the 2Fe subcluster of the [FeFe]-hydrogenase H cluster on the HydF scaffold. *Proceedings of the National Academy of Sciences* **2010,** *107* (23), 10448-10453.

63.   Czech, I.; Silakov, A.; Lubitz, W.; Happe, T., The [FeFe]-hydrogenase maturase HydF from Clostridium acetobutylicum contains a CO and CN− ligated iron cofactor. *FEBS Letters* **2010,** *584* (3), 638-642.

64.   Vallese, F.; Berto, P.; Ruzzene, M.; Cendron, L.; Sarno, S.; De Rosa, E.; Giacometti, G. M.; Costantini, P., Biochemical Analysis of the Interactions between the Proteins Involved in the [FeFe]-Hydrogenase Maturation Process. *Journal of Biological Chemistry* **2012,** *287* (43), 36544-36555.

65.   Posewitz, M. C.; King, P. W.; Smolinski, S. L.; Zhang, L.; Seibert, M.; Ghirardi, M. L., Discovery of Two Novel Radical S-Adenosylmethionine Proteins Required for the Assembly of an Active [Fe] Hydrogenase. *Journal of Biological Chemistry* **2004,** *279* (24), 25711-25720.

66.   Shepard, E. M.; Duffus, B. R.; George, S. J.; McGlynn, S. E.; Challand, M. R.; Swanson, K. D.; Roach, P. L.; Cramer, S. P.; Peters, J. W.; Broderick, J. B., [FeFe]-Hydrogenase Maturation: HydG-Catalyzed Synthesis of Carbon Monoxide. *Journal of the American Chemical Society* **2010,** *132* (27), 9247-9249.

67.   Driesener, R. C.; Duffus, B. R.; Shepard, E. M.; Bruzas, I. R.; Duschene, K. S.; Coleman, N. J. R.; Marrison, A. P. G.; Salvadori, E.; Kay, C. W. M.; Peters, J. W.; Broderick, J. B.; Roach, P. L., Biochemical and Kinetic Characterization of Radical S-Adenosyl-l-methionine Enzyme HydG. *Biochemistry* **2013,** *52* (48), 8696-8707.

68.   Kriek, M.; Martins, F.; Challand, M. R.; Croft, A.; Roach, P. L., Thiamine Biosynthesis in Escherichia coli: Identification of the Intermediate and By-Product Derived from Tyrosine. *Angewandte Chemie International Edition* **2007,** *46* (48), 9223-9226.

69.   Kuchenreuther, J. M.; George, S. J.; Grady-Smith, C. S.; Cramer, S. P.; Swartz, J. R., Cell-free H-cluster Synthesis and [FeFe] Hydrogenase Activation: All Five CO and CN$^-$ Ligands Derive from Tyrosine. *PLoS ONE* **2011,** *6* (5), e20346.

70.   Kuchenreuther, J. M.; Myers, W. K.; Suess, D. L. M.; Stich, T. A.; Pelmenschikov, V.; Shiigi, S. A.; Cramer, S. P.; Swartz, J. R.; Britt, R. D.; George, S. J., The HydG Enzyme Generates an $Fe(CO)_2(CN)$ Synthon in Assembly of the FeFe Hydrogenase H-Cluster. *Science (New York, N.Y.)* **2014,** *343* (6169), 424-427.

71.   Broderick, J. B.; Duffus, B. R.; Duschene, K. S.; Shepard, E. M., Radical S-Adenosylmethionine Enzymes. *Chemical reviews* **2014,** *114* (8), 4229-4317.

72.   Kuchenreuther, J. M.; Britt, R. D.; Swartz, J. R., New Insights into [FeFe] Hydrogenase Activation and Maturase Function. *PLoS ONE* **2012,** *7* (9), e45850.

73.   Shepard, E. M.; Mus, F.; Betz, J. N.; Byer, A. S.; Duffus, B. R.; Peters, J. W.; Broderick, J. B., [FeFe]-Hydrogenase Maturation. *Biochemistry* **2014,** *53* (25), 4090-4104.

74.   Quitterer, F.; List, A.; Eisenreich, W.; Bacher, A.; Groll, M., Crystal Structure of Methylornithine Synthase (PylB): Insights into the Pyrrolysine Biosynthesis. *Angewandte Chemie International Edition* **2012,** *51* (6), 1339-1342.

75.   Nicolet, Y.; Rubach, J. K.; Posewitz, M. C.; Amara, P.; Mathevon, C.; Atta, M.; Fontecave, M.; Fontecilla-Camps, J. C., X-ray Structure of the [FeFe]-Hydrogenase Maturase HydE from Thermotoga maritima. *Journal of Bioogical Chemistry* **2008,** *283* (27), 18861-18872.

76.   Nicolet, Y.; Rohac, R.; Martin, L.; Fontecilla-Camps, J. C., X-ray snapshots of possible intermediates in the time course of synthesis and degradation of protein-bound Fe4S4 clusters. *Proceedings of the National Academy of Sciences* **2013,** *110* (18), 7188-7192.

CHAPTER 2

[FEFE]-HYDROGENASE OXYGEN INACTIVATION IS INITIATED BY THE
MODIFICATION AND DEGRADATION OF THE H-CLUSTER 2FE SUBCLUSTER

Contribution of Authors and Co-Authors

Manuscript(s) in Chapter(s) 2, 3, 5, 6, Appendix D

Author: Kevin D. Swanson

Contributions: Experimental design, enzyme purification, involvement in all experiments

Co-Author: Michael W. Ratzloff

Contributions: FTIR spectroscopy

Co-Author: David W. Mulder

Contributions: Enzyme expertise, experimental design

Co-Author: Jacob H. Artz

Contributions: Protein expression and purification, FTIR experiments, crystal screens,
and finalization of crystal structure

Co-Author: Shourjo Ghose

Contributions: Mass spectrometry

Co-Author: Andrew Hoffman

Contributions: Mass Spectrometry

Co-Author: Spencer White

Contributions: Protein expression

Contribution of Authors and Co-Authors (Continued)

Co-Author: Oleg A. Zadvornyy

Contributions: Collecting and processing X-ray diffraction data, solving structure

Co-Author: Joan B. Broderick

Contributions: Experimental design and interpretation

Co-Author: Brian Bothner

Contributions: Experimental design and interpretation

Co-Author: Paul W. King

Contributions: Experimental design and interpretation

Co-Author: John W. Peters

Contributions: Experimental design and interpretation

Manuscript Information Page

Kevin D. Swanson, Michael W. Ratzloff, David W. Mulder, Jacob H. Artz, Shourjo
Ghose, Andrew Hoffman, Spencer White, Oleg A. Zadvornyy, Joan B. Broderick, Brian
Bothner, Paul W. King John W. Peters

Status of Manuscript:

____ Prepared for submission to a peer-reviewed journal

____ Officially submitted to a peer-review journal

____ Accepted by a peer-reviewed journal

__X_ Published in a peer-reviewed journal

Abstract

The [FeFe]-hydrogenase catalytic site H cluster is a complex iron sulfur cofactor that is sensitive to oxygen (O_2). The O_2 sensitivity is a significant barrier for production of hydrogen as an energy source in water-splitting, oxygenic systems. Oxygen reacts directly with the H cluster, which results in rapid enzyme inactivation and eventual degradation. To investigate the progression of O_2-dependent [FeFe]- hydrogenase inactivation and the process of H cluster degradation, the highly O_2-sensitive [FeFe]-hydrogenase HydA1 from the green algae *Chlamydomonas reinhardtii* was exposed to defined concentrations of O_2 while monitoring the loss of activity and accompanying changes in H cluster spectroscopic properties. The results indicate that H clusterdegradation proceeds through a series of reactions, the extent of which depend on the initial enzyme reduction/oxidation state. The degradation process begins with O_2 interacting and reacting with the 2Fe subcluster, leading to degradation of the 2Fe subcluster and leaving an inactive [4Fe-4S] subcluster state. This final inactive degradation product could be reactivated *in vitro* by incubation with 2Fe subcluster maturation machinery, specifically HydF^{EG}, which was observed by recovery of enzyme activity.

Introduction

[FeFe]-hydrogenases are found in bacteria and lower eukaryotes, and are commonly involved in the recycling of reduced electron carriers that accumulate during anaerobic metabolism[1]. [FeFe]-hydrogenases catalyze reversible H_2 activation at very high rates and thus are attractive targets for bioengineering efforts aimed at coupling microbial H_2 production to oxygenic photosynthesis[2-3]. However, [FeFe]-hydrogenases are rapidly inactivated upon exposure to O_2, the byproduct of water oxidation[4-5]. In [FeFe]-hydrogenases, proton reduction occurs at a complex bridged FeS cluster termed the H cluster. The H cluster exists as a regular [4Fe-4S] subcluster bridged to an organometallic 2Fe subcluster through a protein cysteine thiolate. The 2Fe subcluster is coordinated by unique non-protein ligands including CO, CN, and dithiomethylamine (Figure2.1)[6-10]. The O_2 sensitivity has been attributed to redox reactions with O_2, and subsequent destruction of the H cluster by reactive oxygen species (ROS), rendering the enzyme irreversibly inactivated[11].

Although all of the characterized [FeFe]-hydrogenases have been shown to be sensitive to O_2 inactivation, enzymes from different sources have varying sensitivity to O_2, which has been attributed largely to differences in the access of the active sites to O_2[5, 12-16]. Computational studies have revealed putative channels that are proposed to function in the diffusion of gases, including O_2, to and from the active site[13].
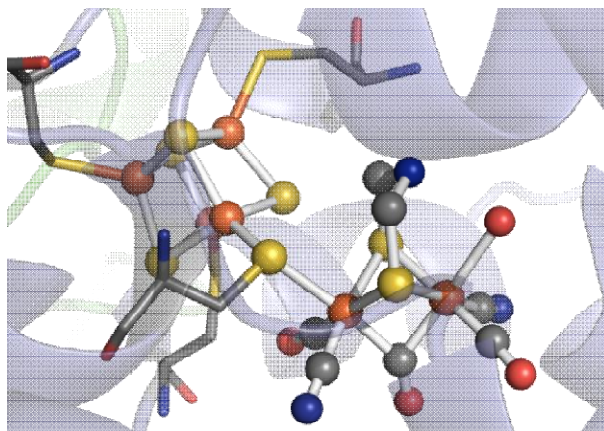
Figure 2.1. H cluster ball-and-stick representation with carbon, nitrogen, oxygen, sulfur, and iron atoms colored grey, blue, red, yellow, and rust respectively (PDB 3C8Y).

It was also discovered through computational analysis and enzymatic assays of site directed variants that constricting the gas channels can decrease the sensitivity of the [FeFe]-hydrogenase to O_2 but not to a significant enough degree to be useful for applications in technology[12-13, 15-16]. A random mutagenesis approach was used to screen thousands of [FeFe]-hydrogenase variants leading to isolation of a more O_2 tolerant variant with several site substitutions. The effect of each mutation was individually tested, and showed that each contributed to an additive effect on the overall O_2 tolerance of the [FeFe]-hydrogenase[16].

Theoretical studies of inactivation have measured the thermodynamics of O_2 binding and reactivity with the H cluster, and probed the subsequent reaction steps that ultimately lead to enzyme degradation. The models suggest that initiation of O_2 interaction with hydrogenase catalysis is dependent on the oxidation state, coordination environment and redox activity of the Fe sites[17-20]. In the H cluster reaction models, O_2 binds at the distal Fe, which is assigned to the (I) oxidation state for H_{ox} with a "loosely"

bound water. Reaction of the bound O_2 with Fe(I) leads to formation of a terminally

bound -OOH or -O_2^- species. Further reaction cycles of the terminal "O" species with H^+

generates H_2O_2 or iron-peroxide as end-products[19]. Alternatively, 2Fe subcluster

oxidation, or O atom insertion into the distal Fe terminal CO ligand can release CO_2[19].

The exact chemical nature of the O-species produced from O_2 reactions at the H cluster

remain to be experimentally validated. A recent experimental and theoretical study of

anaerobic, oxidative inactivation of CrHydA1[21] proposed that the inactivation mechanism

proceeds *via* reversible, and slower irreversible inactivation processes. Reversible

inactivation involved H_2 binding to different thermally available conformers of the H-

cluster, with ligand rearrangements on Fe_d that led to protection from O_2 inactivation.

Irreversible inactivation occurred at high (positive) potentials and was modeled as a slow

oxidation of H_{ox}, rendering the H cluster susceptible to nucleophilic attack and

subsequent H cluster disruption[21].

Structural and biophysical studies on how O_2 reacts with the H cluster to cause

inactivation are challenging, and there are limited experimental studies on this process[4, 22]. A mechanism of H cluster degradation by O_2 has been proposed from the results of X-

ray absorption spectroscopy (XAS) studies in which reactive O_2 species produced at the

2Fe subcluster result in enzyme inactivation by destruction of the [4Fe4S] subcluster[11, 23].

Those results contrast with previous models whereby O_2 accesses and binds to the 2Fe

subcluster to form ROS or other end-products that can readily degrade the 2Fe subcluster

followed by loss of enzyme activity[19]. It has been observed earlier that exposure of

[FeFe]-hydrogenases to either O_2 or light (photolysis) led to the formation of an H_{ox}-CO

like EPR or IR signal[24-26]. The photolytic effect is known to lead to CO release, which can re-bind to the same enzyme, or another enzyme in a process termed "cannibalization"[25-26]. O_2 caused both irreversible and reversible inactivation, where reversible inactivation was proposed to occur *via* formation of an "O"-adduct with an EPR signal similar to H_{ox}-CO. A mechanism for the O_2 induced formation of the O-adduct has not been determined.

In order to reexamine the mechanistic process of O_2 inactivation of [FeFe]hydrogenases, we have exposed the [FeFe]-hydrogenase from *Chlamydomonas reinhardtii* (CrHydA1) to low titers of O_2 while monitoring changes in the biochemical activity and changes in Fourier transform infrared (FTIR) and Ultraviolet–visible (UVVis) spectroscopic properties. The FTIR results indicate that H cluster reacts with O_2 and undergoes a series of reactions to produce a mixture of intermediates, the populations of which depend on the initial reduction/oxidation state of the H cluster. Ultimately, oxidative destruction results in the loss of the 2Fe subcluster and formation of a [4Fe-4S] subcluster state observed with UV-Vis and in the X-ray crystal structure. This inactivation/degradation end product could be reactivated *in vitro* by incubation with the 2Fe subcluster specific maturation machinery, as observed by enzyme activity assays.

Methods

Protein Preparation

Heterologous expression and purification of CrHydA1 in *Escherichia coli* was done as previously described[27-28]. The protein was purified under anaerobic conditions in

a MBraun anaerobic chamber (MBraun USA). All buffers were degassed under vacuum before purification. CrHydA1 isolation from cell extracts was performed using a two-step chromatography process of ion-exchange over diethylaminoethanol (DEAE, GE Lifesciences) Sepharose followed by affinity capture on Strep-Tactin (IBA) resin[28]. Strep-Tactin bound enzyme was eluted in 50 mM Tris buffer (pH 8.0) containing 300 mM NaCl, 5% glycerol, 5 mM sodium dithionite (NaDT), and 2 mM desthiobiotin. Purity was verified by sodium dodecyl sulfate polyacrylamide gel electrophoresis (SDS-PAGE), and the concentration determined by Bradford assay. CrHydA1 was prepared in the H_{ox} state by serial concentration and dilution in NaDT-free buffer until the FTIR spectra consisted primarily of H_{ox}. CrHydA1 was prepared in the H_{ox}-CO state by brief sparging under 100% CO gas, and 10 min incubation, in a sealed serum vial. Aliquots of CrHydA1 were prepared in H_{red}-H_2 by 10 evacuation flush cycles with 100% H_2 on a Schlenk line fitted with an O_2 trap.

HydF was obtained by expression of *hydF* in the background of HydE and HydG (HydF^{EG}) in *E. coli* strain BL21 (DE3). The *hydE*, *hydF*, and *hydG* from *Clostridium acetobutylicum* were individually cloned into pET-Duet, pRSF-Duet, and pCDF-Duet, respectively[29]. The cloned copy of *hydF* contained a N-terminal 6xHis tag[29]. Cells were grown in LB Miller growth medium supplemented with streptomycin (50 mg L^{-1}), kanamycin (30 mg L^{-1}), ampicillin (100 mg L^{-1}), 0.5% w/v glucose (~25 mM), 2 mM ferric ammonium citrate and 50 mM phosphate buffer (final pH of medium was 7.4). All cultures were grown aerobically at 25 °C until an OD_{600} of 0.5. Cultures were sparged with 100% argon for 20 min, and induced with 1.5 mM isopropyl β-D-

1thiogalactopyranoside (IPTG). Cysteine (2 mM) and sodium fumarate (25 mM) were added immediately after IPTG addition. Cultures were sparged with argon at 25°C overnight.

HydF^{EG} was purified in an anaerobic chamber (Coy Labs, Grass Lake MI) as previously described[29]. Cells were harvested by centrifugation and cell pellets stored at - 80 °C. Cells were lysed by resuspension in buffer composed of 10 mM HEPES, pH 7.4, 0.5 M KCl, 5% glycerol, 1 mM dithiothreitol, 20 mM imidazole, 20 mM MgCl$_2$, 1 mM PMSF, 1% Triton X-100, 140 µg ml^{-1} DNAse and RNAse, and 120 µg ml^{-1} lysozyme. The cell lysate was stirred for 1 hour at room temp, and centrifuged in gas tight bottles at 38,000 x g for 30 min. The His-HydF^{EG} was purified from the supernatant by immobilized metal chromatography on a TALON cobalt column (GE Life Sciences).

The column was loaded and washed with 15 column volumes of 20 mM HEPES pH 7.4, 0.5 M KCl, 5% glycerol, 1 mM dithiothreitol, and 20 mM imidazole. Purified HydF^{EG} was eluted with wash buffer containing 200 mM imidazole. HydF^{EG} was collected and concentrated anaerobically with 30 kDa Amicon Ultra-15 centrifugal concentrators (Millipore). The HydF^{EG} was loaded onto a G25 PD-10 desalting column (GE Life Sciences) to remove imidazole and eluted with 50 mM HEPES pH 7.4, 0.5 M KCl, 5% glycerol, and 1 mM dithiothreitol. HydF^{EG} was flash frozen in liquid N$_2$ and stored at – 80 °C or in liquid N$_2$ until further use.

Preparation of Oxygen Treated CrHydA1

O$_2$ gas standards were prepared using septum-sealed 123 ml Wheaton vials.

Dilutions were prepared using a gas-tight syringe (Hamilton) to remove gas from a 100%

O_2 standard (equilibrated to atmospheric pressure) and injecting the O_2 into vials

containing 100% N_2 at atmospheric pressure. Standards of 100%, 4%, 1%, and 0.1% O_2

were used for all of the O_2 additions. Samples used to measure the FTIR spectra of O_2

treated CrHydA1 were prepared as follows: H_{ox} (Figures 2.2 and 2.3), O_2 was injected by

gas-tight syringe into the headspace above an aliquot of 75 µL of 45 mg mL^{-1} CrHydA1

in a septum-sealed 825 µL conical vial; H_{ox}-CO (Figure 2.2, Figure S1), a 15 µL aliquot

of 70 mg mL^{-1} H_{ox} CrHydA1 was injected via gas-tight syringe into a septum-sealed 825

µL conical vial that had previously been flushed with 100% CO. O2 was then injected by

gas-tight syringe into the headspace of the conical vial; H_{red}-H_2 (Figure 2.2), 70 µL of 30

mg mL^{-1} H_{ox} CrHydA1 in a septum-sealed 825 µL conical vial, along with 3 similar

empty conical vials, underwent 10 vacuum/100% H_2 exchanges on a Schlenk line, and

incubated for 1 h at 4 °C in the Mbraun. A 10 µL aliquot of this enzyme sample was

transferred to each one of the empty, H_2-treated vials via gas-tight syringe. O_2 was then

injected by a gas-tight syringe into the headspace of each vial; H_{red}-DT (Figures 2.2 and

S2) was prepared in the MBraun glovebox by adding NaDT (20 mM final) to 50 µL of 50

mg mL^{-1} H_{ox} CrHydA1 (45 mg mL^{-1} final) and mixed via pipetting for 30 s. A 15 µL

aliquot was transferred to a 825 µL conical vial, and then sealed with a septum. O_2 was

injected by gas-tight syringe into the headspace of the conical vials. In all cases, the

conical vials contained a micro stir bar, and stirred while on an ice bath, Final O_2

concentrations ranged from 0.01-24.7% (v/v). In order to minimize pressure increases

due to gas injection, the appropriate standard was used to keep the injection volume less

than 5% of the vial volume (with the exception of the 24.7% CO sample shown in Figure S1). An aliquot of CrHydA1 was removed from the septum-sealed vial using gas-tight syringe and loaded in a custom gas-tight FTIR sample cell[30]. A summary of the O_2 concentration and molar ratios is given in Table S1. Control experiments were performed to estimate the repeatability of O_2 injections, with O_2 concentrations determined by GC (Agilent Technologies). The standard deviation for O_2 injections is estimated to be SD= +/-(% O_2 x 0.15) or +/- 15% of each individual injection (Table S2).

FTIR Spectroscopy

Spectra were collected as described previously with a Nicolet 6700 FTIR spectrometer (Thermo Fisher Scientific) equipped with a Globar IR source, a CaF_2 beam splitter, and a liquid-nitrogen-cooled mercury cadmium telluride (MCT) detector[30]. All of the spectra were collected at room temperature (21 °C). The custom-built sample chamber consists of a covered aluminum box designed to minimize external light interference with the sample. The OMNIC software was configured to report absorbance spectra, and absorbance baselines were fit to these data using a manually adjusted spline.

Ultraviolet-Visible Spectroscopy

A 100 µl aliquot of 3 mg mL^{-1} H_{ox} CrHydA1 was prepared in the glove box under 100% N_2, transferred into low volume 1 cm path-length quartz cuvette and septum sealed. The O_2 reaction was initiated by injecting O_2 (at 0.001%, 17% or 300%) with a gas-tight syringe into the headspace of cuvette with the enzyme solution at 4°C, cooled with a peltier cooler. A micro-stir bar provided agitation of the solution in the cuvette.

The reaction of CrHydA1 with O_2 was monitored by UV-Vis every min for 200-300 min, by scanning over a 250-750 nm range at 1 nm intervals. UV-Vis spectra were recorded on a Cary 4000 UV-Visible spectrophotometer.

Activity Assays

Activities of CrHydA1 were assayed by H_2 evolution from reduced methyl viologen. Reaction volumes of 0.6 or 2 ml were placed in 3 or 10 ml Wheaton vials, respectively, which contained 5 mM methyl viologen (MV), 10 mM NaDT, 50 mM Tris, 300 mM NaCl, 5% glycerol, and between 25 ng-4 µg of enzyme per assay. Hydrogen production was detected by gas chromatography (Agilent Technologies).

Mass Spectrometry

Protein digests were performed with 1.5 mg ml^{-1} CrHydA1, 12.5 ug ml^{-1} Trypsin Gold (Promega), 50 mM Tris-HCl pH 8, 300 mM NaCl, and 5% glycerol. Reactions were allowed to proceed overnight in a 37 °C heat block, and complete digestion was verified by sodium dodecyl sulfate polyacrylamide gel electrophoresis (SDS-PAGE). Reactions were transferred into septum sealed vials with a N_2 headspace. The digestion product was diluted up to a 1000 fold in 50/50 water/Acetonitrile and transferred to screw capped auto sampler vials for LCMS.

An Agilent 1100 series HPLC system coupled to an Agilent Chip Cube integrated microfluidics reverse-phase nano-HPLC system was used. Trapping and analytical separations were performed with an Agilent C18 HPLC-Chip (G4240-62001, 40 nl trap column and 75 µm x 43 mm analytical). Chromatography solvents were H_2O with 0.1%

(v/v) formic acid for channel "A" and acetonitrile for channel "B". The HPLC program was held at 7% B from 0.0 to 2.0 min, then ramped from 7 to 35% B from 2.0 to 20.0 min. The gradient was then ramped from 35 to 95% B from 22 to 27 min. The mass spectrometer was an Agilent 6520 Q-TOF with a dual-ESI source: resolution approximately 20,000 and accuracy 3 ppm. Spectra were collected in positive mode from 50 to 1700 m/z at 2 Hz for both MS and MS/MS, with adaptive acquisition time for highly-abundant ions.

The resulting MS/MS data were analyzed using the PEAKS 6.0 software package and searching the CrHydA1 protein sequence. Peptide mass tolerance was 10 ppm and fragment mass tolerance 0.5 Da. Variable modifications were set to sulfonic acid 47.97, sulfinic acid 31.98, and oxidation or hydroxylation of cysteine 15.99.

Crystallization and Structure Determination

CrHydA1 (1 mL at 10 mg mL^{-1}) in NaDT free buffer was exposed to 0.01% O2 for 2 hrs in a 4.5 mL Wheaton vial. Enzyme activity was measured at the end of the 2 hr period (50 μmol min^{-1}mg^{-1}). An aliquot of the sample was set aside for trypsin digest and MS analysis, and the rest of the sample was concentrated to 30 mg mL^{-1} for crystallization. CrHydA1 was crystallized anaerobically in a MBraun glove box at room temperature using micro-capillary batch diffusion with a precipitation solution of 25.5% polyethylene glycol 8000 as precipitate and 0.085 M sodium cacodylate (pH 6.5), 0.17 M sodium acetate trihydrate, and 1 mM dithionite. After allowing the crystals to form for 23 weeks, they were mounted on cryo-loops and flash frozen in liquid nitrogen. Data were collected at the Stanford Synchrotron Radiation Lightsource (SSRL) on beam line

BL12-1 at 1.75 Å wavelength. The data was processed using XDS[31], and scaled with

Pointless and Aimless[32]. The structure was solved using molecular replacement using

AutoMR (CCP4 suite of programs) with CrHydA1 (PDB ID, 3LX4)[33]. The structure was

built using COOT with further refinement using REFMAC5 using NCS and B factor

restraints. The final model was solved to 2.23 Å with an R factor of 24.1% and an R free

of 27.7% (Table S4, Table S5). Atomic coordinates were deposited in the PDB

(code 4ROV).

In vitro Reactivation of O_2 Inactivated CrHydA1

Reactivation of the O_2 inactivated CrHydA1 was performed with the addition of

N-terminal His tagged-HydF^{EG} at different molar ratios to obtain a 300 µl total volume in

3 ml crimp sealed anaerobic Wheaton vials. CrHydA1 was allowed to reactivate at 37 °C

in a water bath for 1 h, and reactivation was followed by measuring the H_2 production

activity as described above.

Results

FTIR Analysis and Comparison of H_{ox}, H_{red}-NaDT, H_{red}-H_2 and H_{ox}-CO

To investigate how differences in the oxidation state and/or site occupancy of the

2Fe subcluster of CrHydA1 affect the process of O_2 damage, reducing agents NaDT and

H_2, and the competitive inhibitor CO were each added to oxidized (H_{ox}) CrHydA1.

These enzyme samples were then exposed to O_2 and monitored by FTIR. CrHydA1 was

initially prepared in the H_{ox} state with major peaks observed at 1804, 1940, 1964, 2071

and 2089 cm^{-1} (Figure 2.2a, red). Exposure of the H$_{ox}$ CrHydA1 to ~0.01% O$_2$ (Figure 2.2a black spectrum) for 2 h resulted in the loss of H$_{ox}$ features and an increase in features assigned to H$_{ox}$-CO and the O$_2$-damaged cluster, discussed in more detail in the time course discussion. A control experiment (Figure S3) on a duplicate sample in the absence of O$_2$ showed only slight change in the accumulation of H$_{ox}$ signal due to auto-oxidation.

CrHydA1 in the H$_{ox}$ state was exposed to CO to make H$_{ox}$-CO (Figure 2.2b, red spectrum). The expected shift of vCO and vCN peaks to higher wavenumbers were observed as previously reported for CO-inhibited [FeFe]-hydrogenases, with vCO peaks at 1809, 1963, 1969, 2013, and vCN peaks at 2082, and 2091 cm^{-1}[26, 34-35]. The enzyme was then exposed to ~2.4% O$_2$. H$_{ox}$-CO was exposed to larger percentages of oxygen in order to see if any attenuation of FTIR signal could be observed. After approximately 2 h of O$_2$ exposure, the FTIR spectrum indicated the peaks assigned to H$_{ox}$-CO remained relatively unchanged (Figure 2.2b, red vs. black spectrum). Small peaks appeared, which are attributed to degradation of some residual H$_{ox}$ species, and this may have also contributed to the slight increase in H$_{ox}$-CO signal intensity after O$_2$ exposure. Enzyme in the H$_{ox}$-CO state was also treated with higher amounts of O$_2$ (up to ~24.7%, Figure S1), and the resulting FTIR spectra again showed significantly less degradation compared to oxidized and reduced preparations, consistent with other observations that H$_{ox}$-CO is stable to oxidative reactions with O$_2$ [4-5, 11, 36].

Equilibration of H$_{ox}$ CrHydA1 under 100% H$_2$ led to a collective shift in the vCO peaks, consistent with ligand exchange and electronic transitions at the H cluster associated with H$_2$ activation[30, 37]. Figure 2.2c shows the spectrum of H$_2$-reduced

CrHydA1 with principle vCO peaks, assigned to a mixed population of reduced

intermediates, observed at 1792, 1882, 1891, 1916, 1933, 1953, and 1963 cm^{-1}
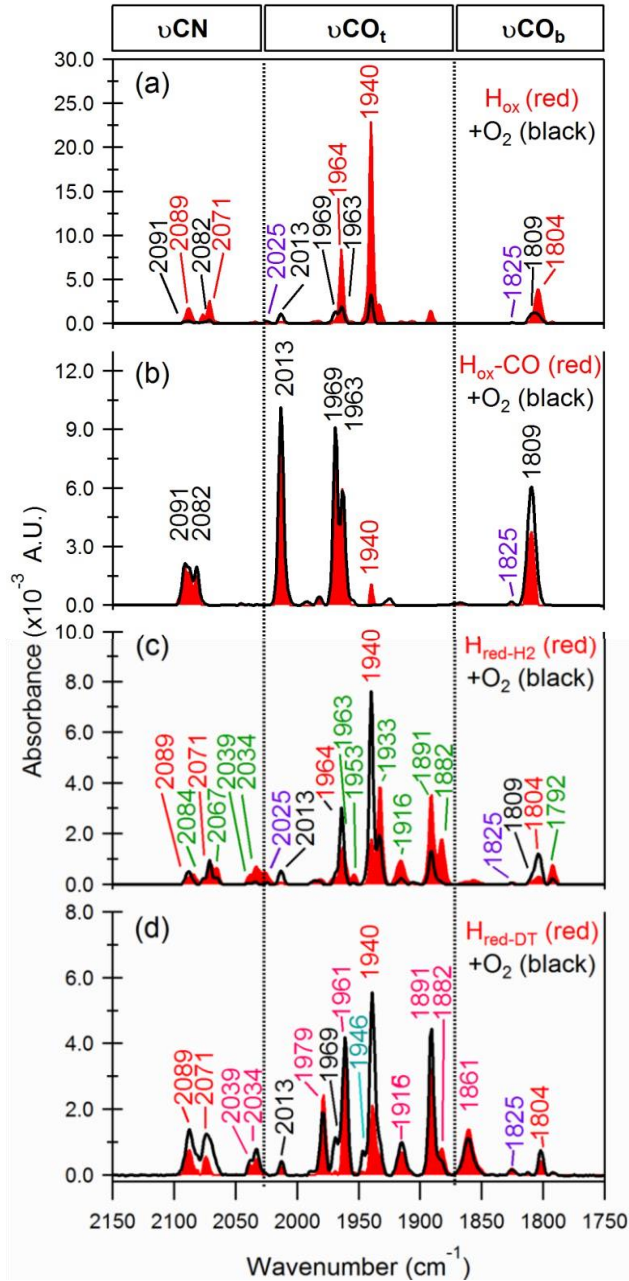
Figure 2.2. FTIR spectra of CrHydA1 samples exposed to O$_2$. The solid red spectra are prior to O$_2$ injection, and black traces after 2 h exposure to O$_2$. (a) H$_{ox}$, ~0.01% O$_2$; (b) H$_{ox}$-CO, ~2.4% O$_2$; (c) H$_{red}$-H$_2$, ~0.01% O$_2$; (d) H$_{red}$-NaDT, ~0.01% O$_2$. Wavenumbers in red, H$_{ox}$; black, H$_{ox}$-CO; green, H$_{red}$-H$_2$; magenta H$_{red}$-NaDT; purple, oxidative damage and cyan, unassigned.

(Figure 2.2c, red spectrum)[30, 37-38]. Additional peaks associated with H_{ox}-CO were also seen in the starting sample, possibly arising from a slight amount of O_2 exposure during H_2 treatment. Exposure of H_{red}-H_2 CrHydA1 to ~0.01% O_2 for 2 h, in the presence of 100% H_2 atmosphere led to attenuation of the 1792, 1882, 1891, 1916, and 1933 cm^{-1} peaks (Figure 2.2c, red vs. black spectrum). This was accompanied by an increase in peak intensities assigned to H_{ox} at 1804, 1940, and 1964 cm^{-1} together with a small increase in peak intensities assigned to H_{ox}-CO at 1969 and 2013 cm^{-1}. Thus, degradation of the H_2-reduced CrHydA1 is likely to involve initial formation of $H_{ox,}$ with subsequent interaction with O_2 leading to formation of H_{ox}-CO and eventual 2Fe subcluster degradation.

When H_{ox} CrHydA1 was treated with NaDT (20 mM final concentration, a 20fold excess), the initial spectrum (Figure 2.2d, red spectrum) showed νCO peaks previously assigned to reduced intermediates at 1861, 1882, 1891, 1916, 1961, and 1979 cm^{-1} [30]. Compared to H_{ox} (Figure 2.2a), the NaDT-treated CrHydA1 showed less signal attenuation after exposure to O_2 (Figure 2.2d, red vs. black spectra), with only a small loss of 2Fe subcluster signal after 2 h of exposure to ~0.05% O_2. Regarding νCO peak intensities, the O_2 treatment produced new peaks at 1946 cm^{-1} and 1969 cm^{-1}, a slight increase in peak intensities at 1916, and 2013 cm^{-1}, and larger increases in peak intensities at 1804 and 1940 cm^{-1}. The increases at 1804 and 1940 cm^{-1} are assigned to an increase in the population of H_{ox}, and the changes at 1969 and 2013 cm^{-1} are assigned to an increase in the population of H_{ox}-CO. The appearance of H_{ox} is similar to the

sequence observed for O_2 exposure of H_2-reduced CrHydA1, again consistent with O_2 inactivation involving at least one H_{ox}-dependent reaction pathway. It should be noted that the presence of NaDT complicates conclusions drawn from this experiment, as it both reduced CrHydA1 and scavenged O_2. NaDT also reacts with O_2 to form ROS, which in turn reacts with CrHydA1 to exact inactivation. However, titrations of the NaDTreduced CrHydA1 with increasing amounts of O_2, led to similar transitions observed for H_{ox} CrHydA1, that is formation of both the H_{ox}-CO and O_2 damage signals (Figure S2).

FTIR Time Series of O_2 Exposed H_{ox} CrHydA1

In order to observe O_2-induced transitions in the 2Fe subcluster by FTIR on the timescales of full spectral collection (512 scans, ~8 min), CrHydA1 prepared in the Hox state (with vCO modes at 1804, 1940, 1964 cm 1) was incubated under a low (~0.01%) O_2 partial pressure at 4 °C, and FTIR spectra were collected at approximately ~25 min intervals (Figure 2.3). Based on an O_2 titration series (Figure S4) we selected 0.01% O_2

Table 2.1. Rate constants for O_2 induced changes in CrHydA1 and CaI H_{ox} νCO peak intensities, and H_2 evolution activities.

[1] $k= -[\ln(y/y_0)]/t$ $(s^{-1}\,\mu M^{-1})$

[2] (a) Goldet, G., et al. 2009. *JACS*. 131:14979; (b) Stripp, S.T., et al. 2009. *PNAS*.

Enzyme	[1] $k\Delta H_{ox}$ ΔIR signal, (s-1 μM-1)		[1] $k$inact H_2 evolution activity (s-1 μM-1)	[2] Ref. $k$inact (s-1 μM-1)
CrHydA1	(Δ1940) 3.0 x 10^{-4}	(Δ1964) 2.0 x 10^{-4}	2.0 x 10^{-4}	4.3 x 10^{-4} (a) 2.2 x 10^{-3} (b)
CaI	(Δ1945) 9.0 x 10^{-6}	(Δ1800) 1.2 x 10^{-6}	6.4 x 10^{-6}	5.1 x 10^{-6} (b)

106(41):17331.
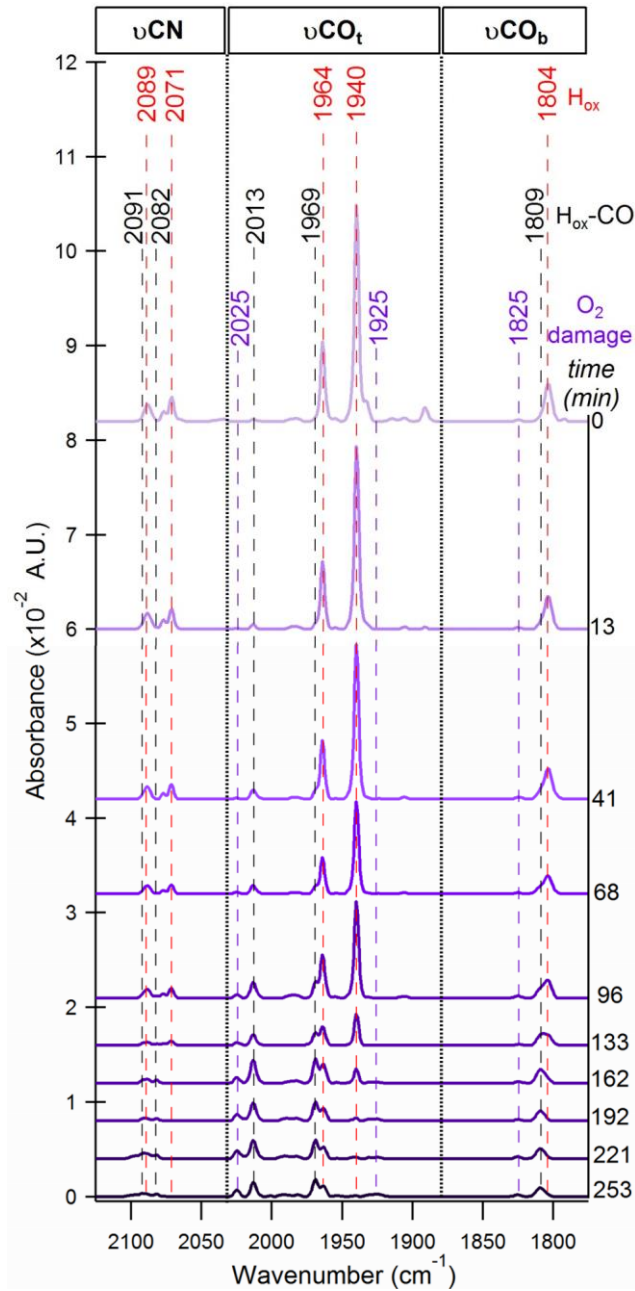
Figure 2.3. Time course of the FTIR spectra of H_{ox} CrHydA1 exposed to ~0.01% O_2. The initial H_{ox} signal (1804, 1940, 1964, 2071, and 2089 cm^{-1}) gradually decays, and the spectrum transitions to a characteristic H_{ox}-CO signal with νCO peaks at 1809, 1963, 1969, and 2013 cm^{-1}. Signals assigned to O_2 damaged clusters are shown in purple.

for the time-course experiment in order to allow the timescales of oxidative transitions to

match the timeframe of IR sampling and data collection. Under 0.01% O_2, the H_{ox} signal

gradually attenuated and transitioned to H_{ox}-CO, with primary νCO peaks at 1809, 1963,

and 2013 cm^{-1}. A near complete transition of H_{ox} to H_{ox}-CO was observed after ~200 min

of O_2 exposure. The decay rates of H_{ox} specific νCO signals at 1940 and 1964 cm^{-1} were

calculated from normalized absorbance measurements to be $k_{Hox} \approx 10^{-4}$ s^{-1} μM^{-1} (Table 2.1,

see also Table S3). These rates matched well to the inactivation rates $k_{inact} \approx 10^{-4}$ s^{-1} μM^{-1}

of H_2 evolution activity (Table 2.1). We also measured the change in the FTIR spectra of

Clostridium acetobutylicum HydA (CaI) prepared in H_{ox} and exposed to a ~30-fold

higher concentration (~0.28%) of O_2. This enzyme is ~100-fold less sensitive to O_2

inactivation than CrHydA1[5] thus was expected to have slower kinetics of O_2induced

changes in FTIR spectral features. A time-course spectrum (Figure S5) of CaI exposed to

~0.28% O_2 shows a slower decay rate of H_{ox} peak intensities, and subsequent appearance

of H_{ox}-CO signals, than for CrHydA1 (Table 2.1, see also Table S3). These differences

match to the comparatively slower (~100-fold) inactivation rate of CaI versus CrHydA1

(Table 2.1, see also Table S3). As observed for CrHydA1 there is good agreement

between the rate of loss of H_{ox} signal intensity, $k_{Hox} \approx 10^{-6}$ s^{-1} μM^{-1} O_2, and the

inactivation rate of H_2 evolution activity by O_2, $k_{inact} \approx 10^{-5}$ to 10^{-6} s^{-1} μM^{-1} O_2. For both

enzymes, prolonged periods of O_2 exposure appeared to have led to higher order effects

on νCO signal decay. These components were not included in the fitting parameters of

Tables 2.1 and S3 used to calculate k_{Hox}.
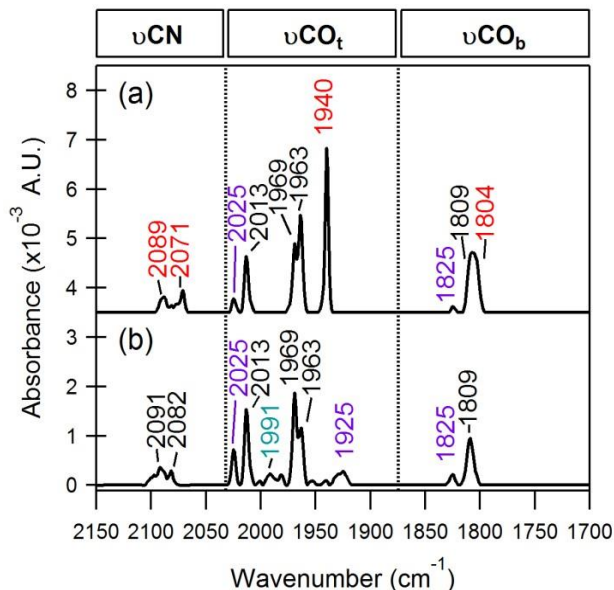
Figure 2.4. FTIR spectra of H_{ox} CrHydA1 after long-term exposure to 0.01% O_2. Scans taken at (a) 133 min, and (b) 253 min, after exposure to O_2. Wavenumber coloring is as described in Figure 2.2.

The percentage of H_{ox}-CO formed after O_2 exposure of H_{ox} (change in primary vCO peaks from 1804, 1940, and 1964 cm^{-1} to 1809, 1963 and 1969 cm^{-1}) was estimated by using standardized values for vCO peak heights, normalized to mg of enzyme, for an anaerobically prepared CrHydA1 H_{ox}-CO sample (Figure 2.2b, red spectrum). The amount of O_2-treated H_{ox} CrHydA1 that converted to H_{ox}-CO was determined based on normalizing the vCO peak intensities in the O_2-treated sample to the H_{ox}-CO standard. The amount of CrHydA1 that converted to H_{ox}-CO was ~20% after 133 min (Figure 2.4a) of ~0.01% O_2 exposure, where the rest of the signal loss is likely due to complete degradation of the 2Fe subcluster, which is observed at 253 min (Figure 2.4b). The O_2induced H_{ox}-CO signal appeared simultaneously with the loss of H_{ox}, and slowly decreased in intensity after 133 min (Figure 2,3). After a longer period of exposure, the loss of H_{ox}-CO was accompanied by the appearance of new vCO peaks at 1825, 1925 and

2025 cm^{-1} (Figure 2.4b). These peaks were specific for oxidatively damaged H cluster, but since the overall 2Fe subcluster signal is degrading and other states are growing in (H$_{ox}$-CO) and decaying (H$_{ox}$), it is not currently possible to determine whether these peaks arise from a single or multiple H cluster state(s). These putative vCO bands at 1825, 1925 and 2025 cm^{-1} might arise from oxygenation of a bridging thiolate, which was observed to induce a 6-19 cm^{-1} upshift of the vCO IR bands[39]. It is possible that O$_2$ or a byproduct of O$_2$ led to a similar effect on CrHydA1 vCO bands (see Figures 2.4a and 2.4b)[39]. In depth DFT calculations on O$_2$ binding to the H cluster propose reaction pathways that include both oxygenation of Fe$_d$ and oxidation of 2Fe[40-41]. In this case, the resulting oxidation of the 2Fe subcluster would also cause an upshift in the vCO bands, again consistent with the observed upshifts in CrHydA1 H$_{ox}$ spectrum after O$_2$ exposure.

<u>UV-Vis of O2 Exposed CrHydA1</u>

Ultraviolet visible (UV-Vis) spectroscopy was employed to monitor the [4Fe-4S] cluster during O$_2$ exposure. The absorption spectra of holo-CrHydA1, CrHydA1 expressed in the absence of HydE, HydF and HydG and lacking the 2Fe subcluster (CrHydA1ΔEFG), and the O$_2$ inactivated CrHydA1 all showed a broad 415-420 nm absorbance feature associated with S to Fe charge transfer bands of FeS clusters. CrHydA1ΔEFG contains only a [4Fe-4S] subcluster inserted by E. coli's FeS cluster assembly machinery[42]. The difference between the spectra of CrHydA1ΔEFG and holo-CrHydA1 (Figures 2.5b and 2.5c, red and blue trace, respectively) shows that the spectra for CrHydA1^{ΔEFG} appears to be red-shifted and the difference in signal at 450 nm accounts for 11% of the total absorbance. This absorbance difference could be due to

CrHydA1$^{\Delta EFG}$ being in a more oxidized state, differences in Fe-loading per-mol of

enzyme, or the presence of the 2Fe subcluster causing a blue shift of the 450 nm

absorbance peak in holo-CrHydA1.
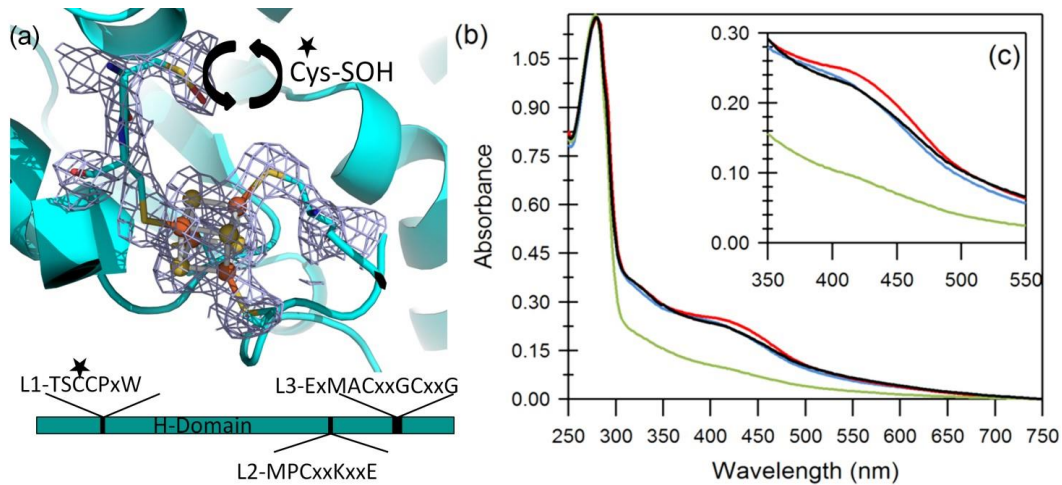
Figure 2.5. Crystal structure and UV-Vis of O_2 inactivated CrHydA1. (a) Electron density map contoured at 2σ showing extra electron density in the H cluster environment including oxidized Cys 169. The conserved [FeFe]-hydrogenase motifs are depicted below the ribbon diagram with Cys 169 (starred). (b) The full spectrum of reduced immature CrHydA1$^{\Delta EFG}$ (——), and of holo-CrHydA1 (——) after inactivation with 0.001% O_2 2 h (——), or with 3 atm of 100% O_2 for 3 h (——). (c) A close-up view of the 350-550 nm region.

Inactivation of CrHydA1 by exposure to ~0.001% and 17% O_2 for 2 h was

monitored by H_2 evolution activity and UV-Vis spectroscopy. The initial activity was

500 µmol min^{-1}mg^{-1}, which declined after the 2 h O_2 treatment to 12 µmol min^{-1} mg^{-1}.

CrHydA1 that was not exposed to O_2 did not show a decrease in specific activity, nor any

change in the UV-vis spectra. The blue trace in Figure 2.5b and 2.5c is the starting

spectrum of holo-CrHydA1, and the black trace is after 2 h incubation with 0.001% O_2,

the orange trace is after 2 h incubation with 17% O_2. The difference spectra between

holo-CrHydA1 (Figures 2.5b and 2.5c, blue trace) and O_2 inactivated CrHydA1 (Figures 2.5b and 2.5c, black and orange traces) did not reveal significant differences (data not shown), suggesting that most of the S☐Fe charge transfer absorption is maintained after O_2 inactivation This result is consistent with stability of the [4Fe-4S] cluster against O_2 damage. CrHydA1 that was exposed to large amounts of O_2 (3 atm of 100% O_2 for 3 h) exhibited a significant decay in the peak at 420 nm (Figures 2.5b and 2.5c, green trace).

In-vitro Activation of O_2 Inactivated CrHydA1

CrHydA1 that had been O_2 inactivated could be in vitro activated with HydFEG (Figure S7) and activity could be recovered to ~80% 0f as purified activity. The remaining population of enzyme that was inactivateable is likely due to degradation products that were further degraded to possibly [3Fe-4S] cluster, [2Fe-2S] cluster, or completely stripped of cluster[39]. This data suggests there is a significant population of enzyme containing intact [4Fe-4S] after O_2 exposure. It had been previously shown that HydF^{EG} is sufficient for activating CrHydA1$^{\Delta EFG}$ [29], and that activation of CrHydA1$^{\Delta EFG}$ requires the assembly of a preformed [4Fe-4S] cluster[42].

Structural Characterization of O_2 Inactivated CrHydA1

CrHydA1 inactivated by O_2 readily crystallized and the structure was determined to 2.3Å resolution. The resulting structure was very similar to the previously characterized structure of purified CrHydA1 expressed in the absence of [FeFe]-hydrogenase maturases HydE, HydF, and HydG with an overall r.m.s. deviation between the two structures of 0.29 Å [42]. The structure revealed a vacant 2Fe subcluster site and an

intact [4Fe-4S] subcluster (Figure 2.5a) and an open channel leading from the surface to the site left vacant in absence of the 2Fe subcluster. This suggests that the O_2 inactivated CrHydA1 is the appropriate conformation and is consistent with the observation that oxygen inactivated CrHydA1 can be reactivated by the H cluster maturation machinery. In addition, the structure revealed three Cys residues (amino acids 88, 169, and 238) to have additional electron density around the sulfur atoms which can be modeled and refined suggesting sulfenic acid (R-SOH) at positions Cys 169 (which functions in proton-transfer to the H-cluster(124)) and Cys 238 (surface localized) and sulfinic acid (R-SOOH) at position Cys 88 (surface localized). No modifications of the four Cys residues that function to coordinate the H cluster (Cys 170, 225, 417, and 421) were detected. The extra electron density at Cys 169 is best explained as a reaction product of the sulfur group with ROS, which might arise from O_2 binding at the 2Fe subcluster. It is possible that the modifications of the surface Cys 88 and 238 might arise from diffusion of ROS out of the catalytic site. Due to the importance of Cys 169, we used MS analysis to confirm the presence of sulfenic acid at the Cys 169 position observed in the X-ray structure (Figure S6). Thus this residue may also play an important role in inactivation. Although O_2 damage is evident from the X-ray and analytical structures, the [4Fe-4S] subcluster was intact with no evidence of O_2 damage.

Discussion

The results of recent studies in which X-ray Absorption Spectroscopy (XAS) was
used to monitor O_2 damage of CrHydA1 were interpreted to indicate that after O_2 binding
and reaction with the 2Fe subcluster, the initial target of H cluster degradation was the
[4Fe-4S] subcluster[11, 23]. These studies were conducted with high concentrations of O_2
and in one study with the additional presence of high concentrations of NaDT. For
example, Stripp $et\ al.$ exposed ~ 30 nmol of CrHydA1 equilibrated in the H_{ox} state to
~20% O_2 over a period of 15 min[11], whereas in Lambertz $et\ al.$ exposed 8 nmol of NaDT
reduced CrHydA1 to air saturated buffer (~330 μM or 21% O_2) for ~17 min[23]. In
contrast, for the comparative study with FTIR (Figure 2.3), we monitored H_{ox} 2Fe
subcluster degradation with slightly more enzyme (~68 nmol), but exposed to ~2500x
less (~0.137 μM in solution as determined by Henry's Law or ~0.01% headspace partial
pressure) concentrated O_2 in solution over a ~17x longer time period. As mentioned
above, several experiments were conducted with different amounts of O_2 in order to
determine the amount that caused inactivation on timescales that allowed for detection of
intermediates. Thus, the amount of O_2 used extended the time-frame of inactivation, and
allowed for a combined use of FTIR and UV-Vis spectroscopies to monitor the integrity
of both the 2Fe and [4Fe-4S] subclusters. Higher amounts of O_2 led to faster inactivation
times and more rapid loss of 2Fe IR signals (Figure S4), whereas [4Fe-4S] signals
persisted longer (Figures 2.5b and 2.5c). Similar experimental setups were performed to
allow the use of additional analytical techniques (biochemical assays, and UV-Vis

spectroscopies, mass spectrometry, and X-ray crystallography) to follow the fate of the 2Fe subcluster and [4Fe-4S] subcluster during the inactivation process.

FTIR analysis of CrHydA1 incubated in the presence of ~0.01% O_2 in the absence of exogenously added reducing agents exhibited attenuation of the H_{ox} state. The attenuation of the H_{ox} signal tracked nearly 1:1 with loss of enzyme hydrogen production activity and is strong evidence that the 2Fe subcluster of the H cluster is the initial site of O_2 inactivation. In addition to the loss of H_{ox} signal due to O_2, signals commonly associated with H_{ox}-CO state appeared. This observation suggests that O_2 degrades the 2Fe subcluster, liberating CO, and that the proportion of H cluster that transitions to the H_{ox}-CO state is a result of the free CO binding to remaining intact clusters. CO liberation and CO binding to intact enzyme in H_{ox} is also thought to occur during photoillumination of the [FeFe]-hydrogenases[34]. These observations are consistent with free CO being a potent inhibitor (K_i≈0.1 μM)[5] of [FeFe]-hydrogenases.

The changes that occur when CrHydA1 is exposed to O_2 appear to occur to a greater extent and at a higher rate when poised in the H_{ox} state. Enzyme poised in H_{ox}CO, H_{red}-H_2, and H_{red}-NaDT were less prone to O_2-dependent decay. CrHydA1 equilibrated under H_2 or NaDT reduced also showed limited degradation compared to H_{ox}, with a majority of 2Fe subcluster signal being maintained at 1.2% to 2% O_2 respectively after 2 h (NaDT data shown in Figure S2). The data suggests that an H cluster that is coordinately saturated with an occupied distal Fe ligand exchangeable site is more resistant to O_2 damage and provide strong support of this site as the initial site of O_2 binding and attack along the pathway of H cluster degradation[4-5, 11, 19-22].

The addition of CO had the greatest protective effect with no observable decay of H_{ox}-CO

up to 24.7% O_2 (Figure S1) over 2 h of exposure, consistent with previous

electrochemical observations[4-5, 11]. The H_2 and NaDT treated CrHydA1 exposed to O_2

initially transitions into H_{ox} prior to degradation indicated by the observed appearance of

the 1940 cm^{-1} feature. Subsequently, similar degradation products are observed in the

NaDT- and H_2-treated CrHydA1 samples as were observed with H_{ox} samples, with the

transient appearance of H_{ox}-CO specific FTIR features.

The O_2 inactivated CrHydA1 was capable of being reactivated by the addition of

HydF^{EG} suggesting that the inactivated enzyme has a damaged or absent 2Fe subcluster.

Further, as described above, both UV-Vis spectroscopy and structural characterization

indicated the presence of an intact [4Fe-4S] subcluster that was stable long after activity

attenuated. Interestingly, the X-ray crystal structure and UV-Vis of O_2 inactivated

CrHydA1 strongly resembled CrHydA1 expressed in the absence of maturases

(CrHydA1$^{\Delta EFG}$). Previous studies probing H cluster degradation using comparatively

higher concentrations of O_2 either with[23] or without[11] NaDT proposed that the

degradation of the [4Fe-4S] subcluster preceded 2Fe subcluster degradation, whereby

ROS was generated by O_2 binding and reaction at the 2Fe subcluster. Under the

conditions of our study in which CrHydA1 was exposed to O_2 in the absence of NaDT,

the [4Fe-4S] subcluster seems fairly resistant to degradation. We do however see

evidence for the oxidation of the non-coordinating active site Cys (Cys 169) perhaps

through the formation of ROS[41]. Exposure of either the O_2 degradation intermediate

observed here or CrHydA1$^{\Delta EFG}$ to high concentrations of O_2 resulted in the eventual

destruction of the [4Fe-4S] subcluster, as evidenced by reduction and eventual loss of the S→Fe charge transfer bands at ~420 nm.

Thus, based on the experimental evidence presented here, we propose that the mechanism of O_2 attack on CrHydA1 first involves degradation of the more labile 2Fe subcluster, followed by attack on the more robust [4Fe-4S] subcluster. The titration data suggests that the reaction sequence is independent of O_2 concentration, but occurs at a concentration dependent rate. High (>1%) O_2 levels led to fast 2Fe subcluster degradation and did not allow for the reliable detection of inactivation intermediates by our FTIR set-up.

Conclusion

The inactivation of [FeFe]-hydrogenase by O_2 is defined by steps that involve the diffusion of gases into close proximity of the catalytic site, followed by redox/chemical steps of O_2 reaction with the H cluster. Our results are consistent with theoretical models[19] and indicate that the latter process proceeds *via* oxidative breakdown of the 2Fe subcluster, initially releasing CO that can bind to secondary targets (e.g., other enzymes). Further exposure results in the eventual formation of a stable break-down product with an intact [4Fe-4S] subcluster and a vacant 2Fe subcluster site capable of being reactivated by 2Fe subcluster specific maturation machinery. Long-term and/or high concentration O_2 exposure is required for oxidative damage of the [4Fe-4S] subcluster and complete H cluster degradation as evidenced by the previous XAS/EXAFS studies.

Based on our results, [FeFe]-hydrogenase inactivation from O_2 exposure essentially

reverses the maturation pathway of H cluster insertion into immature CrHydA1, and

suggests that H clusters inactivated by low concentration O_2 exposure *in vitro* could be

substrates for reactivation by HydF[EG].

 AUTHOR INFORMATION
 Corresponding Authors
*paul.king@nrel.gov
*john.peters@chemistry.montana.edu
 Author Contributions
§
These authors contributed equally.
Notes
The authors declare no competing financial interest.

References

1.   Vignais, P. M.; Billoud, B., Occurrence, classification, and biological function of hydrogenases: an overview. *Chemical reviews* **2007,** *107* (10), 4206-72.

2.   Turner, J.; Sverdrup, G.; Mann, M. K.; Maness, P.-C.; Kroposki, B.; Ghirardi, M.; Evans, R. J.; Blake, D., Renewable hydrogen production. *International Journal of Energy Research* **2008,** *32* (5), 379-407.

3.   McKinlay, J. B.; Harwood, C. S., Photobiological production of hydrogen gas as a biofuel. *Current opinion in biotechnology* **2010,** *21* (3), 244-51.

4.   Baffert, C.; Demuez, M.; Cournac, L.; Burlat, B.; Guigliarelli, B.; Bertrand, P.; Girbal, L.; Leger, C., Hydrogen-activating enzymes: activity does not correlate with oxygen sensitivity. *Angewandte Chemie (International ed. in English)* **2008,** *47* (11), 2052-4.

5.   Goldet, G.; Brandmayr, C.; Stripp, S. T.; Happe, T.; Cavazza, C.; Fontecilla-Camps, J. C.; Armstrong, F. A., Electrochemical kinetic investigations of the reactions of [FeFe]-hydrogenases with carbon monoxide and oxygen: comparing the importance of gas tunnels and active-site electronic/redox effects. *J Am Chem Soc* **2009,** *131* (41), 14979-89.

6.   Silakov, A.; Wenk, B.; Reijerse, E.; Lubitz, W., (14)N HYSCORE investigation of the H-cluster of [FeFe] hydrogenase: evidence for a nitrogen in the dithiol bridge. *Physical chemistry chemical physics : PCCP* **2009,** *11* (31), 6592-9.

7.   Nicolet, Y.; Piras, C.; Legrand, P.; Hatchikian, C. E.; Fontecilla-Camps, J. C., Desulfovibrio desulfuricans iron hydrogenase: the structure shows unusual coordination to an active site Fe binuclear center. *Structure* **1999,** *7* (1), 13-23.

8.   Peters, J. W.; Lanzilotta, W. N.; Lemon, B. J.; Seefeldt, L. C., X-ray crystal structure of the Fe-only hydrogenase (CpI) from Clostridium pasteurianum to 1.8 angstrom resolution. *Science (New York, N.Y.)* **1998,** *282* (5395), 1853-8.

9.   Berggren, G.; Adamska, A.; Lambertz, C.; Simmons, T. R.; Esselborn, J.; Atta, M.; Gambarelli, S.; Mouesca, J. M.; Reijerse, E.; Lubitz, W.; Happe, T.; Artero, V.; Fontecave, M., Biomimetic assembly and activation of [FeFe]-hydrogenases. *Nature* **2013,** *499* (7456), 66-69.

10.   Pandey, A. S.; Harris, T. V.; Giles, L. J.; Peters, J. W.; Szilagyi, R. K., Dithiomethylether as a Ligand in the Hydrogenase H-Cluster. *Journal of the American Chemical Society* **2008,** *130* (13), 4533-4540.

11.   Stripp, S. T.; Goldet, G.; Brandmayr, C.; Sanganas, O.; Vincent, K. A.; Haumann, M.; Armstrong, F. A.; Happe, T., How oxygen attacks [FeFe] hydrogenases from photosynthetic organisms. *Proceedings of the National Academy of Sciences* **2009,** *106* (41), 17331-17336.

12.   Ghirardi, M. L.; Cohen, J.; King, P.; Schulten, K.; Kim, K.; Seibert, M. In *[FeFe]-hydrogenases and photobiological hydrogen production*, 2006; pp 63400X-63400X-6.

13.   Cohen, J.; Kim, K.; King, P.; Seibert, M.; Schulten, K., Finding gas diffusion pathways in proteins: application to O2 and H2 transport in CpI [FeFe]-hydrogenase and the role of packing defects. *Structure* **2005,** *13* (9), 1321-9.

14.   King, P. W.; Svedruzic, D.; Cohen, J.; Schulten, K.; Seibert, M.; Ghirardi, M. L. In *Structural and functional investigations of biological catalysts for optimization of solar-driven H2 production systems*, 2006; pp 63400Y-63400Y-9.

15.   Lautier, T.; Ezanno, P.; Baffert, C.; Fourmond, V.; Cournac, L.; Fontecilla-Camps, J. C.; Soucaille, P.; Bertrand, P.; Meynial-Salles, I.; Leger, C., The quest for a functional substrate access tunnel in FeFe hydrogenase. *Faraday discussions* **2011,** *148*, 385-407; discussion 421-41.

16.   Bingham, A. S.; Smith, P. R.; Swartz, J. R., Evolution of an [FeFe] hydrogenase with decreased oxygen sensitivity. *International Journal of Hydrogen Energy* **2012,** *37* (3), 2965-2976.

17.   Bruska, M. K.; Stiebritz, M. T.; Reiher, M., Regioselectivity of H cluster oxidation. *J Am Chem Soc* **2011,** *133* (50), 20588-603.

18.   Stiebritz, M. T.; Finkelmann, A. R.; Reiher, M., Oxygen Coordination to the Active Site of Hmd in Relation to [FeFe] Hydrogenase. *European Journal of Inorganic Chemistry* **2011,** *2011* (7), 1163-1171.

19.   Stiebritz, M. T.; Reiher, M., Hydrogenases and oxygen. *Chemical Science* **2012,** *3* (6), 1739-1751.

20.   Kubas, A.; De Sancho, D.; Best, R. B.; Blumberger, J., Aerobic damage to [FeFe]-hydrogenases: activation barriers for the chemical attachment of O2. *Angewandte Chemie (International ed. in English)* **2014,** *53* (16), 4081-4.

21.   Fourmond, V.; Greco, C.; Sybirna, K.; Baffert, C.; Wang, P.-H.; Ezanno, P.; Montefiori, M.; Bruschi, M.; Meynial-Salles, I.; Soucaille, P.; Blumberger, J.; Bottin, H.; De Gioia, L.; Léger, C., The oxidative inactivation of FeFe hydrogenase reveals the flexibility of the H-cluster. *Nat Chem* **2014,** *6* (4), 336-342.

22.   Liebgott, P.-P.; Leroux, F.; Burlat, B.; Dementin, S.; Baffert, C.; Lautier, T.; Fourmond, V.; Ceccaldi, P.; Cavazza, C.; Meynial-Salles, I.; Soucaille, P.; Fontecilla-Camps, J. C.; Guigliarelli, B.; Bertrand, P.; Rousset, M.; Léger, C., Relating diffusion along the substrate tunnel and oxygen sensitivity in hydrogenase. *Nat Chem Biol* **2010,** *6* (1), 63-70.

23.   Lambertz, C.; Leidel, N.; Havelius, K. G. V.; Noth, J.; Chernev, P.; Winkler, M.; Happe, T.; Haumann, M., O(2) Reactions at the Six-iron Active Site (H-cluster) in [FeFe]-Hydrogenase. *The Journal of biological chemistry* **2011,** *286* (47), 40614-40623.

24.   Kowal, A. T.; Adams, M. W.; Johnson, M. K., Electron paramagnetic resonance studies of the low temperature photolytic behavior of oxidized hydrogenase I from Clostridium pasteurianum. *The Journal of biological chemistry* **1989,** *264* (8), 4342-8.

25.   Albracht, S. P.; Roseboom, W.; Hatchikian, E. C., The active site of the [FeFe]-hydrogenase from Desulfovibrio desulfuricans. I. Light sensitivity and magnetic hyperfine interactions as observed by electron paramagnetic resonance. *Journal of biological inorganic chemistry : JBIC : a publication of the Society of Biological Inorganic Chemistry* **2006,** *11* (1), 88-101.

26.   Roseboom, W.; De Lacey, A. L.; Fernandez, V. M.; Hatchikian, E. C.; Albracht, S. P., The active site of the [FeFe]-hydrogenase from Desulfovibrio desulfuricans. II. Redox properties, light sensitivity and CO-ligand exchange as observed by infrared spectroscopy. *Journal of biological inorganic chemistry : JBIC : a publication of the Society of Biological Inorganic Chemistry* **2006,** *11* (1), 102-18.

27.   King, P. W.; Posewitz, M. C.; Ghirardi, M. L.; Seibert, M., Functional Studies of [FeFe] Hydrogenase Maturation in an Escherichia coli Biosynthetic System. *Journal of bacteriology* **2006,** *188* (6), 2163-2172.

28.   Yacoby, I.; Tegler, L. T.; Pochekailov, S.; Zhang, S.; King, P. W., Optimized Expression and Purification for High-Activity Preparations of Algal [FeFe]-Hydrogenase. *PLoS ONE* **2012,** *7* (4), e35886.

29.   McGlynn, S. E.; Shepard, E. M.; Winslow, M. A.; Naumov, A. V.; Duschene, K. S.; Posewitz, M. C.; Broderick, W. E.; Broderick, J. B.; Peters, J. W., HydF as a scaffold protein in [FeFe] hydrogenase H-cluster biosynthesis. *FEBS Letters* **2008,** *582* (15), 2183-2187.

30.   Mulder, D. W.; Ratzloff, M. W.; Shepard, E. M.; Byer, A. S.; Noone, S. M.; Peters, J. W.; Broderick, J. B.; King, P. W., EPR and FTIR analysis of the mechanism of H2 activation by [FeFe]-hydrogenase HydA1 from Chlamydomonas reinhardtii. *J Am Chem Soc* **2013,** *135* (18), 6921-9.

31.   Kabsch, W., XDS. *Acta crystallographica. Section D, Biological crystallography* **2010,** *66* (Pt 2), 125-32.

32.   Evans, P., Scaling and assessment of data quality. *Acta crystallographica. Section D, Biological crystallography* **2006,** *62* (Pt 1), 72-82.

33.   Vagin, A. a. T., A, MOLREP: an automated program for Molecular Replacement. *Journal of Applied Crystallography* **1997,** *30* (6), 1022-1025.

34.   Pierik, A. J.; Hulstein, M.; Hagen, W. R.; Albracht, S. P., A low-spin iron with CN and CO as intrinsic ligands forms the core of the active site in [Fe]-hydrogenases. *European journal of biochemistry / FEBS* **1998,** *258* (2), 572-8.

35.   Chen, Z.; Lemon, B. J.; Huang, S.; Swartz, D. J.; Peters, J. W.; Bagley, K. A., Infrared studies of the CO-inhibited form of the Fe-only hydrogenase from Clostridium pasteurianum I: examination of its light sensitivity at cryogenic temperatures. *Biochemistry* **2002,** *41* (6), 2036-43.

36.   Bennett, B.; Lemon, B. J.; Peters, J. W., Reversible carbon monoxide binding and inhibition at the active site of the Fe-only hydrogenase. *Biochemistry* **2000,** *39* (25), 7455-60.

37.   Adamska, A.; Silakov, A.; Lambertz, C.; Rudiger, O.; Happe, T.; Reijerse, E.; Lubitz, W., Identification and characterization of the "super-reduced" state of the H-cluster in [FeFe] hydrogenase: a new building block for the catalytic cycle? *Angewandte Chemie (International ed. in English)* **2012,** *51* (46), 11458-62.

38.   Silakov, A.; Kamp, C.; Reijerse, E.; Happe, T.; Lubitz, W., Spectroelectrochemical characterization of the active site of the [FeFe] hydrogenase HydA1 from Chlamydomonas reinhardtii. *Biochemistry* **2009,** *48* (33), 7780-6.

39.   Nicolet, Y.; Rohac, R.; Martin, L.; Fontecilla-Camps, J. C., X-ray snapshots of possible intermediates in the time course of synthesis and degradation of protein-bound

Fe4S4 clusters. *Proceedings of the National Academy of Sciences* **2013,** *110* (18), 7188-7192.

40.   Cornish, A. J.; Gartner, K.; Yang, H.; Peters, J. W.; Hegg, E. L., Mechanism of proton transfer in [FeFe]-hydrogenase from Clostridium pasteurianum. *The Journal of biological chemistry* **2011,** *286* (44), 38341-7.

41.   Kettenhofen, N. J.; Wood, M. J., Formation, reactivity, and detection of protein sulfenic acids. *Chemical research in toxicology* **2010,** *23* (11), 1633-46.

42.   Mulder, D. W.; Ortillo, D. O.; Gardenghi, D. J.; Naumov, A. V.; Ruebush, S. S.; Szilagyi, R. K.; Huynh, B.; Broderick, J. B.; Peters, J. W., Activation of HydA(DeltaEFG) requires a preformed [4Fe-4S] cluster. *Biochemistry* **2009,** *48* (26), 6240-8.

CHAPTER 3

THE PHYSIOLOGICAL FUNCTIONS AND STRUCTURAL DETERMINANTS OF CATALYTIC BIAS IN THE [FEFE]-HYDROGENASES OF *CLOSTRIDIUM PASTEURIANUM* STRAIN W5

Contribution of Authors and Co-Authors

Manuscript(s) in Chapter(s) 2, 3, 5, 6, Appendix D

Author: Jesse B. Therien

Contributions: Sequencing and qRT-PCR experiments

Co-Author: Jacob H. Artz

Contributions: Data interpretation, Bioinformatics

Co-Author: Saroj Poudel

Contributions: Bioinformatics

Co-Author: Trinity L. Hamilton

Contributions: qRT-PCR design and interpretation

Co-Author: Zhengfeng Liu

Contributions: sequencing

Co-Author: Seth M. Noone

Contributions: Sequencing

Co-Author: Michael W. W. Adams

Contributions: Interpretation of data

Contribution of Authors and Co-Authors (Continued)

Co-Author: Paul W. King

Contributions: Interpretation of data

Co-Author: Donald A. Bryant

Contributions: Sequencing

Co-Author: Eric S. Boyd

Contributions: Design of bioinformatics studies

Co-Author: John W. Peters

Contributions: Experimental design and interpretation

64

Jesse B. Therien, Jacob H. Artz, Saroj Poudel, Trinity L. Hamilton, Zhenfeng Liu, Seth M. Noone, Michael W. W. Adams, Paul W. King, Donald A. Bryant, Eric S. Boyd, John W. Peters

Jesse B. Therien[1], Jacob H. Artz[1], Saroj Poudel[2], Trinity L. Hamilton[1*], Zhenfeng Liu[3, †], Seth M. Noone[4], Michael W. W. Adams[5], Paul W. King[6], Donald A. Bryant[1, 3], Eric S. Boyd[2], John W. Peters[1#]

Department of Chemistry and Biochemistry, Montana State University, Bozeman, Montana[1]; Department of Microbiology and Immunology, Montana State University, Bozeman, Montana[2]; Department of Biochemistry and Molecular Biology, The Pennsylvania State University, University Park, Pennsylvania[3]; National Renewable Energy Laboratory, Biosciences Center, Golden, Colorado[4]; Department of Biochemistry & Molecular Biology, University of Georgia, Athens, Georgia[5].

Running Title: Insights into hydrogen metabolism in *C. pasteurianum*

#Corresponding Author: John W. Peters, *Department of Chemistry and Biochemistry, Montana State University, Bozeman, MT 59717, USA*
john.peters@chemistry.montana.edu

Present address: Department of Biological Sciences, University of Cincinnati, Cincinnati, Ohio, USA*

[†]**Present address**: Dornsife College of Letters, Arts, and Sciences, University of Southern California, AHF 232, Los Angeles, CA 90089

Jesse Therien <jessetherien@gmail.com>,
Jacob Artz <jacob.artz@msu.montana.edu>,
Saroj Poudel <saroz189@gmail.com>,
Trinity Hamilton <trinity.hamilton@uc.edu>,
Zhenfeng Liu < zhenfenl@usc.edu>,
Noone, Seth <Seth.Noone@nrel.gov>,
Mike Adams <adams@bmb.uga.edu>
King, Paul <paul.king@nrel.gov>,
Donald A. Bryant" <dab14@psu.edu>,
Eric Boyd <eboyd@montana.edu>,
John Peters <john.peters@chemistry.montana.edu>,

Abstract

Background

The first generation of biochemical studies of complex, iron-sulfur-cluster-containing [FeFe]-hydrogenases and Mo-nitrogenase were carried out on enzymes purified from *Clostridium pasteurianum* (strain W5). These studies suggested that two distinct [FeFe]-hydrogenases are expressed differentially under nitrogen-fixing and non-nitrogen-fixing conditions. As a result, the first characterized [FeFe]-hydrogenase (CpI) is presumed to have a primary role in central metabolism, recycling reduced electron carriers that accumulate during fermentation via proton reduction. A role for capturing reducing equivalents released as hydrogen during nitrogen fixation has been proposed for the second hydrogenase, CpII. Biochemical characterization of CpI and CpII indicated CpI has extremely high hydrogen production activity in comparison to CpII, while CpII has elevated hydrogen oxidation activity in comparison to CpI when assayed under the same conditions. This suggests that these enzymes have evolved a catalytic bias to support their respective physiological functions.

Results

We identified four hydrogenases: three [FeFe]-hydrogenases, one of which had not previously been known, and one [NiFe]-hydrogenase in the published genome of C. pasteurianum (strain W5). Quantitative real-time PCR experiments show markedly reduced levels of CpI gene expression together with concomitant increases in CpII gene expression under nitrogen-fixing conditions. Structure-based analyses of the CpI and CpII

sequences reveals variations in their catalytic sites that may contribute to their alternative physiological roles.

Conclusions

This work demonstrates that the physiological roles of CpI and CpII are to evolve and to consume hydrogen, respectively, in concurrence with their catalytic activities in vitro, with CpII capturing excess reducing equivalents under nitrogen fixation conditions. Comparison of the primary sequences of CpI and CpII and their homologs provides an initial basis for identifying key structural determinants that modulate hydrogen production and hydrogen oxidation activities.

Background

The genus Clostridium includes a diverse group of Gram-positive, spore-forming anaerobes [1]. In general, clostridia gain their energy from the conversion of hexose sugars to butyrate, acetate, and CO_2. During this process reduced electron carriers in the form of ferredoxin accumulate and must be recycled for sustained fermentative energy metabolism. C. pasteurianum recycles reduced ferredoxin by coupling electrons and protons to form hydrogen (H_2) through the activity of a hydrogenase.

Clostridium pasteurianum strain W5 was the first free-living, nitrogen-fixing organism to be isolated [2]. For over 100 years, it has been a model for studying the biochemistry of nitrogen fixation and H_2 metabolism. The first generation of biochemical studies of complex iron-sulfur clusters involved in catalysis by an [FeFe]-hydrogenase and by Mo-nitrogenase were carried out with enzymes purified from C. pasteurianum strain W5 [3]. Indeed, ferredoxin was first discovered in C. pasteurianum strain W5 [4], and the first preparations of a soluble hydrogenase were also obtained from this organism [5]. Subsequently, the presence of a second [FeFe]-hydrogenase (CpII) was revealed [6], and its physical and catalytic properties were studied along with those of CpI [7]. CpI was proposed to evolve H_2 to recycle electron carriers during fermentative growth in the presence of fixed nitrogen [7]. CpII was proposed to function under nitrogen-fixing conditions to capture reducing equivalents in the form of H_2 which is an obligate byproduct of nitrogenase-catalyzed reduction of nitrogen to ammonia. This is consistent with the observations that CpII accumulates at a higher cellular concentration during diazotrophic

growth [6]. Comparison of the rates of H_2 evolution and oxidation revealed that CpI produces H_2 550-times faster than CpII (5,500 vs. 10 μmol of H_2/min·mg respectively) while it oxidizes H_2 about 30% slower than CpII (24,000 vs. 34,000 μmol of H_2/min·mg respectively) [8]. Typically, [FeFe]-hydrogenases have characteristically high catalytic rates for H_2 production [8]. Therefore, the two [FeFe]-hydrogenases exhibit a strong "catalytic bias," which is manifested most profoundly as the adaptation of CpII toward H_2 oxidation.

In this work we have revisited the hypotheses that under non-nitrogen fixing conditions CpI functions to reduce protons during the recycling of electron carriers during fermentation, while CpII functions in H_2 oxidation under diazotrophic conditions. The genome of C. pasteurianum ATCC 6013 (strain W5) [9] was subjected to homology searches using known hydrogenase sequences as queries to determine the complement of encoded hydrogenases, their sequences and their gene context. Using these data, we analyzed the transcript abundance of each hydrogenase under nitrogen-fixing and nitrogen-replete culture conditions to assign physiological roles for CpI and CpII. Furthermore, detailed primary amino acid structural-based comparison together with phylogenetic analysis provide insights into the determinants of the profound catalytic bias observed for these two related enzymes.

RESULTS AND DISCUSSION

Genome. The sequencing of the C. pasteurianum strain W5 (CpW5) genome was carried out independently of the recently published complete genome [9]. Our analysis resulted in a draft genome consisting of 14 contigs and 4.2 Mbp that shares 99.97% average nucleotide identity with the published genome (Supplemental Figure 1). The published complete genome contains 4.3 Mbp, which suggests that our genome is nearly complete. In particular, the sequences of the genes encoding all four hydrogenases discussed in the present study are identical to those in the complete genome [9]. Like the genomes of other clostridial species [10-12], the %GC content of CpW5 was low at 30.0%. C. pasteurianum NRRL B-598, which is an oxygen-tolerant species, is also related to CpW5 and has a genome size that is ~50% larger, comprising 6.1 Mbp [13]. According to SEED Viewer [14], which does not include sequences from these C. pasteurianum genomes (i.e. ATCC 6013 DSM 525 and NRRL B-598), the closest neighbors with completed genomes are Clostridium acetobutylicum (3.94 Mbp) [15], Clostridium botulinum (3.89 Mbp) [16], Clostridium novyi NT (2.55 Mbp) [17], and Clostridium sporogenes ATCC 15579 (4.09 Mbp) [18].

Hydrogenases. The genome of CpW5 encodes the two characterized [FeFe]-hydrogenases, CpI and CpII, and an additional homolog designated CpIII, as well as one (previously annotated) [NiFe]-hydrogenase [19], together with all of the necessary genes for hydrogenase maturation. These sequence data therefore allow us to carry out the first

comparative analysis of the primary sequence of CpII since it was biochemically characterized more than two decades ago [7].

The sequences of CpI and CpII are 33% identical, with a 45% identity and 61% similarity over the conserved region (Fig. 1), which suggests that these two enzymes have generally conserved protein architectures. A homology model of CpII (Fig. 2) based on the solved crystal structure of CpI [20] and generated using SwissModel [21], as well as amino acid sequence alignment, indicate the absence of accessory domains in CpII that are present in CpI. The CpI sequence contains conserved cysteine residues for each cluster that sequentially bind clusters [2Fe-2S] (FS2), the distal [4Fe-4S] cluster (FS4C), the medial [4Fe-4S] cluster (FS4B) and the proximal [4Fe-4S] cluster (FS4A). In contrast, the N-terminus of CpII lacks the cysteine residues responsible for binding accessory clusters FS2 and FS4C (Fig. 2). However, conserved regions binding the two Fe atoms of the catalytic site, known as the H-cluster, and two [4Fe4S] accessory clusters were identified in CpII. CpIII, which has thus far not been biochemically characterized, has a unique N-terminal arrangement of cysteines. Sequence alignment reveals that the FS4A binding motif is conserved, while the FS4B motif lacks two of the four cysteine residues that typically ligate this cluster (Fig. 1).

```
          10        20        30        40        50        60        70        80
....|....|....|....|....|....|....|....|....|....|....|....|....|....|....|....|
MKTIIINGVQFNTDEDTTILKFARDNNIDISALCFLNNCNNDINKEICTVEVEGTGLVTACDTLIEDGMIINTNSDAVN
MKTIILNGNEVHTDKDITILELARENNVDIPTLCFLKDCGN-FGKGGVCMVEVEGKGFRAACVAKVEDGMVINTESDEVK
-------------------------------------------------------------------------MN-------
------------------MKSEYNDLFKSLIDAYYKDDFDEFIKKALSDSTVNKEELSNIISSFCGVELKYT-------
------------------MNNKYIELFKSLVDSYYNDTFDSFVYHILSDEEVDKKELSKVISSLCGVSVEFK-------
                                  2             2    2             2

          90       100       110       120       130       140       150       160
....|....|....|....|....|....|....|....|....|....|....|....|....|....|....|....|
EKIKSRISQLLDIHEFICGCNRRENCEFLKLVITKYKARASKPFLPKDKTEYVDERSKSLTVDRTICLICGRCVNACGKN
ERIKKRVSMLLDRHEFICGCSRRENCEFLKLVIKTKAKASKPFLPEDKDALVDNRSKAIVIDRSHCVICGRCVAACKQH
-----------SKHKFT--------------DIR---------VPIE------KDNPSIMRHEELCVRCKVCKVCTEE
----------DKDTYIKD---------LKNAIKN------YNSDHK---IVTKIRDCSVDCADENGKTSCQKSCPFD
----------DTETYISE---------LKKAISN------YKCTDN---IVEKIKECDSSCHSNEGETPCQKSCPFD
           C    C    C       C                               B    B  B  A

         170       180       190       200       210       220       230       240
....|....|....|....|....|....|....|....|....|....|....|....|....|....|....|....|
TETYAMKFLNKNGKTIIGAEDEKCFDDTNCLLCGQCIIACFVAALSEK-SHMDRVKNALNAPEKHVIVAMAPSVRASIGE
TSTCSIQFIKKDGQRAVGTVDDVCLDDSTCLLCGQCVIACFVAALEK-SHIEKVQEALNDPKKHVIVAMAPSVRTAMGE
ISVYGHYDLEKTGDKAI------------CIYCGQCANVCEVYSITEV-SDVQQVKDAINDPDKIVIFQTSPSVRVSLGE
AILIDEANKTSYIDKDL-----------CTDCGFCVEGCPNGSILDKVEFIPLAN--LLKEKQPVIAAVAPAITGQFGD
AILVDKNTKTSHIQKDL-----------CTDCGMCITSCESGSILDKIEFMPLLN--LFKNNETVIAAVAPAIAGQFGE
                             A  A A   B                               *

         250       260       270       280       290       300       310       320
....|....|....|....|....|....|....|....|....|....|....|....|....|....|....|....|
LFNMGFGVDVTGKIYTALRQLGFDKIFDINFGADMTIMEEATELVQRIENN-GPFPMFTSCCPGWVRQAENYYPELLNNL
LFKMGYGKDVTGKLYTALRMLGFDKVFDINFGADMTIMEEATELLGRVKNN-GPFPMFTSCCPAWVRLAQNYHPELLDNL
AFGMEPGTYVEDKMAAVLKNLGADYVFDTTFGADLTITEEASELVQRITSGNGTLPQFTSCCPAWVEFVEIYYPELINNL
DVTIDQ-------LRTAFKKVGFADMIEVAFFADMLTLKEACFNAHVKSK-DDLMITSCCPMWVGMLKRVYKDMVKYV
NVSLEM-------LRTAFKKVGFADMVEVAFFADMLTIKEAPFNELVNSK-DDLMITSCCPMWVSMIRKIYKDLARHV
               *                               H

         330       340       350       360       370       380       390       400
....|....|....|....|....|....|....|....|....|....|....|....|....|....|....|....|
SSAKSPQQIFGTASKTYYPSISGLDPKNVFTVTVMPCTSKKFEADRPQMEKD-------GLRDIDAVITTRELAKMIKDA
SSAKSPQQIFGTASKTYYPSISGIAPEDVYTVTIMPCNDKKYEADIPFMETN-------SLRDIDASLTTRELAKMIKDA
SSSKSPILMQGPTIKTYFAKKAAIDPKKIVNVAVTPCTAKKYEITRAEKNDAGKYYNDENIRDMDYVITVRELSNWIKED
SPSVSBMIAAGRVIKTLNS--------NCKVVFVGPCIAKKAESKNKDIEGD-----------IDFVLTFEEVKNIFESL
SPSVSBMIASGRVIKKLNP--------NCKVVFIGPCIAKKAESRSQDISDA-----------IDFVLTFEELKGIFDVL
                                 *H

         410       420       430       440       450       460       470       480
....|....|....|....|....|....|....|....|....|....|....|....|....|....|....|....|
KTIPFAKLEDSEADPAMGEYSGACAIFGATGGVMEAALRSAKDFAENAELED--IEYKQVRGLNGIKEAEVEINNNKYN-V
KTIKFADLEDGEVDPAMGTYSGACAIFGATGGVMEAAIRSAKDFAENKELEN--VDYTEVRGPFKGIKEAEVEIAGNKLN-V
KIEFKALQGAEFDSLLSRGSGGGIIFGITGGVMESAIRTAYYYITKKNPPKDLYNLEAVGNMDGIREAQVTIGDYTIN-I
NINPSELPE--DPSTDYASREGRLYARTGGVSISVSEAVAKLFPEK-------------------KDLFKS
DIDPEKLPE---THTKSYASREGRLYGRTGGVSTSVDEAVKRIFPNK-------------------HHLFKS

         490       500       510       520       530       540       550       560
....|....|....|....|....|....|....|....|....|....|....|....|....|....|....|....|
AVINGASNLFKFMKSGMINEKQYHFIEVMACHGGCVNGGGQPHVNPKDLEKVDIKKVRASVLYNQDE-HLSKRKSHENTA
AVINGASNFFEFMKSGKMNEKQYHFIEVMACPGGCINGGGQPHVNALDRENVDYRKLRASVLYNQDKNVLSKRKSHDNPA
AIVHGTANARKLIEKVKSGEKKYDFVEVMTCRGGCIGGGGQPKVKIPMADKVR--QKRIAGLYNKDQ-SVTQRLAHENPD
VQANGVIECKKILEKAQNGEVAANFIEGMGCVGGCVGGVGGPKALIPKEKGREKVNEFAENSNVKISLES-------DQMKKI
TKVDGVKDCKDILNKTQAGNIGANFLEGMGCVGGCVGGVGGPKAIVHKDQGRESVNKTAESSEIKISVDS-------ERMKDI
                              H    H

         570       580       590
....|....|....|....|....|....|
LVKMYQNYFGKPGEGRAHEILHFKYKK--------  Cpl
IIKMYDSYFGKPGEGLAHKLLHVKYTKDKNVSKHE  Cal
ITKVYDEFFKKPLSPLAEELLHTVYSSKKHILGE-  CpII
LNMLNITSAKDFMDEEKIKIFEREF----------  CpIII
LSRIGINSIEDFGDKSKVDIFERRF----------  CaIII
```

Figure 3.1 (legend on following page)

Figure 3.1. Protein sequence alignment of the [FeFe]-hydrogenases of C. pasteurianum W5 and C. acetobutylicum. Residues ligating FeS clusters are indicated with A, B, C, or 2 to denote the cluster they ligate; H – the H-cluster, A – proximal cluster (FS4A), B – FS4B, C – FS4C, and 2 – FS2. Key residues within a 5 angstrom radius of the H-cluster are denoted with a star. These residues are conserved among representatives of phylogenetically clustering members of groups containing CpI/CaI, CpII and CpIII/CaIII.

The [FeFe]-hydrogenase sequences encoded in the CpW5 genome contain the evolutionarily conserved H-cluster motifs; ^{299}**CCP**x, ^{354}**PC**xx**K**, and ^{495}ExMx**C**xx**GC**xxG (numbered according to CpI) (Fig. 1) [22]. These motifs include all of the H-cluster binding cysteines, (H in figure 1). Phylogenetic clustering of the H-cluster domains of clostridial [FeFe]-hydrogenases has shown a variety of distinct clusters, designated A1-A5, A7, A8, and B1-B3 [23]. Group A2, which includes CpI, is comprised of soluble, H_2-producing enzymes. CpII, which lacks the [2Fe-2S] cluster as well as one of the [4Fe-4S] clusters, is classified as an A3 hydrogenase. Members of group B2, that includes CpIII, have an average size of 450 amino acids and an additional characteristic cysteine residue in the P1 motif (TS**C**CCPxW) of the H-cluster [24]. No hydrogenases of this type have been biochemically characterized to date, and it is unclear if these sequences produce active hydrogenases. The overall subunit architecture of the hydrogenase places CpI as a M3 hydrogenase, comprising an H-cluster, three [4Fe-4S] clusters, and an additional [2Fe-2S] cluster [25].

The [NiFe]-hydrogenase gene cluster of CpW5 contains the required accessory genes (hypABCEFD and hoxN) downstream of the structural genes, hyaAB, which encode the

large and small subunits, respectively. The predicted protein sequence of the large subunit contains previously described [26] L1 and L2 motifs characteristic of membrane-bound, uptake hydrogenases. The L1 and L2 motifs encompass the highly conserved cysteine pairs (CxxC) near each terminus that ligate the NiFe center. Unlike [FeFe]-hydrogenases, maturases for the [NiFe]-hydrogenase are often found in a single gene cluster with the structural genes [27], as is the case for the CpW5 genome. This gene cluster is not co-localized with any other hydrogenase or nitrogenase genes. The gene for the hydrogenase large subunit (hyaB) clusters phylogenetically with other clostridia in group 1 [24] (data not shown), which comprises membrane-associated uptake hydrogenases [26].
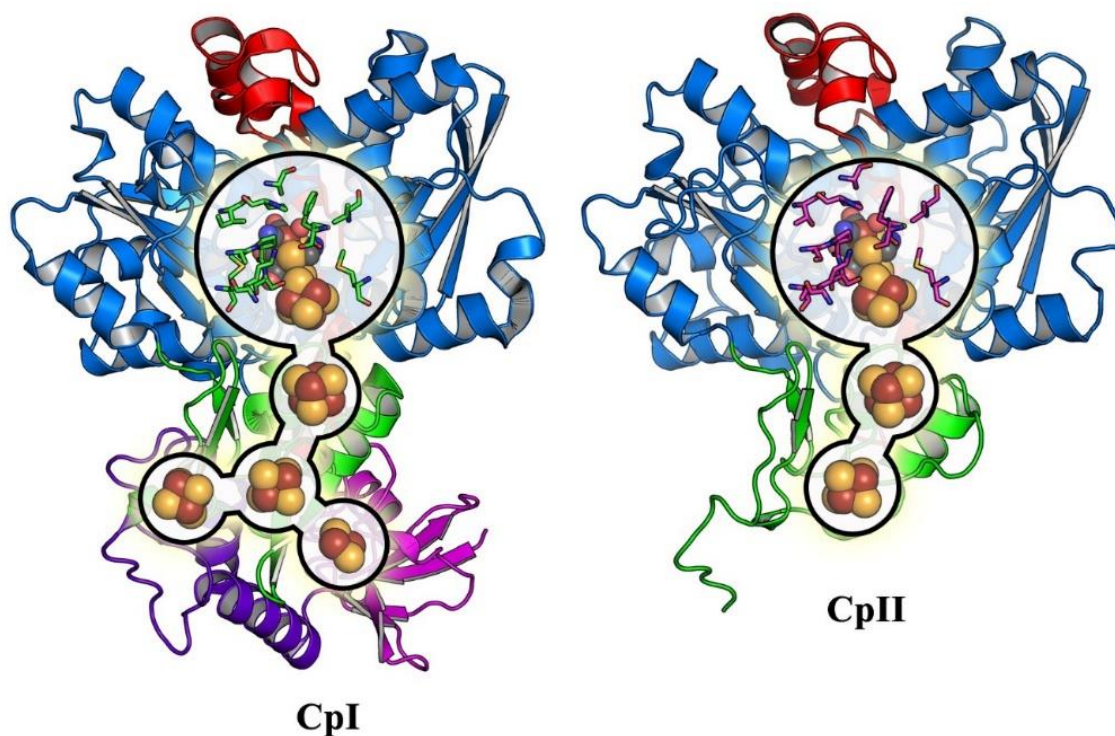
Figure 3.2. Comparison of overall protein structure of CpI and the CpII homology model

Transcriptional and physiological analyses. Quantitative real-time PCR assays were

performed to compare the transcript abundance of each CpW5 hydrogenase under both

non-nitrogen-fixing and nitrogen-fixing conditions.
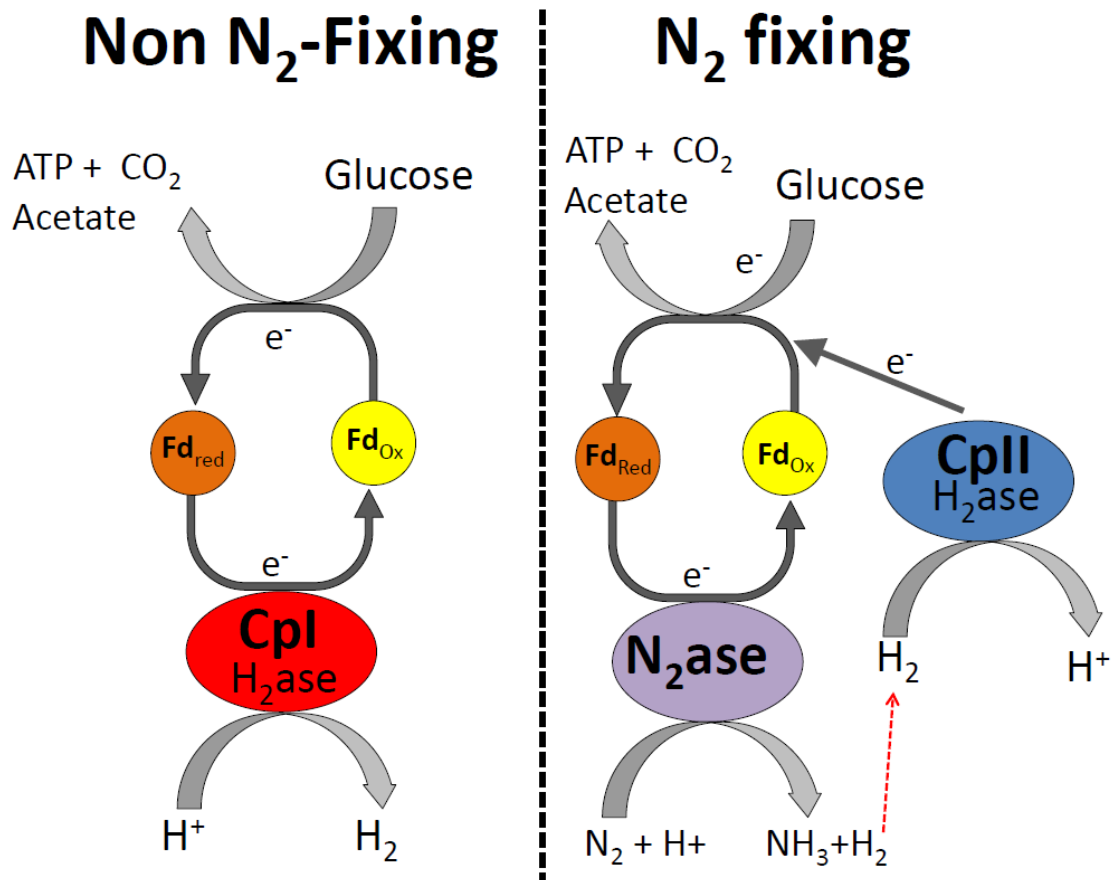
Figure 3.3. Proposed metabolic functions of CpI and CpII in C. pasteurianum. CpI acts as an electron sink under standard fermentative conditions, while CpII acts to recycle reducing equivalents in H_2 during nitrogen fixation. It should be noted that the [NiFe]-hydrogenase may also function alongside CpII to recycle reducing equivalents, although this hydrogenase probably makes a smaller contribution than CpII to H_2 oxidation.

Transcript levels for CpI decreased under nitrogen-fixing conditions (2.9-fold change)

while CpII transcripts increased (7.5-fold change). The transcript levels of CpIII and the

[NiFe]-hydrogenase were low with and without fixed nitrogen, with relative transcript

abundances approximately 100-fold lower than those for CpI or CpII, as based on the amplification threshold for each gene. CpIII transcript levels decreased slightly under diazotrophic conditions (2.0-fold change), while [NiFe]-hydrogenase transcripts underwent an 8.7-fold increase. Despite this increase in transcript abundance for the [NiFe]-hydrogenase, the relative transcript abundance of the [NiFe]-hydrogenase was approximately 10-fold lower than the CpII transcript abundance under nitrogen-fixing conditions. Thus, low levels of [NiFe]-hydrogenase transcripts are present under both nitrogen replete and nitrogen-fixing conditions.

Collectively, the abundance of hydrogenase transcripts agrees with previously established protein expression conditions and supports a rational model of hydrogenase usage by CpW5: CpI, which is known to be abundantly expressed under standard, non-nitrogen-fixing fermentative conditions [28], functions to dispose of excess reducing equivalents as H_2, whereas under diazotrophic conditions, dinitrogen reduction by Mo-nitrogenase consumes a large amount of electrons and therefore subverts the need for an electron-consuming, proton-reducing enzyme.

In contrast, CpII has an exceptionally low H_2 production activity [29] and thus it is unlikely that it is capable of removing excess reducing equivalents. Rather, its high H_2 oxidation activity and almost negligible proton reduction capacity is consistent with this hydrogenase functioning in the uptake direction. This H_2 oxidation is of particular importance for recycling electrons from the nitrogenase-produced H_2 and feeding those electrons back into

the reductant-consuming, nitrogen-fixing metabolism. In this model, CpII thereby acts to recycle reducing equivalents, mitigating loss of electrons from H_2 produced by nitrogenase (Fig. 3). The [NiFe]-hydrogenase has a similar transcriptional profile to CpII, which is up-regulated under nitrogen-fixing conditions. This suggests that it may also have a role in recapturing reducing equivalents, as has been previously demonstrated for [NiFe]-hydrogenases in aerobic, nitrogen-fixing organisms [30-33], but our data suggest a much lower abundance of [NiFe]-hydrogenase transcripts compared to CpII transcripts. The qRT-PCR data are consistent with previous observations that CpII is expressed primarily under nitrogen-fixing conditions and that CpI and CpII account for the majority of the total hydrogenase activity observed during protein purification [6, 29].

The different catalytic rates and metabolic functions of CpI and CpII provide a unique system for the study of catalytic bias. The specific catalytic abilities of these hydrogenases function to enhance one direction of the reaction while minimizing the other; they demonstrate the complex interplay between the metabolic niche of a protein and the structural fine-tuning it must possess in order to perform a particular function. There is a large selective advantage to having an enzyme with very low rates of proton reduction, such as CpII, because such enzymes are likely to be operating near equilibrium under nitrogen-fixing conditions, and the slow rates of proton reduction would reduce the loss of precious reducing equivalents.

Of more than 40 fully sequenced genomes of Clostridium species, all but two (C. kluyveri and C. butyricum) encode nitrogenase and a [NiFe]-hydrogenase. The two exceptions have genes encoding three or more [FeFe]-hydrogenases, suggesting that one or more of the [FeFe]-hydrogenases serves to consume H_2 and thereby supplants the need for a [NiFe]-hydrogenase during nitrogen fixation.

Structural basis for catalytic bias in [FeFe]-hydrogenases.

CpI and CpII display substantial differences in the ability to reduce protons and oxidize H_2, and we hypothesize that these differences are due to structural differences and thus to their amino acid sequences. Comparison of activities among hydrogenases does not reveal a trend in H_2 oxidation to production ratios based on the differing FeS cluster binding motifs [34]. It is currently unclear to what extent the presence of additional clusters contributes to differences in catalytic biases amongst these hydrogenases. Most likely, a suite of structural features is responsible for tuning the directionality of a given hydrogenase. The particular amino acids involved in gas channel lining [35], proton transfer [36], electron transfer, and H-cluster ligand environment [37] may all play a role.

Although the motifs coordinating H-clusters are conserved across [FeFe]-hydrogenases, amino acids in the second coordination sphere are not conserved. For example, three residues near the 2Fe subcluster, A230, I268, and M353 in CpI, are S99, T137, and T223 in CpII (Fig. 4). These differences highlight how variation in the second coordination sphere may play a role in modulating catalytic bias. Previous work by Knorzer et al. [37]

showed that Thr (T137 in CpII) is the most frequent substitution for a Met (residue 353 in CpI) that is adjacent to the μ-CO of the 2Fe subcluster, in 409 CpI homologs. These authors used site-directed substitution to change M353 to L353 in CpI and observed a significant decrease in H_2 production (to 15% of wild type (WT) enzyme) and a small decrease in H_2 oxidation (to 74% of WT), which they attributed to a lower turnover rate [37]. This suggests that a close proximity of this residue to 2Fe influences the enzymatic preference for H_2 oxidation or production, and that Leu results in an enzyme that favors oxidation to a greater degree relative to one that has Met.
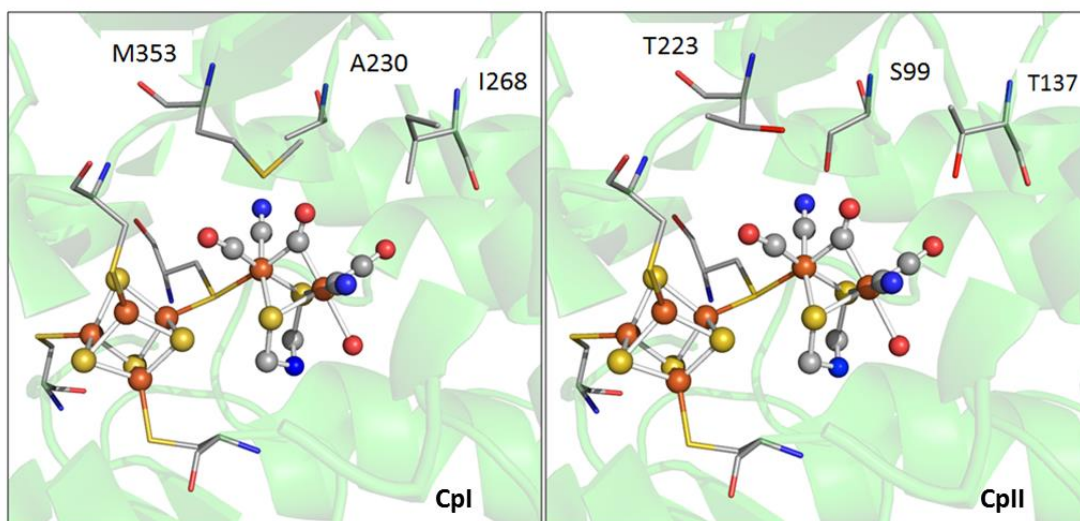
Figure 3.4. A zoomed in comparison of several possible key residues in the active site that influence catalytic bias, including, alanine 230, isoleucine 268, and methionine 353 in CpI, which correspond to a serine, threonine, and threonine in CpII, respectively.

A further comparison of the crystal structure of CpI with the CpII homology model revealed 14 potential sites (four at the FS4B, one at the FS4A, and nine in the H-cluster region) that may influence the redox potential of the FeS centers and thereby alter the catalytic bias (Fig. 5). By cross-checking these residues with their conservation percentage

and phylogenetic signal (K-statistic) among [FeFe]-hydrogenases, it is evident that most of these 14 residues are under strong selective pressure, demonstrating the functional importance of these residues and positions. Most likely, the determinants of catalytic bias are not found at a single site, but are rather a suite of residues that act in concert with one another. Future studies will focus on these 14 key residues using a site-directed mutagenesis approach.
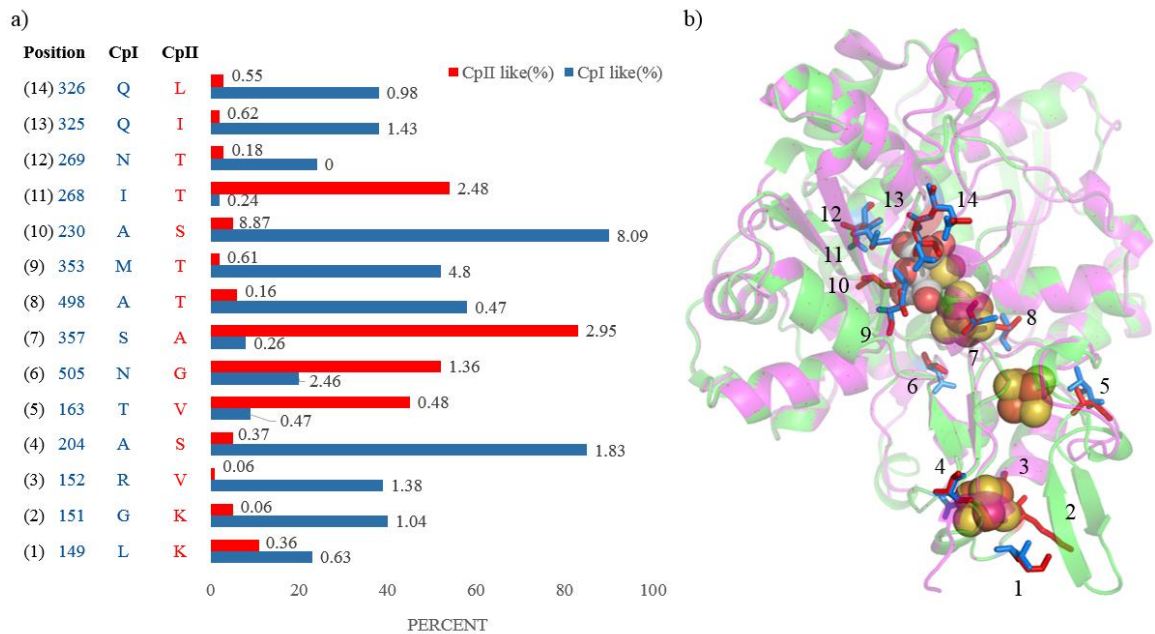
Figure 3.5. (a) Percent conservation of either CpI- or CpII-type residues among 829 [FeFe]-hydrogenase sequences is displayed in blue and red, respectively, along the X-axis. The Y-axis displays sites corresponding to the model depicted in (b), where CpII is superimposed with CpI, and 14 sites have been identified that may tune the FeS cluster potential. Residues are numbered according to CpI. The number at the end of each bar in (a) is the K-value, or phylogenetic signal, that corresponds to the amino acid at that position. A value of 1 or greater shows a high degree of phylogenetic signal, or conservation, and can be interpreted to indicate that this residue is under strong selective pressure.

Conclusions.

In this work the complement of hydrogenases from CpW5 was analyzed to provide better insights into the H_2 metabolism of this organism. The genome revealed sequences of three [FeFe]-hydrogenases and a [NiFe]-hydrogenase that allowed, for the first time, a comparison of the deduced amino acid sequences of the two biochemically characterized [FeFe]-hydrogenases, CpI and CpII, which have a sequence similarity of 61%. Targeted transcriptional analyses implicated a role for CpII in recapturing the reducing equivalents that are produced as H_2 as part of Mo-nitrogenase catalysis during growth under nitrogen-fixing conditions. A role for CpII in H_2 uptake is consistent with the previously observed catalytic bias of CpII toward H_2 oxidation. CpII probably evolved to be a poor proton-reducing enzyme, thereby limiting potential loss of H_2 under nitrogen-fixing conditions when the availability of reducing equivalents may be growth-limiting. A comparison of the CpI and CpII sequences in the context of their respective phylogenetic and structural relationships reveal several likely determinants of catalytic bias, which can be studied by characterization of site-specific variants of these [FeFe]-hydrogenases.

MATERIALS AND METHODS

Growth conditions. Freeze-dried C. pasteurianum strain W5 (ATCC® 6013™) was obtained from ATCC and rehydrated with Difco™ Reinforced Clostridial (DRC) Medium following the ATCC protocol. Sealed 25 ml glass serum vials (Wheaton) containing 10 ml of DRC medium under a headspace of 10% H_2-10% CO_2-80% N_2 were then inoculated with the rehydrated culture and incubated at 37°C following ATCC propagation procedures

for this organism. Agar plates prepared with DRC medium were used to store C. pasteurianum strain W5 for further use. Plates were incubated at 37°C for 24-48 hours and were then stored at room temperature in an anaerobic chamber.

For genome sequencing, cultures were inoculated from a single colony from a DRC agar plate that was inoculated into a sealed 25-ml serum vials containing 10 ml of the same medium. Cells were grown under a headspace of 10% H_2-10% CO_2-80% N_2 by overnight incubation at 37°C. An aliquot (1 ml) of the culture was spun down at 14,000 x g at room temperature before extracting DNA.

Genome sequencing. Total genomic DNA of C. pasteurianum strain W5 was extracted using a Promega Wizard® Plus SV minipreps DNA purification system. The concentration (220 ng/µL) was determined by a NanoDrop 1000 Spectrophotometer ($Abs_{260/280} = 2.04$). Genomic DNA was submitted to the Genomics Core Facility at The Pennsylvania State University for 454 pyrosequencing [38]. Reads were assembled with the Newbler assembler (ver. 2.6; Roche) into 145 contigs of at least 500 bp with 116 of those contigs predicted to form six large scaffolds. Read depth was about 19X.

Gaps were closed by PCR using primers designed approximately 200 bases from the end of each contig. GoTaq® 2x Master Mix (Promega, Madison, WI) was used for the amplification reactions in a Techne Touchgene Gradient Thermal Cycler (Techne, Bulington, NJ). Amplicons were then purified either directly using QIAquick PCR

Purification Kit or from agarose gels using the Qiaex II Gel Extraction Kit (Qiagen, Valencia, CA). Purified PCR products were sequenced by Davis Sequencing in Davis, CA, and sequence data were assembled using BioEdit (v7). The final assembled reads were compared to the recently published closed genome [9] using the ANI calculator tool with default settings [39] using previously described methods [40, 41]. This Whole Genome Shotgun project has been deposited at DDBJ/EMBL/GenBank under the accession LFYL00000000. The version described here is version LFYL01000000.

The genome was annotated using the RAST (Rapid Annotation using Subsystem Technology) prokaryotic genome annotation server [14]. The amino acid sequence of the H-cluster domain of CpI was used as a BLAST query against a database of the amino acid sequences encoded by the draft genome. All matches with an expect value (e-value) below 1.0 were aligned using ClustalW to determine whether they contained previously published signature motifs L1, L2, and L3 found in [FeFe]-hydrogenases.

For qRT-PCR, cultures were inoculated from a single colony from a DRC agar plate into a sealed 25-ml serum vial containing 10 ml of the same medium. Cells were grown under a headspace of 10% H_2-10% CO_2-80% N_2 by overnight incubation at 37°C. 1-5 ml of overnight culture was used to inoculate 50 ml of both DM-11 [42] (N+; containing NH_4Cl and $(NH_4)_2SO_4$) and DM-11-N (N-; fixed nitrogen free) media to an $OD_{650} = 0.020$ and were then sparged with 10% H_2-10% CO_2-80% N_2 for 10 minutes and incubated overnight. This was repeated after which point a C_2H_2 reduction assay [43] was

performed to ensure that the N-culture contained nitrogenase activity. In sealed 120-mL

serum vials, 1 mL (N+) cell culture was added to 50 mL of N+ media, and 6 mL of (N-)

cell culture were added to 50 mL of N- media, in order to give an initial $OD_{650} = 0.020$

for each culture. The vials were once again sparged with the gas mix and incubated

overnight at 37°C. The following day, another C_2H_2 reduction assay was performed to

verify nitrogenase activity. Samples (500 µl) were mixed with 1 ml of RNAprotect

Bacterial Reagent® (Qiagen, Valencia, CA) and either subjected to RNA extraction

immediately or frozen at -20°C until later RNA extraction.

Preparation of total RNA. Total RNA was extracted from C. pasteurianum strain W5 using

a RNeasy® Mini Kit (Qiagen, Valencia, CA) according to the manufacturer's protocol.

For N+ conditions, theOD_{650} of the cell culture was 0.9, while for N- cultures it was 0.4.

Note that N- cultures reach stationary phase at a density of nearly half the N+ cultures. In

both cases, cells were in the exponential phase at the time of harvesting. The DNase

treatment step used the RQ1 RNase-Free DNase (Promega, Madison, WI) and a re-

purification using the RNeasy® Mini Kit. The RNA concentration was determined using

Qubit® RNA Assay Kit (Life Technologies, Carlsbad, CA), and the RNA solution was

stored at -20 °C until further analysis.

Quantitative RT-PCR (qRT-PCR).   Integrated DNA Technologies SciTools qPCR

online primer designing software was used to design primers for the four hydrogenases

(CpI, CpII, CpIII and the large subunit of the [NiFe]-hydrogenase). The nitrogenase α-

subunit, nifD, and the 16S rRNA small subunit (Supplemental Table 1), served controls, to which expression was normalized. qRT-PCR was performed on a Rotor-Gene-Q real-time PCR detection system *(Qiagen, Valencia, CA)* using the Power SYBR® *green RNA-to-C_T™* 1-Step Kit (Life Technologies, Carlsbad, CA) according to the included protocol. Briefly, each reaction consisted of 10 µL Power SYBR® Green PCR master mix, 100 nM each of the forward and reverse primers, 100 ng of RNA template, and nuclease-free H_2O to a final volume of 20 µL. Cycling conditions were 40 minutes at 48°C, 10 minutes at 95°C, and then 40 cycles of 15 seconds at 95°C, and then one minute at 60°C. Reactions were performed in triplicate with control reaction mixtures containing no reverse transcriptase. Each transcriptional experiment was repeated a minimum of three times using RNA isolated from separate cultures. Primer efficiencies for DNA were 0.98 for 16S, 0.97 for CpI, 0.92 for CpII, 0.84 for CpIII, and 0.88 for nifD, using a DNA concentration of 145ng µl^{-1} to 0.145ng µl^{-1}.

Bioinformatics. Homologs of CpI were compiled from the Integrated Microbial Genomes (IMG) database [44] using BLASTp, resulting in 829 protein sequences. CpI and CpII, along with 829 homologs, were subjected to a multiple sequence alignment (MSA) using the Muscle algorithm as implemented in MEGA (vers. 6) [45] with default settings. Residues at each aligned position were removed if they were found to be identical in both CpI and CpII. For each of the remaining residues the degree of conservation (as a percent) among the 829 homologs was calculated using the MSA. SWISS-MODEL [46] was used to generate a homology model of CpII, based upon the known structure of CpI [20]. Pymol

[47] was then used to superimpose CpII onto CpI with a structure-based alignment. Based on this superimposition, functionally important residues that differed between CpI and CpII were selected. Sites examined included the proton transfer channel [48] and the protein sphere around the H-cluster, as well as the proximal and medial [4Fe-4S] clusters. Using this set of criteria, a total of 14 residues were identified in the FeS cluster regions that potentially differentiate the functionality of these enzymes.

The large subunit of [FeFe]-hydrogenase (HydA) contains an H-cluster domain containing at least ~350 residues [25, 26]. In addition to the H cluster, hydA often encodes diverse N-terminal (F-cluster) and C-terminal (C-cluster) domains. To minimize bias in phylogenetic reconstruction, the alignment containing the 829 homologous hydrogenases, as well as CpI and CpII, was trimmed to contain just the H-cluster domain, as previously described [49]. A phylogenetic tree of the H-cluster alignment block was constructed using a maximum likelihood method, i.e. RaxML, using the following parameters: gamma rate distribution, fixed base frequencies, and the BLOSUM62 substitution matrix [50]. The tree was rooted to Nar1 proteins from Homo sapiens (NP_036468, NP_071938) and Danio rerio (A2RRV9). The phylogenetic signal (K-statistic) associated with the distribution of the 14 individual amino acids at each of the identified alignment positions, as they are distributed on the H-cluster phylogenetic tree, was quantified using the program multiphylosignal within the Picante package [51] as implemented with the base package R. The K statistic compares the observed signal in the distribution of a trait (e.g., particular amino acid usage at a specific alignment position) on a phylogeny to the signal under a Brownian motion

model of evolution [52]. Values of K that are close to 1 imply a Brownian motion for the evolution of that trait (or some degree of phylogenetic signal) while values greater than 1 indicate strong phylogenetic signal. K values closer to zero or which are negative correspond to a random or convergent pattern of evolution for that trait.

Based on the H-cluster phylogenetic tree constructed above, 39 hydrogenase homologs that grouped phylogenetically with CpI and 39 homologous hydrogenases that grouped with CpII were identified. These 78 hydrogenases along with CpI and CpII were aligned and subjected to phylogenetic reconstruction as described above. The F- and C-cluster domains of the hydrogenases were identified using BLASTp against the Conserved Domain Database (CDD) and the CDSEARCH/cdd v3.13 algorithm [53] (version 3.13) using an e-value of 0.01 as previously described [24]. These CpI- and CpII- like hydrogenases were categorized into modular structures based on the presence of identified F- and C- clusters as described previously [24]. The modular structure was then overlaid onto the respective tree to determine the extent to which phylogeny predicts the distribution of F- and C-clusters. The genomes of organisms with the previously identified 78 hydrogenase homologs were screened for NifH using BLASTp and the NifH sequence from Cp as a search query. The distribution of nifH in the genomes of the respective taxa was also mapped onto the respective phylogenetic trees (Supplementary information figures 2 and 3). Interactive Tree Of Life (iTOL) was used to project the phylogenetic trees [54].

Declarations

List of Abbreviations

CpW5: Clostridium pasteurianum ATCC 6013 (strain W5); CpI: [FeFe]-hydrogenase 1 from CpW5; CpII: [FeFe]-hydrogenase 2 from CpW5; CpIII: [FeFe]-hydrogenase 3 from CpW5; WT: wild type

Consent for publication

Not applicable

Availability of Data

Data will be made available upon request.

Competing interests

The authors declare no competing interests

Authors' contributions

J.B.T. performed Clostridial growth and qRT-PCR experiments, J.H.A. and S.P. carried out bioinformatics studies. J.B.T. and J.H.A. wrote the document. E.S.B., T.L.H., and J.W.P contributed to experimental design and manuscript revision. Z.L., S.M.N., and D.A.B. sequenced the genome. P.W.K and M.W.W.A. contributed to data interpretation. All authors read and approved the final manuscript.

References

1. Patakova P, Linhova M, Rychtera M, Paulova L, Melzoch K: *Novel and neglected issues of acetone-butanol-ethanol (ABE) fermentation by clostridia:* Clostridium *metabolic diversity, tools for process mapping and continuous fermentation systems*. Biotechnol Adv 2013, *31*:58-67.

2. Winogradsky S: Recherches sure l'assimilation de l'azote libre de l'atmosphere par les microbes. *Archives des science biologique* 1895, 3:297-352.

3. Dalton H, Morris JA, Ward MA, Mortenson LE: Purification and some properties of molybdoferredoxin, a component of nitrogenase from Clostridium pasteurianum. *Biochemistry* 1971, 10:2066-2072.

4. Mortenson LE, Valentine RC, Carnahan JE: An electron transport factor from *Clostridium pasteurianum. Biochem Biophys Res Commun* 1962, 7:448-452.

5. Valentine RC, Mortenson LE, Carnahan JE: *The hydrogenase system of* Clostridium pasteurianum. J Biol Chem 1963, *2*38:1141-1144.

6. Chen J-S, Blanchard DK: Isolation and properties of a unidirectional H2-oxidizing hydrogenase from the strictly anaerobic N2-fixing bacterium Clostridium pasteurianum W5. *Biochem Biophys Res Commun* 1978, 84:1144-1150.

7. Adams MW, Mortenson LE: The physical and catalytic properties of hydrogenase II of *Clostridium pasteurianum*. A comparison with hydrogenase I. *J Biol Chem* 1984, 259:7045-7055.

8. Adams MW: The structure and mechanism of iron-hydrogenases. *Biochim Biophys Acta* 1990, 1020:115-145.

9. Rotta C, Poehlein A, Schwarz K, McClure P, Daniel R, Minton NP: *Closed genome sequence of* Clostridium pasteurianum *ATCC 6013*. Genome Announ 2015, *3:e01596*

10. Sakaguchi Y, Hayashi T, Kurokawa K, Nakayama K, Oshima K, Fujinaga Y, Ohnishi M, Ohtsubo E, Hattori M, Oguma K: The genome sequence of *Clostridium botulinum* type C neurotoxin-converting phage and the molecular mechanisms of unstable lysogeny. *Proc Natl Acad Sci USA* 2005, 102:17472-17477.

11. Sedlar K, Kolek J, Skutkova H, Branska B, Provaznik I, Patakova P: Complete genome sequence of *Clostridium pasteurianum* NRRL B-598, a non-type strain producing butanol. *J Biotechnol* 2015, 214:113-114.

12. Yutin N, Galperin MY: A genomic update on clostridial phylogeny: Gram-negative spore formers and other misplaced clostridia. *Environ Microbiol* 2013, 15:2631-2641.

13. Kolek J, Sedlář K, Provazník I, Patáková P: *Draft genome sequence of* Clostridium pasteurianum *NRRL B-598, a potential butanol or hydrogen producer*. Genome Announ 2014, *2:e00192-14*.

14. Overbeek R, Olson R, Pusch GD, Olsen GJ, Davis JJ, Disz T, Edwards RA, Gerdes S, Parrello B, Shukla M *et al*: The SEED and the Rapid Annotation of microbial genomes using Subsystems Technology (RAST). *Nucl Acids Res* 2014, 42(D1):D206-D214.

15. Nolling J, Breton G, Omelchenko MV, Makarova KS, Zeng QD, Gibson R, Lee HM, Dubois J, Qiu DY, Hitti J *et al*: Genome sequence and comparative analysis of the

solvent-producing bacterium *Clostridium acetobutylicum*. *J Bacteriol* 2001, 183:4823-4838.

16.   Sebaihia M, Peck MW, Minton NP, Thomson NR, Holden MTG, Mitchell WJ, Carter AT, Bentley SD, Mason DR, Crossman L *et al*: Genome sequence of a proteolytic (Group I) *Clostridium botulinum* strain Hall A and comparative analysis of the clostridial genomes. *Genome Res* 2007, 17:1082-1092.

17.   Bettegowda C, Huang X, Lin J, Cheong I, Kohli M, Szabo SA, Zhang X, Diaz LA, Jr., Velculescu VE, Parmigiani G *et al*: The genome and transcriptomes of the anti-tumor agent *Clostridium novyi-NT*. *Nat Biotechnol* 2006, 24:1573-1580.

18.   Poehlein A, Riegel K, Konig SM, Leimbach A, Daniel R, Durre P: Genome sequence of *Clostridium sporogenes* DSM 795(T), an amino acid-degrading, nontoxic surrogate of neurotoxin-producing Clostridium botulinum. *Standards in genomic sciences* 2015, 10:40.

19.   Pyne ME, Utturkar S, Brown SD, Moo-Young M, Chung DA, Chou CP: *Improved draft genome sequence of* Clostridium pasteurianum *Strain ATCC 6013 (DSM 525) using a hybrid next-generation sequencing approach*. Genome Announc 2014, *2*:e00790-14.

20.   Peters JW, Lanzilotta WN, Lemon BJ, Seefeldt LC: X-ray crystal structure of the Fe-only hydrogenase (CpI) from Clostridium pasteurianum to 1.8 angstrom resolution. *Science* 1998, 282:1853-1858.

21.   Arnold K, Bordoli L, Kopp J, Schwede T: The SWISS-MODEL workspace: a web-based environment for protein structure homology modelling. *Bioinformatics* 2006, 22:195-201.

22.   Schmidt O, Drake HL, Horn MA: Hitherto unknown [Fe-Fe]-hydrogenase gene diversity in anaerobes and anoxic enrichments from a moderately acidic fen. *Appl Environ Microbiol* 2010, 76(6):2027-2031.

23.   Calusinska M, Joris B, Wilmotte A: Genetic diversity and amplification of different clostridial [FeFe] hydrogenases by group-specific degenerate primers. *Lett Appl Microbiol* 2011, 53:473-480.

24.   Calusinska M, Happe T, Joris B, Wilmotte A: The surprising diversity of clostridial hydrogenases: a comparative genomic perspective. *Microbiology* 2010, 156:1575-1588.

25.   Meyer J: [FeFe] hydrogenases and their evolution: a genomic perspective. *Cell Mol Life Sci* 2007, 64:1063-1084.

26.   Vignais PM, Billoud B: Occurrence, classification, and biological function of hydrogenases: an overview. *Chem Rev* 2007, 107:4206-4272.

27.   Casalot L, Rousset M: Maturation of the [NiFe] hydrogenases. *Trends Microbiol* 2001, 9:228-237.

28.   Adams MW, Eccleston E, Howard JB: *Iron-sulfur clusters of hydrogenase I and hydrogenase II of* Clostridium pasteurianum. Proc Natl Acad Sci USA 1989, *86*:4932-4936.

29.   Adams MWW, Mortenson LE: *The purification of hydrogenase II (uptake hydrogenase) from the anaerobic N$_2$-fixing bacterium* Clostridium pasteurianum. Biochim Biophys Acta 1984, *766*:51-61.

30.   Hamilton TL, Ludwig M, Dixon R, Boyd ES, Dos Santos PC, Setubal JC, Bryant DA, Dean DR, Peters JW: Transcriptional profiling of nitrogen fixation in *Azotobacter vinelandii*. *J Bacteriol* 2011, 193:4477-4486.

31.   Laane C, Haaker H, Veeger C: *On the efficiency of oxidative phosphorylation in membrane vesicles of* Azotobacter vinelandii *and of* Rhizobium leguminosarum *bacteroids*. Eur J Biochem 1979, *97*:369-377.

32.   Walker CC, Yates MG: The hydrogen cycle in nitrogen-fixing *Azotobacter chroococcum*. *Biochimie* 1978, 60:225-231.

33.   Walker CC, PartridgeE CDP, Yates MG: *The effect of nutrient limitation on hydrogen production by nitrogenase in continuous cultures of* Azotobacter chroococcum. Microbiology 1981, *124*:317-327.

34.   Mulder DW, Shepard EM, Meuser JE, Joshi N, King PW, Posewitz MC, Broderick JB, Peters JW: *Insights into FeFe -hydrogenase structure, mechanism, and maturation*. Structure 2011, *19*:1038-1052.

35.   Liebgott P-P, de Lacey AL, Burlat B, Cournac L, Richaud P, Brugna M, Fernandez VM, Guigliarelli B, Rousset M, Léger C et al: *Original design of an oxygen-tolerant [NiFe] hydrogenase: major effect of a valine-to-cysteine mutation near the active site*. J Am Chem Soc 2011, *133*:986-997.

36.   Morra S, Maurelli S, Chiesa M, Mulder DW, Ratzloff MW, Giamello E, King PW, Gilardi G, Valetti F: *The effect of a C298D mutation in CaHydA [FeFe]-hydrogenase: Insights into the protein-metal cluster interaction by EPR and FTIR spectroscopic investigation*. Biochim Biophys Acta *1857:98-106.*

37.   Knörzer P, Silakov A, Foster CE, Armstrong FA, Lubitz W, Happe T: *Importance of the protein framework for catalytic activity of [FeFe]-hydrogenases*. J Biol Chem 2012, *287*:1489-1499.

38.   Mardis ER: *Next-generation DNA sequencing methods*. Annu Rev Genomics and Human Genet 2008, *9*:387-402.

39.   Rodriguez-R LM KK: The enveomics collection: a toolbox for specialized analyses of microbial genomes and metagenomes. *PeerJ Preprints* 2016, 4:e1900v1.

40.   Goris J, Konstantinidis KT, Klappenbach JA, Coenye T, Vandamme P, Tiedje JM: DNA-DNA hybridization values and their relationship to whole-genome sequence similarities. *Int J Syst Evol Microbiol* 2007, 57:81-91.

41.   Rodriguez-R L, Konstantinidis K: *Bypassing cultivation to identify bacterial species*. Microbe *9:111-118.*

42.   Mallette MF, Reece P, Dawes EA: *Culture of* Clostridium pasteurianum *in defined medium and growth as a function of sulfate concentration*. Appl Microbiol 1974, *28*:999-1003.

43.   Hardy RWF, Holsten RD, Jackson EK, Burns RC: *The acetylene-ethylene assay for N₂ fixation: laboratory and field evaluation*. Plant Physiol 1968, *43*:1185-1207.

44.   Markowitz VM, Chen I-MA, Palaniappan K, Chu K, Szeto E, Grechkin Y, Ratner A, Jacob B, Huang J, Williams P *et al*: IMG: the integrated microbial genomes database and comparative analysis system. *Nucl Acids Res* 2012, 40:D115-D122.

45.   Tamura K, Stecher G, Peterson D, Filipski A, Kumar S: *MEGA6: Molecular Evolutionary Genetics Analysis version 6.0*. Mol Biol Evol 2013, 30:2725-2729.

46.   Schwede T, Kopp J, Guex N, Peitsch MC: SWISS-MODEL: an automated protein homology-modeling server. *Nucleic Acids Res* 2003, 31:3381-3385.

47.   Delano WL: The PyMOL Molecular Graphics System. 2002.

48.   Cornish AJ, Gartner K, Yang H, Peters JW, Hegg EL: Mechanism of proton transfer in [FeFe]-hydrogenase from Clostridium pasteurianum. *J Biol Chem* 2011, 286:38341-38347.

49.   Mulder DW, Boyd ES, Sarma R, Lange RK, Endrizzi JA, Broderick JB, Peters JW: Stepwise [FeFe]-hydrogenase H-cluster assembly revealed in the structure of HydA(DeltaEFG). *Nature* 2010, 465:248-251.

50.   Stamatakis A: RAxML version 8: a tool for phylogenetic analysis and post-analysis of large phylogenies. *Bioinformatics* 2014, 30:1312-1313.

51.   Kembel S: An introduction to the picante package. 2010.

52.   Blomberg SP, Garland J, T.,, Ives AR: Testing for phylogenetic signal in comparative data: behavioral traits are more labile. *Evolution* 2003, 57:717-745.

53.   Marchler-Bauer A, Derbyshire MK, Gonzales NR, Lu S, Chitsaz F, Geer LY, Geer RC, He J, Gwadz M, Hurwitz DI *et al*: CDD: NCBI's conserved domain database. *Nucl Acids Res* 2015, 43(Database issue):D222-226.

54.   Letunic I, Bork P: Interactive Tree Of Life (iTOL): an online tool for phylogenetic tree display and annotation. *Bioinformatics* 2007, 23:127-128.

CHAPTER 4

DEVELOPMENT OF HYDROGENASE EXPRESSION AND EPR CPI
SPECTROSCOPIC DECONVOLUTION

Introduction

The two closely related hydrogenases described in the previous chapter, CpI and

CpII, immediately provide the basis for an excellent model system through which to

study catalytic bias, where bias is defined as the ratio of the maximal forward catalytic

rate over the maximal reverse rate. CpI is well known as one of nature's best hydrogen

production catalysts, while CpII is an unusual [FeFe]-hydrogenase, in that it

preferentially functions as a hydrogen oxidizer. In order to develop this model system

and examine the contributions of the secondary coordination sphere around both the H-

cluster and conduit array, expression and purification systems needed to be developed.

Upon acquiring pure protein, EPR spectroscopy was used as the main method of

characterization, as this technique is acutely sensitive to [FeS] clusters. However, the

EPR signals that result from the characterization of both CpI and CpII are a complex

amalgamation of overlapping signals[1], wherein these signals arise from each of the F-

clusters as well as the H-cluster[2-4]. Thus, the deconvolution of the complex spectra,

wherein the signal is separated into its constituent parts, was necessary to probe how the

properties of each individual [FeS] cluster contribute to the observed catalytic bias.

In order to do this, high-quality EPR data must be accumulated over a range of

conditions. Simulations are then used to match the observed complex spectra with a

combination of individually-contributing spin systems. This work has precedent in both

Complex I[5-6], as well as the molybdenum-containing, NAD^+-dependent FdsABG formate

dehydrogenase from *Ralstonia eutropha*.[7] In the case of Complex I, five EPR active

signals have been identified and deconvoluted, though the electron relay contains eight

FeS clusters. For FdsABG formate dehydrogenase four out of six FeS clusters have been

identified.

CpI, with a predicted five EPR active centers, and CpII, with only three predicted

EPR active centers, represent more tractable problems than the above systems.   By

identifying the spin characteristics of particular clusters in the conduit array important

mechanistic details may be understood, namely, how properties of individual clusters

give rise to the observed catalytic features. This further opens the door to site-directed

mutagenesis, and the ability to specifically influence the conduit array. While this

technique does require large amounts of protein and must be subjected to difficult

analysis, it is best to analyze conduit arrays in a 'holo' state, where mutations have not

been introduced to knockout particular FeS clusters. Mutations may result in decoupling

the spin between systems or otherwise perturbing the EPR signals such that a chemically

relevant state is not observed.   Surprisingly, despite CpI and CpII both having been

subjected to significant EPR study[1-2, 4, 8-12], spectral deconvolution has not been

attempted, and thus little is known about each FeS cluster in the conduit array.

<u>Expression and Purification of CpI</u>

The development of an expression protocol for CpI required overcoming several difficulties, namely, the formation of a large amount of [FeS] clusters, including the complex, maturase-requiring H-cluster, as well as overcoming the general oxygen sensitivity of enzyme.

<u>Development of Plasmid System</u>

In order to fully mature CpI, the gene has to be co-expressed with the HydE, HydF, and HydG proteins. Therefore, two accommodate all four genes into one plasmid system the pET-duet vector system was used. This system has two gene expression sites per plasmid, and several different plasmids have been developed with distinct antibiotic resistances, allowing for multiple plasmids to co-express protein in culture. The lab already had a vector, pCDF-duet, for the expression of HydF and HydG, this plasmid was named pCDF *FG*.

The CpI gene was digested out of a previous construct from the lab that had a C-terminal His-tag using the NcoI/SalI restriction enzymes, and was cloned into the pET-duet vector with a strep-II tag, in order to allow for a more gentle, higher-purity purification. The pET-duet vector already had *HydE* in the second cloning site, and the vector was named pETdt*CpI*E*, with the asterisk designating the position of the strep tag. This plasmid was then sequence-verified through Davis Sequencing, as well as analyzed by a restriction digest.

Expression of CpI*EFG

The pETdtCpI*E and pCDF FG plasmids were co-transformed into E. coli BL21

(DE3) ΔiscR chemically-competent cells. The iscR gene regulates the iron sulfur cluster

expression, and by using a knockout strain, the [FeS] clusters may be overexpressed. The

transformants were plated on LB plates with standard concentrations of both ampicillin

and chloramphenicol, to select for cells that had retained both plasmids.

5-10 colonies from the LB plates were picked and used to inoculate a 100 mL

overnight culture, supplemented with 100 µg/mL carbenicillin, 30 µg/mL kanamycin (for

the competent cells), and 30 µg/mL chloramphenicol, with growth at 37 °C and shaking

at 250 RPM. After 16 hours of growth, 4 mL of culture was used to inoculate 1 L flasks,

with the media having been pre-heated to 37 °C. Growth was allowed to proceed at 37

°C and 250 RPM until an O.D. of 0.5 was reached, typically around four hours of growth.

Expression was performed on the benchtop under argon sparging, where cultures

were supplemented with 25 mM sodium fumarate, 2.5 mM ferric ammonium citrate, 1.5

mM isopropyl β-D-1-thiogalactopyranoside (IPTG), and 2 mM cysteine hydrate, added in

that order. Thus, the cultures were allowed to become anaerobic under argon

concomitant with the induction of gene expression. Sparging continued overnight (~18

hours).

Following the expression of CpI, all further steps had to be treated in a strictly

anaerobic manner. Therefore, the Coy Chamber (Coy Laboratories, Grass Lake, MI) was

used to harvest cells into 1 L gas-tight centrifuge bottles. These bottles were then spun at

7500 g for 5 min. The resultant cell pellet was then scraped from the bottle, placed in a

falcon tube, flash-frozen in liquid nitrogen, and stored in the -80 °C freezer until further use. Prior to harvesting an aliquot of media was removed and used for a whole-cell activity assay of hydrogenase activity. Further purification was only carried out on cultures displaying high activity, defined as greater than 1000 nmol H_2 min^{-1} mL^{-1} as measured by gas chromatography.

During the development of the expression protocol, it was found that several factors were critical for the generation of active hydrogenase. Ammonium Fe(III) citrate of the brown, not green variety, (sigma 09714-250G), L-cysteine hydrochloride hydrate (Sigma C121800), and TB media specifically from EMD (1.01629.9010). LB media, as well as TB media from other sources, were found to be inferior for hydrogenase expression. Supplementation of 0.5% weight/volume of D-glucose to the expression culture immediately prior to inoculation was also found to aid in improving hydrogenase expression.

Hydrogenase Activity Assays

Hydrogenase activity was measured using a Shimadzu GC-8A with a thermal conductivity detector. Briefly, 2 mL reactions were set up in 10 mL crimp-sealed vials containing 5 mM methyl viologen (MV), 10 mM NaDT, 50 mM Tris, 300 mM NaCl, 5% glycerol, and between 25 ng-4 µg of enzyme per assay. For the whole cell assays, 0.1% triton was added to ensure cell lysis.

CpI Purification

To purify CpI, frozen cell pellets were resuspended at 5mL/gram of cell pellet in 50 mM Tris pH 8, 5 mM NaCl, 5% weight/volume glycerol, and 10 mM sodium dithionite (NaDT), 140 µg ml-1 DNAse and RNAse, 120 µg ml-1 lysozyme, and EDTA-free protease inhibitor tablets to the recommended concentration (Roche Diagnostics, 05892791001). The cells were stirred under argon with 1% Triton X-100 for lysis. After one hour the lysate was placed in gas-tight centrifuge bottles, and centrifuge at 50,000 x g for 30 min.

The clarified lysate was purified using a two-step protocol, first over a diethylaminoethanol (DEAE GE Life Sciences) sepharose ion-exchange column, followed by affinity capture using Strep-Tactin resin (IBA). For the DEAE column, elution was performed with 300 mM NaCl. This eluate was then concentrated to a volume of ~12 mL prior to loading onto the Strep column. Elution from the strep column was performed with 5 mM desthiobiotin (DTB), resulting in a single brown band eluting from the column. This pure protein was further concentrated, and then assessed for purity using sodium dodecyl sulfate polyacrylamide gel electrophoresis (SDS-PAGE) and the concentration was measured using the Bradford assay.

For later experiments, the apo form of CpI was purified. The same protocol was able to be followed, but without co-transformation of the pCDF *FG* plasmid. This allowed for the spectroscopic characterization of the apo enzyme, as well as the synthetically reconstituted varieties.

CpII Expression and Purification

The CpII gene, having been sequenced as described in the previous chapter, was codon-optimized for expression in *E. coli*, and synthesized by GenScript with a C-terminal Strep tag. Expression was carried out identically to CpI, but with the pACYC vector containing genes for HydE, HydF, and HydG. Overexpression was verified using SDS-PAGE. It was found that the CpII protein, though soluble, was easily degraded, most probably by proteases in the cell. Attempts to quickly purify away the proteases were unsuccessful. First, a DEAE column was run similar to with CpI, and no CpII was found to elute from the column. As an alternative, a cation exchange column (ToyoPearl CM-650C, Tosoh Bioscience, LLC) was employed instead. This method also failed to produce purified CpII.

A one-step Streptactin purification was attempted next, with the clarified cell lysate being loaded directly onto the strep column. A small amount of partially-purified protein was present, so the method still needed to be refined. It was discovered that anaerobic lysis with the Parr bomb (Parr Instruments) for two cycles of 25 min at 1500 PSI lead to better purification. A further innovation was to lower the O.D. of induction to 0.2-0.25, and increase the resuspension volume of the cell pellet to 10 mL/g of cells. This allowed for the production of pure protein at around 0.3 mg/L of cell culture. The expression of apo-CpII was not found to be stable; the presence of the H-cluster likely serves to stabilize the protein.

Figure 4.1. An SDS-PAGE gel depicting purified CpII, with the inset showing a photograph of the purified brown CpII in a crimp-sealed vial.

Spectral Deconvolution of CpI

Pure CpI was reconstituted with the synthetic PDT 2Fe subcluster, which features a carbon at the bridging position of the dithiomethyl bridge. This reduces the enzymatic turnover rate by around 1000-fold[13], which means that, for potentiometric experiments, the redox potential remains stable enough to freeze samples. EPR spectroscopy was used across a range of potentials to analyze CpI, as described in the following chapter.
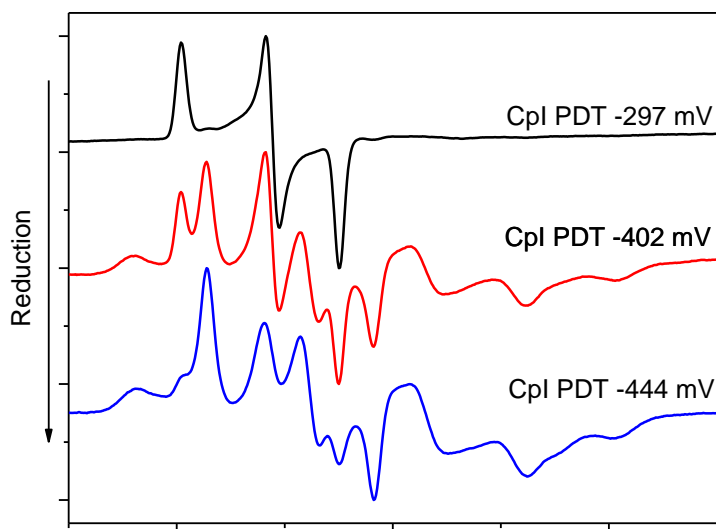
Fig 4.2. Potentiometric titration series of CpI reconstituted with PDT shows the H_{ox} signal at -297 mV, and a complicated set of signals growing in at more negative potentials

The spectral features identified represent the combination of the paramagnetic response by each of the three [4Fe-4S] clusters, distal [2Fe-2S] cluster, and H-cluster, for a total of five different clusters. However, to further complicate matters, the H-cluster may be found in a variety of states.

To perform the spectral deconvolution, a highly detailed set of data first had to be collected, with power saturation and temperature dependence data collected for each potential that was analyzed. This allowed for a careful discrimination of spectroscopic figures, where sets of peaks that correspond to one another, and therefore to a particular [Fe-S] cluster, could be isolated. By determining which features had similar temperature relaxation and power relaxation properties, an initial set of spin systems could be identified.
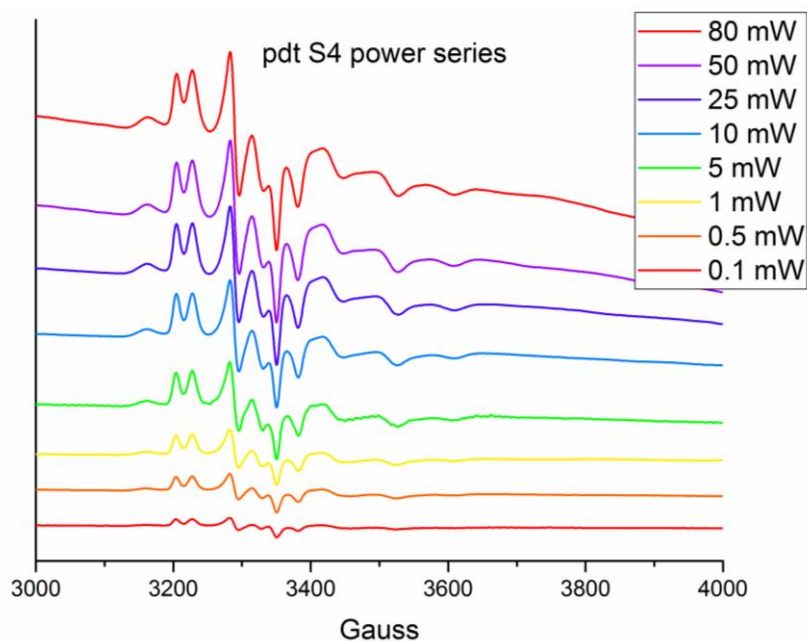
Fig 4.3. Power saturation series of PDT-CpII at -381 mV.
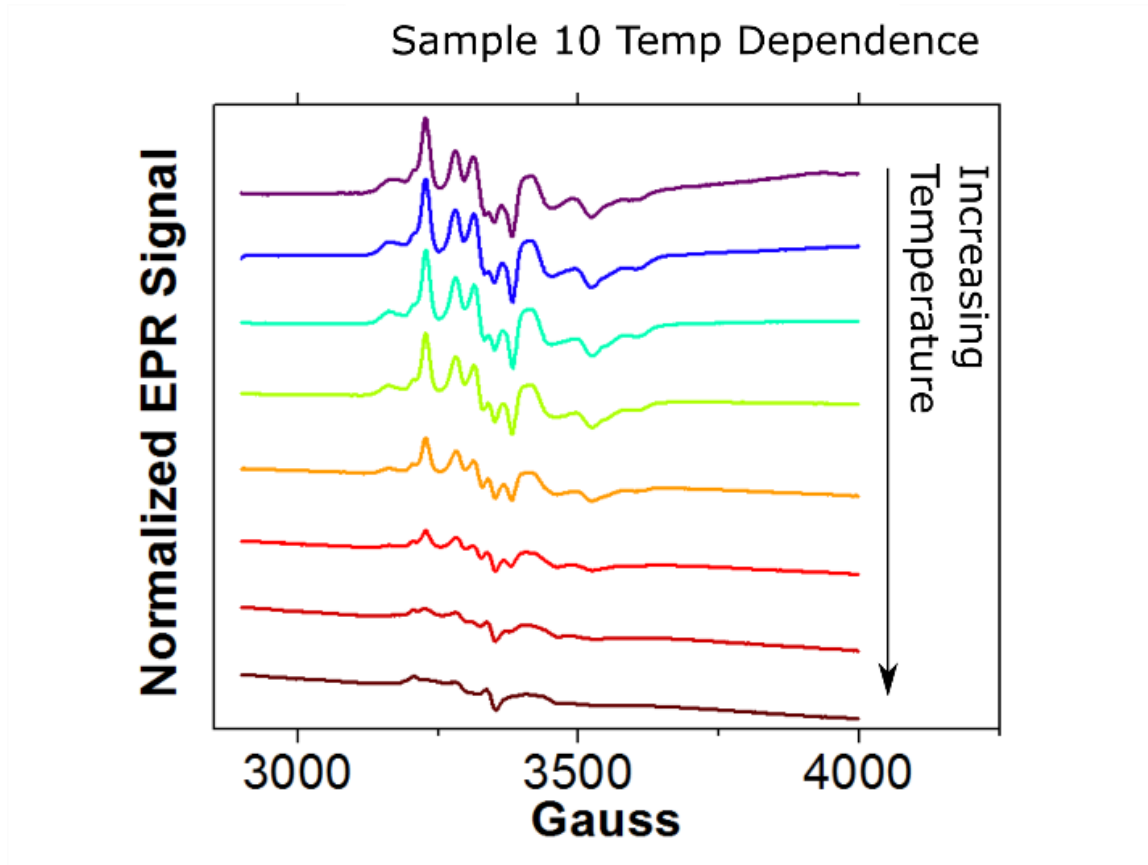
Fig 4.4. EPR Temperature relaxation series of PDT CPI at -418 mV, from T=5K (Purple) to 60K (Brown).

Spectral Deconvolution Using EasySpin

Once the given spectroscopic features had been identified, they could be further analyzed using Stefan Stoll's EasySpin, a package for MatLab that is capable of simulating EPR data across a variety of parameters. In this case, the 'Pepper' function was used to simulate the continuous-wave data that was collected. Experimental spectra were loaded, and the fitting was accomplished with the 'esfit' command. G-strain was used as a line broadening parameter, as is customary for the simulation of [Fe-S] clusters. The line broadening accounts for inhomogeneity in the sample, which among other

factors, may arise from the protein framework adopting slightly different confirmations.

Each script for the spectral deconvolution would define the particular spin systems in

terms of *g*-value, a *g*-strain parameter, and a system weight (the weight is simply relative

to the other weights of additional systems). Fitting was carried out primarily using the

Nelder/Mead simplex algorithm was a scale/shift baseline parameter.
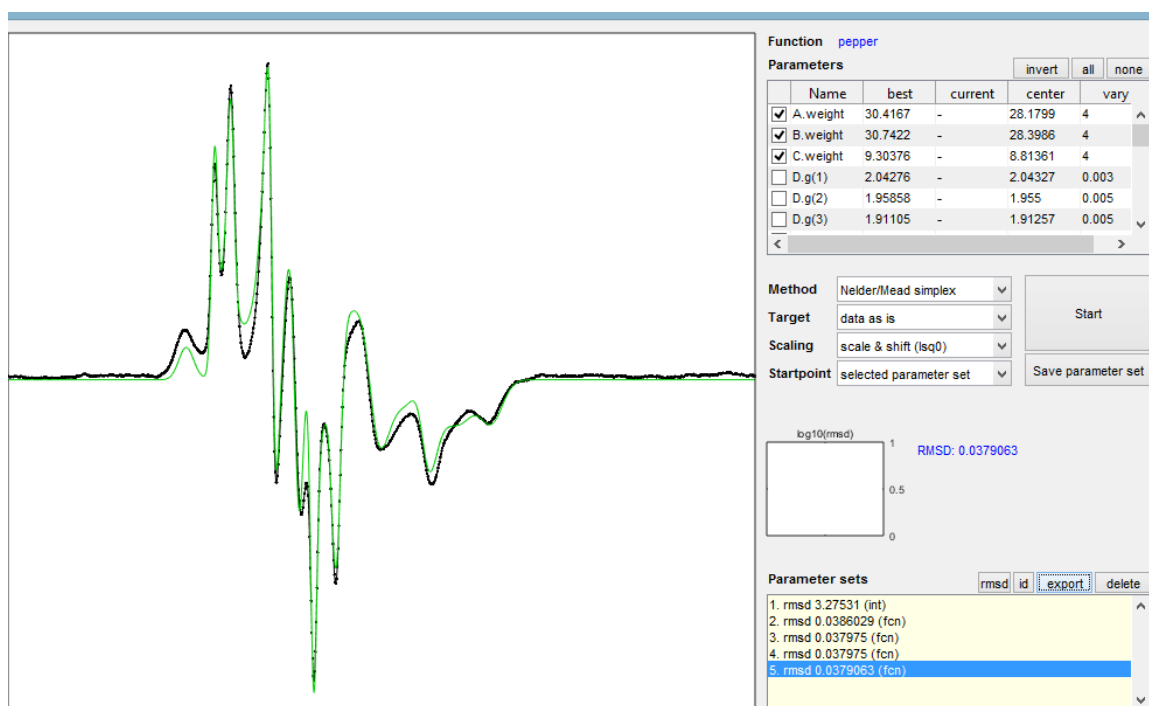
Fig 4.5. The CpI simulation (Green) is overlaid against the experimental data (Black) showing a close agreement of the fit to the experimental spectrum.

```
Exp.Range = [290 400];
Exp.mwFreq = 9.3845;
Temperature = 15;
SimOpt.Method = 'perturb';
FitOpt.Method = 'simplex';
[B,spc]=textread('C:\Users\f12j699\Documents\BETCy\EPR\pdtCpI1mW15K_S8_BC.txt
');
Sys1.g = [2.09246, 2.03873, 2.00144]; % Hox, % Bennet C
Sys1.gStrain = [0.0071146, 0.00718816, 0.00632224];
Sys1.weight = 30.4167;
Sys2.g = [2.07693, 2.00552, 1.98197]; %Bennet D
Sys2.gStrain = [0.00677033, 0.0148354, 0.00914997];
Sys2.weight = 30.7422;
Sys3.g = [2.0832, 2.0135, 2.0195]; % Bennet E
Sys3.gStrain = [0.0079013, 0.00898677, 0.0097];
Sys3.weight = 9.30376;
Vary1.weight = 0.0001;
Vary2.weight = 0.0001;
Vary3.weight = 0.0001;
Sys4.g = [2.04276, 1.95858, 1.91105]; %2Fe values (Meyer, Mulder)

Sys4.gStrain = [0.0152, 0.0263428, 0.0238841];

Sys4.weight = 38.3001;
Vary4.weight = 0.00001;
Sys5.g = [2.07771, 1.95165, 1.88]; %Distal 4Fe?

Sys5.gStrain = [0.0152289, 0.0161676, 0.0249999];

Sys5.weight = 37.3828;
Vary5.weight = 0.0001;
Sys6.g = [2.12031, 1.90922, 1.85579]; % Poorly simulated hyperfine?

Sys6.gStrain = [0.0170733, 0.0130418, 0.0192118];

Sys6.weight = 37.5543;
Vary6.weight = 0.0001;
 |
esfit
('pepper',spc,{Sys1,Sys2,Sys3,Sys4,Sys5,Sys6},{Vary1,Vary2,Vary3,Vary4,Vary5,
Vary6},Exp,SimOpt,FitOpt)
```

Fig 4.6. Example script for simulation of CpI EPR data.

The final fit represents the summation of each component that is contributing to the observed experimental spectra, with excellent agreement (Figure 4.5). The spin systems used here for -402 mV (Figure 4.6) may also be used to describe the CpI data across a range of potentials, albeit with changing component weights. The observed deconvolution arises from the well-known H_{ox} signal from the H-cluster, as well as another, minor contribution from the CO-inhibited state of the H-cluster, as has been

previously described. The remaining four components arise from each of the F-clusters in the conduit array, their individual assignments are described in the following chapter.

　　　With the spectral deconvolution complete, individual components could be fit to the Nernst equation, and the midpoint potential of each cluster could therefore be determined. For CpI, each [FeS] cluster was found to have a midpoint potential near the Hox potential or slightly more negative. Future efforts will focus on spin quantization of each spectral component to derive further insights into how each accessory cluster impacts catalytic bias.

Model	Nernst_ES2 (User)
Equation	A*((10^((M-x)/59.4))/(1+10^((M-x)/59.4)))
Plot	Hox
A	0.98564 ± 0.03004
M	-376.13389 ± 3.95479
Reduced Chi-	0.00235
R-Square(CO	0.98726
Adj. R-Square	0.98599
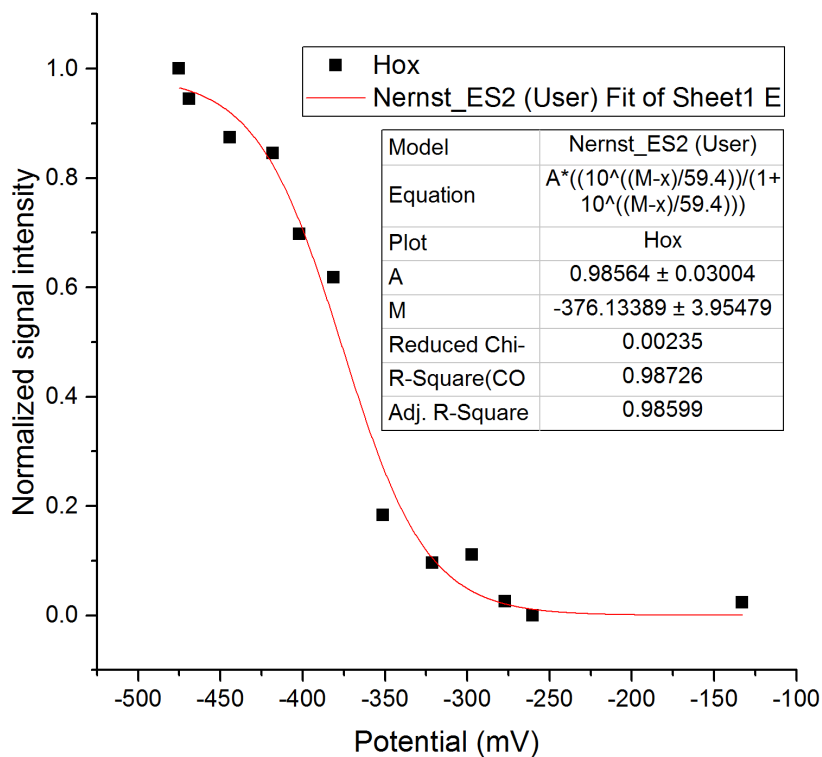
Fig 4.7. Example of potentiometric titration data, where a particular signal is fit to the Nernst equation, and the midpoint potential is thereby identified (-376 mV for this signal)

Spectral Deconvolution of CpII

The spectral deconvolution of CpII was able to proceed according to the methodology developed for CpI. First, the potentiometric titration was performed, as described in chapter 6. Power saturation and temperature relaxation profiles were gathered across the range of data sets, and spectroscopically distinct features were visually separated. These were then used as starting parameters to simulate data in EasySpin (Figures 4.8 and 4.9). The deconvolution of the CpII spectra was much more straightforward, as CpII only has two, rather than four, accessory clusters in the conduit array. Four systems were found to be contributing to the spectra, and are described in detail in chapter 6.
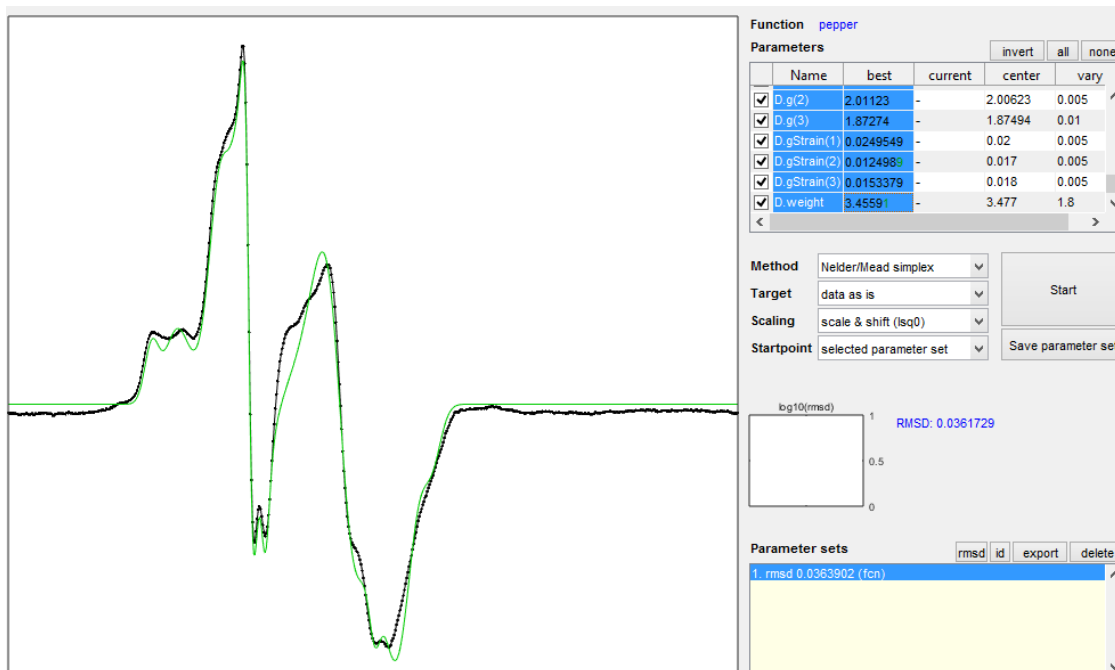
Fig 4.8. Example fit of CpII simulation data (Green) to experimental data (black) shows close agreement.

```
Exp.Range = [300 400];
Exp.mwFreq = 9.3845;
Exp.nPoints = 640;
SimOpt.Method = 'matrix';
FitOpt.Method = 'simplex';
[B,spc]= textread ('C:\Users\f12j699\Documents\BETCy\CpII EPR\May
EPR\CpII_BC.txt');
Sys1.g = [2.02358, 2.01396, 2.00761];
Vary1.g = [0.005, 0.005, 0.005];
Sys1.gStrain = [0.0138151, 0.00637545, 0.0114746];
Vary1.gStrain = [0.005, 0.0035, 0.005];
Sys1.weight = 0.254684;
Vary1.weight = .08;
Sys2.g = [2.09771, 2.00271, 1.9145];
Vary2.g = [0.008, 0.01, 0.01];
Sys2.gStrain = [0.0148059, 0.00719075, 0.00971432];
Vary2.gStrain = [0.01, 0.01, 0.005];
Sys2.weight = 1.89531;
Vary2.weight = 3.9;
Sys3.g = [2.03702, 1.94076, 1.89758];
Vary3.g = [0.01, 0.01, 0.01];
Sys3.gStrain = [0.0229713, 0.0257773 0.0253084];
Vary3.gStrain = [0.005, 0.005, 0.005];
Sys3.weight = 10.3652;
Vary3.weight = 7;
Sys4.g = [2.07547, 2.01123, 1.87274];
Vary4.g = [0.003, 0.005, 0.01];
Sys4.gStrain = [0.0249548, 0.0124989, 0.0153379];
Vary4.gStrain = [0.005, 0.005, 0.005];
Sys4.weight = 3.45591;
Vary4.weight = 1.8;
Sys5.g = [2.086, 2.008, 2.008];
Vary5.g = [0.001, 0.005, 0.004];
Sys5.weight = 3;
Vary5.weight =2.5;

    esfit
('pepper',spc,{Sys1,Sys2,Sys3,Sys4},{Vary1,Vary2,Vary3,Vary4},Exp,SimOpt,FitO
pt);
```

Fig 4.9. Example script for the simulation of CpII data.

Conclusions

The expression, purification, spectroscopic characterization, and deconvolution of

CpI and CpII has paved the way for a variety of biochemical and spectroscopic

experiments that will serve to further elucidate the properties of [FeFe]-hydrogenases,

particularly in regard for the determinants of catalytic bias. The heterologous expression

of CpII has heretofore not been reported, and represents a major step towards

understanding how the conduit array influences catalytic bias. These efforts, as well as

interpretation of the deconvoluted signals, are described more fully in the following

chapters.

References

1.   Bennett, B.; Lemon, B. J.; Peters, J. W., Reversible carbon monoxide binding and inhibition at the active site of the Fe-only hydrogenase. *Biochemistry* **2000,** *39* (25), 7455-60.

2.   Adams, M. W., The mechanisms of H2 activation and CO binding by hydrogenase I and hydrogenase II of Clostridium pasteurianum. *The Journal of biological chemistry* **1987,** *262* (31), 15054-61.

3.   Adams, M. W., The structure and mechanism of iron-hydrogenases. *Biochimica et biophysica acta* **1990,** *1020* (2), 115-45.

4.   Mulder, D. W.; Ratzloff, M. W.; Shepard, E. M.; Byer, A. S.; Noone, S. M.; Peters, J. W.; Broderick, J. B.; King, P. W., EPR and FTIR analysis of the mechanism of H2 activation by [FeFe]-hydrogenase HydA1 from Chlamydomonas reinhardtii. *J Am Chem Soc* **2013,** *135* (18), 6921-9.

5.   Ohnishi, T., Iron-sulfur clusters/semiquinones in complex I. *Biochimica et biophysica acta* **1998,** *1364* (2), 186-206.

6.   Wright, J. J.; Salvadori, E.; Bridges, H. R.; Hirst, J.; Roessler, M. M., Small-volume potentiometric titrations: EPR investigations of Fe-S cluster N2 in mitochondrial complex I. *J Inorg Biochem* **2016**.

7.   Niks, D.; Duvvuru, J.; Escalona, M.; Hille, R., Spectroscopic and Kinetic Properties of the Molybdenum-containing, NAD+-dependent Formate Dehydrogenase from Ralstonia eutropha. *Journal of Biological Chemistry* **2016,** *291* (3), 1162-1174.

8.   Adams, M. W.; Mortenson, L. E., The physical and catalytic properties of hydrogenase II of Clostridium pasteurianum. A comparison with hydrogenase I. *The Journal of biological chemistry* **1984,** *259* (11), 7045-55.

9.   Adams, M. W.; Eccleston, E.; Howard, J. B., Iron-sulfur clusters of hydrogenase I and hydrogenase II of Clostridium pasteurianum. *Proceedings of the National Academy of Sciences* **1989,** *86* (13), 4932-4936.

10.   Kowal, A. T.; Adams, M. W.; Johnson, M. K., Electron paramagnetic resonance studies of the low temperature photolytic behavior of oxidized hydrogenase I from Clostridium pasteurianum. *The Journal of biological chemistry* **1989,** *264* (8), 4342-8.

11.   Telser, J.; Benecky, M. J.; Adams, M. W.; Mortenson, L. E.; Hoffman, B. M., EPR and electron nuclear double resonance investigation of oxidized hydrogenase II (uptake) from Clostridium pasteurianum W5. Effects of carbon monoxide binding. *Journal of Biological Chemistry* **1987,** *262* (14), 6589-6594.

12.   Lubitz, W.; Ogata, H.; Rüdiger, O.; Reijerse, E., Hydrogenases. *Chemical reviews* **2014,** *114* (8), 4081-4148.

13.   Berggren, G.; Adamska, A.; Lambertz, C.; Simmons, T. R.; Esselborn, J.; Atta, M.; Gambarelli, S.; Mouesca, J. M.; Reijerse, E.; Lubitz, W.; Happe, T.; Artero, V.; Fontecave, M., Biomimetic assembly and activation of [FeFe]-hydrogenases. *Nature* **2013,** *499* (7456), 66-69.

CHAPTER 5

POTENTIOMETRIC EPR SPECTRAL DECONVOLUTION OF CPI [FEFE]-
HYDROGENASE REVEALS ACCESSORY CLUSTER PROPERTIES

<u>Contribution of Authors and Co-Authors</u>

Manuscript(s) in Chapter(s) 2, 3, 5, 6, Appendix D

Author: Jacob H. Artz

Contributions: Expression and purification of all protein, sample preparation, potentiometric titrations, EPR data collection, EPR data processing, wrote document

Co-Author: David W. Mulder

Contributions: Aided in potentiometric titrations, all data collecting and processing

Co-Author: Michael W. Ratzloff

Contributions: FTIR data collection and interpretation

Co-Author: Axl X. LeVan

Contributions: Aided in protein expression and purification

Co-Author: S. Garret Williams

Contributions: Synthesis and reconstitution of synthetic H-cluster and h-cluster analog

Co-Author: Michael W. W. Adams

Contributions: Interpretation of EPR results

Co-Author: Anne K. Jones

Contributions: Experimental design and interpretation

<u>Contribution of Authors and Co-Authors (Continued)</u>

Co-Author: Paul W. King

Contributions: Experimental design and interpretation

Co-Author: John W. Peters

Contributions: Experimental design and interpretation

Manuscript Information Page

Jacob H. Artz, David W. Mulder, Michael W. Ratzloff, Saroj Poudel, Axl X. LeVan, S. Garrett Williams, Michael W. W. Adams, Anne K. Jones, Eric S. Boyd, Paul W. King, John W. Peters

Potentiometric EPR spectral deconvolution of CpI [FeFe]-hydrogenase reveals accessory cluster properties

Jacob H. Artz[a], David W. Mulder[b], Michael W. Ratzloff[b], Axl X. LeVan[a], S. Garrett Williams[c], Michael W. W. Adams[d], Anne K. Jones[c], Paul W. King[b], John W. Peters*[a]

[a] Department of Chemistry and Biochemistry, 224 Chemistry and Biochemistry Building, Montana State University, Bozeman, MT, 59717 [b] National Renewable Energy Laboratory, 15013 Denver West Parkway, Biosciences Center, Golden, CO 80401 [c] School of Molecular Sciences, Arizona State University, PO Box 871604, Tempe, AZ 85287, USA [d] B216B Life Sciences Complex, Department of Biochemistry, The Univeristy of Georgia, Athens, GA 30602

*Corresponding author: john.peters@chemistry.montana.edu

Abstract

CpI [FeFe]-hydrogenase has been a model hydrogenase for understanding mechanisms of biological H_2 activation. Here, a new methodology for the study of CpI is introduced. CpI synthetically reconstituted with the propanedithiolate ligand severely impedes catalytic turnover, allowing previously unobserved highly-reduced states to be characterized via electron paramagnetic resonance spectroscopy. This reveals possible new insights into the mechanism of CpI. Not only may this methodology be used to further study additional hydrogenases, but this information may lead towards the design of novel hydrogen-evolving catalysts.

Introduction:

Hydrogenases reversibly and efficiently reduce protons to hydrogen using a series of [FeS] clusters[1]. The catalytic site is the H-cluster, consisting of a [4Fe4S] cubane with a cysteine thiolate linkage to a 2Fe subcluster, which is comprised of a [2Fe-2S] motif decorated with a dithiomethylamine bridge and several carbon monoxide and cyanide ligands[2-4]. CpI features a branched chain of accessory clusters (F-clusters) organized as stem of two [4Fe-4S] clusters that diverges towards either a [4Fe-4S] or [2Fe-2S] cluster, whereas a related hydrogenase, CpII, has only the two [4Fe-4S] F-cluster stem[5]. Currently, it is not clear how the properties of the accessory clusters contribute to the observed catalytic properties of the two enzymes. Previous midpoint potential measurements of CpI demonstrated the F-cluster potentials group around a value of -420 mV[5], although a more fine-grained approach to better resolve midpoint potential values has yet to be undertaken. In this work EPR spectroscopy has been employed on CpI at a variety of potentials in order to deconvolute the EPR spectra, and thereby link specific EPR features back to the identification of the midpoint potential of each FeS cluster.

In order to understand the catalytic abilities of hydrogenases specifically, and [FeS] cluster-containing enzymes in general, it is critical to delineate how each [FeS] cluster influences catalysis. [FeFe]-hydrogenases offer an excellent model system, as they are configured in a variety of ways[6] that directly influence the catalytic bias of a given hydrogenase. Here, CpI is used as the system of study given that it is a profound hydrogen producer[7], and understanding the structure-function relationship that contributes to hydrogen production may aid in the design and implementation not just of

novel hydrogen producing catalysts, but of any catalysis where the goal is to perform a difficult reduction (i.e., nitrogen fixation).

Previous EPR studies have failed to distinguish F-clusters from one another[8], as the signals are complex and overlapping. To overcome these issues a detailed data set of EPR spectra consisting of power and temperature series across a range of potentials has allowed individual contributions to the overall spectra to be parsed, revealing the E_m's of each [FeS] cluster.

Bennet et. al. have previously identified three spin systems in CpI[8], although the EPR spectra unambiguously show several other weaker, broad contributions that remain unaccounted for, though are proposed to arise from hyperfine couplings. Atta et. al. have generated an N-terminal truncation of CpI in order to specifically isolate the [2Fe2S] accessory cluster[9]; EPR on this protein shows a nearly-axial rhombic signal with g-values of 2.047, 1.954, and 1.911. A potentiometric titration of this protein revealed the E_m to be -400 mV.

Methods:

Protein Expression: Heterologous protein expression was performed using the pET-Duet plasmid encoding either CpI or CaI, as has been described previously[10-12]. However, in the case of the CpI protein, no maturase genes were present, yielding the apo form of the enzyme. A two-step purification of the CpI was performed, wherein the protein was first purified over an anion exchange column (diethylaminoethanol sepharose, GE LifeSciences), and then using affinity chromatography via Strep-tactin

resin (IBA). The purity of the protein was verified using SDS-PAGE and western blot with anti-strep antibody.

Synthetic reconstitution: CpI was prepared with either the naturally-occurring adt ligand or the pdt ligand, according the specifics of each experiment. Cluster incorporation was verified with FTIR.

FTIR: Spectra were collected on a Nicolet 6700 FTIR spectrometer as reported previously[13].

Potentiometric titrations: Potentiometric titrations were performed under strictly anaerobic conditions in an mBraun glove box at room temperature. Protein was loaded on a G25 column in order to remove dithionite, and eluted with 50 mM Tris, 200 mM NaCl, and 5% glycerol. The protein was then briefly treated with 1 mM thionin in order to oxidize the protein, and run over the G25 column again. This oxidized protein was added to a continuously-stirred sample cell for potentiometric titrations, along with 5 µM of the following redox-active dyes: indigo disulfonate, phenosafrinin, benzyl viologen, and methyl viologen, a final concentration of 10% glycerol, and a total cell volume of 3200 µL. The potential was measured using a Ag/AgCl ORP electrode, and increasingly low potentials were reached by titrating in 2mM or 10 mM sodium dithionite. Samples were withdrawn 200 µL at a time, loaded into EPR tubes, and flash frozen in liquid nitrogen.

EPR Spectroscopy: CW X-band EPR spectroscopy was carried out on a Bruker E500 equipped with a helium cryostat. Spectra were collected at a frequency of 9.38 GHz, 1 mW power, 15K, and a modulation frequency of 100 kHz, although the power ranged from 0.1 mW to 80 mW for power series measurements, and the temperature was varied from 4K to 80K for temperature series data. EPR simulations were carried out in MatLab using Stefan Stoll's EasySpin package[14].

Results:

Previously, a potentiometric titration on the holo form of CaI had been attempted, but it began to evolve hydrogen near -400 mV at the hydrogen couple, causing rapid drift towards more positive potentials. Lower potentials were therefore unable to be reached. In order to solve this drift problem, a titration was performed on unmaturated CpI protein that lacks a functional catalytic H-cluster. This method resulted in a spectra series that has protein features that do not change significantly between an oxidized and a reduced state. The overall EPR signal is broad, and can be closely simulated as a compilation of only three rhombic spin systems for an enzyme composed of five F-clusters.

In order to procure a more relevant spectroscopic view of the CpI titration series, it was necessary to synthetically reconstitute the enzyme, with a propane dithiolate bridging ligand instead of the native azadithiolate. The methyl group in the bridgehead position is predicted to alter proton transfer to and from the H-cluster, nearly eliminating hydrogen catalysis, while still retaining nearly all the F-cluster spectroscopic features

observed in native CpI. While there was some drift towards more positive potentials observed due to a low level of residual catalytic turnover, the samples were frozen immediately effectively trapping the reduced states. This titration series showed a clear progression from the well-characterized rhombic H_{ox} signal (all F-clusters are in the diamagnetic 2+ oxidation state) to a reduced spectrum at around -402 mV as has been previously reported[8], to an even-more reduced, and more complex broad signal that is indicative of intensive coupling of multiple, reduced, F-clusters at these low potentials (below -440 mV), possibly with contributions from the super reduced state of the H-cluster as well, wherein the cubane may be in the EPR-active 1^+ state.

In order to verify the quality of synthetic reconstitution, unmaturated CpI enzyme was reconstituted and examined via FTIR. The spectra show a high level of H-cluster incorporation and compared favorably to previous results[3]. In addition, the CO-inhibited state[5, 8] was observed.

The potentiometric titration of pdt-reconstituted CpI was performed across a range from -133 mV to -475 mv, with twelve samples being collected for CW X-band EPR. At the more positive potentials, the typical H_{ox} signal, with g-values of 2.092, 2.039, and 2.00 was observed. Several other signals began to grow in as the potential decreased towards -402 mV. At this potential, a very complex spectra was observed, which could be simulated as a series of six spin systems, including the well-characterized H_{ox} and H_{ox}-CO ($g = 2.083, 2.014, 2.020$) states, although the Hox-CO represented a minor spin contribution to the signal relative to the other observed spin systems. At lower potentials, the H_{ox} signal decreases in intensity, and the other features, presumably arising

from each of the F-clusters, broadened out, and the spectra could be simulated by a series of three different spin systems (Figure 5.1).

EPR spectral simulations were carried out with the 'Pepper' function of EasySpin. Previously identified spin systems (Hox[15], HoxCO[15], the two Bennet systems[8], and the Atta FS2 component[9]) were used as a starting point, with an additional system later being added, both to account for another [4Fe-4S] cluster in the conduit array, and to improve fitting. The combination of these six systems successfully accounts for the experimentally observed spectra (Figure 5.2). Individual system g-values and weights are presented in Table 5.1. At -402 mV all clusters have a similar contribution to the overall spectrum, with the exception of a weak contribution from the H_{ox}-CO signal. Out of the four remaining previously unassigned signals, each was proposed to result from one of the four F-clusters. FS2 was attributed to the system with g-values of 2.043, 1.959, and 1.911, based on similarity to values previously reported from a CpI truncation mutant[9]. Similarly, the signal attributed to FS4C, with g-values of 2.078, 1.952, and 1.88, closely resembles the EPR of a truncated CaI mutant that lacks F-clusters. The remaining two clusters have g-values of 2.077, 2.006, 1.982, and 2.120, 1.909, 1.856. These two systems could not be assigned with certainty, however, FS4B has tentatively been assigned to the g=2.12 system on the basis of having a broader signal that likely corresponds with more coupling.

The EPR signal observed between -444 mV, which essentially demonstrates the five non-H_{ox} signals, and -469 mV, broadens substantially at 15K. While this can be simulated closely by three spin systems without invoking any spin coupling, the

simulated line widths for each system are unreasonably broad. Simulations that are likely

to be more biologically relevant involve the addition of electron-electron coupling

between the three spin systems, as well as an added component of H-strain to simulate a

small degree of hyperfine coupling. It seems plausible, therefore, that the three [4Fe-4S]

F-clusters are coupled to one another at low potentials, similar to what has been reported

in eight-iron ferredoxins[16]. Having deconvoluted each spectra to examine the contribution

of each spin system, it was possible to fit each particular FeS cluster to the one-electron

Nernst curve.

Discussion:

The potentiometric titration of apo-CpI revealed a complex, broad spectra that

increased in intensity at more negative potentials. Given the lack of the 2Fe subcluster,

these signals are most likely arising from the F-clusters themselves. The broadness of the

features suggests interactions between the clusters, where hyperfine and/or electron-

electron coupling may play a role. The exact nature of these interactions has yet to be

determined, although it is a possibility that the exchange interaction has led to an

averaging of the spin systems, contributing to the inability to fully resolve these signals.

The lack of this signal broadening at moderate potentials in pdt-CpI suggests that the

fully assembled H-cluster withdraws electrons from the F-cluster, diminishing the overall

level of coupling. That the midpoint potential measured for the pdt-CpI in this

experiment is within the range of error suggested[17] for the adt-CpI suggests that

exchanging the bridging atom of the 2Fe subcluster has not dramatically altered the electronic properties of either the H-cluster or the conduit array.

The utilization of synthetic active site reconstitution with the unnatural pdt ligand has allowed for the study of CpI at low potentials, showing for the first time extensive spin coupling at these potentials.

The midpoint potential of the CpI F-clusters is more negative than the CpI H-cluster, with potential assignments of -372, -368, -372, and -360 mV, for FS4A, B, and C, and FS2, respectively, although these numbers represent the positive boundary for potentials; the actual potentials may be lower. The result of F-clusters with a more negative potential than the H-cluster is that electron flow is directed from the conduit to the H-cluster, thereby favoring proton reduction.

The broad signals at low potential are still of an unknown source, though two distinct possibilities arise. Either 1) the F clusters are all reduced, and the broad signals are a result of coupling between the clusters, or 2) the H-cluster becomes further reduced to an EPR active state. This distinction is critical for accurate assignment of midpoint potentials to the F-clusters. Though the H_{ox} signal E_m is definitively at -375 mV in this experiment, the intensity of F-cluster signals clearly did not stop increasing, even at the most negative potentials.

FTIR has been employed on the recycled -469 and -475 mV EPR samples in order to check for FTIR stretching mode shifts compared to the H_{ox} signal, which would indicate that the reduced EPR state is due to the super reduced state of the H-cluster. Unfortunately, the sample is still undergoing turnover during the concentration step

necessary for FTIR, and this provides enough time for the potential to drift, resulting in the characteristic H_{ox} FTIR signal. Additional experiments will be necessary in order to unambiguously determine the origin of the low-potential signals. Perhaps the use of either the SDT or ODT ligand[3] will catalytically disable the hydrogenase to a sufficient degree that potentiometric drift is no longer an issue.

Another consequence of the model that is provided here is that the [2Fe-2S] F-cluster is at a more positive potential than the H-cluster, and may therefore help direct electrons in the H_2 oxidation direction. The presence of two terminal FeS clusters, each capable of interacting with distinct redox partners, may explain the ability of this enzyme to function bidirectionally.

Collectively, the midpoint potentials of the H- and F-clusters of CpI suggest that electron flow through the enzyme has been tuned by evolution, such that there is enough of a gradient in the E_m to efficiently direct electron flow. This is corroborated, in part, by current bioinformatics work that suggests that there has been coevolution between the protein environment surrounding the both the H-cluster and the F-clusters[18-20]. Current work suggests that suites of residues in the outer coordination sphere serve in conjunction with one another to adjust the E_m of each FeS cluster.

It is as of yet unclear the extent to which each residue in the outer coordination sphere of the [FeFe]-hydrogenase H- and F-clusters is involved in redox tuning, although it is possible if not probable that longer-range effects play a role in catalytic bias[21]. Rational site-directed mutagenesis studies will need to be carried out in order to resolve this question.

In these titrations enzymatic turnover was observed by watching the potential, as monitored by the potentiostat, return to more positive values following the addition of dithionite as a reductant. For pdt-CpI, the drift was not observed until -418 mV, growing more severe at lower potentials. This corresponds approximately with the disappearance of the Hox EPR signal, while each of the F-clusters can be strongly seen at -400 mV and below.

Conclusions:

In this text a new methodology for the study of [FeFe]-hydrogenases has been outlined, wherein the use of a synthetically reconstituted enzyme with extremely low turnover may be used to study previously uncharacterized states of CpI. Further, the ability to spectrally deconvolute each of the components of the complex EPR spectra represents a major advancement in the ability to recognize the contributions of each F-cluster to the overall catalytic ability of the enzyme. These insights will help elucidate the determinants of catalytic bias, allowing for the design of unidirectional catalysts.
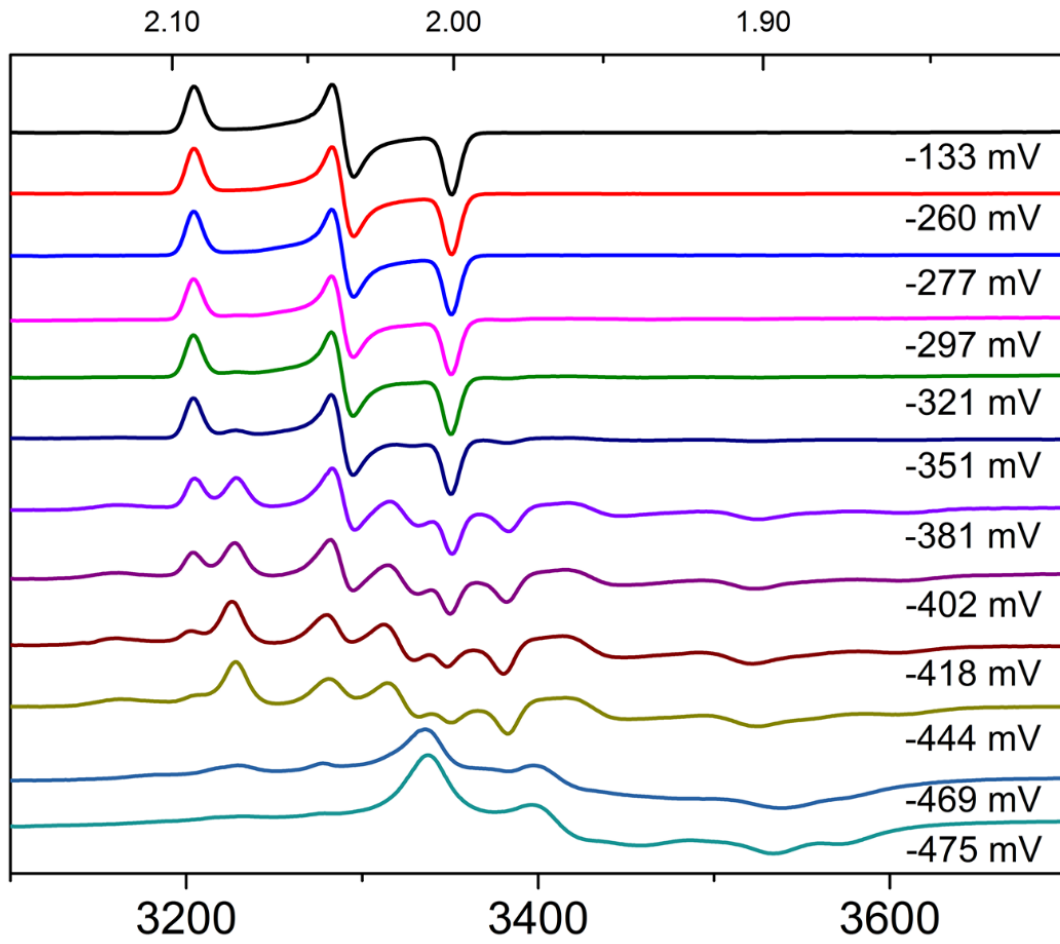
Figure 5.1 Potentiometric titration of CpI (pdt).
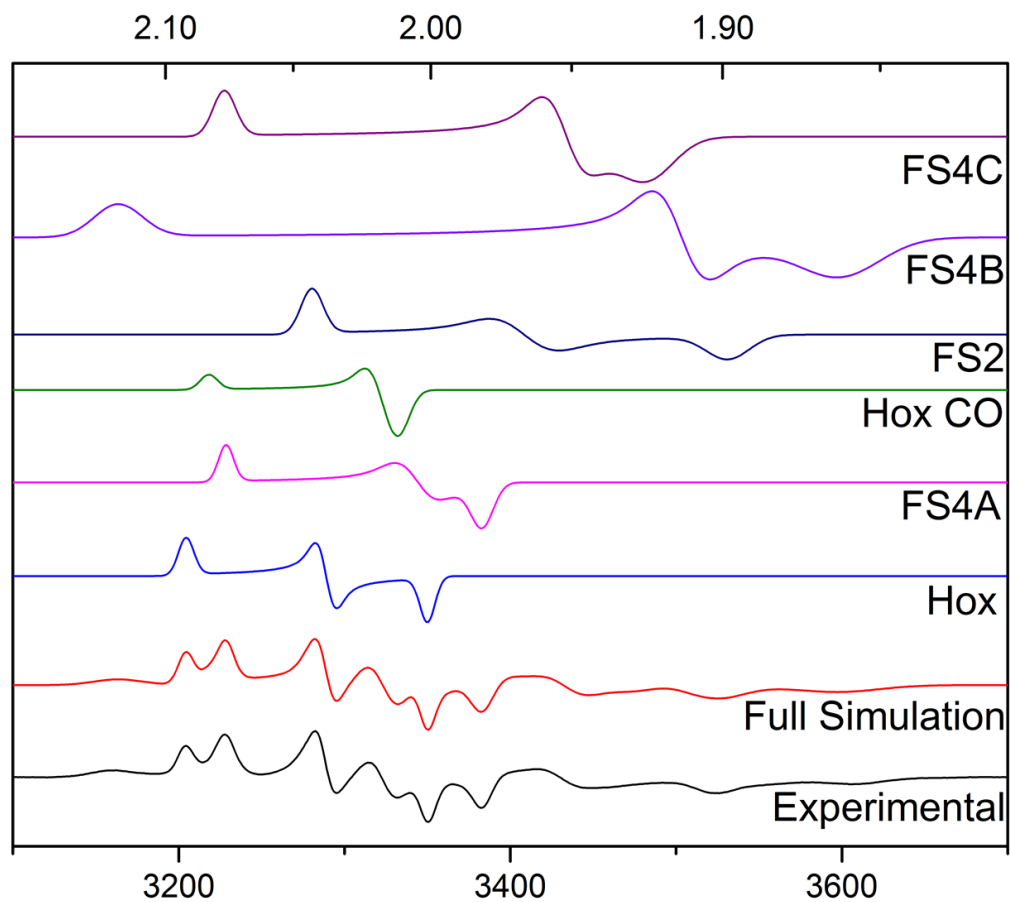
Figure 5.2. Spectral deconvolution of pdt-CpI.

Spin System	g	g	g	System weight %	Proposed cluster
1	2.092	2.039	2.00	16.56	Hox
2	2.077	2.006	1.982	16.73	FS4A?
3	2.083	2.014	2.020	5.06	Hox CO
4	2.043	1.959	1.911	20.85	FS2
5	2.078	1.952	1.88	20.35	FS4C
6	2.120	1.909	1.856	20.44	FS4B?

Table 5.1. Proposed spectral deconvolution simulation values of CpI at -402 mV

References

1.   Vignais, P. M.; Billoud, B., Occurrence, classification, and biological function of hydrogenases: an overview. *Chemical reviews* **2007,** *107* (10), 4206-72.
2.   Peters, J. W.; Lanzilotta, W. N.; Lemon, B. J.; Seefeldt, L. C., X-ray crystal structure of the Fe-only hydrogenase (CpI) from Clostridium pasteurianum to 1.8 angstrom resolution. *Science (New York, N.Y.)* **1998,** *282* (5395), 1853-8.
3.   Berggren, G.; Adamska, A.; Lambertz, C.; Simmons, T. R.; Esselborn, J.; Atta, M.; Gambarelli, S.; Mouesca, J. M.; Reijerse, E.; Lubitz, W.; Happe, T.; Artero, V.; Fontecave, M., Biomimetic assembly and activation of [FeFe]-hydrogenases. *Nature* **2013,** *499* (7456), 66-69.
4.   Lubitz, W.; Ogata, H.; Rüdiger, O.; Reijerse, E., Hydrogenases. *Chemical reviews* **2014,** *114* (8), 4081-4148.
5.   Adams, M. W., The structure and mechanism of iron-hydrogenases. *Biochimica et biophysica acta* **1990,** *1020* (2), 115-45.
6.   Meyer, J., [FeFe] hydrogenases and their evolution: a genomic perspective. *Cell. Mol. Life Sci.* **2007,** *64* (9), 1063-1084.
7.   Kowal, A. T.; Adams, M. W.; Johnson, M. K., Electron paramagnetic resonance studies of the low temperature photolytic behavior of oxidized hydrogenase I from Clostridium pasteurianum. *The Journal of biological chemistry* **1989,** *264* (8), 4342-8.
8.   Bennett, B.; Lemon, B. J.; Peters, J. W., Reversible carbon monoxide binding and inhibition at the active site of the Fe-only hydrogenase. *Biochemistry* **2000,** *39* (25), 7455-60.
9.   Atta, M.; Lafferty, M. E.; Johnson, M. K.; Gaillard, J.; Meyer, J., Heterologous biosynthesis and characterization of the [2Fe-2S]-containing N-terminal domain of Clostridium pasteurianum hydrogenase. *Biochemistry* **1998,** *37* (45), 15974-80.
10.   King, P. W.; Svedruzic, D.; Cohen, J.; Schulten, K.; Seibert, M.; Ghirardi, M. L. In *Structural and functional investigations of biological catalysts for optimization of solar-driven H2 production systems*, 2006; pp 63400Y-63400Y-9.
11.   Yacoby, I.; Tegler, L. T.; Pochekailov, S.; Zhang, S.; King, P. W., Optimized Expression and Purification for High-Activity Preparations of Algal [FeFe]-Hydrogenase. *PLoS ONE* **2012,** *7* (4), e35886.
12.   Kuchenreuther, J. M.; Britt, R. D.; Swartz, J. R., New Insights into [FeFe] Hydrogenase Activation and Maturase Function. *PLoS ONE* **2012,** *7* (9), e45850.
13.   Mulder, D. W.; Ratzloff, M. W.; Shepard, E. M.; Byer, A. S.; Noone, S. M.; Peters, J. W.; Broderick, J. B.; King, P. W., EPR and FTIR analysis of the mechanism of H2 activation by [FeFe]-hydrogenase HydA1 from Chlamydomonas reinhardtii. *J Am Chem Soc* **2013,** *135* (18), 6921-9.
14.   Stoll, S., Chapter Six-CW-EPR Spectral Simulations: Solid State. *Methods in enzymology* **2015,** *563*, 121-142.
15.   Adams, M. W., The mechanisms of H2 activation and CO binding by hydrogenase I and hydrogenase II of Clostridium pasteurianum. *The Journal of biological chemistry* **1987,** *262* (31), 15054-61.

16.   Mathews, R.; Charlton, S.; Sands, R. H.; Palmer, G., On the nature of the spin coupling between the iron-sulfur clusters in the eight-iron ferredoxins. *The Journal of biological chemistry* **1974,** *249* (13), 4326-8.

17.   Adams, M. W.; Eccleston, E.; Howard, J. B., Iron-sulfur clusters of hydrogenase I and hydrogenase II of Clostridium pasteurianum. *Proceedings of the National Academy of Sciences* **1989,** *86* (13), 4932-4936.

18.   Poudel, S.; Tokmina-Lukaszewska, M.; Colman, D. R.; Refai, M.; Schut, G. J.; King, P. W.; Maness, P. C.; Adams, M. W.; Peters, J. W.; Bothner, B.; Boyd, E. S., Unification of [FeFe]-hydrogenases into three structural and functional groups. *Biochimica et biophysica acta* **2016,** *1860* (9), 1910-21.

19.   Boyd, E. S.; Hamilton, T. L.; Swanson, K. D.; Howells, A. E.; Baxter, B. K.; Meuser, J. E.; Posewitz, M. C.; Peters, J. W., [FeFe]-hydrogenase abundance and diversity along a vertical redox gradient in Great Salt Lake, USA. *International journal of molecular sciences* **2014,** *15* (12), 21947-66.

20.   Peters, J. W.; Schut, G. J.; Boyd, E. S.; Mulder, D. W.; Shepard, E. M.; Broderick, J. B.; King, P. W.; Adams, M. W. W., [FeFe]- and [NiFe]-hydrogenase diversity, mechanism, and maturation. *Biochimica et Biophysica Acta (BBA) - Molecular Cell Research* **2015,** *1853* (6), 1350-1369.

21.   Abou Hamdan, A.; Dementin, S.; Liebgott, P.-P.; Gutierrez-Sanz, O.; Richaud, P.; De Lacey, A. L.; Rousset, M.; Bertrand, P.; Cournac, L.; Léger, C., Understanding and Tuning the Catalytic Bias of Hydrogenase. *Journal of the American Chemical Society* **2012,** *134* (20), 8368-8371.

CHAPTER 6

EPR AND FTIR SPECTROSCOPY PROVIDES INSIGHTS INTO THE
MECHANISM OF [FEFE]-HYDROGENASE CPII

<u>Contribution of Authors and Co-Authors</u>

Manuscript(s) in Chapter(s) 2, 3, 5, 6, Appendix D

Author: Jacob H. Artz

Contributions: Expression and purification of all protein, sample preparation,
potentiometric titrations, EPR data collection, EPR data processing, wrote document

Co-Author: David W. Mulder

Contributions: Aided in potentiometric titrations, all data collecting and processing

Co-Author: Michael W. Ratzloff

Contributions: FTIR data collection and interpretation

Co-Author: Saroj Poudel

Contributions: Bioinformatic studies

Co-Author: Axl X. LeVan

Contributions: Aided in protein expression and purification

Co-Author: Michael W. W. Adams

Contributions: Interpretation of EPR reults

Co-Author: Eric S. Boyd

Contributions: Experimental design and interpretation

Contribution of Authors and Co-Authors (Continued)

Co-Author: Paul W. King

Contributions: Experimental design and interpretation

Co-Author: John W. Peters

Contributions: Experimental design and interpretation

Manuscript Information Page

Jacob H. Artz, David W. Mulder, Michael W. Ratzloff, Saroj Poudel, Axl X. LeVan, ,
Michael W. W. Adams, Eric S. Boyd, Paul W. King, John W. Peters*

Status of Manuscript:

__X_ Prepared for submission to a peer-reviewed journal

____ Officially submitted to a peer-review journal

____ Accepted by a peer-reviewed journal

____ Published in a peer-reviewed journal

EPR AND FTIR SPECTROSCOPY PROVIDES INSIGHTS INTO THE MECHANISM OF [FEFE]-HYDROGENASE CPII

Jacob H. Artz[a], David W. Mulder[b], Michael W. Ratzloff[b], Saroj Poudel[a], Axl X. LeVan[a], Michael W. W. Adams[c] Eric S. Boyd[a], Paul W. King[b], John W. Peters*[a]

[a] Department of Chemistry and Biochemistry, 224 Chemistry and Biochemistry Building, Montana State University, Bozeman, MT, 59717 [b] National Renewable Energy Laboratory, 15013 Denver West Parkway, Biosciences Center, Golden, CO [d]B216B Life Sciences Complex, Department of Biochemistry, The University of Georgia, Athens, GA 30602

*Corresponding author: john.peters@chemistry.montana.edu

Keywords: [FeFe]-hydrogenase, *Clostridium pasteurianum*, CpI, CpII, FeS cluster, EPR

Abstract

Unidirectional catalysts may be of great technological importance across a variety of fields, and yet the determinants of this unique catalytic feature remain largely unknown. Here, a unique model system of [FeFe]-hydrogenases, CpI and CpII, are used as a basis for defining features that may contribute to this profound catalytic bias. CpII is expressed and purified heterologously for the first time, allowing for in-depth electron paramagnetic and Fourier Transform Infrared spectroscopic characterizations. Compared to CpI, CpII is found to have accessory clusters that differ in their midpoint potentials. A previously unobserved oxidative inactivation suggests that CpII may in fact undergo a catalytic mechanism distinct from CpI. These insights collectively suggest ways that the structure of [FeFe]-hydrogenases may tune the metal sites in order to provide a defined catalytic outcome.

Introduction

Catalytic bias, defined as the ratio of the maximal forward rate over the maximal reverse rate[1], is fundamentally important for an understanding of catalytic mechanisms[2]. For many catalytic reactions it may be preferable to favor a forward reaction (or prevent the reverse reaction), thereby leading to an accumulation of product. So far the contributors to catalytic bias remain largely undetermined, particularly in enzymes. Thus, a model system of [FeFe]-hydrogenases has been identified for the study of catalytic bias.

Clostridium pasteurianum strain W5 has a long been a model system for the study of hydrogen metabolism[3], and was the source of the first [FeFe]-hydrogenase to be crystallized[4]. Before this, however, hydrogenases from *Cp*W5 was the subject of intense scrutiny. During the purification of [FeFe]-hydrogenase I, or CpI, it was found that the cellular lysate had a different ratio of hydrogen production to oxidation than the purified protein[5]. This led directly to the discovery of a second [FeFe]-hydrogenase, CpII[6], that was found to be expressed in greater quantities during diazotrophic conditions[7]. Biochemical analysis revealed that CpII functions almost exclusively as a hydrogen oxidizer, which dramatically differentiates it from CpI. CpI produces hydrogen at 5500 μmol of H_2/min·mg , while CpII only produces hydrogen at 10 μmol of H_2/min·mg[8]. CpII, however, is a better hydrogen oxidizer, with a rate of 34,000 μmol of H_2/min·mg , compared to only 24,000 μmol of H_2/min·mg for CpI[8].

Subsequent sequence analysis of CpI and CpII revealed strong homology between the enzymes, with nearly 45% sequence identity over the conserved regions of the proteins, although CpII lacks an N-terminal region responsible for binding one [4Fe-4S] cluster and one [2Fe-2S] cluster. Analyses of Fe content and sequence homology suggest that CpII shares a conduit array of two [4Fe-4S] clusters in common with CpI, along with the catalytic H-cluster. The H-cluster is itself a [4Fe-4S] cubane with a cysteine thiolate linkage to a 2Fe subcluster[4], which is further ligated by the diatomic carbon monoxide, and cyanide ligands, as well as a dithiomethylamine bridge[9].

The conservation of the H-cluster as the site of catalysis suggests several possibilities for modulating the profound catalytic bias observed between CpI and CpII. Tuning of the secondary coordination sphere around either the H-cluster, or accessory [FeS] cluster conduit array, or, most probably, both, works to alter the kinetic properties of the catalytic cycle[10], thereby favoring hydrogen oxidation in the case of CpII. Previous comparison of the amino acid sequences of CpI and CpII demonstrate that the proton channel[11] is strictly conserved, as are amino acids directly lining the proposed gas channel[12]. Catalytic bias between CpI and CpII is therefore thought to arise from differences in the amino acids surrounding the H- and F- clusters, of which 14 key residues have been identified.

The motivation of this study, therefore, was to delineate the spectroscopic features of the CpII hydrogenase in the context of what has been observed for CpI, and compare the two

enzymes in order to identify the specific contributors of proton reduction that are
conspicuously absent from CpII. EPR was used to analyze midpoint potentials of each
[FeS] cluster, and FTIR was further employed as a spectroscopic handle for the active
site[13].

Methods:

Protein Expression: CpII was synthesized by GenScript with a C-terminal Strep tag.
Expression was carried out with the maturase genes[14], with cultures being induced for
expression at room temperature with IPTG when the O.D.$_{600}$ reached 0.25. Cells were
then frozen, resuspended in buffer at 10 ml/gram of cells, with protease inhibitor,
DNAse, and lysozyme. Lysis was carried out in a Coy anaerobic chamber (Coy
Laboratories, Grass Lake, MI) using a Parr bomb (Parr Instruments), with two cycles at
1500 PSI. The lysate was harvested, and centrifuged at 58,000 x g for 1 hour at 4 °C.
Clarified lysate was then purified in a single step over an anaerobic strep column.

FTIR: Spectra were collected on a Nicolet 6700 FTIR spectrometer as previously
reported[13].

Potentiometric titrations: Potentiometric titrations were performed under strictly
anaerobic conditions in an mBraun glove box at room temperature. Protein was loaded
on a G25 column in order to remove dithionite, and eluted with 50 mM Tris, 200 mM
NaCl, and 5% glycerol. The protein was then briefly treated with 1 mM thionin in order

to oxidize the protein, and run over the G25 column again. This oxidized protein was added to a continuously-stirred sample cell for potentiometric titrations, along with 5 µM of the following redox-active dyes: indigo disulfonate, phenosafrinin, benzyl viologen, methyl viologen, and methylene blue, a final concentration of 10% glycerol, and a total cell volume of 3200 µL. The potential was measured using a Ag/AgCl ORP electrode, and increasingly low potentials were reached by titrating in 2mM or 10 mM sodium dithionite. Samples were withdrawn 200 µL at a time, loaded into EPR tubes, and flash frozen in liquid nitrogen. 15 EPR samples were collected from -28 mV (sample 1) through -462 mV (sample 15), although the last sample was only 150 µL.

EPR Spectroscopy: CW X-band EPR spectroscopy was carried out on a Bruker E500 equipped with a helium cryostat. Spectra were collected at a frequency of 9.38 GHz, 1 mW power, 15K, and a modulation frequency of 100 kHz, although the power ranged from 0.1 mW to 80 mW for power series measurements, and the temperature was varied from 4K to 80K for temperature series data. EPR simulations were carried out in MatLab using Stefan Stoll's EasySpin package[15], with the 'Pepper' function.

Results:

The CpII titration was carried out from -28 mV to -466 mV (Figure 6.1), with noticeable drift towards more positive potential beginning around -350 mV, and becoming severe at the lowest potentials. A somewhat weak signal, with g-values of 2.024, 2.014, and 2.008, is present throughout the samples and is perhaps indicative of a non-catalytic state. While

this signal was simulated with g-values corresponding to a rhombic system, line broadening makes the actual signal appear nearly isotropic. Additional features grow in below -350 mV, consistent with where turnover was observed electrochemically. It should be noted that, while this enzyme was under turnover conditions, the relative rate of proton reduction by CpII was low enough that this experiment was tractable.

Deconvolution of CpII (Figure 6.2) was performed using the 'Pepper' function of EasySpin. The temperature and power series data, which were collected at each potential during the titration, were critical in determining the contributions of each spin system to the overall observed complex spectra. In addition to several rhombic signals likely arising from the F-clusters, there appears to be a signal corresponding to enzyme turnover, perhaps the H_{ox} signal.

Deconvolution of the CpII at low potential revealed the presence of a weak isotropic signal at g=2.01, and three stronger rhombic signals. The isotropic signal corresponds to the inactive or resting state of the enzyme, while the other three signals likely arise from the H- and F-clusters. Unlike CpI at this potential, the systems represent a variety of different weights. The strongest signal at this potential, g=2.037, 1.941, and 1.900, has been assigned to FS4A' on the basis of having a broad signal suggestive of coupling. The H-active signal has been assigned to the system with g-values of 2.075, 2.011, and 1.872, while FS4B' has been assigned to the system corresponding to g-values 2.098, 2.002, and 1.9145. (Table 6.1)

FTIR of CpII shows that CpII undergoes changes under either H_2 or NaDT in glycine pH10 buffer, relative to oxidized samples (Figure 6.3). Unreactivity to CO suggests the presence of a bound ligand on the distal Fe of the H-cluster. There were very minor changes in the sample poised at -442 mv, with a weak 1959 cm-1 appearing and 2082 cm-1 disappearing. Sample #12 (-399 mV), 2082 cm-1 was also a little weaker relative to 2108 cm-1, but was otherwise the same as the starting sample. This suggests that the majority of the changes in the EPR are likely from reduction of the F-clusters. The presence of mediators may be aiding turnover of the enzyme, which resulted in more changes in the IR under H_2 for samples that were recycled from the potentiometric titration.

An additional FTIR experiment was performed in order to test the reactivity of the H-cluster to both H_2 and CO gas (Figure 6.4). The initial FTIR spectra corresponds to one that is similar to the H-inactive state, and, when treated with CO, shows no change. Upon H_2 reduction of the non-treated, inactive sample, peaks corresponding to the reduced H-cluster appear. Subsequent treatment with CO shows more peak shifts that are similar to values reported for the CpI CO-inhibited state.

Having deconvoluted each spectra to examine the contribution of each spin system, it was possible to fit each particular FeS cluster to the one-electron Nernst curve. Midpoint potential values were found to be -414, -385, and $\leq$ -426 mV, for signals assigned to FS4A', FS4B', and the H-act signal, respectively (Figure 6.5). In the case of the H-act signal, the potentiometric titration did not reach low enough potential to

conclusively rule out the possibility of having a midpoint potential below -426 mV. This number should therefore be treated as an upper bound to the potential of this cluster.

Discussion:

CpII shows enzymatic turnover from -351 mV, increasing at more negative potentials. Midpoint potentials of the CpII clusters were found to be less than or equal to -426 mV, - 414 mV, and -385 mV. These signals have been attributed to the H-cluster, FS4A', and FS4B', respectively. CpII thereby demonstrates how the potentials of clusters in the conduit array relative to the H-cluster cause the enzyme to be functionally unidirectional. FTIR data shows distinct differences between CpII, as shown here, and previously reported CpI spectra. Thus, the various states of CpI and CpII do not have a direct one-to-one correspondence, rather, CpII is mechanistically distinct. The combination of EPR and FTIR data, along with the potential drift witnessed during the potentiometric titration, suggest that CpII is primarily in an inactive state at potentials above approximately -350 mV. The inactive state is characterized by an isotropic EPR signal with a g-value of 2.01, and FTIR peaks at 1999, 1985, and 1827. By reducing CpII further, activity is observed, and additional features grow in as measured by EPR. For the FTIR, new peaks at 1967 and 1788 are observed. Only the reduced state is susceptible to CO inhibition, and this treatment reveals further changes in the FTIR. It is suspected that the oxidative inhibition is directly related to the catalytic differences that are profoundly distinct between CpI and CpII.

This model of catalytic bias in CpII is essentially a kinetic argument, wherein the specific properties of each enzyme have different abilities to lower the activation energy in a given direction of the enzyme. Bias as presented here is a kinetic effect, given that the measurements are based on catalytic rate, or V_{max}, and the thermodynamic equilibrium cannot be different between the two systems, given that the enzymes have been compared under identical dye-based or electrochemical conditions. CpI and CpII are similar in terms of their ability to lower the activation energy for hydrogen oxidation, while in the opposite direction, proton reduction, only CpI can effectively lower the barrier. In this model the E_m's of the [FeS] clusters are thought to be one of the enzyme properties that influence bias. Further detailed analyses will be necessary to fully understand how similar yet distinct structural features contribute to profoundly different enzyme function.

Conclusions:

The first heterologous purification of CpII has allowed for an in-depth investigation into the features of [FeFe]-hydrogenases that contribute to proton reduction. EPR data suggests that the midpoint potentials of the accessory clusters may be poised to favor fast hydrogen oxidation, rather than proton reduction. Further, a unique oxidative inactivation and reductive activation has been observed, and it is probable that this has strong mechanistic importance for the observed catalytic function of CpII.
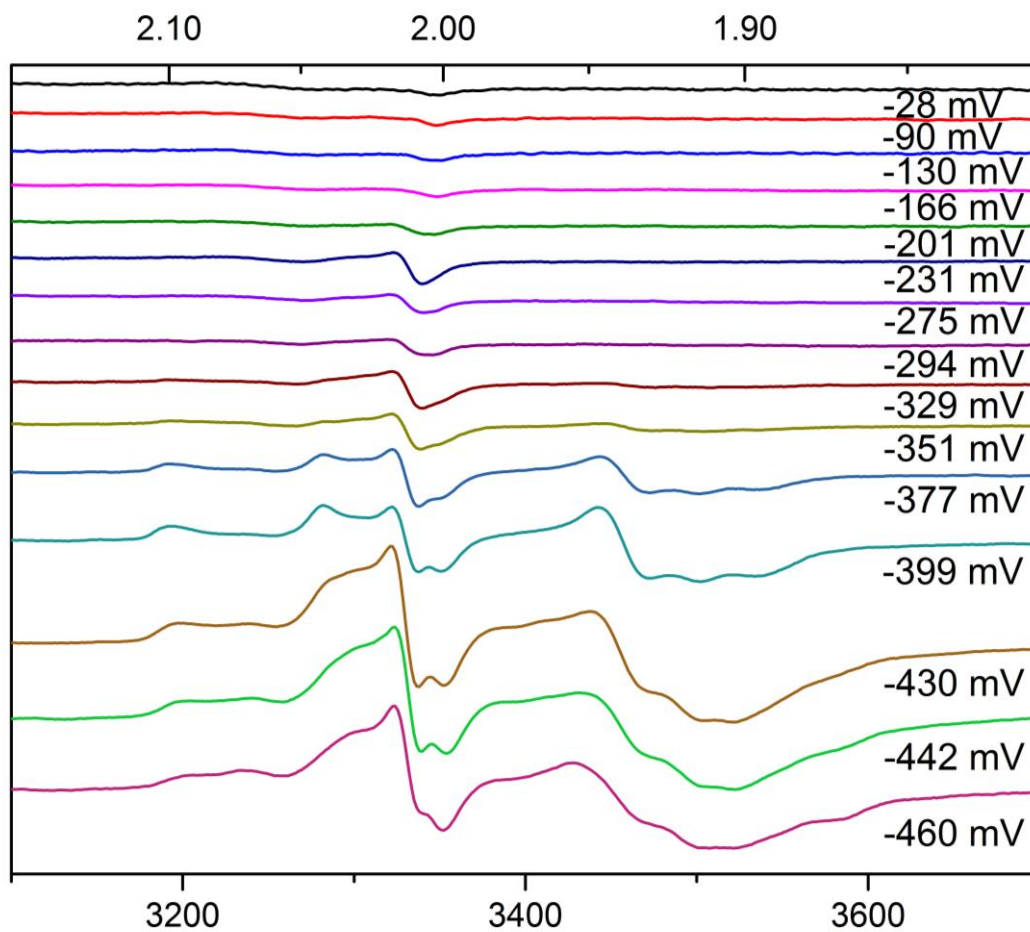
Figure 6.1 Potentiometric titration of CpII (mV potential vs SHE of each sample is displayed in the legend), with g-values displayed on the upper x-axis, and Guass displayed on the lower x-axis.
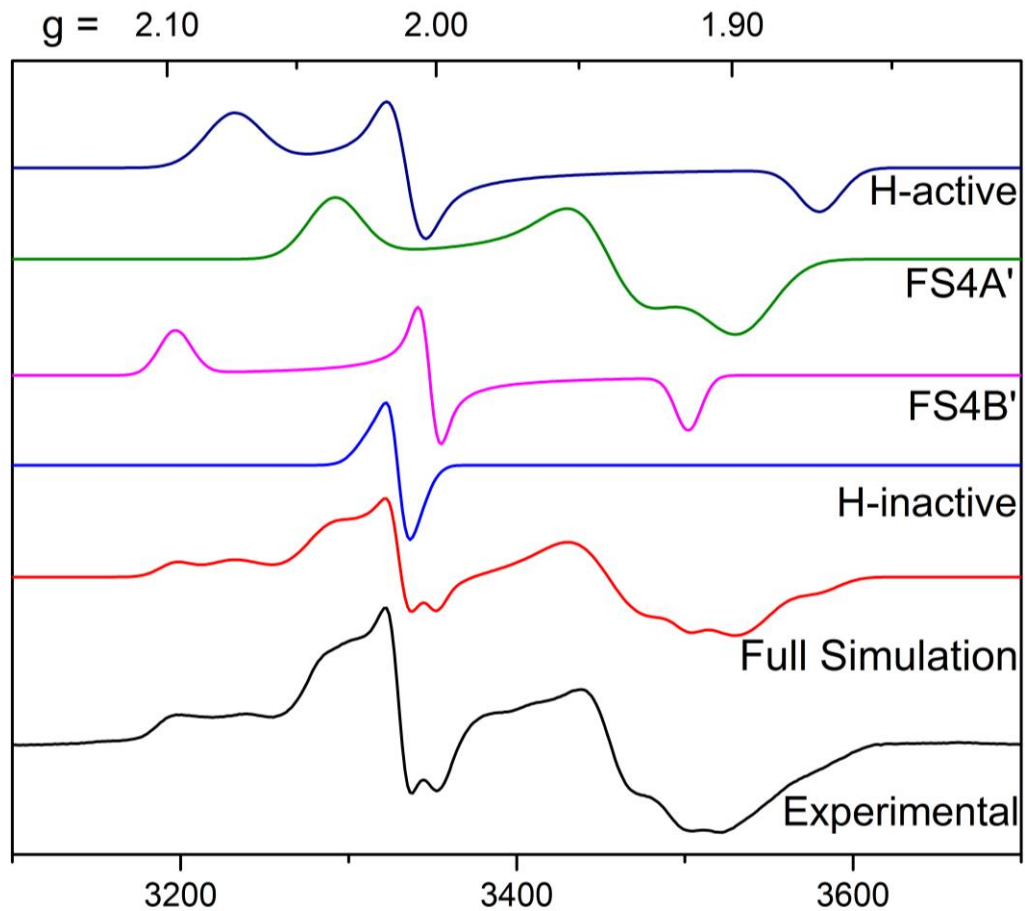
Figure 6.2 CpII deconvolution.

	Gz	Gx	Gy	G strain	G strain	G strain	Weight	Proposed cluster
Sys1	2.024	2.014	2.008	0.014	0.006	0.011	1.59	H-inact
Sys2	2.098	2.002	1.9145	0.015	0.007	0.010	11.87	FS4B'
Sys3	2.037	1.941	1.900	0.023	0.026	0.025	64.91	FS4A?
Sys4	2.075	2.011	1.872	0.025	0.012	0.015	21.64	H-act

Table 6.1. CpII deconvolution values of proposed clusters
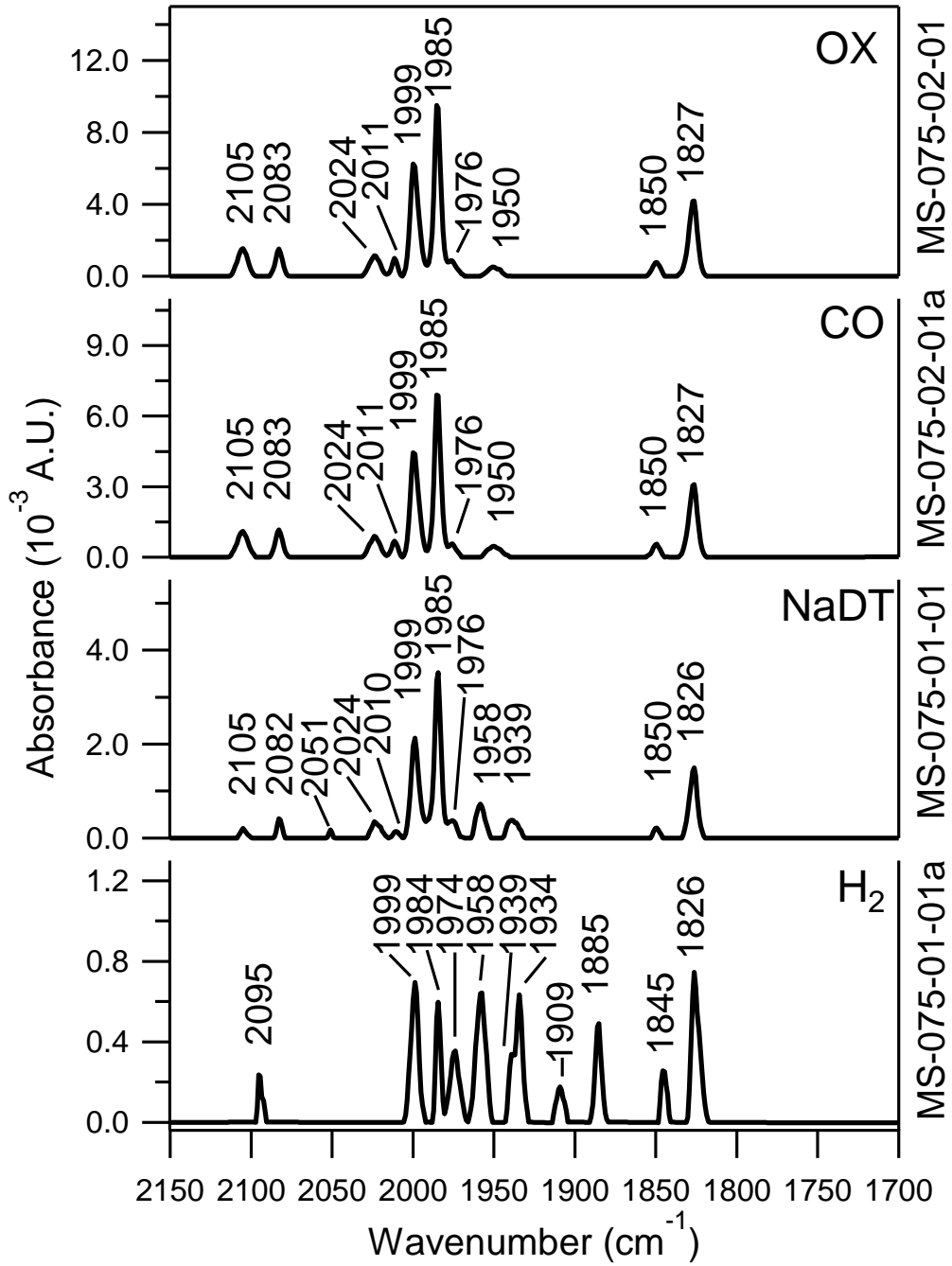
Figure 6.3 FTIR of CpII under different treatments
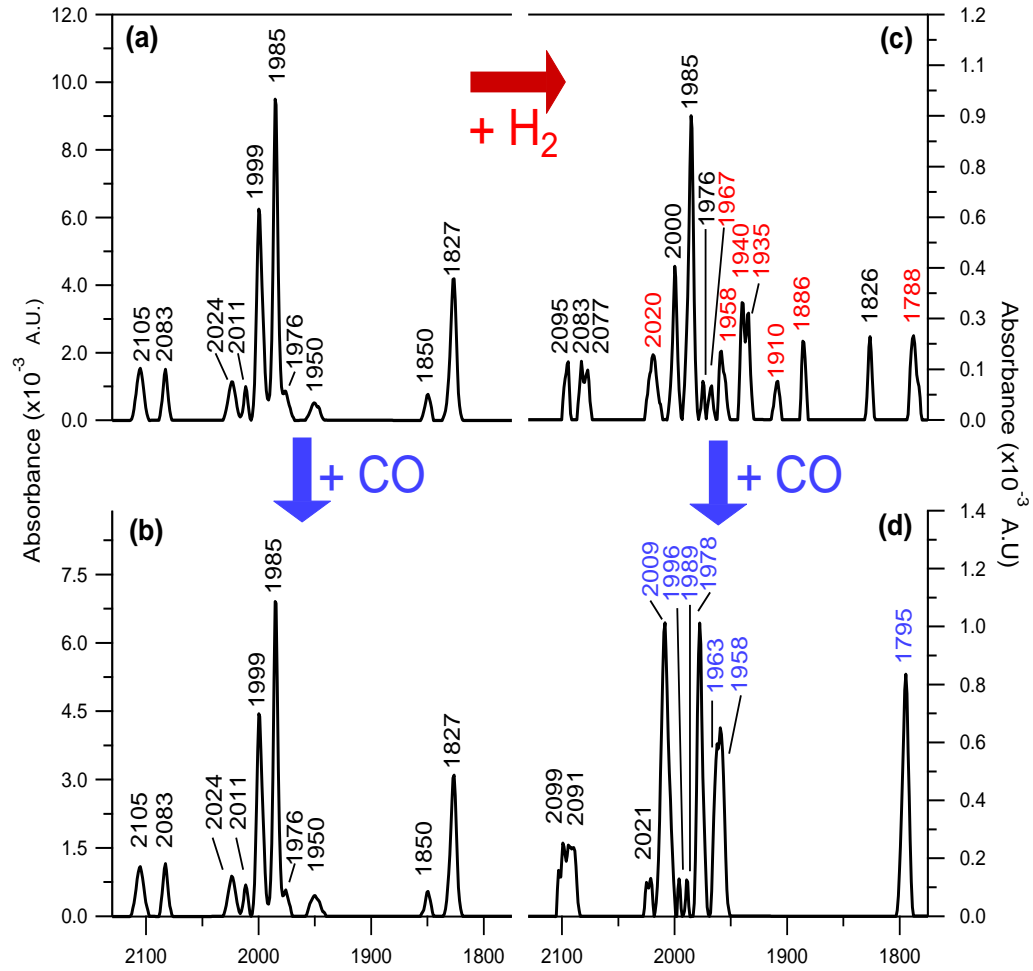
Figure 6.4: Representative FTIR spectra of CpII with varying chemical treatments. (a) As-isolated (also oxidized with thionine-not shown) when treated with CO shows no reaction (b). When activated with H_2, redox transitions are clearly seen, with new features highlighted in red (c). When subsequently treated with CO, further transitions are seen, with new features highlighted in blue (d).
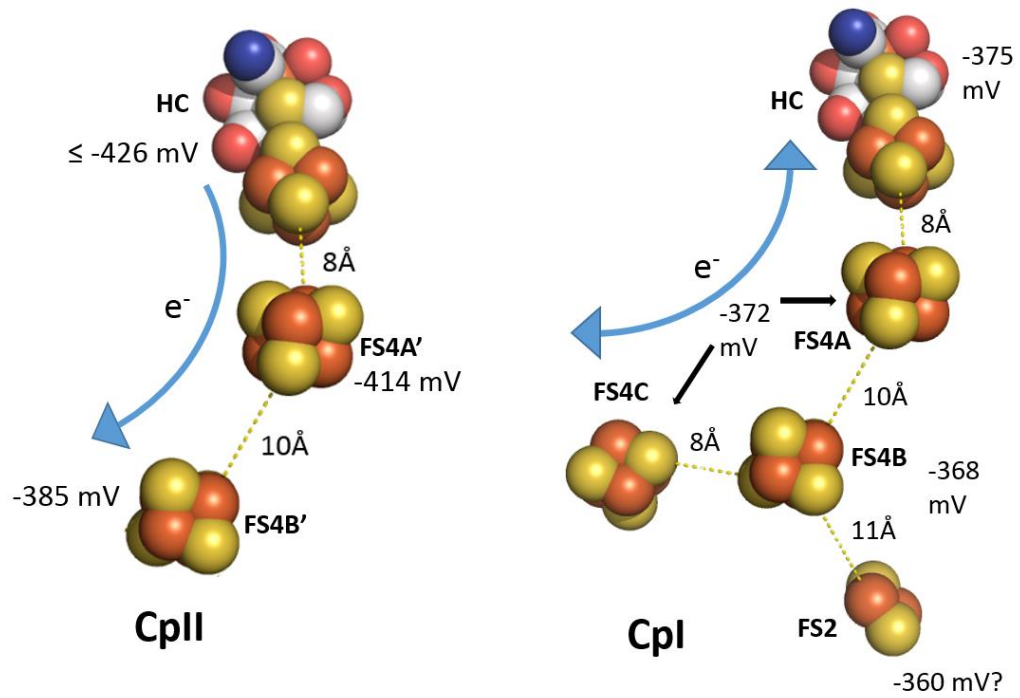
Figure 6.5 Mechanistic proposal as to how midpoint potentials of clusters influence catalytic bias

References

1.   Abou Hamdan, A.; Dementin, S.; Liebgott, P.-P.; Gutierrez-Sanz, O.; Richaud, P.; De Lacey, A. L.; Rousset, M.; Bertrand, P.; Cournac, L.; Léger, C., Understanding and Tuning the Catalytic Bias of Hydrogenase. *Journal of the American Chemical Society* **2012,** *134* (20), 8368-8371.

2.   Li, B.; Elliott, S. J., The Catalytic Bias of 2-Oxoacid:ferredoxin Oxidoreductase in CO2: evolution and reduction through a ferredoxin-mediated electrocatalytic assay. *Electrochimica Acta* **2016,** *199*, 349-356.

3.   Winogradsky, S., Recherches sure l'assimilation de l'azote libre de l'atmosphere par les microbes. *Archives des science biologique* **1895,** *3* (4), 297-352.

4.   Peters, J. W.; Lanzilotta, W. N.; Lemon, B. J.; Seefeldt, L. C., X-ray crystal structure of the Fe-only hydrogenase (CpI) from Clostridium pasteurianum to 1.8 angstrom resolution. *Science (New York, N.Y.)* **1998,** *282* (5395), 1853-8.

5.   Chen, J.-S.; Mortenson, L. E., Purification and properties of hydrogenase from Clostridium pasteurianum W5. *Biochimica et Biophysica Acta (BBA) - Protein Structure* **1974,** *371* (2), 283-298.

6.   Chen, J.-S.; Blanchard, D. K., Isolation and properties of a unidirectional H2-oxidizing hydrogenase from the strictly anaerobic N2-fixing bacterium Clostridium pasteurianum W5. *Biochemical and biophysical research communications* **1978,** *84* (4), 1144-1150.

7.   Adams, M. W.; Mortenson, L. E., The physical and catalytic properties of hydrogenase II of Clostridium pasteurianum. A comparison with hydrogenase I. *The Journal of biological chemistry* **1984,** *259* (11), 7045-55.

8.   Adams, M. W., The structure and mechanism of iron-hydrogenases. *Biochimica et biophysica acta* **1990,** *1020* (2), 115-45.

9.   Peters, J. W.; Schut, G. J.; Boyd, E. S.; Mulder, D. W.; Shepard, E. M.; Broderick, J. B.; King, P. W.; Adams, M. W. W., [FeFe]- and [NiFe]-hydrogenase diversity, mechanism, and maturation. *Biochimica et Biophysica Acta (BBA) - Molecular Cell Research* **2015,** *1853* (6), 1350-1369.

10.   Knörzer, P.; Silakov, A.; Foster, C. E.; Armstrong, F. A.; Lubitz, W.; Happe, T., Importance of the Protein Framework for Catalytic Activity of [FeFe]-Hydrogenases. *Journal of Biological Chemistry* **2012,** *287* (2), 1489-1499.

11.   Cornish, A. J.; Gartner, K.; Yang, H.; Peters, J. W.; Hegg, E. L., Mechanism of proton transfer in [FeFe]-hydrogenase from Clostridium pasteurianum. *The Journal of biological chemistry* **2011,** *286* (44), 38341-7.

12.   Lautier, T.; Ezanno, P.; Baffert, C.; Fourmond, V.; Cournac, L.; Fontecilla-Camps, J. C.; Soucaille, P.; Bertrand, P.; Meynial-Salles, I.; Leger, C., The quest for a functional substrate access tunnel in FeFe hydrogenase. *Faraday discussions* **2011,** *148*, 385-407; discussion 421-41.

13.   Mulder, D. W.; Ratzloff, M. W.; Shepard, E. M.; Byer, A. S.; Noone, S. M.; Peters, J. W.; Broderick, J. B.; King, P. W., EPR and FTIR analysis of the mechanism of H2 activation by [FeFe]-hydrogenase HydA1 from Chlamydomonas reinhardtii. *J Am Chem Soc* **2013,** *135* (18), 6921-9.

14.   King, P. W.; Posewitz, M. C.; Ghirardi, M. L.; Seibert, M., Functional Studies of [FeFe] Hydrogenase Maturation in an Escherichia coli Biosynthetic System. *Journal of bacteriology* **2006,** *188* (6), 2163-2172.

15.   Stoll, S., Chapter Six-CW-EPR Spectral Simulations: Solid State. *Methods in enzymology* **2015,** *563*, 121-142.

CHAPTER 7

POINT MUTATIONS IN CPI AND CPII ALTER CATALYTIC BIAS AS MEASURED
BY ELECTROCHEMISTRY

Introduction

Hydrogenases have long been studied via protein film electrochemistry (PFE)[1], due to the wealth of information the technique is capable of providing. At a basic level, the electrochemistry provides a readout of activity as a function of potential, which, in the case of hydrogenases, relates directly to either proton reduction or hydrogen oxidation[2] (Figure 7.1). Enzyme is directly deposited onto an electrode, which immobilizes it and allows activity to be monitored as a function of the known applied potential[3]. PFE is able to provide insights about catalytic bias (does the enzyme favor hydrogen production or hydrogen oxidation?), information about the Km's of gaseous substrates (H_2, O_2, and CO), and provides a simple platform for measuring hydrogenases across a range of other conditions, including pH and temperature[2-4]. PFE is therefore able to provide a detailed set of information about hydrogenases, with the additional advantage that it requires very little sample volume. Mecahnistic details may also be gleaned from the shape of circular voltammetry traces[5]. One drawback, however, is that the exact amount of sample that adheres to the elctrode is not known[6], making it intractable to directly measure certain kinetic parameters.

Traditional [FeFe]-hydrogenases are thought to function as CaI, which shares 71% identity with the crystallographically characterized CpI[7-8]. CaI hydrogenase is excellent at proton reduction when adhered to the electrode[9], performs substantially less

well at hydrogen oxidation and is fully reversible. This suggest CpI ought to behave in a similar manner, though despite being a main hydrogenase of study, significant electrochemical characterization has not previously been performed. Depending on the pH, a typical E_m may be around -400 mV for the hydrogen couple[10]. Although certain [FeFe]-hydrogenases have been thoroughly characterized[9, 11], the breadth of natural hydrogenase variation is as of yet poorly researched, although it is clear that CaI and related enzymes do not represent the only catalytic profiles for [FeFe]-hydrogenases, with some known to prefer hydrogen oxidation to a greater or lesser degree.
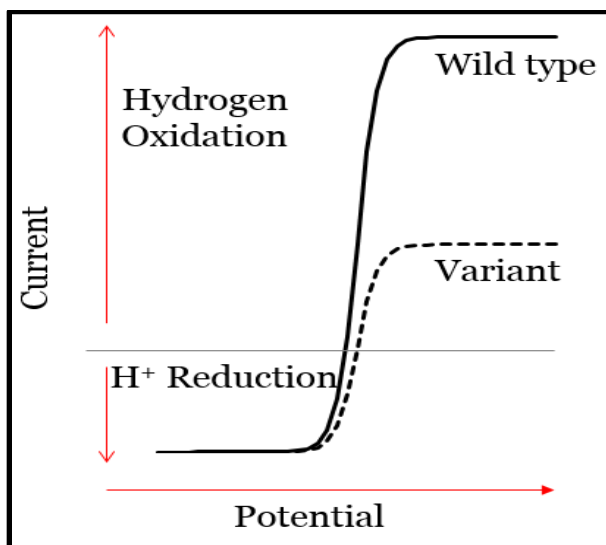
Figure 7.1. Idealized electrochemical data for two proteins with a different catalytic bias

In this work PFE was first employed on purified CpI and CpII hydrogenases. Targeted amino acid variations were then introduced in order to deliberately shift the catalytic bias, or the electrochemical readout from the electrode, from CpI-like to CpII-like, or the reciprocal, from CpII-like to CpI-like. While a variety of other redox tuning experiments have been employed in different enzymes[12-14], the CpI/CpII model system

represents a fascinating case study for the contributors to catalytic bias, given the overall

sequence similarity of the hydrogenases[15]. PFE represents an ideal technique for the

study of the variants, as it provides a rapid readout with only minimal sample.

Methods

Bioinformatic Network Analysis

All the homologous sequences of CpI and CpII (n=714) that were extracted using

the Integrated Microbial Genomes (IMG)[16] were subjected to multiple sequence

alignment using standalone clustalw[17] with default settings. Only residues that varied

between both CpI and CpII in the second coordination sphere of the cofactors were

considered for further network analysis. A binary table was generated to identify the

presence or absence of the residues identified in CpI and CpII in all the 714 homologs[18].

A Pearson correlation was then calculated to determine the highly correlated residues in

both CpI and CpII using the plugin Network Analyzer present in Cytoscape[19]. Cytoscape

was used to generate the network using the correlation matrix generated earlier. A force

directed organic layout was used to visualize the network in Cytoscape. Each unique

identified residue was denoted as node while the edges between nodes represent the

degree of correlation between the nodes.

Mutagenesis Experiments:

Initial mutagenesis was carried out on CpI to make it more CpII-like, that is, make

the variant a better hydrogen oxidizer than the WT CpI. Three residues near the active

site, M353, I268, and A230, were chose for mutation due to their proximity to the active site, and their strong phylogenetic conservation. Forward and reverse primers were designed to separately introduce each of these mutations into the CpI plasmid that was already in use in the lab. The successful introduction of each mutation into CpI was verified through sequencing of the plasmid (Davis), resulting in three distinct CpI to CpII-like individual variants: M353T, I268T, and A230S.

The second generation of experiments were done by ordering an expression plasmid with the desired mutations introduced directly into the strep-tagged hydrogenase sequence (GenScript). Sequencing data was sent with each gene as quality control. The network analysis was used to examine which amino acids may be most likely to confer either CpI-like or CpII-like properties, and these amino acids were chose for experiments. CpI was made more CpII-like by the introduction of three CpII-type amino acids around the H-cluster, for CpI I268T S357A N505G (CpI TAG). CpII was made CpI-like by I325Q L326Q T353M (CpII QQM) mutations around the H-cluster. (Numbering according to alignment with CpI sequence).

Protein Purification:

The purification of both CpI and CpII hydrogenases were carried out as described previously. The variant hydrogenases were purified according to the most closely related WT enzyme. CpI A230S, CpI I268T, CpI M353T, and CpI TAG were purified according to the CpI protocol, while CpII QQM was purified according to the CpII protocol.

Electrochemistry

Electrochemistry was carried out under anaerobic conditions at 25 °C

using a Pyrolytic Graphite Electrode (PGE) rotating at 3500 RPM. Conditions

where not otherwise indicated are pH 8, and a scan rate of 20 mV/S.

Results and Discussion

Electrochemistry of CpI and CpII

Initial experiments were performed in order to provide a baseline

characterization of both CpI and CpII (Figure 7.2). CpI was found to behave as a

canonical [FeFe]-hydrogenase, with a strong bias towards proton reduction, and a

fully reversibly cyclic voltammogram (CV). In contrast, CpII was found to

oxidatively inactivate at relatively mild potentials (-200 mV vs SHE), and could

then be reactivated at more negative potentials (more reducing conditions).

To further pursue the ability of CpII to oxidatively inactivate in comparison to

CpI, additional CV scans were performed with varying scan rates (Figure 7.3). Cyclic

voltammograms of CpI and CpII at different scan rates show that CpII inactivates on a

faster timescale (i.e. at faster scan rates). CpI was found to oxidatively inactivate at

substantially harsher conditions than required to oxidatively inactivate CpII, with slower

scan rates and more positive potentials required for inactivation.. The bottom panel shows

the ease of which CpII oxidatively inactivates and the complex reactivation process

which may occur at two different potentials (one occurring at approximately -200

mV and the other at approximately -450 mV). The oxidative inactivation of CpII is in agreement with the EPR and FTIR data previously collected, and suggests that CpII is mechanistically distinct from CpI.
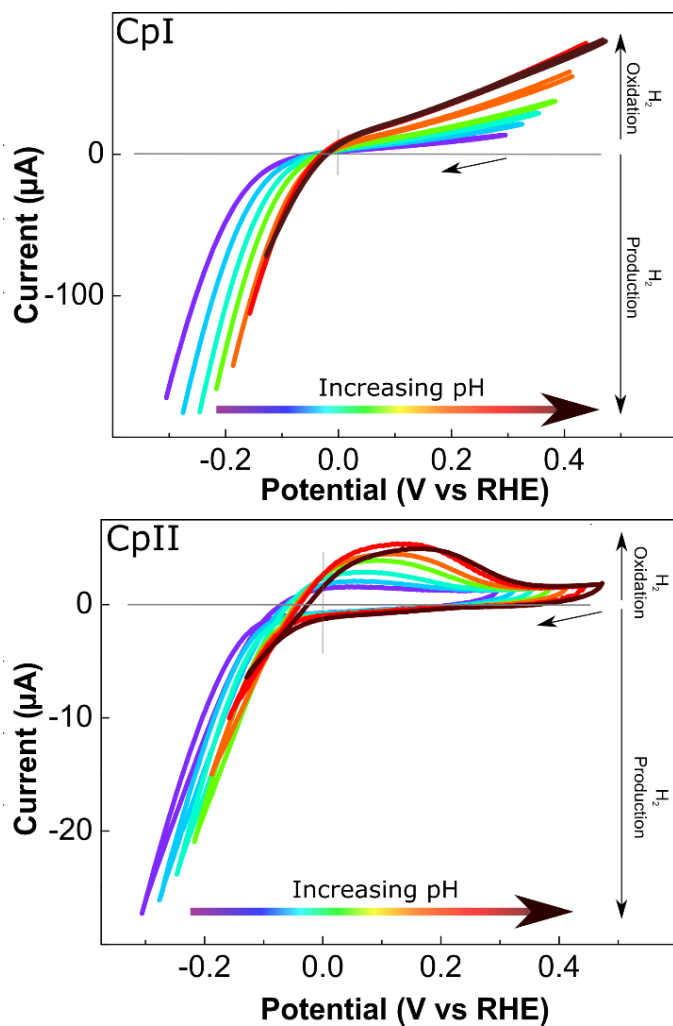
Figure 7.2. Cyclic voltammograms of CpI (top panel) and CpII (bottom panel) immobilized on a PGE under 1 atm hydrogen at various pH values (spanning the range from pH 8.0 to pH 5.0 in intervals of 0.5 pH units. Other experimental conditions are: 25°C, electrode rotation rate 3500 rpm, potential scan rate 20 mV s^{-1}. Arrows indicate the point and direction at which potential cycling commences.
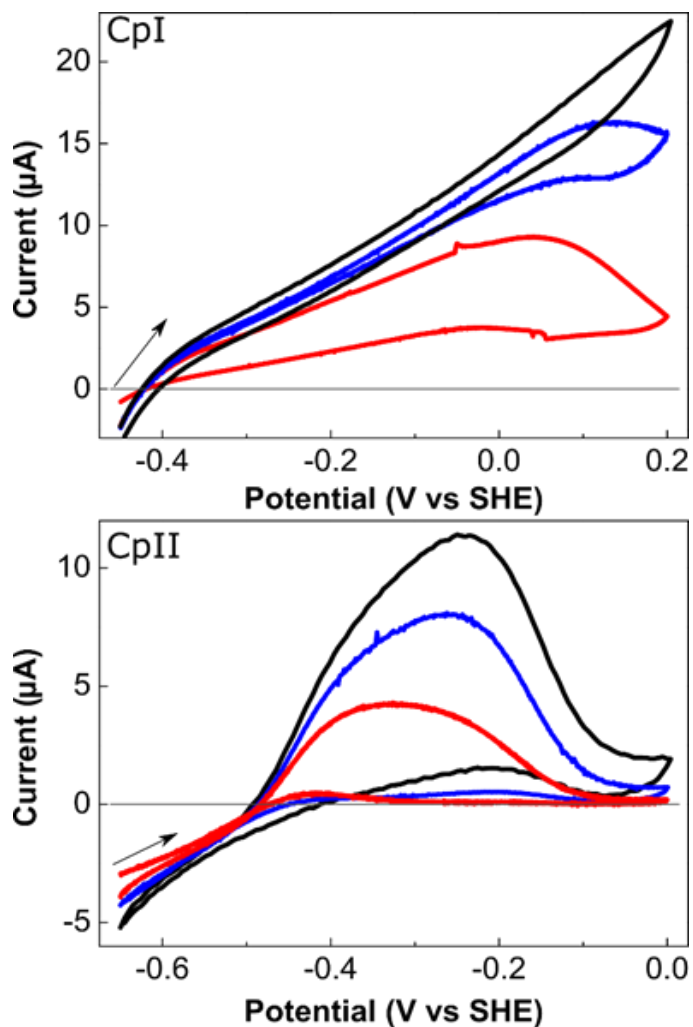
Figure 7.3. Cyclic voltammograms of CpI (top panel) and CpII (bottom panel) immobilized on a PGE under 1 atm hydrogen at various potential scan rates (spanning from 20 mV s^{-1} (black), 10 mV s^{-1} (blue), to 0.1 mV s^{-1} (red) for CpI (top) or CpII (bottom). Other experimental conditions are: T = 25°C, electrode rotation rate 3500 rpm, at pH 7.0 for CpI and pH 8.0 for CpII. Arrows indicate the point and direction at which potential cycling commences.

Electrochemistry of CpI Variants

CpI A230S, I268T, and M353T were compared to WT CpI (Figure 7.4).

Qualitatively, the electrocehmical traces were very similar, indicating that the hydrogen

catalysis is likely the same mechanism for the variant enzymes as the wild type.

However, in the case of all three variants, the amino acid substitutions reduced catalytic activty to a substantial degree, with CpI I268T and M353T retaining very little activity. This result is surprising, given that each amino acid change was among the natural variations found at those positions among the different [FeFe]-hydrogenases. To further determine the cause for the lower activities among the variants, we measured the K_m for H_2 for the native and variant forms of CpI (Figure 7.5). The K_m's were measured by chronoamperometry, where the current is measured as a function of time, in this case, oxidative current under H_2 is examined.
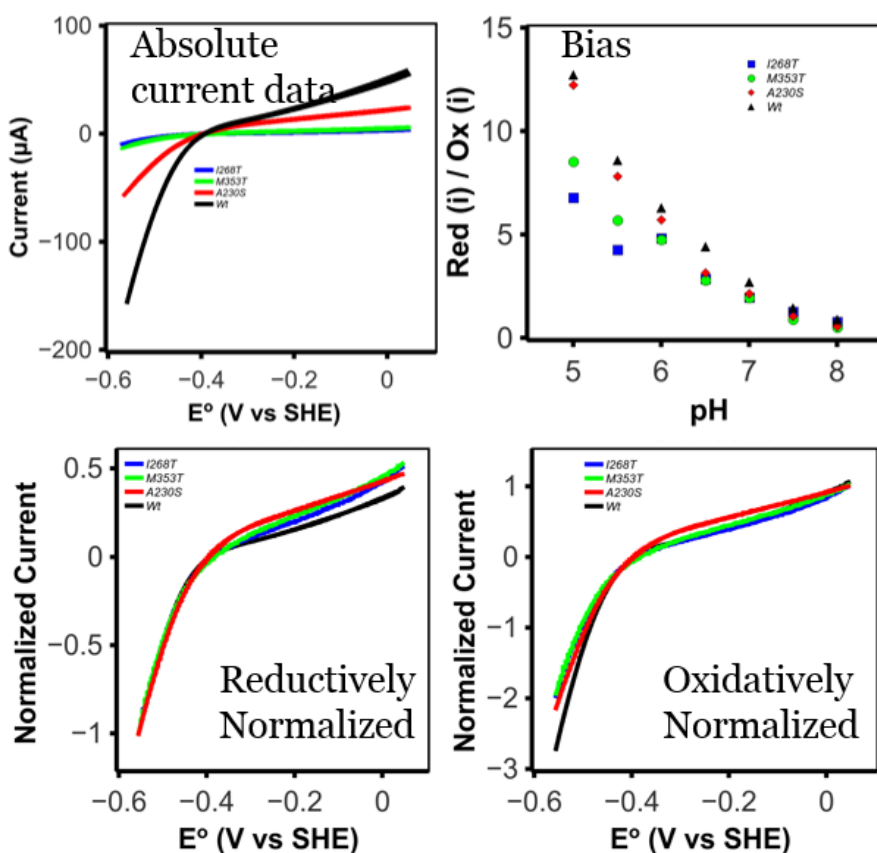
Figure 7.4. Continuous wave voltammograms of CpI and variants, with relative catalytic bias plotted in the top right figure. Absolute current in the top left depicts the decrease in current among the variant enzymes, while the bottom two traces show normalized current.
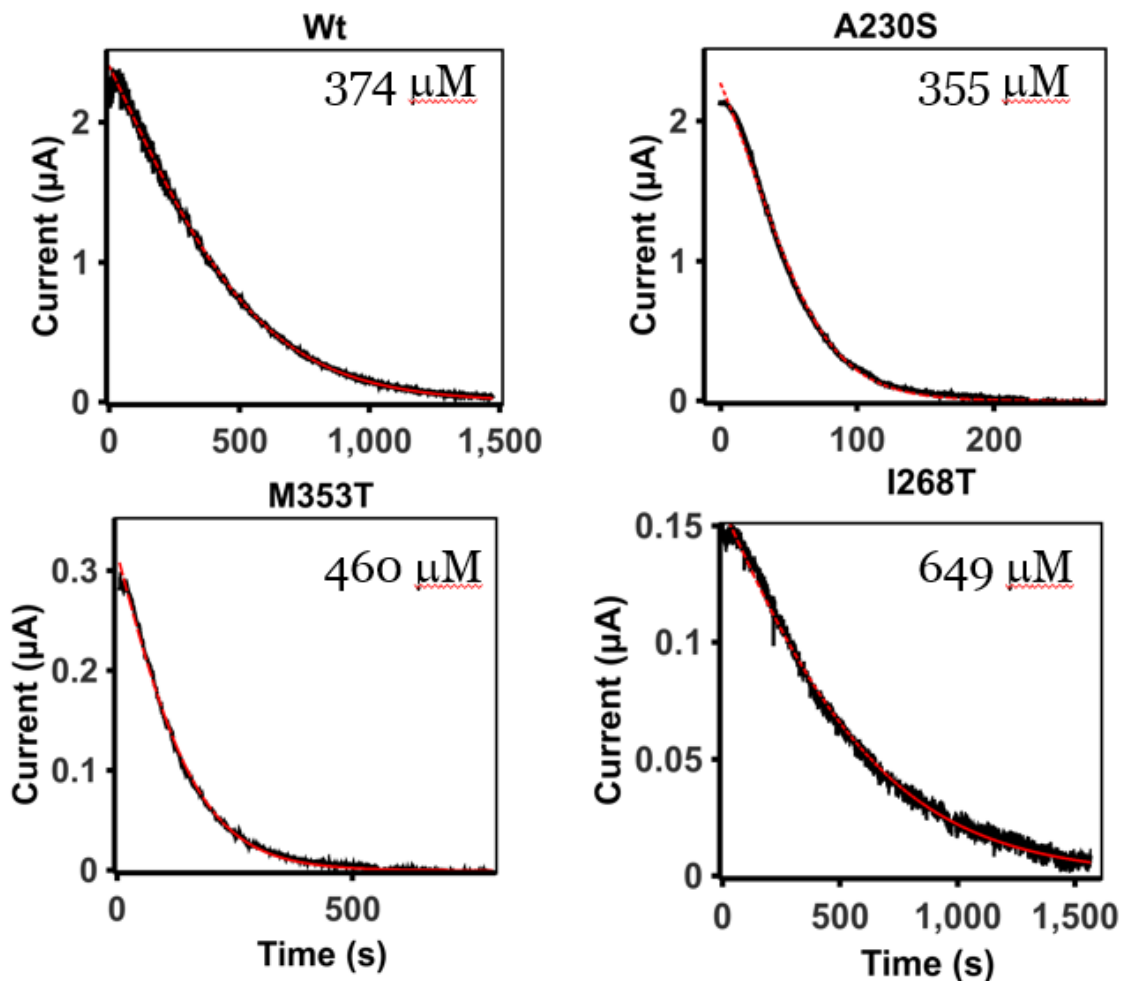
Figure 7.5. Chronoamperometry plots depicting the K_m of H_2 in WT CpI and the three CpI variants.

The K_m's measured for the WT CpI and A230S, I268T, and M353T variants, respectively, were 374, 355, 649, and 460 µM. The values are all close to the solubility limit of H_2 in aqueous solutions, and therefore represent lower limits for K_m values. The relatively similar K_m values suggests that the reduced activity among the variants is due to a K_{cat} effect, where the enzymatic turnover is lower among the variants.

Introduction of Multiple Variants to CpI and CpII

That single amino acid variants did not shift the catalytic bias of CpI towards that of CpII suggests that individual amino acid substitutions are not enough to change the bias of these enzymes, rather, suites of mutations are necessary in order to tune them. Thus, a network analysis was undertaken in order to predict which amino acids may work in concert to tune the second coordination sphere of the H-cluster (Figure 7.6). In total 14 residues from the second coordination sphere were in CpI and CpII, and the interrelatedness of these residues was hypothesized to be responsible for bias tuning.

For the first sets of variants based on the cluster analysis, suits of residues in CpI that were evolutionarily conserved (>50%) were considered. The amino acids most strongly conserved and found together in CpI homologs were Q325, Q326, and M353. It was therefore hypothesized that these three amino acids are integral to the ability of CpI to function as it does as a proton reducer. Thus, these three amino acids were substituted into CpII to make CpII more CpI-like.
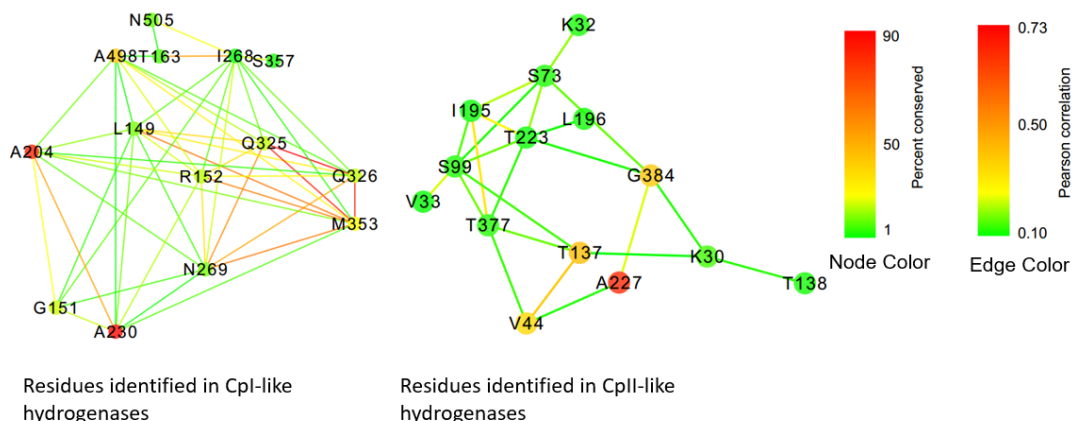
Fig 7.6. Network map depicting the covariance of 14 residues identified around the iron-sulfur cluster in the CpI (left panel) and CpII (right panel) hydrogenase. Each unique residue identified is given as a node and the edges between the nodes represent significantly correlated residues. Node color represents the percent conserved when compared to the entire genomes while edge color represents the Pearson correlation between each residue.

Similarly, the H-cluster coordination environment amino acids in the CpII family that were highly correlated and evolutionarily conserved (>50%) were T137, A227, and G384. These three amino acids are hypothesized to confer superior hydrogen-oxidizing catalytic abilities, and were therefore introduced into a single CpI variant in order to test whether these would increase H_2 oxidation activity. Both the CpI TAG and CpII QQM enzymes were then purified and subjected to PFE experiments.
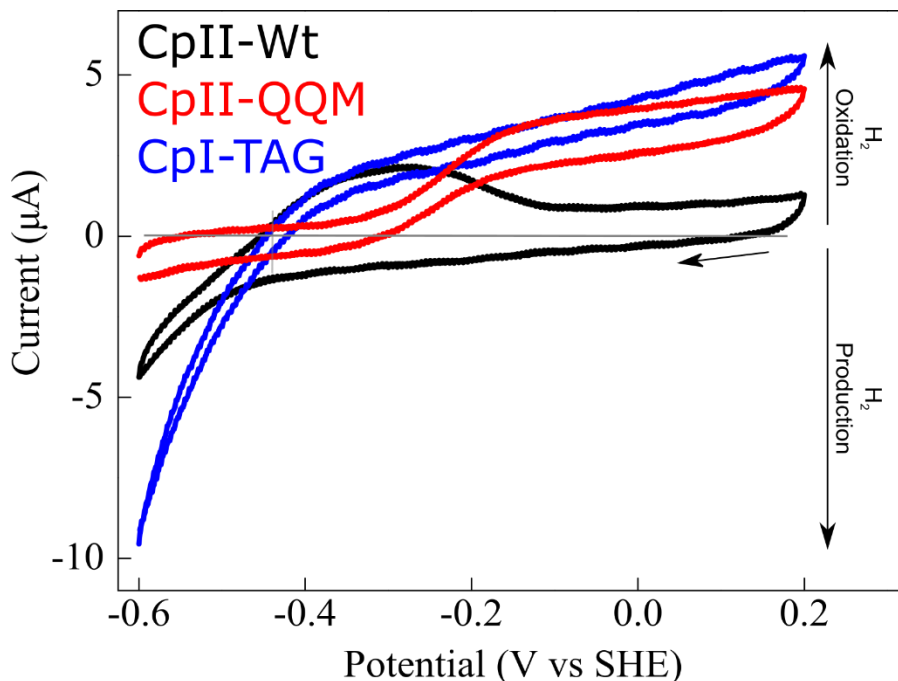
Figure 7.7 The cyclic voltammetry plot of CpII WT (black) is compared to CpII QQM (red) and CpI TAG (blue)

The CpI to CpII-like CpI TAG variant has an electrochemistry trace that qualitatively resembles that of CpI WT (Figure 7.7), or the individual amino acid substitutions as described previously. The activity, however, is lower than the WT enzyme. These three amino acids are therefore insufficient to alter the catalytic bias of CpI towards H2 oxidation activity. Thus, it may be the case that additional amino acids in the H-cluster environment are necessary to confer H2 oxidation bias, or it may be that amino acids in the F-cluster environment act to tune the potential of the F-clusters, thereby influencing catalytic bias. Probably the F- and H-cluster environments work in concert to direct electrons to and from the active site.
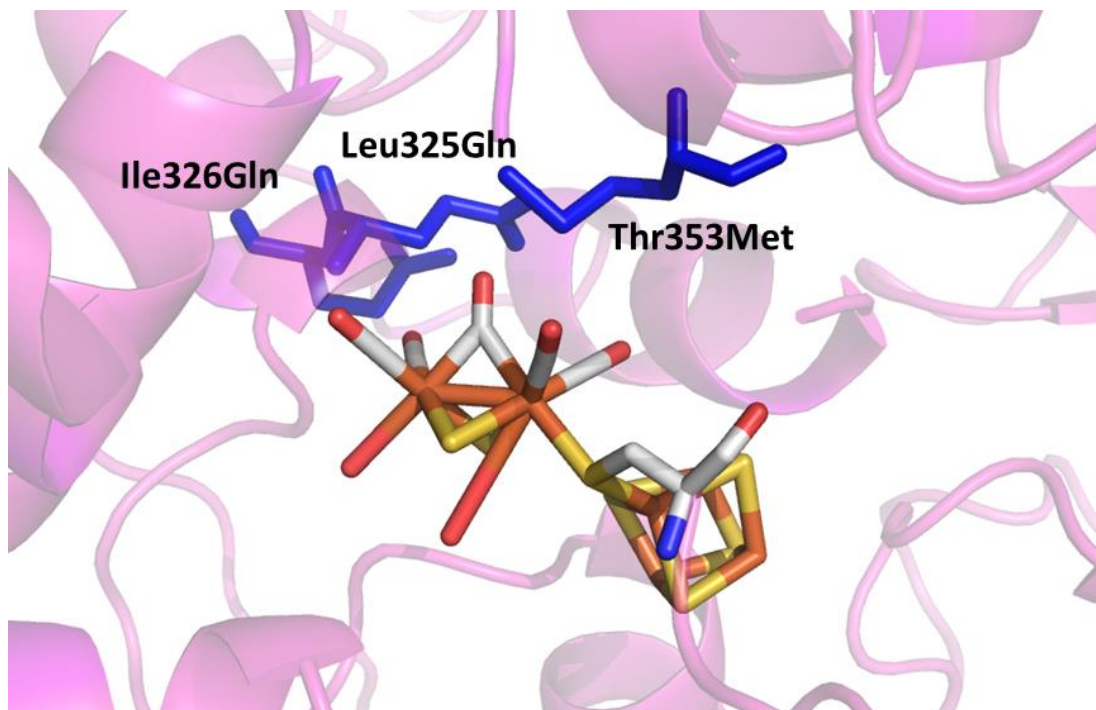
Fig 7.8. The H-cluster environment of CpII, showing the CpI-type amino acids in blue. These amino acids eliminate oxidative inactivation and bias the hydrogenase towards hydrogen oxidation

The CpII QQM variant was tuned in its catalytic bias to a significant degree compared to WT CpII (Figure 7.7). As evidenced by the electrochemical trace, the oxidative inactivation that is found in CpII was fully eliminated in CpII QQM, and is, in that regard, functionally much more similar to CpI in its function. However, CpII QQM is still a poor proton reducer, in contrast to CpI, which suggests that a combination of other amino acid substitutions in the H-cluster and/or F-cluster environments are needed to fully alter the catalytic profile. It should be noted that extended range effects cannot be ruled out in either case. That CpII QQM functionally lacks the ability to reduce protons in comparison to its ability to oxidize hydrogen suggests that the catalyst is highly biased, that is, it is nearly unidirectional. It is interesting to note that this hydrogenase behaves

very differently from what has previously observed biologically, and it represents an

excellent case study for further probing the determinants of either hydrogen oxidation or

proton reduction in [FeFe]-hydrogenases. Furthermore, CpII QQM may represent a key

catalyst for hydrogen oxidation, as in the use of fuel cells or other potential applications.

A depiction of the CpII QQM variant may be found in figure 5.8

References

1.   Lubitz, W.; Ogata, H.; Rüdiger, O.; Reijerse, E., Hydrogenases. *Chemical reviews* **2014,** *114* (8), 4081-4148.

2.   Armstrong, F. A.; Evans, R. M.; Hexter, S. V.; Murphy, B. J.; Roessler, M. M.; Wulff, P., Guiding Principles of Hydrogenase Catalysis Instigated and Clarified by Protein Film Electrochemistry. *Accounts of Chemical Research* **2016,** *49* (5), 884-892.

3.   Evans, R. M.; Armstrong, F. A., Electrochemistry of Metalloproteins: Protein Film Electrochemistry for the Study of E. coli [NiFe]-Hydrogenase-1. In *Metalloproteins: Methods and Protocols*, Fontecilla-Camps, J. C.; Nicolet, Y., Eds. Humana Press: Totowa, NJ, 2014; pp 73-94.

4.   Vincent, K. A.; Parkin, A.; Lenz, O.; Albracht, S. P. J.; Fontecilla-Camps, J. C.; Cammack, R.; Friedrich, B.; Armstrong, F. A., Electrochemical Definitions of O2 Sensitivity and Oxidative Inactivation in Hydrogenases. *Journal of the American Chemical Society* **2005,** *127* (51), 18179-18189.

5.   Morra, S.; Valetti, F.; Sadeghi, S. J.; King, P. W.; Meyer, T.; Gilardi, G., Direct electrochemistry of an [FeFe]-hydrogenase on a TiO2 Electrode. *Chemical Communications* **2011,** *47* (38), 10566-10568.

6.   Butt, J. N.; Filipiak, M.; Hagen, W. R., Direct electrochemistry of Megasphaera elsdenii iron hydrogenase. Definition of the enzyme's catalytic operating potential and quantitation of the catalytic behaviour over a continuous potential range. *European journal of biochemistry / FEBS* **1997,** *245* (1), 116-22.

7.   King, P. W., Designing interfaces of hydrogenase–nanomaterial hybrids for efficient solar conversion. *Biochimica et Biophysica Acta (BBA) - Bioenergetics* **2013,** *1827* (8–9), 949-957.

8.   Peters, J. W.; Lanzilotta, W. N.; Lemon, B. J.; Seefeldt, L. C., X-ray crystal structure of the Fe-only hydrogenase (CpI) from Clostridium pasteurianum to 1.8 angstrom resolution. *Science (New York, N.Y.)* **1998,** *282* (5395), 1853-8.

9.   Madden, C.; Vaughn, M. D.; Díez-Pérez, I.; Brown, K. A.; King, P. W.; Gust, D.; Moore, A. L.; Moore, T. A., Catalytic Turnover of [FeFe]-Hydrogenase Based on Single-Molecule Imaging. *Journal of the American Chemical Society* **2012,** *134* (3), 1577-1582.

10.   Adams, M. W., The structure and mechanism of iron-hydrogenases. *Biochimica et biophysica acta* **1990,** *1020* (2), 115-45.

11.   Parkin, A.; Cavazza, C.; Fontecilla-Camps, J. C.; Armstrong, F. A., Electrochemical investigations of the interconversions between catalytic and inhibited states of the [FeFe]-hydrogenase from Desulfovibrio desulfuricans. *J Am Chem Soc* **2006,** *128* (51), 16808-15.

12.   Marshall, N. M.; Garner, D. K.; Wilson, T. D.; Gao, Y. G.; Robinson, H.; Nilges, M. J.; Lu, Y., Rationally tuning the reduction potential of a single cupredoxin beyond the natural range. *Nature* **2009,** *462* (7269), 113-6.

13.   Bhagi-Damodaran, A.; Petrik, I. D.; Marshall, N. M.; Robinson, H.; Lu, Y., Systematic Tuning of Heme Redox Potentials and Its Effects on O2 Reduction Rates in a Designed Oxidase in Myoglobin. *Journal of the American Chemical Society* **2014,** *136* (34), 11882-11885.

14.   Liu, J.; Chakraborty, S.; Hosseinzadeh, P.; Yu, Y.; Tian, S.; Petrik, I.; Bhagi, A.; Lu, Y., Metalloproteins Containing Cytochrome, Iron–Sulfur, or Copper Redox Centers. *Chemical reviews* **2014,** *114* (8), 4366-4469.

15.   Adams, M. W., The mechanisms of H2 activation and CO binding by hydrogenase I and hydrogenase II of Clostridium pasteurianum. *The Journal of biological chemistry* **1987,** *262* (31), 15054-61.

16.   Markowitz, V. M.; Chen, I.-M. A.; Palaniappan, K.; Chu, K.; Szeto, E.; Grechkin, Y.; Ratner, A.; Jacob, B.; Huang, J.; Williams, P.; Huntemann, M.; Anderson, I.; Mavromatis, K.; Ivanova, N. N.; Kyrpides, N. C., IMG: the integrated microbial genomes database and comparative analysis system. *Nucleic Acids Research* **2012,** *40* (D1), D115-D122.

17.   Larkin, M. A.; Blackshields, G.; Brown, N. P.; Chenna, R.; McGettigan, P. A.; McWilliam, H.; Valentin, F.; Wallace, I. M.; Wilm, A.; Lopez, R.; Thompson, J. D.; Gibson, T. J.; Higgins, D. G., Clustal W and Clustal X version 2.0. *Bioinformatics (Oxford, England)* **2007,** *23* (21), 2947-8.

18.   Assenov, Y.; Ramírez, F.; Schelhorn, S.-E.; Lengauer, T.; Albrecht, M., Computing topological parameters of biological networks. *Bioinformatics (Oxford, England)* **2008,** *24* (2), 282-284.

19.   Smoot, M. E.; Ono, K.; Ruscheinski, J.; Wang, P. L.; Ideker, T., Cytoscape 2.8: new features for data integration and network visualization. *Bioinformatics (Oxford, England)* **2011,** *27* (3), 431-2.

CHAPTER 8

CONCLUDING REMARKS

The formation of reduced end products is of critical importance for nearly all facets of civilization. As dependency on energy grows, it becomes increasingly important to develop clean and efficient catalysts, however, many current catalysts perform equally well under both the forward and reverse directions for a reaction. By creating a catalyst that has a strong preference for a forward reaction, thereby eliminating the back reaction, end products may be accumulated much more easily.

In this work [FeFe]-hydrogenases are examined as a model system in which to study catalytic bias, specifically, which structural features contribute to the production or consumption of H_2 gas. The mechanistic understandings from this work may be generalizable across various systems, including the reduction of dinitrogen to ammonia gas, which is critical for fertilizer, or the reduction of carbon dioxide to various reduced organic compounds.

Having introduced hydrogenases, in the next chapter a description of the oxygen degradation of *Chlamydomonas reinhardtii* [FeFe]-hydrogenase was presented. The oxygen intolerance of hydrogenase is currently one of the main mechanistic inhibitors to biological hydrogen production. This work demonstrates that minimal oxygen damage to the active site may be overcome.

In the third chapter, the background model system of CpI and CpII [FeFe] hydrogenases were described, wherein the metabolic contexts and sequences of these

hydrogenases are discussed in detail. This study lays the groundwork for understanding how to relate the spectroscopic and biochemical properties back to typical hydrogen metabolism. This system is further illustrative of how biology has exploited catalytic bias in order to optimize electron flow under differing metabolic conditions.

In the next three chapters, the spectroscopic characterization of CpI and CpII are further illuminated, demonstrating novel properties of both CpI and CpII. The spectroscopy has been used to develop a mechanistic model for the catalytic bias observed in this model system, where CpII is capable of shutting down enzyme activity if the hydrogen uptake is not advantageous to the system. The ability to express and purify CpII, combined with the advanced EPR characterization and spectral deconvolution methods, represent a major advance in the ability to relate the properties of multiple EPR centers back to catalytic properties.

In the final chapter the electrochemistry of CpI and CpII are outlined in great detail, demonstrating further evidence of the unique capabilities of these enzymes, and the conditions under which they function. Finally, it is demonstrated that changing the catalytic properties of these enzymes requires concerted amino acid changes, but, by changing a few key residues, the catalytic bias of the hydrogenase may be profoundly shifted. This represents a fertile area for additional research, where hypotheses derived from bioinformatics analyses may directly lead to innovation in catalysis design and properties.

Cumulatively, this research has furthered an understanding of elements that contribute to electron flow through enzymes, with dramatic implications for the design of synthetic catalysts.

APPENDICES

APPENDIX A

SUPPLEMENTAL MATERIAL TO CHAPTER 2
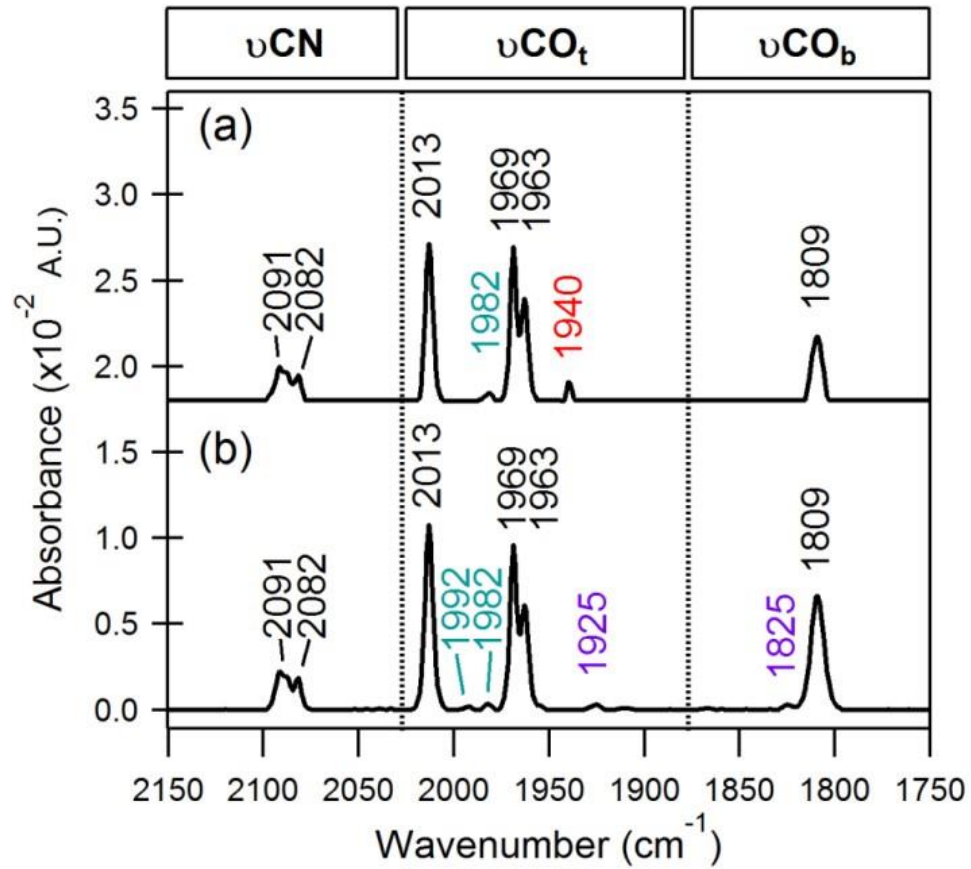
Figure s1. FTIR spectra of CrHydA1 H_{ox}-CO before (a), and after (b) 2 h exposure to 24.2% O_2 at 4 °C. CrHydA1 concentration 70 mg^{-1} ml^{-1}. The principle νCO peaks are colored as Hox-CO (black), H_{ox} (red), O_2 damaged (purple), unassigned (cyan).
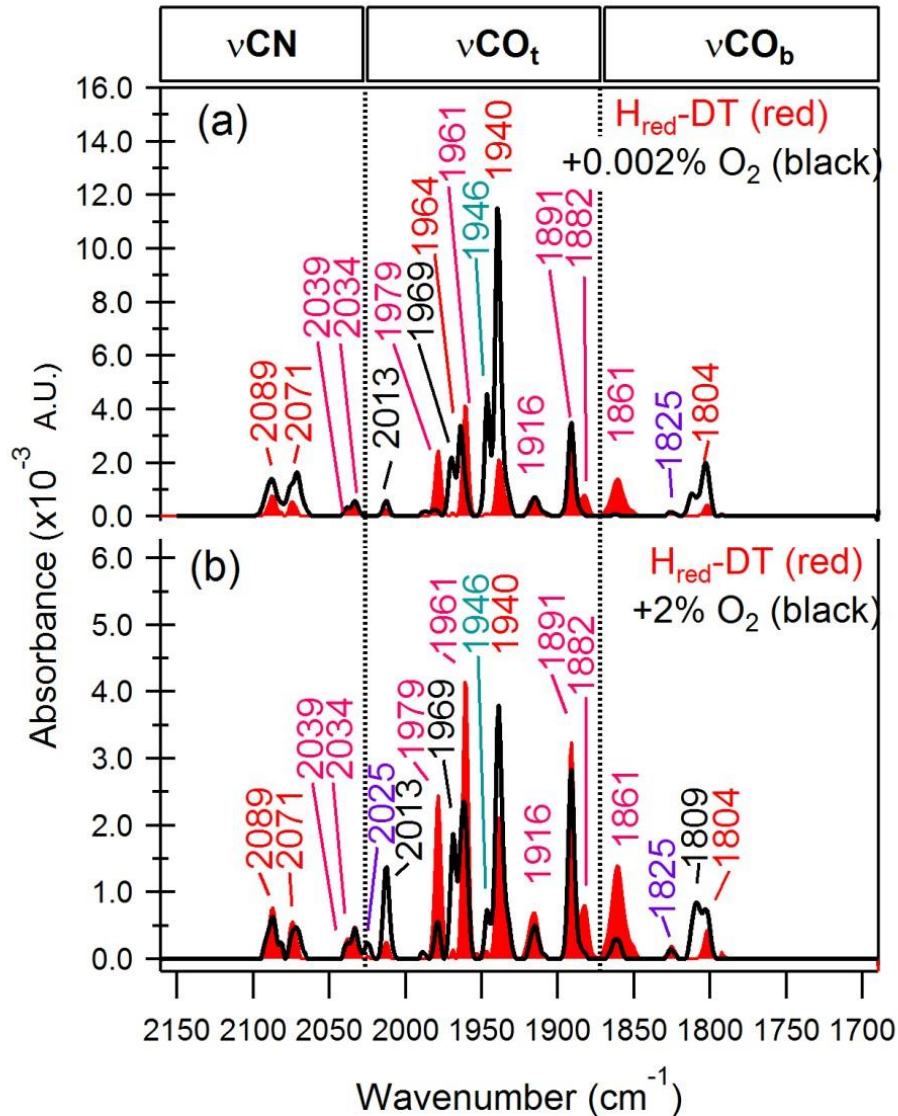
Figure S2. FTIR spectra of O₂ titration of NaDT-treated CrHydA1. (a) After 2 h of exposure to 0.002% O₂. (b) After 2 h exposure to 2% O₂. While there are additional features that may be a result of the interaction of NaDT and O₂, similar trends are observed here as seen in H_{ox} experiments. The growth of H_{ox}-CO and of signals assigned to O₂ damage, (1825 and/or 2025 cm⁻¹) are seen here. The vCO and vCN peaks are colorcoded as; H_{ox}-CO (black), H_{ox} (red), H_{red}-DT (magenta) O₂ damaged (purple), unassigned (cyan).
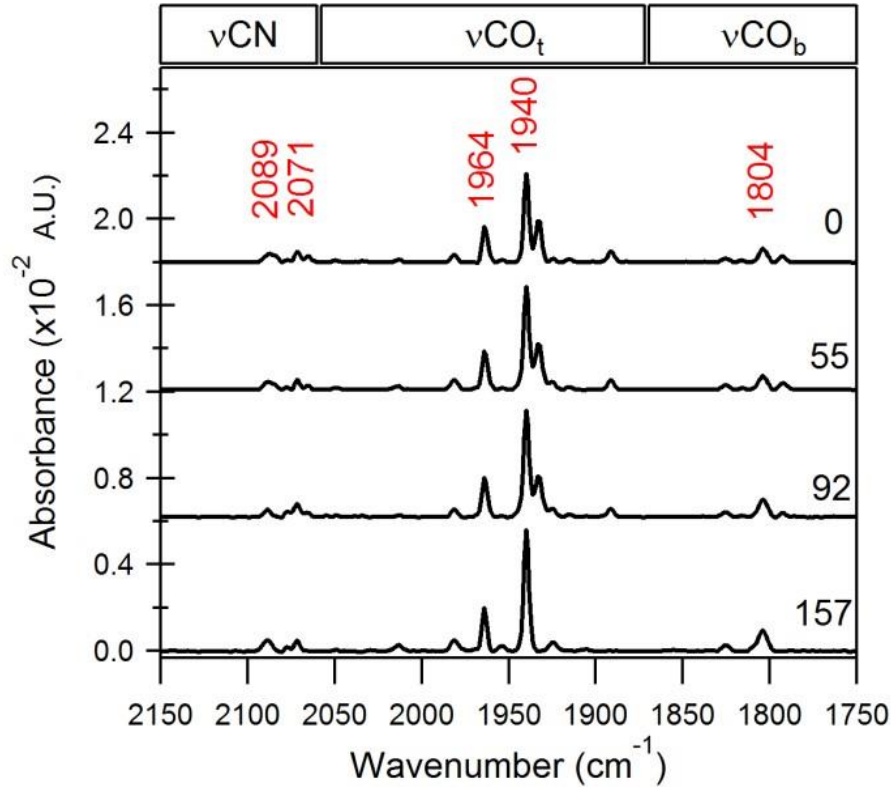
Figure S3. FTIR time-course of non-O_2 treated CrHydA1 under N2 atmosphere. CrHydA1 (59 mg mL^{-1}) was buffer exchanged by G-25 into NaDT-free buffer as described in the Experimental Section, but minus the O_2 injection. Time (min) is indicated on the right of the spectra. The increase in the H_{ox} specific 1940 cm^{-1} vCO peak along with the decrease in the H_{red} vCO peaks at 1891 and 1933 cm^{-1} indicates autooxidation of a small fraction of residual H_{red}.4
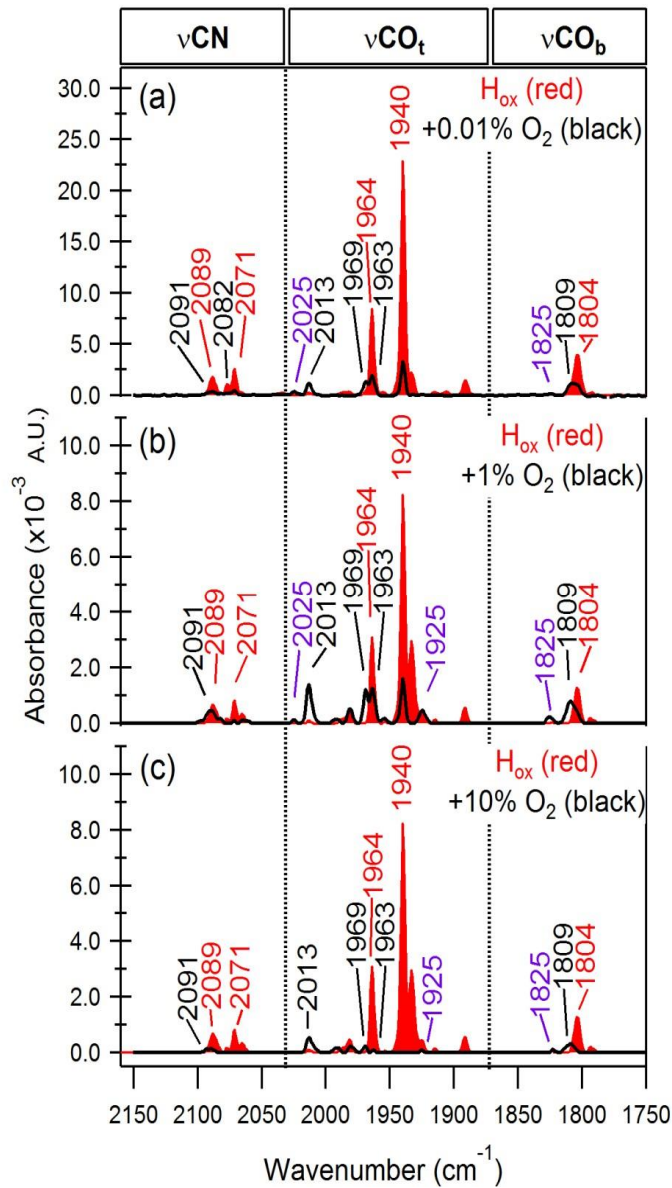
Figure S4. FTIR spectra of O_2 titration of H_{ox} CrHydA1. (a) H_{ox} CrHydA1 at 45 mg mL^{-1} (red) and after 133 min exposure to 0.01% O_2 (black), (b) H_{ox} CrHydA1 at 40 mg mL^{-1} (red) and after 120 min exposure to 1% O_2 (black), (c) H_{ox} CrHydA1 at 40 mg mL^{-1} (red) and after 120 min exposure to 10% O_2 (black).
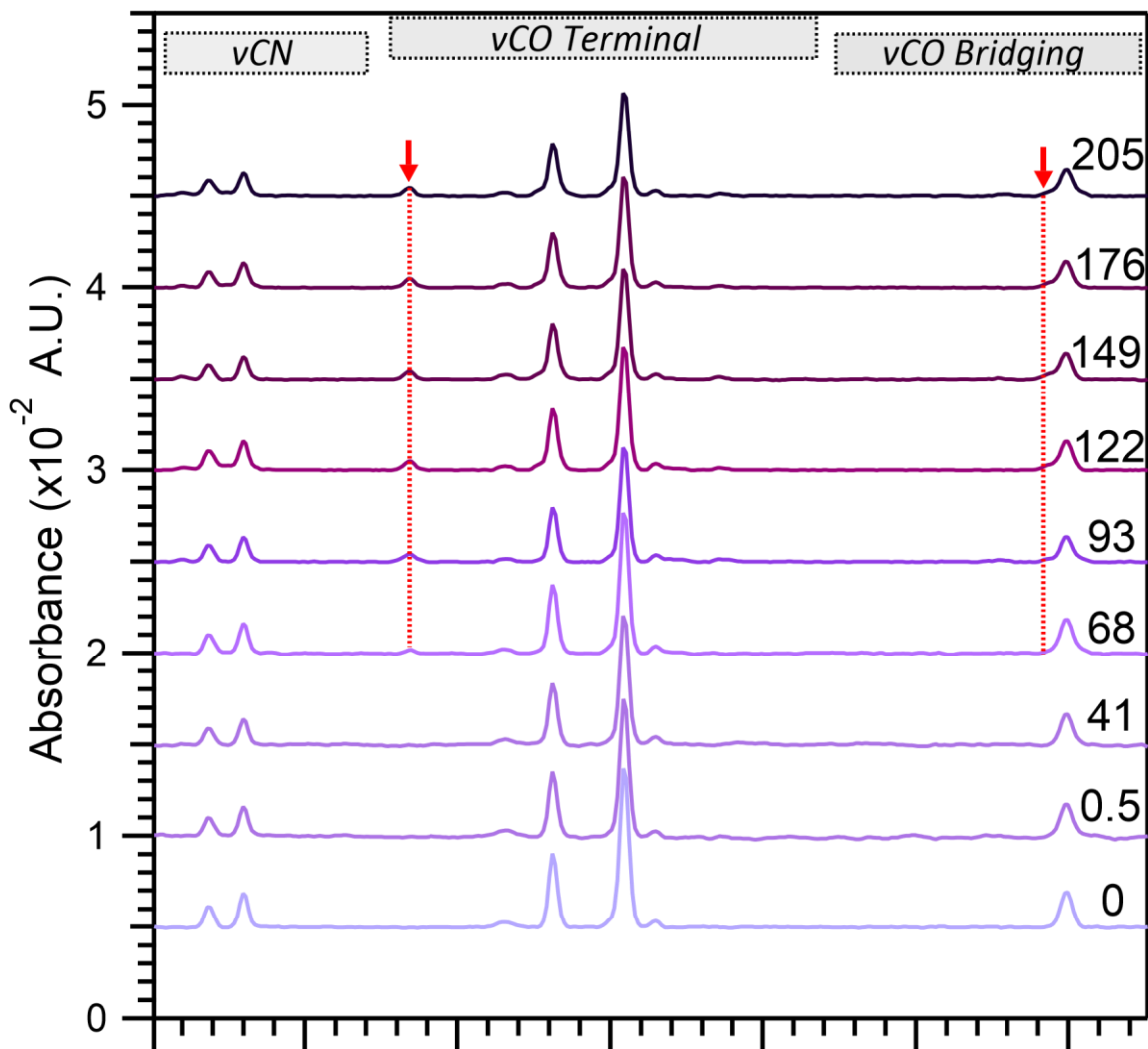
Figure S5. FTIR spectral time course of the 2Fe subcluster in CaI that was exposed to 0.28% O_2. CaI was prepared in the H_{ox} state and exposed to 0.28% O_2 at 4 °C with magnetic stirring. Aliquots were removed at the time intervals indicated on the right (in min, with increasing time from bottom to top), and analyzed by FTIR. The red dashed lines and arrows indicate the appearance of νCO peaks assigned to the H_{ox}-CO state of CaI (2016 and 1807 cm^{-1}).
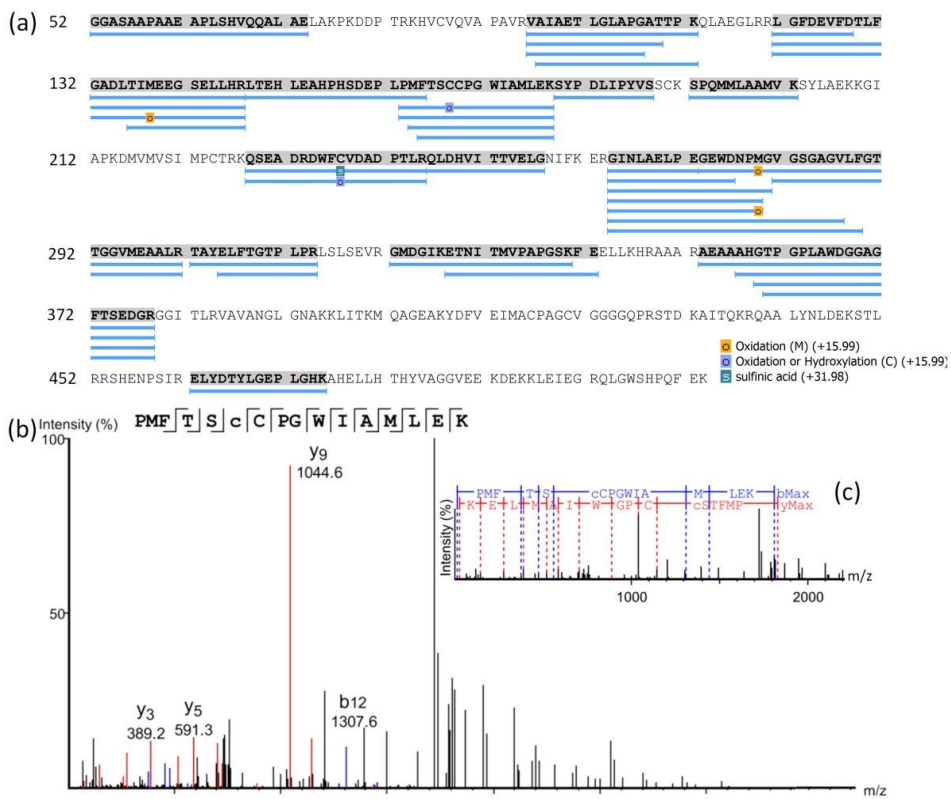
Figure S6 CrHydA1 (1o mg mL^{-1}) was exposed to ~0.1% O$_2$ for 2 h. The enzyme activity was monitored by gas chromatography, after the activity decayed to 50 µmol min^{-1} mg^{-1} the sample was allowed to equilibrate in an anaerobic Coy chamber for 30 min. The enzyme was then subjected to a trypsin digest and analyzed by mass spectrometry as described in the Experimental Section of the manuscript. Peptides were searched for by nonspecific cleavage, which increased coverage, likely due to fragmentation during HPLC and ionization.[1] No peptides were identified when using a nonspecific cleavage search against a non-CrHydA1 protein sequence. (a) Sequence coverage of CrHydA1 (60%) with modifications indicated at the bottom right of the coverage map. (b) Mass spectra of the peptide fragment that corresponds to sulfenic acid and site 169. (c) Annotated spectrum with alignment.

(1) König S., Zeller M., Peter-Katalinic J., Roth J., Sorg C., Vogl T. *J. Am. Chem. Soc. Mass Spectrom.* **2001**, 12, 1180
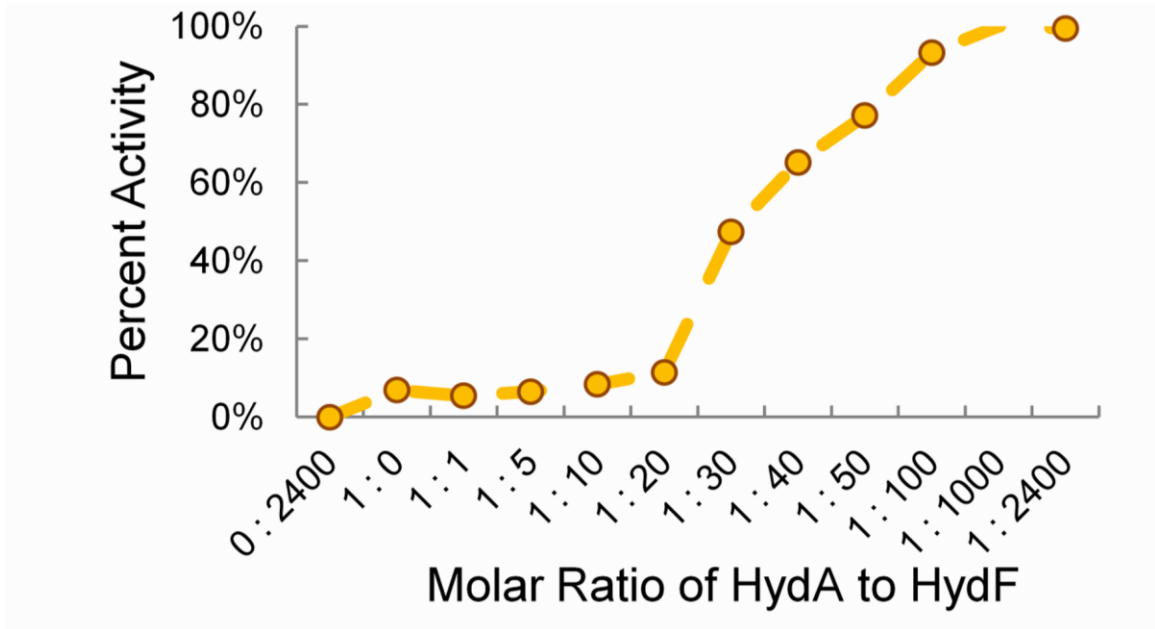
Figure s7. Titration of CrHydA1 (labeled as "HydA") with HydF^{EG}. Poor incorporation of 2Fe subcluster into HydF during heterologous expression in *E. coli* results in the need for large ratios of HydF to CrHydA1 to reach full activation.

Treatment	Mole ratio (O$_2$:CrHydA1)	Final O$_2$ Headspace (%, SD = +/- 0.15*%)	Time (min)	Figure	Experiment
H$_{ox}$	0.06	0.01	133	Figures 4.2a and 4.3	FTIR
	5.07	1.02	120	Figure S4	FTIR
	50.43	10.15	120	Figure S4	FTIR
H$_{ox}$-CO	39.3	2.47	120	Figure 4.2b	FTIR
	392.99	24.69	120	Figure S1	FTIR
H$_{red}$-H$_2$	1.25	0.02	120	Figure 4.2c	FTIR
H$_{red}$-DT	0.06	0.002	120	Figure S2	FTIR
	1.25	0.05	120	Figure 4.2d	FTIR
	51.05	2.06	120	Figure S2	FTIR
H$_{ox}$	0.06	0.001	120	Figures 4.5b and 4.5c	UV-Vis
	1000	17	120	Figures 4.5b and 4.5c	UV-Vis
	17,647	300	180	Figures 4.5b and 4.5c	UV-Vis

Table S1. Summary of O$_2$ concentrations and O2:CrHydA1 molar ratios for FTIR experiments.

Vial	Injection volume (μL)	[a] O$_2$ (nmol)	[b] Molarity (mol^{-1} L^{-1} O$_2$)	[c] pO$_2$ (atm)	[d] O$_2$ %
1	50	14	3 E-04	0.0069	0.84
2	50	15	3 E-04	0.0072	0.88
3	50	12	2.4 E-04	0.0059	0.71
4	50	15	3 E-04	0.0070	0.85
5	50	19	4 E-04	0.0090	1.10
Average ± SD		15 ± 2			0.88 ± 0.14

Table S2. Average and standard deviation values of %O$_2$ used for O2 treatments.

[a] The O$_2$ peak area from GC was converted to nmol O2 based on a O$_2$ standard curve.

[b] Molarity=O2 (nmol)/injection volume (μL).

[c] pO2=nRT/V, where n/V is "molarity", T=298K.

[d] %O2=pO2/barometric pressure. Barometric pressure was 0.82 atm in Golden, CO.

Enzyme	T (K)	Barometric Pressure (atm)	[O₂][a]		k (s[-1])[b]		k_{Hox} (s-1 µM O2-1)
			%	µM	□1945 cm⁻¹	□1940 cm⁻¹	
CaI	277	0.82	0.28	3.2	1.2 X 10⁻³		7.0 X 10⁻⁶
CrHydA1	277	0.82	0.010	0.11	-	2.0 X 10⁻³	3.0 X 10⁻⁴
CrHydA1	277	0.82	0.13	1.49	-	2.1 X 10⁻²	2.4 X 10⁻⁴

Table S3. FTIR time-course fits and experimental conditions used to calculate O2 induced transitions in CaI and CrHydA1.

[a] molar concentration = [% O_2*barometric pressure(atm)/(T(K)*0.082056)]*0.03181

[b] k (s[-1]) = -[ln(A)/A_0)]/t (s). "A" is taken as the H_{ox} specific peak at 1945 cm^{-1} for CaI, and at 1940 cm⁻¹ for CrHydA1.

Data Collection	CrHydA1
Wavelength (Å)	1.734
Unit cell parameters a, b, c (Å) α, β, γ (°)	77.6, 71.0, 94.7 90.0, 91.9, 90.0
Space group	P 1 21 1
Resolution range (Å)	34.73-2.29 (2.241-2.29*)
Total reflections	288694
Unique reflections	45032
R-merge(%)	11 (40*)
I/σ (I)	6.6 (3.1*)
Completeness (%)	96 (87*)
Redundancy	6.4 (5.9*)

Refinement

Resolution limits (Å)	35-2.3
No of used reflections	39011

No of protein atoms	6282
R factor (%)	20.9
R free (%)	25.2
Ramachandran Favorite regions (%)	95.9
Ramachandran Allowed regions (%)	4.1
Ramachandran Outliers (%)	0.0
R.m.s. deviations from ideal values, bond lengths of refined atoms(Å)	0.019
Angels (Å)	2.09
Average B, all atoms (A^2)	49.48
Wilson B-factor (A^2)	25.6

* Values in parentheses are for the highest resolution shell.

Table S4. Data collection and refinement statistics for O2 exposed CrHydA1

APPENDIX B

PHYLOGENETIC TREE OF [FEFE]-HYDROGENASE SEQUENCES
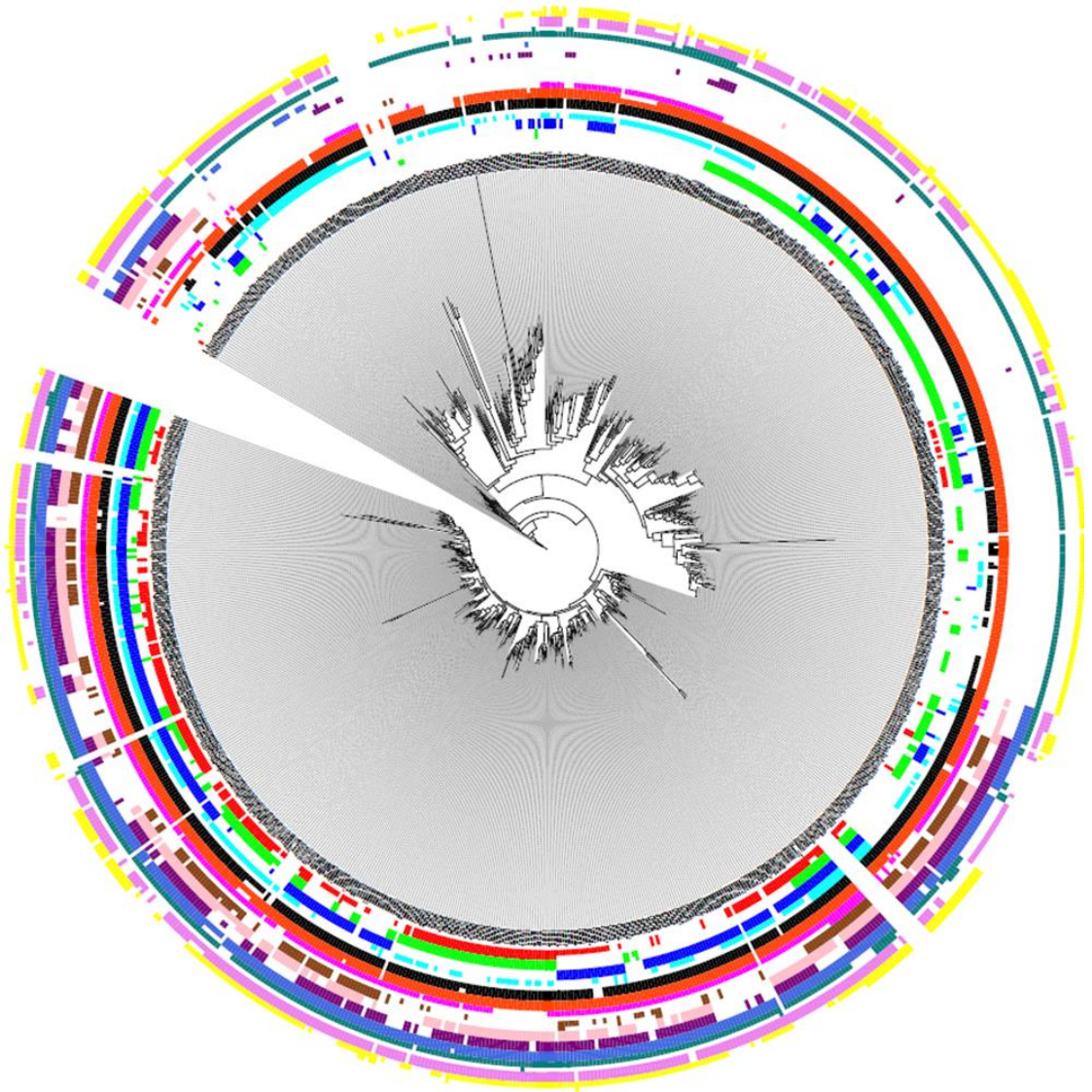
Supplemental figure 8. Phylogenetic tree of [FeFe]-hydrogenase sequences depicting presence of either CpI- or CpII -type amino acids in each of the fourteen sites described as possibly contributing to catalytic bias.

APPENDIX C

GENE SEQUENCES FOR CPI TAG AND CPII QQM

Gene Name: CpII QQM, Length: 1416bp, Vector Name: pUC57, Codon Optimization: No
Start with: CATATG
Sequence:
AACAGCAAGCACAAATTCACCGACATTCGTGTTCCGATCGAAAAGGATAACCCGAGCATTATGCGTCACG
AGGAACTGTGCGTGAAGTGCAAAGTTTGCAAGAAAGTGTGCACCGAGGAAATCAGCGTGTATGGTCACTA
CGACCTGGAGAAGACCGGCGATAAAGCGATCTGCATTTATTGCGGCCAGTGCGCGAACGTTTGCCCGGTG
TACAGCATTACCGAAGTTAGCGACGTGCAGCAAGTTAAGGATGCGATCAACGACCCGGATAAAATCGTTA
TTTTCCAAACCAGCCCGAGCGTGCGTGTTAGCCTGGGCGAGGCGTTTGGTATGGAACCGGGCACCTATGT
TGAGGATAAGATGGCGGCGGTGCTGAAAAACCTGGGTGCGGACTACGTTTTCGATACCACCTTTGGCGCG
GACCTGACCATTACCGAGGAAGCGAGCGAACTGGTGCAGCGTATCACCAGCGGCAACGGTACCCTGCCGC
AATTCACCAGCTGCTGCCCCGGCGTGGGTGGAGTTTGTTGAAATTTACTATCCGGAGCTGATCAACAACCT
GAGCAGCAGCAAGAGCCCGCAGCAAATGCAGGGTCCGACCATTAAAAACCTACTTTGCGAAGAAAGCGGCG
ATTGATCCGAAGAAAATCGTGAACGTTGCGGTGACCCCGTGCACCGCGAAGAAATATGAGATCACCCGTG
CGGAAAAGAACGACGCGGGTAAATACTATAACGATGAGAACATTCGTGACATGGATTACGTGATCACCGT
TCGTGAACTGAGCAACTGGATTAAAGAGGACAAAATCGAATTCAAGGCGCTGCAGGGCGCGGAGTTTGAT
AGCCTGCTGAGCCGTGGTAGCGGTGGCGGTATCATTTTCGGCATCACCGGCGGTGTTATGGAAAGCGCGA
TTCGTACCGCGTACTATTACATCACCAAGAAAAACCCGCCGAAGGACCTGTATAACCTGGAGGCGGTTGG
TAACATGGATGGCATTCGTGAAGCGCAAGTGACCATCGGTGACTACACCATCAACATTGCGATCGTTCAC
GGCATGGCGAACGCGCGTAAACTGATCGAGAAGGTGAAAAGCGGTGAAAAGAAATATGACTTTGTTGAGG
TGATGACCTGCCGTGGCGGTTGCATTGGCGGTGGCGGTCAGCCGAAGGTTAAAATCCCGATGGCGGATAA
AGTGCGTCAAAAACGTATTGCGGGCCTGTACAACAAGGACCAGAGCGTTACCCAACGTCTGGCGCACGAG
AACCCGGACATCACCAAGGTGTACGATGAATTCTTTAAGAAGCCGCTGAGCCCGCTGGCGGAGGAACTGC
TGCACACCGTGTACAGCAGCAAGAAACACATTCTGGGCGAGAGCGCGTGGAGCCACCCGCAGTTCGAAAAA
ATAA
End with: GTCGAC

Item 2: Custom Cloning (shippable)
Target Vector: pET-21b(+), Vector Map: N
Cloning Site: NdeI-SalI,

Item 1: Gene Synthesis (non-shippable)
Gene Name: CpI I268TS357A N505G, Length: 1764bp, Vector Name: pUC57, Codon
Optimization: No
Start with: CAT
Sequence:
atgAAAACCATTATTATTAACGGCGTGCAGTTTAACACCGATGAAGATACCACCATTCTGAAATTTGCGC
GTGATAACAACATTGATATTAGCGCGCTGTGCTTTCTGAACAACTGCAACAACGATATTAACAAATGCGA
AATTTGCACCGTGGAAGTGGAAGGCACCGGCCTGGTGACCGCGTGCGATACCCTGATTGAAGATGGCatg
ATTATTAACACCAACAGCGATGCGGTGAACGAAAAAATTAAAAGCCGTATTAGCCAGCTGCTGGATATTC
ATGAATTTAAATGCGGCCCGTGCAACCGTCGTGAAAACTGCGAATTTCTGAAACTGGTGATTAAATATAA
AGCGCGTGCGAGCAAACCGTTTCTGCCGAAAGATAAAACCGAATATGTGGATGAACGTAGCAAAAGCCTG
ACCGTGGATCGTACCAAATGCCTGCTGTGCGGCCGTTGCGTGAACGCGTGCGGCAAAAACACCGAAACCT
ATGCGatgAAATTTCTGAACAAAAACGGCAAAACCATTATTGGCGCGGAAGATGAAAAATGCTTTGATGA
TACCAACTGCCTGCTGTGCGGCCAGTGCATTATTGCGTGCCCGGTGGCGGCGCTGAGCGAAAAAAGCCAT
atgGATCGTGTGAAAAACGCGCTGAACGCGCCGGAAAAACATGTGATTGTGGCGatgGCGCCGAGCGTGC
GTGCGAGCATTGGCGAACTGTTTAACatgGGCTTTGGCGTGGATGTGACCGGCAAAATTTATACCGCGCT
GCGTCAGCTGGGCTTTGATAAAATTTTTGATACCAACTTTGGCGCGGATatgACCATTatgGAAGAAGCG
ACCGAACTGGTGCAGCGTATTGAAAACAACGGCCCGTTTCCGatgTTTACCAGCTGCTGCCCGGGCTGGG
TGCGTCAGGCGGAAAACTATTATCCGGAACTGCTGAACAACCTGAGCAGCGCGAAAAGCCCGCAGCAGAT
TTTTGGCACCGCGAGCAAAACCTATTATCCGAGCATTAGCGGCCTGGATCCGAAAAACGTGTTTACCGTG
ACCGTGatgCCGTGCACCGCGAAAAAATTTGAAGCGGATCGTCCGCAGatgGAAAAAGATGGCCTGCGTG
ATATTGATGCGGTGATTACCACCCGTGAACTGGCGAAAatgATTAAAGATGCGAAAATTCCGTTTGCGAA
ACTGGAAGATAGCGAAGCGGATCCGGCGatgGGCGAATATAGCGGCGCGGGCGCGATTTTTGGCGCGACC
GGCGGCGTGatgGAAGCGGCGCTGCGTAGCGCGAAAGATTTTGCGGAAAACGCGGAACTGGAAGATATTG
AATATAAACAGGTGCGTGGCCTGAACGGCATTAAAGAAGCGGAAGTGGAAATTAACAACAACAAATATAA
CGTGGCGGTGATTAACGGCGCGAGCAACCTGTTTAAATTTatgAAAAGCGGCatgATTAACGAAAAACAG
TATCATTTTATTGAAGTGGatgGCGTGCCATGGCGGCTGCGTGGGCGGCGGCGGCCAGCCGCATGTGAACC
CGAAAGATCTGGAAAAAGTGGATATTAAAAAAAGTGCGTGCGAGCGTGCTGTATAACCAGGATGAACATCT
GAGCAAACGTAAAAGCCATGAAAACACCGCGCTGGTGAAAatgTATCAGAACTATTTTGGCAAACCGGGC
GAAGGCCGTGCGCATGAAATTCTGCATTTTAAATATAAAAAAAGCGCGTGGAGCCATCCGCAGTTTGAAA
AATAA
End with: GTCGAC

Item 2: Custom Cloning (shippable)
Target Vector: pET-21b(+), Cloning Site: NdeI-SalI,

<u>APPENDIX D</u>

BIOCHEMICAL AND STRUCTURAL PROPERTIES OF A THERMOSTABLE
MERCURIC ION REDUCTASE FROM *METALLOSPHAERA SEDULA*

Contribution of Authors and Co-Authors

Manuscript(s) in Chapter(s) 2, 3, 5, 6, Appendix D

Author: Jacob H. Artz

Contributions: Biochemical assays, crystal structure refinement, authored manuscript

Co-Author: Spencer N. White

Contributions: Enzyme purification, crystallization, and data collection

Co-Author: Oleg A. Zadvornyy

Contributions: Crystal data collection, crystal structure solution, interpretation of data

Co-Author: Corey J. Fugate

Contributions: Expertise in enzyme expression and purification

Co-Author: Danny Hicks

Contributions: Help with biochemical assays

Co-Author: George H. Gauss

Contributions: Assistance with crystal data collection

Co-Author: Matthew C. Posewitz

Contributions: Experimental design and interpretation

Co-Author: Eric S. Boyd

Contributions: Phylogenetics of MerA-containing species

Co-Author: John W. Peters

Contributions: Experimental design and interpretation

Manuscript Information Page

Jacob H. Artz, Spencer N. White, Oleg A. Zadvornyy, Corey J. Fugate, Danny Hicks,
George H. Gauss, Matthew C. Posewitz, Eric S. Boyd, John W. Peters
Frontiers in Bioengineering and Biotechnology, section Process and Industrial
Biotechnology.

Biochemical and structural properties of a thermostable mercuric ion reductase from *Metallosphaera sedula*

Jacob H. Artz[1], Spencer N. White[1], Oleg A. Zadvornyy[1], Corey J. Fugate[1], Danny Hicks[1], George H. Gauss[1], Matthew C. Posewitz[2], Eric S. Boyd[3,4], John W. Peters[1]

[1]Department of Chemistry and Biochemistry, Montana State University, Bozeman, MT, USA

[2]Department of Chemistry and Geochemistry, Colorado School of Mines, Golden, CO, USA

[3]Department of Microbiology and Immunology, Montana State University, Bozeman, MT, USA

[4]Thermal Biology Institute, Montana State University, Bozeman, MT, USA

Correspondence: John W. Peters, Department of Chemistry and Biochemistry, Montana State University, Bozeman, MT 59717, john.peters@chemistry.montana.edu, 406-994-7212

Abstract

Mercuric ion reductase (MerA), a mercury detoxification enzyme, has been tuned by evolution to have high specificity for mercuric ions (Hg^{2+}) and to catalyze their reduction to a more volatile, less toxic elemental form. Here, we present a biochemical and structural characterization of MerA from the thermophilic crenarchaeon *Metallosphaera sedula*. MerA from *M. sedula* is a thermostable enzyme, and remains active after extended incubation at 97 °C. At 37 °C, the NADPH oxidation-linked Hg^{2+} reduction specific activity was found to be 1.9 µmol/min·mg, increasing to 3.1µmol/min·mg at 70 °C. *M. sedula* MerA crystals were obtained and the structure was solved to 1.6 Å, representing the first solved crystal structure of a thermophilic MerA. Comparison of both the crystal structure and amino acid sequence of MerA from *M. sedula* to mesophillic counterparts provides new insights into the structural determinants that underpin the thermal stability of the enzyme.

1.   Introduction

The ionic form of mercury, which is one of the most toxic metals known to biology (Gertrud Huber, 1989;Nies, 2003;Vetriani et al., 2005), is naturally present at elevated concentrations in many hydrothermal vents, hot springs, and acid mine drainage fluids (Batten and Scow, 2003;Simbahan et al., 2005;Vetriani et al., 2005;King et al.,

2006;Boyd et al., 2009;Wang et al., 2011). In these environments biology utilizes a finely tuned protein catalyst termed the mercuric reductase (MerA) (encoded by the *merA* gene) in order to reduce toxic ionic mercury (Hg^{2+}) to the far less toxic, volatile, and elemental form (Hg^0). The reaction catalyzed by MerA follows the reaction scheme of $NADPH + Hg^{2+} \rightarrow NADP^+ + Hg^0$ (Barkay et al., 2003). MerAs, which are part of the disulfide oxidoreductase family (Fox and Walsh, 1982) are ancient enzymes, having arisen in high temperature environments after the great oxidation event ~2.4 billion years ago (Barkay et al., 2010). Since that time evolution has finely tuned MerA through recruitment of regulatory and transport proteins (Boyd and Barkay, 2012) to serve a diversity of organisms, including both Archaea and Bacteria, that encounter Hg^{2+} ions in less extreme mesophilic settings, while retaining extremely high stability and substrate specificity. These characteristics of mercuric reductases lend them to possible sensor applications, wherein the redox properties of the enzyme could be coupled to an amplifiable electrical signal. A stable mercuric reductase may also be used to potentially mitigate mercury contamination.

Metallosphaera sedula (*Mse*), isolated previously from Pisciarelli Solfatara in Naples, Italy (Gertrud Huber, 1989), has a minimum and maximum temperature for growth range of 50 °C to 80 °C (Auernik et al., 2008a). Pisciarelli Solfatara itself contains a variety of thermal features that range in temperature from ~30 °C to nearly 100 °C, and a pH range of 1.5 to around 6.0 with elevated concentrations of heavy metals, including Hg^{2+} at concentrations up to 0.005 g/kg (Huber et al., 2000). The genome sequence of *Mse* was completed in 2008, (Auernik et al., 2008b), making it possible to identify mechanisms of Hg^{2+} tolerance at the genomic level. The *mer* operon in *Mse* includes both MerA and MerH, where MerH may aid metal trafficking to the MerR transcription factor (Schelert et al., 2013).

A variety of MerAs have been characterized previously, most notably a protein encoded on a transposon isolated from *Pseudomonas aeruginosa* which is termed Tn*501* (Fox and Walsh, 1982), as well as MerA from *Bacillus cereus* (*Bc*MerA) (Schiering et al., 1991) and a MerA from a deep brine environment, termed ATII-LCL (Sayed et al., 2013). Collectively, these biochemical studies have revealed MerAs that exhibit K_m values for Hg^{2+} that range from 9 to 70 µM and specific activities that range from 1.05 to 50 µmol/min·mg. Structural characterization was first carried out on *Bc*MerA (Schiering et al., 1991) and later on Tn*501* (Ledwidge et al., 2005). Most recently the Tn*501* structure has been solved in complex with Hg^{2+}(Lian et al., 2014) . Structural characterization confirmed that MerA is a member of the disulfide oxidoreductase (DSOR) protein family, which adopt a βαββαβ fold and which are known to catalyze pyridine-dependent substrate reduction with a characteristic active site CXXXXC motif (Argyrou and Blanchard, 2004). Some MerAs also harbor an additional N-terminal GMTCXXC motif (Boyd and Barkay, 2002) that assists in metal recruitment (Ledwidge et al., 2005). A third pair of conserved cysteines are located in a flexible region on the c-terminal domain, and are responsible for delivering mercuric ions to the active site of the opposing monomer (Lian et al., 2014).

Despite these advances, the structural characterization of a MerA from a thermophile has yet to be conducted, even though this is critical for understanding the

properties of enzymes involved in mercury detoxification of high-temperature environments where mercury concentrations are very high. Structural characterization is important for both understanding the thermophilic origins of the protein (Barkay et al., 2010;Boyd and Barkay, 2012) as well as for possible incorporation into stable biotechnologies. Here, we report biochemical and structural characterization of a thermostable MerA from the aerobic thermoacidophilic Crenarchaeon *Mse* (*Mse*MerA).

2. Materials and Methods

2.1 Bioinformatics

MerA homologs were compiled from the Department of Energy-Integrated Microbial Genomes database using BLASTp and the *Tn501* MerA as a query. Representative homologs were screened for conserved residues that define MerA (as described above) and those protein sequences with these residues were aligned using CLUSTALX (version 2.0.8) specifying the Gonnet 250 protein substitution matrix and default gap extension and opening penalties (Larkin et al., 2007) with dihydrolipoamide dehydrogenase from *Magnetospirillum magneticum* AMB-1 (YP_423326), *Thermus thermophilus* HB27 (YP_005669), and *Pseudomonas fluorescens* Pf0-1 (YP_351398) serving as outgroups. N terminal 'NmerA' sequence was trimmed from the alignment block as previously described (Barkay et al., 2010) and the phylogeny of MerA was evaluated with PhyML (ver. 3.0.1) (Guindon et al., 2010) using the LG amino acid substitution matrix with a discrete 4 category gamma substitution model and a defined proportion of invariant sites. A consensus phylogenetic tree was projected from 100 bootstrap replications using FigTree (ver. 1.2.2) (http://tree.bio.ed.ac.uk/UH).

Structural superimpositions were generated by the program UCSF Chimera (Pettersen et al., 2004). The protein sequence of *Mse*MerA was blasted with NCBI BLASTp. The top eight hits were compared with mesophilic mercuric reductases from *Staphylococcus aureus*, *Bacillus cereus*, *Pseudomonas aeruginosa,* and a sequence from a hydrothermal deep-sea brine environment, ATII-LCL (Sayed et al., 2013). It should be noted that while the ATII-LCL sequence was isolated from a hydrothermal vent system with a temperature of 68 ℃, the optimum temperature for activity was shown to be 30-50 ℃ (Sayed et al., 2013), indicating that it is not adapted to the thermal regime from where it was isolated or that the environment from where it was isolated is variable with respect to temperature. VADAR was used to evaluate the surface area and charged residue percentage of MerA homologs (Willard et al., 2003) while the ProtParam tool available from ExPASy was used to calculate the aliphatic index of MerA homologs (Gasteiger et al., 2005).

2.2 Expression and Purification

*Mse*MerA DSM 5348 sequence was codon-optimized and synthesized by GenScript USA Inc with an N-terminal 6x His-tag. The gene was cloned into MCS1 of pETDuet-1 and transformed into *E. coli* BL21DE3 cells (Novagen). Sequence-based confirmation of *Mse*MerA transformation was performed by Davis Sequencing, Inc (1450 Drew Ave, Suite 100, Davis, California).

Fifty milliliters of Luria-Bertani (LB) broth supplemented with 0.5 mM riboflavin and 0.1 g/L ampicillin was inoculated with recombinant *E. coli* cells containing *Mse*MerA and shaken at 250 rpm at room temperature overnight. One liter of LB medium, as described above, was inoculated with 2 mL from the overnight culture, and shaken at 250 rpm until an OD_{600} of 0.5-0.7 was reached. Two mM IPTG was added, and expression was carried out for four hours, after which the cultures were centrifuged at 6,000 x g for 10 min (4 ⁰C), with the resultant cell pellet immediately being flash frozen in liquid nitrogen and stored at -80 ᵒC. Each liter of cell culture yielded 3.0 to 3.5 g of cell paste.

Cell paste was subjected to three freeze/thaw cycles to facilitate lysis, after which cells were re-suspended in 5 mL Buffer A (100 mM NaCl, 50 mM MOPS with a pH of 6.7, 25 mM imidazole) per gram of cells. Lysozyme and deoxyribonuclease (DNase) were added to final concentrations of 0.1 mg/mL along with phenylmethylsulfonyl fluoride (PMSF)-saturated isopropanol to a final concentration of 0.1% v/v, and this mixture was incubated for 30 min at room temperature. Triton X-100 was then added to a final concentration of 1% v/v, and this was mixed for 30 min. The crude lysate was then clarified by centrifugation at 100,000 x g for one hour (4 ⁰C). The resulting clarified lysate was observed to have a yellow color.

Purification of *Mse*MerA was carried out using a 75 mL gradient from 100% Buffer A to 100% Buffer B (100 mL NaCl, 50 mM MOPS with a pH 6.7, 250 mM imidazole) on a 2 mL Ni-NTA column (Qiagen) at 3 mL/min. Seven milliliter fractions were collected and further analyzed with an SDS-PAGE gel. Fractions containing pure protein were combined and concentrated to 10 mg/mL, buffer exchanged to Buffer C (10mM MOPS pH of 6.7), and the protein was then concentrated to 30 mg/mL and flash-frozen in liquid nitrogen. Purity of the protein was confirmed by SDS- and Native PAGE. A yield of 1.5 mg of pure protein per liter of growth culture was achieved.

2.3 Activity Assay

Activity assays were carried out in 100 mM NaCl, 50 mM MOPS with a pH of 6.7, 0.2 mg/mL *Mse*MerA, and 1 mM $HgCl_2$, and these were initiated by the addition of 0.2 mM NADPH, similar to previously established procedures (Fox and Walsh, 1982). For kinetic studies, the concentration of Hg^{2+} ranged from 28.6 µM to 2.77 mM. NADPH oxidation was monitored at 338 nm using a Cary 6000 UV/Vis spectrometer equipped with a 1x1 Peltier. Assays were conducted from 37 to 70 °C, above which temperature the rate of non-enzymatic NADPH oxidation was too high to accurately measure enzymatic activity. In order to determine the thermostability of *Mse*MerA, an aliquot of the enzyme was assayed at 37°C, and the remaining protein was boiled at 97 °C for 100 minutes, after which the enzymatic activity was once again measured at 37 °C.

2.4 Crystallization and Structure Determination

*Mse*MerA crystals were obtained using the hanging drop method. Crystallization drops contained 0.085 M TRIS (pH 8.5), 15% v/v glycerol, 14% w/v PEG400, 0.19 M $LiSO_4$, and 20 mg/mL protein. Crystals were obtained after two weeks, mounted on cryo loops, and shipped to the Stanford Synchrotron Radiation Lightsource for X-ray data

collection. Diffraction data were collected at 100 K using the 12-2 beamline. Diffraction images were indexed, integrated and scaled using HKL2000 (Otwinowski and Minor, 1997).

The structure of *Mse*MerA was solved to 1.6 Å using CCP4 molecular replacement (Cowtan et al., 2011) of Tn*501*MerA (PDB ID: 1ZK7), which shares 37% amino acid identity with *Mse*MerA. Model building was performed in Coot (Emsley et al., 2010) and coordinates were refined to reasonable stereochemistry at a resolution 1.6 Å (Supplemental Table 1) using REFMAC5 (Murshudov et al., 1997). The structure was validated using MolProbity (Chen et al., 2010) and all molecular images were calculated in PyMol (DeLano, 2002). Structural superimpositions were generated both with 1ZK7 (Ledwidge et al., 2005) and 4K7Z (Lian et al., 2014), in which the active site cysteines were substituted by alanines and could be solved in complex with the Hg^{2+} ion.

3. Results

3.1 Thermal Adaptation of *Mse*MerA.

Phylogenetic reconstruction of representative core (NmerA trimmed) MerA sequences revealed a number of deeply branching lineages from thermophilic taxa, consistent with previous analyses that indicate MerA likely originated in a high temperature environment (Schelert et al., 2004). *Mse*MerA clustered among MerA from thermophilic crenarchaeota (Fig. 1). Sequence alignments reveal both the active site CXXXXC motif and c-terminal cysteines that are conserved among all MerA sequences. However, several key differences were observed that may be involved in conferring thermotolerance (Fig 2). Specifically, the thermophilic enzymes are missing regions corresponding to amino acids 66-71 and 130-134 Tn*501* (Tn*501*MerA numbering), suggesting a reduction in loop regions in comparison to the mesophilic enzymes (Fig. 2). Two sets of residues, V317 and Y441, are within putative coordination distance of the active-site mercury. These residues are substituted for an E and F, respectively, in *Mse*MerA and other thermophiles with the exception of *Hydrogenobacter thermophilus* TK-6 (YNP_003432979) and *Hydrogenobaculum* sp. Y04AAS1 (YNP_002121876).
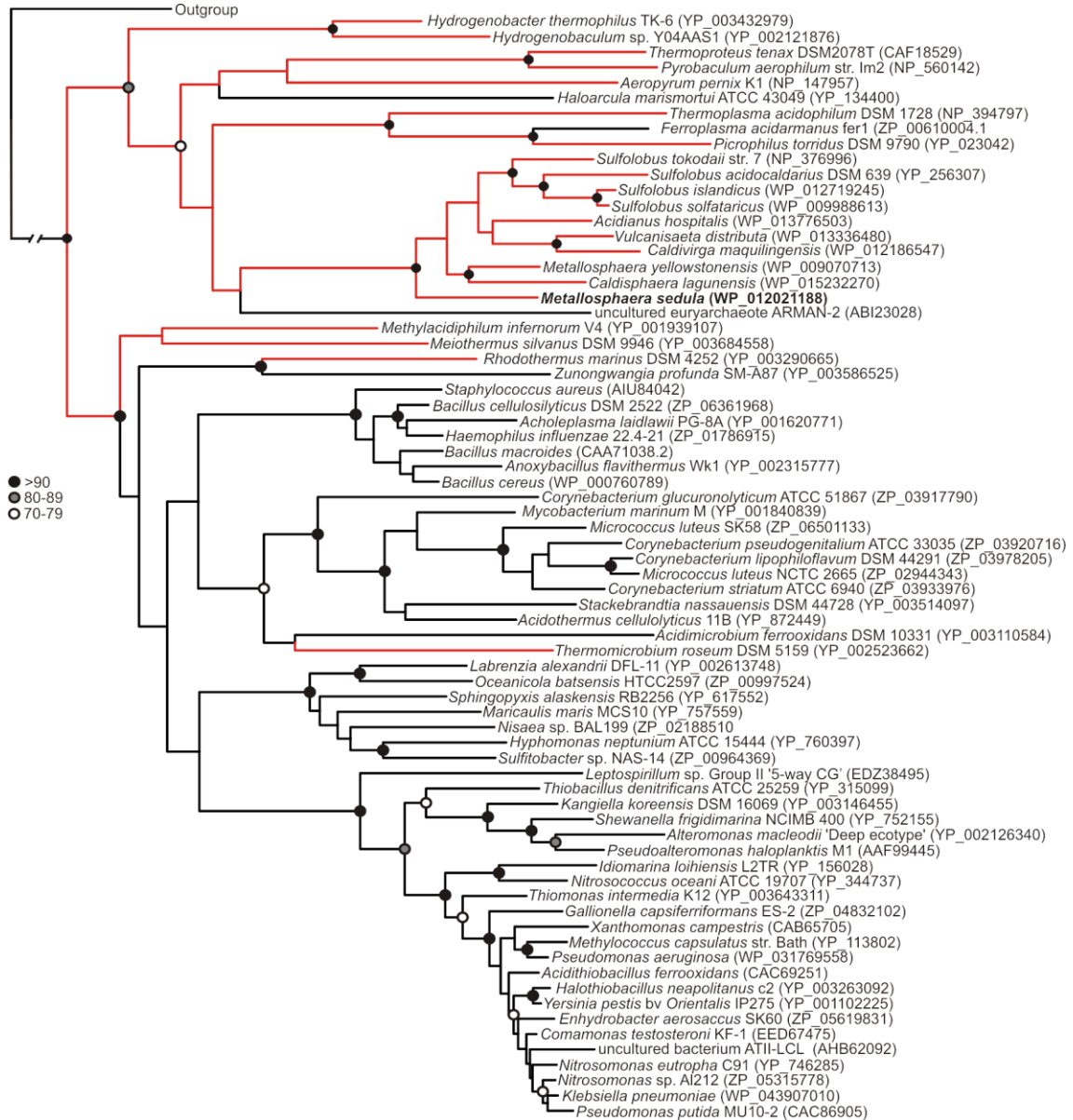
Figure 1. Maximum-likelihood phylogenetic reconstruction of MerAs, with homologs from thermophilic taxa highlighted in red. MseMerA is boldfaced. Bootstrap support is indicated by black (>90), gray (80-89) and open (70-79) circles. Nodes with no symbol exhibited bootstrap values of <70.

A comparison of the *Mse*MerA crystal structure to the previously determined Tn*501*MerA structure (PDB: 1ZK7) (Ledwidge et al., 2005) reveals that the two structures are highly similar, with an overall C-alpha deviation of 1.5 Å rmsd as calculated by Dali Lite(McWilliam et al., 2013). Two particular loop regions are shorter in *Mse*MerA (Fig. 4b). This was further supported by VADAR (Willard et al., 2003),

which calculated a 4% decrease in coil regions in *Mse*MerA. The calculated surface area of *Mse*MerA at 19,966.5 Å^2 is slightly reduced in comparison to Tn*501*MerA, with a surface area of 21217.4 Å^2.


```
                        L1                    L2                   E/V               F/Y
                  70         80        130         140      320        330     450        460
                  ....|....|....|....|..  |....|....|....|..  ..|....|●...|...  .|.●.|....|.
M. sedula WP_012021188     KKAREVTGSEVY------PPFS  VKVNG-----QVIEAEKF  DVLGGRMLEALAGRQG  VHMFPTIAESLRL
V. distributa WP_013336480 NYVSKVLGHEHY------PEFT  VKVNG-----KVIEARRF  DVIGGPMLEALAGKQG  VHVFPTMAESLKL
B. cereus WP_WP_0000760789 HIAKNNPFVG-LHTSAGNVDLA  VEVNGK-----QLSAKRF  DVTLGPQFVYVAAYQG  MAPYLTMAEGIKL
Tn501 WP_031769558         HLRRESPFDAGLPAAAPAVLRE  LTVATADGGTHEVNFDRC  DCTDQPQFVYVAAAAG  LFPYLTMVEGLKL
```

Figure 2. MseMerA aligned with other MerAs reveals two loop regions, L1 and L2, that may be involved in conferring thermostability, and two positions at 326 and 452 (highlighted with stars), where the active site region is different between thermophiles and mesophiles.

MEGA (Tamura et al., 2013) was used to compile an amino acid composition chart for the sequences examined. The thermophiles were observed to have a larger number of positively charged amino acids. VADAR calculated the total charged residues in *Mse*MerA to be 25% of residues compared to 21% of residues in *Tn501*MerA, and 24% in *Bc*MerA. An increase in ionic interactions may therefore represent a factor contributing to MerAs thermal stability (Szilágyi and Závodszky, 2000). The aliphatic index of *Mse,* Tn*501,* and *Bc* MerAs were calculated by ExPASy's ProtParam tool (Gasteiger et al., 2005), and found to be 101.63, 98.65, and 97.86, respectively, again in agreement with *Mse*MerA having higher thermostability (Ikai, 1980).

3.2 Biochemical Characterization

The specific activity of *Mse*Mera was examined from 37 °C to 70 °C (Fig. 3). One unit of activity was defined as 1 µmol NADPH oxidized per minute. At 37 °C the specific activity was found to be 1.9 U/mg, increasing up to 3.1 U/mg at 70 °C. Mercury dependence of *Mse*MerA was determined, with K_m values of 400 and 150 µM at 37 °C and 70 °C, respectively. Specific activity was not determined above 70 °C due to the difficulty of discriminating between enzymatic and non-enzymatic NADPH oxidation at high temperatures. The thermal stability of *Mse*MerA was tested by incubating the enzyme at 97 °C for up to 100 minutes, followed by assessment of enzymatic activity at 37 °C. Even after 100 minutes of incubation at 97 °C no decrease in overall activity was observed when compared to the untreated enzyme (Supplemental Figure 1). The K_{cat} at 70 °C was found to be 23 s^{-1}, with a K_{cat}/K_m of 0.15 µM^{-1}s^{-1}.
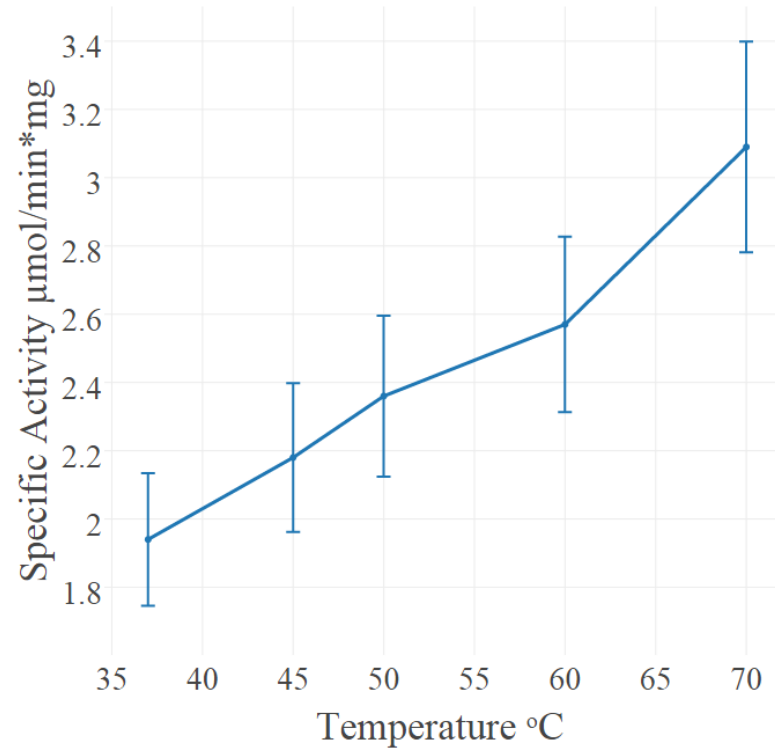
Figure 3.   NADPH oxidation activity of MseMerA incubated at temperatures ranging from 37-70 ºC

	Optimum growth temp ᵒC	Optimum tempera-ture for enzyme activity, ᵒC	K_m, µM		Specific activity, U/mg	Amino Acid substitution at the position V/Y 317/441 (Tn *501* numbering)	Reference
			Hg	NADPH			
M. sedula	50-79	>70	400[a]/150[b]	ND*	1.9[a]/3.1[b]	E/F	This work
*Pa*Tn*501*	25-42	55-65	12	6	12.7	V/Y	(Fox and Walsh, 1982)
ATII-LCL	~68	30-50	8.65	4.35	50	V/Y	(Sayed et al., 2013)
Azotobacter. Chroococcum	26	45	11.11	ND	25	ND	(Ghosh et al., 1999)
Klebsiella pneumoniae	37	40	75	ND	9	V/Y	(Zeroual et al., 2003)
B. cereus	37	ND	30	ND	ND	V/Y	(Rennex et al., 1994)
E. coli R831	37	ND	13	6	1.05	ND	(Schottel, 1978)

Table 1**.** MerA comparison
Abbreviations: ND - not determined
[a] measured at 30 °C
[b] measured at 70 °C

3.3 Structural characterization of *Mse*MerA

     *Mse*MerA crystals were obtained using vapor diffusion in a precipitating solution of 14% polyethylene glycol 4000 and 0.19 M lithium sulfate. These crystals belonged to space group $P22_12_1$ and contained two monomers per asymmetric unit, assembled into one homodimer (Fig 4A). The crystal structure of *Mse*MerA was solved to 1.6 Å, with R and R_{free} values of 16.9% and 19.6%, respectively. Bound FAD was observed, suggesting that these molecules act to stabilize the structure.   No mercury was observed in the active site. As expected based on the sequence alignment, a clear reduction in loop regions was observed in comparison to Tn*501*MerA (Fig. 4B). No electron density for the carboxy terminus of *Mse*MerA was identified from 440-448, including the conserved pair of cysteines at residues 446 and 447. This is in agreement with the carboxy terminus being able to undergo conformational changes during the catalytic cycle (Lian et al., 2014). The solved structure has been deposited in the Protein Data Bank with the accession code
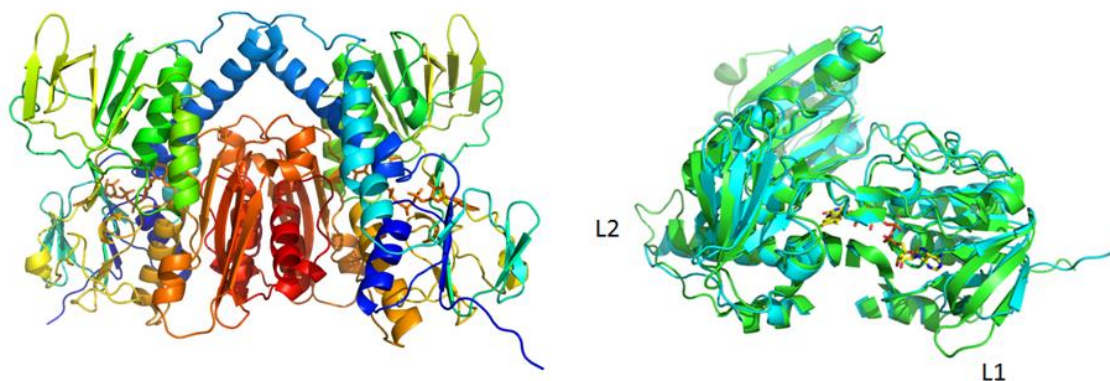
4YWO.

Figure 4 A) Cartoon representation of a dimer of MseMerA with bound FAD. B) Structural superimposition of MseMerA monomer (cyan) with Tn501MerA (green) reveals a decrease in loop regions (labeled L1 and L2) in MseMerA.

4. Discussion

Bioinformatic and phylogenetic data overwhelmingly supports *Mse*MerA being a thermostable protein, as illustrated by features consistent with other enzymes from thermophiles including a reduction in loop regions, a greater percent of charged amino acids, and an overall reduced surface area in comparison to its mesophilic counterpart. Collectively these strategies are likely to interact synergistically to convey the high degree of thermostability observed. Retention of 100% activity after incubation at 97 ℃ for 100 minutes further confirms the highly thermostable nature of *Mse*MerA.

 Though practical constraints made measuring specific activity above 70 °C impossible, catalytic activity was found to increase over the range of 37 °C to 70 °C, with a V_{max} of 3.1 U/mg at 70 °C. This places *Mse*MerA in the range of average activity when compared to other MerAs (Table 1). The K_m for Hg^{2+} of *Mse*MerA was found to decrease from 400 µM at 37 ℃ to 150 µM at 70 °C, indicating a higher affinity for Hg^{2+} ions at elevated temperatures. The K_m of *Mse*MerA is around an order of magnitude higher than that found for other MerAs (Table 1), and may be an adaptive strategy to cope with elevated Hg^{2+} concentrations commonly encountered in the acidic, high temperature environments where *Mse* resides (King et al., 2006;Boyd et al., 2009;Wang et al., 2011).

 The K_{cat} of *Mse*MerA is 23 s^{-1}, which is very similar to the K_{cat} of ATII-LCL at 22.5 s^{-1} (Sayed et al., 2013), and also similar to *Bc*MerA at 12 s^{-1} (Rennex et al., 1994). The higher K_m value observed in *Mse*MerA translates to the lowest overall catalytic efficiency, with a K_{cat}/K_m of 0.15 $µM^{-1}s^{-1}$."

 Though *Pseudomonas aeruginosa* (*Pa*) from which the *Tn501* transposon was isolated is a mesophilic organism, the MerA enzyme was found to have optimal activity at 55-65 ℃, and retained full activity at 37 ℃ even following a ten-minute incubation at 100 ℃ (Nakahara et al., 1985;Vetriani et al., 2005). Intriguingly, phylogenetic analysis indicates that *Tn501*MerA groups closely with the mesophiles (Fig. 1). Conversely,

phylogenetic analysis of MerA from a high temperature brine pool, ATII-LCL (Sayed et al., 2013), was found to group with MerA sequences from mesophilic organisms (Figure 1). While the environment from which ATII-LCL was isolated is at 68 ^oC, the enzyme has maximum activity over a range of 30-50 ^oC, and, when measured at 37 ^oC, was found to be half inactivated after a ten minute incubation at 75 ^oC (Sayed et al., 2013). The ATII-LCLMerA is therefore not nearly as thermostable as *Mse*MerA and is not adapted to its local environment, with respect to the thermal regime, but is adapted with respect to salinity regime.

The structure of *Mse*MerA reveals a dimeric biological assembly, as has been shown with previous structures (Schiering et al., 1991;Ledwidge et al., 2005;Lian et al., 2014). With this architecture, the active site cleft on one monomer interacts with the C-terminal domain of the opposing monomer, (Fig. 5, Table 1). This style of interaction is generally conserved among enzymes of the DSOR family. For example in glutathione reductase, His467, located near the C-terminus of one monomer, is necessary for catalytic function of the opposing monomer (Misra et al., 1985). In MerA, this has been substituted to a catalytically important tyrosine (Rennex et al., 1994).
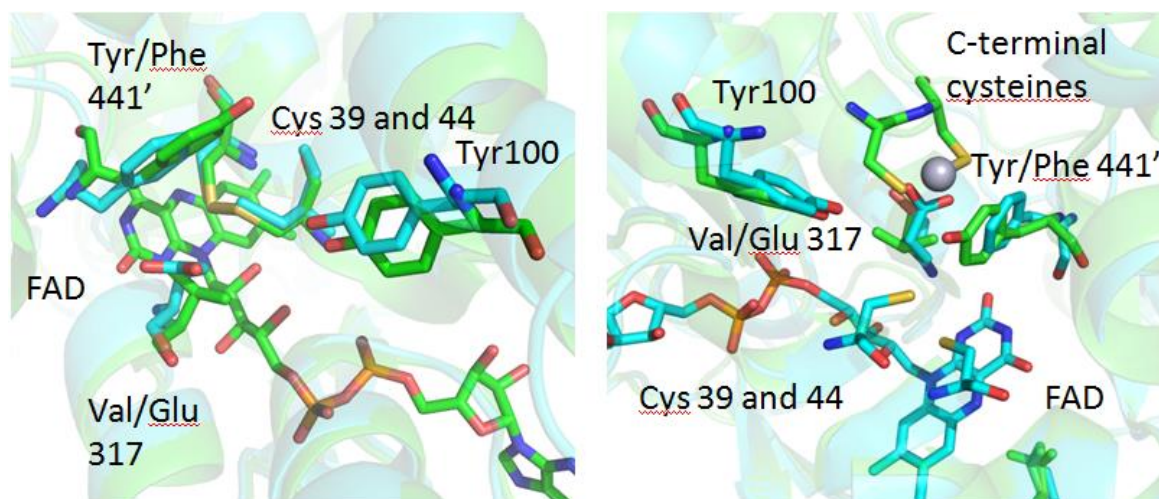

Figure 5 A) Structural superimposition of MseMerA with Tn501MerA 1ZK7 shows the Y441'/V317 amino acids conserved in mesophiles and the F441/E317 amino acids conserved in thermophiles, suggesting an alternative Hg^{2+} coordination strategy in MseMerA. B) An alternative angle of the active site environment of MseMerA superimposed onto Tn501MerA 4K7Z, which depicts the Hg^{2+} ion bound to the c-terminal cysteines. The monomer with the C-terminal cysteines is noted by a 'prime' designation.

Structural superimposition of *Mse*MerA (described here) with the recently solved Tn*501*MerA structure with bound mercury (4K7Z) reveals two specific amino acid substitutions, V317 to E, and Y441' to F', in the active site of *Mse*MerA compared to Tn*501*MerA (numbering is by Tn*501*MerA 4K7Z) (Fig. 5). Another residue thought to be involved in metal coordination, Y100 (in *Bc* structure is Y264) (Schiering et al., 1991), is strictly conserved. For Tn*501*MerA and *Bc*MerA the hydroxyl groups of Y441'

and Y100 likely act in concert to facilitate metal transfer from the C-terminal cysteines to the active site cysteines. In contrast, in *Mse*MerA the F441' in the position of tyrosine in Tn*501*MerA lacks a hydroxyl group to coordinate the Hg^{2+} ion, but a glutamic acid in place of the Tn*501*MerA V317 provides a different residue with which the Hg^{2+} ion could potentially be coordinated.

The conservation of either the V/Y' in mesophiles or the E/F' amino acid pair in thermophiles, along with the observed positions of the amino acids is suggestive of an alternative metal binding strategy for Hg^{2+} ion transfer from the C' cysteine pair to the active site cysteines C42 and C47. In Tn*501*MerA and *Bc*MerA, upon Hg^{2+} ion binding to the C' cysteines, the C' terminal region folds into the catalytic cleft, delivering the mercuric ion (Lian et al., 2014) to the conserved Y100 and Y441', which facilitate transfer to the active site cysteines. Given that *Mse*MerA lacks the Y441 with which to coordinate the Hg^{2+}ion during active site delivery, the E317 is the most rational alternative.

Rennex et al have previously substituted individual amino acids Y441F and Y100F in *Bc*MerA (Rennex et al., 1994). The K_m for Hg^{2+} increased from 30 µM to 39 µM in the case of the Y441F variant, and decreased to 6 µM in the case of the Y100F variant. However, in both cases, the K_{cat}/K_m was decreased around 15-fold. It is therefore likely that the observed low catalytic efficiency of the variant enzymes is due in part to a lack of a residue to coordinate the Hg^{2+} ion, such as the glutamic acid found in *Mse*MerA and other thermophiles. Moreover, Sayed et al (Sayed et al., 2013) previously demonstrated that glutamic acid residues may play a role in Hg^{2+} ion coordination and transfer. However, the active site glutamic acid found in *Mse*MerA is a different site from what Sayed et al (Sayed et al., 2013) have previously characterized. Furthermore, sequence alignment shows that the ATII-LCL enzyme has the V/Y amino acid pair (Table 1).

Both the Tn*501*MerA Y441' and the *Mse*MerA E300 are about 5Å from the active site cysteines, although they coordinate from different positions, with the Y441' coordinating the Hg^{2+} ion almost perpendicular to E317. The different placement and nature of these side chains may help explain the higher K_m observed in *Mse*MerA relative to homologs from mesophilic organisms. Since the high Hg^{2+} concentrations are common features of high temperature environments these differences may reflect adaptations to function at elevated Hg^{2+} concentrations and as such represent the structural determinants of specificity for mercuric reductases. Highly specific stable enzymes, especially those that catalyze oxidation-reduction reactions coupled to the specific molecular recognition, could potentially be used as chemical sensors in which the redox chemistry could be coupled to produce an amplifiable electrical signal.

In conclusion, here we present a characterization of the thermostable mercuric reductase from *M. sedula*. We show that the enzyme is highly resistant to heat treatment while retaining similar catalytic rates to other characterized MerAs. The enzyme appears to have a potentially different way of coordinating Hg^{2+} and has a lower affinity for Hg^{2+} ions than previously characterized enzymes. Considering that *Mse* is a thermophile and its MerA is likely to harbor properties more similar to those of primitive MerA that evolved in a high temperature environments (Barkay et al., 2010), these results may

indicate that the activity of MerA has been refined through evolutionary time to successfully detoxify environmental Hg^{2+} at lower concentrations than those that are naturally present in thermal environments.

5. Acknowledgements

6. References

Argyrou, A., and Blanchard, J.S. (2004). Flavoprotein disulfide reductases: advances in chemistry and function. *Prog Nucleic Acid Res Mol Biol* 78**,** 89-142. doi: 10.1016/s0079-6603(04)78003-4.

Auernik, K.S., Cooper, C.R., and Kelly, R.M. (2008a). Life in hot acid: pathway analyses in extremely thermoacidophilic archaea. *Current Opinion in Biotechnology* 19**,** 445-453. doi: http://dx.doi.org/10.1016/j.copbio.2008.08.001.

Auernik, K.S., Maezato, Y., Blum, P.H., and Kelly, R.M. (2008b). The genome sequence of the metal-mobilizing, extremely thermoacidophilic archaeon Metallosphaera sedula provides insights into bioleaching-associated metabolism. *Appl Environ Microbiol* 74**,** 682-692. doi: 10.1128/aem.02019-07.

Barkay, T., Kritee, K., Boyd, E., and Geesey, G. (2010). A thermophilic bacterial origin and subsequent constraints by redox, light and salinity on the evolution of the microbial mercuric reductase. *Environmental Microbiology* 12**,** 2904-2917. doi: 10.1111/j.1462-2920.2010.02260.x.

Barkay, T., Miller, S.M., and Summers, A.O. (2003). Bacterial mercury resistance from atoms to ecosystems. *FEMS Microbiol Rev* 27**,** 355-384.

Batten, K.M., and Scow, K.M. (2003). Sediment microbial community composition and methylmercury pollution at four mercury mine-impacted sites. *Microbial Ecology* 46**,** 429-441. doi: 10.1007/s00248-003-1005-z.

Boyd, E.S., and Barkay, T. (2012). The mercury resistance operon: from an origin in a geothermal environment to an efficient detoxification machine. *Frontiers in Microbiology* 3. doi: 10.3389/fmicb.2012.00349.

Boyd, E.S., King, S., Tomberlin, J.K., Nordstrom, D.K., Krabbenhoft, D.P., Barkay, T., and Geesey, G.G. (2009). Methylmercury enters an aquatic food web through acidophilic microbial mats in Yellowstone National Park, Wyoming. *Environmental Microbiology* 11**,** 950-959. doi: 10.1111/j.1462-2920.2008.01820.x.

Chen, V.B., Arendall, W.B., 3rd, Headd, J.J., Keedy, D.A., Immormino, R.M., Kapral, G.J., Murray, L.W., Richardson, J.S., and Richardson, D.C. (2010). MolProbity: all-atom structure validation for macromolecular crystallography. *Acta Crystallogr D Biol Crystallogr* 66**,** 12-21.

Cowtan, K., Emsley, P., and Wilson, K.S. (2011). From crystal to structure with CCP4. *Acta Crystallographica Section D: Biological Crystallography* 67**,** 233-234. doi: 10.1107/S0907444911007578.

Delano, W.L. (2002). *The PyMOL Molecular Graphics System* San Carlos, CA, USA.

Emsley, P., Lohkamp, B., Scott, W.G., and Cowtan, K. (2010). Features and development of Coot. *Acta Crystallogr D Biol Crystallogr* 66**,** 486-501.

Fox, B., and Walsh, C.T. (1982). Mercuric reductase. Purification and characterization of a transposon-encoded flavoprotein containing an oxidation-reduction-active disulfide. *Journal of Biological Chemistry* 257**,** 2498-2503.

Gasteiger, E., Hoogland, C., Gattiker, A., Duvaud, S.E., Wilkins, M., Appel, R., and Bairoch, A. (2005). "Protein Identification and Analysis Tools on the ExPASy Server," in *The Proteomics Protocols Handbook,* ed. J. Walker. Humana Press), 571-607.

Gertrud Huber, C.S., Agata Gambacorta, Karl O. Stetter (1989). Metallosphaera sedula gen, and sp. nov. Represents a New Genus of Aerobic, Metal-Mobilizing, Thermoacidophilic Archaebacteria. *Systematic and Applied Microbiology* 12**,** 38-47. doi: 10.1016/S0723-2020.

Ghosh, S., Sadhukhan, P.C., Chaudhuri, J., Ghosh, D.K., and Mandal, A. (1999). Purification and properties of mercuric reductase from Azotobacter chroococcum. *Journal of Applied Microbiology* 86**,** 7-12. doi: 10.1046/j.1365-2672.1999.00605.x.

Guindon, S., Dufayard, J.-F., Lefort, V., Anisimova, M., Hordijk, W., and Gascuel, O. (2010). New Algorithms and Methods to Estimate Maximum-Likelihood Phylogenies: Assessing the Performance of PhyML 3.0. *Systematic Biology* 59**,** 307-321. doi: 10.1093/sysbio/syq010.

Huber, R., Huber, H., and Stetter, K.O. (2000). Towards the ecology of hyperthermophiles: biotopes, new isolation strategies and novel metabolic properties. *FEMS Microbiology Reviews* 24**,** 615-623. doi: 10.1111/j.1574-6976.2000.tb00562.x.

Ikai, A. (1980). Thermostability and aliphatic index of globular proteins. *J Biochem* 88**,** 1895-1898.

King, S.A., Behnke, S., Slack, K., Krabbenhoft, D.P., Nordstrom, D.K., Burr, M.D., and Striegl, R.G. (2006). Mercury in water and biomass of microbial communities in hot springs of Yellowstone National Park, USA. *Applied Geochemistry* 21**,** 1868-1879. doi: http://dx.doi.org/10.1016/j.apgeochem.2006.08.004.

Larkin, M.A., Blackshields, G., Brown, N.P., Chenna, R., Mcgettigan, P.A., Mcwilliam, H., Valentin, F., Wallace, I.M., Wilm, A., Lopez, R., Thompson, J.D., Gibson, T.J., and Higgins, D.G. (2007). Clustal W and Clustal X version 2.0. *Bioinformatics* 23**,** 2947-2948. doi: 10.1093/bioinformatics/btm404.

Ledwidge, R., Patel, B., Dong, A., Fiedler, D., Falkowski, M., Zelikova, J., Summers, A.O., Pai, E.F., and Miller, S.M. (2005). NmerA, the Metal Binding Domain of Mercuric Ion Reductase, Removes Hg2+ from Proteins, Delivers It to the Catalytic Core, and Protects Cells under Glutathione-Depleted Conditions†,‡. *Biochemistry* 44**,** 11402-11416. doi: 10.1021/bi050519d.

Lian, P., Guo, H.-B., Riccardi, D., Dong, A., Parks, J.M., Xu, Q., Pai, E.F., Miller, S.M., Wei, D.-Q., Smith, J.C., and Guo, H. (2014). X-ray Structure of a Hg2+ Complex of Mercuric Reductase (MerA) and Quantum Mechanical/Molecular Mechanical Study of Hg2+ Transfer between the C-Terminal and Buried Catalytic Site Cysteine Pairs. *Biochemistry* 53**,** 7211-7222. doi: 10.1021/bi500608u.

Mcwilliam, H., Li, W., Uludag, M., Squizzato, S., Park, Y.M., Buso, N., Cowley, A.P., and Lopez, R. (2013). Analysis Tool Web Services from the EMBL-EBI. *Nucleic acids research* 41**,** W597-600. doi: 10.1093/nar/gkt376.

Misra, T.K., Brown, N.L., Haberstroh, L., Schmidt, A., Goddette, D., and Silver, S. (1985). Mercuric reductase structural genes from plasmid R100 and transposon Tn501: functional domains of the enzyme. *Gene* 34**,** 253-262. doi: http://dx.doi.org/10.1016/0378-1119(85)90134-9.

Murshudov, G.N., Vagin, A.A., and Dodson, E.J. (1997). Refinement of macromolecular structures by the maximum-likelihood method. *Acta Crystallogr D Biol Crystallogr* 53**,** 240-255.

Nakahara, H., Schottel, J.L., Yamada, T., Miyakawa, Y., Asakawa, M., Harville, J., and Silver, S. (1985). Mercuric reductase enzymes from Streptomyces species and group B Streptococcus. *J Gen Microbiol* 131**,** 1053-1059.

Nies, D.H. (2003). Efflux-mediated heavy metal resistance in prokaryotes. *FEMS Microbiology Reviews* 27**,** 313-339. doi: http://dx.doi.org/10.1016/S0168-6445(03)00048-2.

Otwinowski, Z., and Minor, W. (1997). Processing of X-ray diffraction data collected in oscillation mode. *Macromolecular Crystallography, Pt A* 276**,** 307-326. doi: 10.1016/s0076-6879(97)76066-x.

Pettersen, E.F., Goddard, T.D., Huang, C.C., Couch, G.S., Greenblatt, D.M., Meng, E.C., and Ferrin, T.E. (2004). UCSF Chimera—A visualization system for exploratory research and analysis. *Journal of Computational Chemistry* 25**,** 1605-1612. doi: 10.1002/jcc.20084.

Rennex, D., Pickett, M., and Bradley, M. (1994). In vivo and in vitro effects of mutagenesis of active site tyrosine residues of mercuric reductase. *FEBS Letters* 355**,** 220-222. doi: http://dx.doi.org/10.1016/0014-5793(94)01180-X.

Sayed, A., Ghazy, M.A., Ferreira, A.J.S., Setubal, J.C., Chambergo, F.S., Ouf, A., Adel, M., Dawe, A.S., Archer, J.a.C., Bajic, V.B., Siam, R., and El-Dorry, H. (2013). A novel mercuric reductase from the unique deep brine environment of Atlantis II in the Red Sea. *Journal of Biological Chemistry*. doi: 10.1074/jbc.M113.493429.

Schelert, J., Dixit, V., Hoang, V., Simbahan, J., Drozda, M., and Blum, P. (2004). Occurrence and characterization of mercury resistance in the hyperthermophilic archaeon Sulfolobus solfataricus by use of gene disruption. *J Bacteriol* 186**,** 427-437.

Schelert, J., Rudrappa, D., Johnson, T., and Blum, P. (2013). Role of MerH in mercury resistance in the archaeon Sulfolobus solfataricus. *Microbiology* 159**,** 1198-1208. doi: 10.1099/mic.0.065854-0.

Schiering, N., Kabsch, W., Moore, M.J., Distefano, M.D., Walsh, C.T., and Pai, E.F. (1991). Structure of the detoxification catalyst mercuric ion reductase from Bacillus sp. strain RC607. *Nature* 352**,** 168-172. doi: 10.1038/352168a0.

Schottel, J.L. (1978). The mercuric and organomercurial detoxifying enzymes from a plasmid-bearing strain of Escherichia coli. *Journal of Biological Chemistry* 253**,** 4341-4349.

Simbahan, J., Kurth, E., Schelert, J., Dillman, A., Moriyama, E., Jovanovich, S., and Blum, P. (2005). Community analysis of a mercury hot spring supports occurrence of domain-specific forms of mercuric reductase. *Appl Environ Microbiol* 71**,** 8836-8845. doi: 10.1128/aem.71.12.8836-8845.2005.

Szilágyi, A., and Závodszky, P. (2000). Structural differences between mesophilic, moderately thermophilic and extremely thermophilic protein subunits: results of a comprehensive survey. *Structure* 8**,** 493-504. doi: http://dx.doi.org/10.1016/S0969-2126(00)00133-7.

Tamura, K., Stecher, G., Peterson, D., Filipski, A., and Kumar, S. (2013). MEGA6: Molecular Evolutionary Genetics Analysis version 6.0. *Mol Biol Evol* 30**,** 2725-2729. doi: 10.1093/molbev/mst197.

Vetriani, C., Chew, Y.S., Miller, S.M., Yagi, J., Coombs, J., Lutz, R.A., and Barkay, T. (2005). Mercury Adaptation among Bacteria from a Deep-Sea Hydrothermal Vent. *Applied and Environmental Microbiology* 71**,** 220-226. doi: 10.1128/aem.71.1.220-226.2005.

Wang, Y.P., Boyd, E., Crane, S., Lu-Irving, P., Krabbenhoft, D., King, S., Dighton, J., Geesey, G., and Barkay, T. (2011). Environmental Conditions Constrain the Distribution and

Diversity of Archaeal merA in Yellowstone National Park, Wyoming, U.S.A. *Microbial Ecology* 62**,** 739-752. doi: 10.1007/s00248-011-9890-z.

Willard, L., Ranjan, A., Zhang, H., Monzavi, H., Boyko, R.F., Sykes, B.D., and Wishart, D.S. (2003). VADAR: a web server for quantitative evaluation of protein structure quality. *Nucleic Acids Research* 31**,** 3316-3319.

Zeroual, Y., Moutaouakkil, A., Dzairi, F.Z., Talbi, M., Chung, P.U., Lee, K., and Blaghen, M. (2003). Purification and characterization of cytosolic mercuric reductase from Klebsiella pneumoniae. *Annals of Microbiology* 53**,** 149-160.

CUMULATIVE REFERENCES CITED

Adami, M., M. Martini, and L. Piras. 1995. 'Characterization and enzymatic application of a redox potential biosensor based on a silicon transducer', *Biosensors and Bioelectronics*, 10: 633-38.

Adams, M W, E Eccleston, and J B Howard. 1989. 'Iron-sulfur clusters of hydrogenase I and hydrogenase II of Clostridium pasteurianum', *Proceedings of the National Academy of Sciences*, 86: 4932-36.

Adams, M. W. 1987. 'The mechanisms of H2 activation and CO binding by hydrogenase I and hydrogenase II of Clostridium pasteurianum', *J Biol Chem*, 262: 15054-61.

Adams, M. W. 1990. 'The structure and mechanism of iron-hydrogenases', *Biochim Biophys Acta*, 1020: 115-45.

Adams, M. W., and L. E. Mortenson. 1984a. 'The physical and catalytic properties of hydrogenase II of Clostridium pasteurianum. A comparison with hydrogenase I', *J Biol Chem*, 259: 7045-55.

Adams, Michael W. W., and Leonard E. Mortenson. 1984b. 'The purification of hydrogenase II (uptake hydrogenase) from the anaerobic N2-fixing bacterium Clostridium pasteurianum', *Biochimica et Biophysica Acta (BBA) - Bioenergetics*, 766: 51-61.

Adamska, A., A. Silakov, C. Lambertz, O. Rudiger, T. Happe, E. Reijerse, and W. Lubitz. 2012. 'Identification and characterization of the "super-reduced" state of the H-cluster in [FeFe] hydrogenase: a new building block for the catalytic cycle?', *Angew Chem Int Ed Engl*, 51: 11458-62.

Albracht, S. P., W. Roseboom, and E. C. Hatchikian. 2006. 'The active site of the [FeFe]-hydrogenase from Desulfovibrio desulfuricans. I. Light sensitivity and magnetic hyperfine interactions as observed by electron paramagnetic resonance', *J Biol Inorg Chem*, 11: 88-101.

Argyrou, A., and J. S. Blanchard. 2004. 'Flavoprotein disulfide reductases: advances in chemistry and function', *Prog Nucleic Acid Res Mol Biol*, 78: 89-142.

Armstrong, Fraser A., Rhiannon M. Evans, Suzannah V. Hexter, Bonnie J. Murphy, Maxie M. Roessler, and Philip Wulff. 2016. 'Guiding Principles of Hydrogenase Catalysis Instigated and Clarified by Protein Film Electrochemistry', *Accounts of Chemical Research*, 49: 884-92.

Arnold, K., L. Bordoli, J. Kopp, and T. Schwede. 2006. 'The SWISS-MODEL workspace: a web-based environment for protein structure homology modelling', *Bioinformatics*, 22: 195-201.

Assenov, Yassen, Fidel Ramírez, Sven-Eric Schelhorn, Thomas Lengauer, and Mario Albrecht. 2008. 'Computing topological parameters of biological networks', *Bioinformatics*, 24: 282-84.

Auernik, K. S., C. R. Cooper, and R. M. Kelly. 2008. 'Life in hot acid: pathway analyses in extremely thermoacidophilic archaea', *Curr Opin Biotechnol*, 19: 445-53.

Auernik, K. S., Y. Maezato, P. H. Blum, and R. M. Kelly. 2008. 'The genome sequence of the metal-mobilizing, extremely thermoacidophilic archaeon Metallosphaera sedula provides insights into bioleaching-associated metabolism', *Appl Environ Microbiol*, 74: 682-92.

Baffert, C., M. Demuez, L. Cournac, B. Burlat, B. Guigliarelli, P. Bertrand, L. Girbal, and C. Leger. 2008. 'Hydrogen-activating enzymes: activity does not correlate with oxygen sensitivity', *Angew Chem Int Ed Engl*, 47: 2052-4.

Barkay, T., K. Kritee, E. Boyd, and G. Geesey. 2010. 'A thermophilic bacterial origin and subsequent constraints by redox, light and salinity on the evolution of the microbial mercuric reductase', *Environ Microbiol*, 12: 2904-17.

Barkay, T., S. M. Miller, and A. O. Summers. 2003. 'Bacterial mercury resistance from atoms to ecosystems', *FEMS Microbiol Rev*, 27: 355-84.

Batten, K. M., and K. M. Scow. 2003. 'Sediment microbial community composition and methylmercury pollution at four mercury mine-impacted sites', *Microb Ecol*, 46: 429-41.

Becker, René, Saeed Amirjalayer, Ping Li, Sander Woutersen, and Joost N. H. Reek. 2016. 'An iron-iron hydrogenase mimic with appended electron reservoir for efficient proton reduction in aqueous media', *Science Advances*, 2.

Bennett, B., B. J. Lemon, and J. W. Peters. 2000. 'Reversible carbon monoxide binding and inhibition at the active site of the Fe-only hydrogenase', *Biochemistry*, 39: 7455-60.

Berggren, G., A. Adamska, C. Lambertz, T. R. Simmons, J. Esselborn, M. Atta, S. Gambarelli, J. M. Mouesca, E. Reijerse, W. Lubitz, T. Happe, V. Artero, and M. Fontecave. 2013. 'Biomimetic assembly and activation of [FeFe]-hydrogenases', *Nature*, 499: 66-69.

Bettegowda, C., X. Huang, J. Lin, I. Cheong, M. Kohli, S. A. Szabo, X. Zhang, L. A. Diaz, Jr., V. E. Velculescu, G. Parmigiani, K. W. Kinzler, B. Vogelstein, and S. Zhou. 2006. 'The genome and transcriptomes of the anti-tumor agent Clostridium novyi-NT', *Nat Biotechnol*, 24: 1573-80.

Bingham, Alyssa S., Phillip R. Smith, and James R. Swartz. 2012. 'Evolution of an [FeFe] hydrogenase with decreased oxygen sensitivity', *International Journal of Hydrogen Energy*, 37: 2965-76.

Blomberg, S.P., Jr. Garland, T.,, and A.R. Ives. 2003. 'Testing for phylogenetic signal in comparative data: behavioral traits are more labile', *Evolution*, 57: 717-45.

Bourrez, Marc, Romain Steinmetz, Sascha Ott, Frederic Gloaguen, and Leif Hammarström. 2015. 'Concerted proton-coupled electron transfer from a metal-hydride complex', *Nat Chem*, 7: 140-45.

Boyd, E. S., and T. Barkay. 2012. 'The mercury resistance operon: from an origin in a geothermal environment to an efficient detoxification machine', *Front Microbiol*, 3: 349.

Boyd, E. S., T. L. Hamilton, K. D. Swanson, A. E. Howells, B. K. Baxter, J. E. Meuser, M. C. Posewitz, and J. W. Peters. 2014. '[FeFe]-hydrogenase abundance and diversity along a vertical redox gradient in Great Salt Lake, USA', *Int J Mol Sci*, 15: 21947-66.

Boyd, E. S., S. King, J. K. Tomberlin, D. K. Nordstrom, D. P. Krabbenhoft, T. Barkay, and G. G. Geesey. 2009. 'Methylmercury enters an aquatic food web through acidophilic microbial mats in Yellowstone National Park, Wyoming', *Environ Microbiol*, 11: 950-9.

Broderick, Joan B., Benjamin R. Duffus, Kaitlin S. Duschene, and Eric M. Shepard. 2014. 'Radical S-Adenosylmethionine Enzymes', *Chem Rev*, 114: 4229-317.

Bruno-Barcena, José M., Mari S. Chinn, and Amy M. Grunden. 2013. 'Genome Sequence of the Autotrophic Acetogen Clostridium autoethanogenum JA1-1 Strain DSM 10061, a Producer of Ethanol from Carbon Monoxide', *Genome Announcements*, 1.

Bruska, M. K., M. T. Stiebritz, and M. Reiher. 2011. 'Regioselectivity of H cluster oxidation', *J Am Chem Soc*, 133: 20588-603.

Buckel, Wolfgang, and Rudolf K. Thauer. 2013. 'Energy conservation via electron bifurcating ferredoxin reduction and proton/Na+ translocating ferredoxin oxidation', *Biochimica et Biophysica Acta (BBA) - Bioenergetics*, 1827: 94-113.

Butt, J. N., M. Filipiak, and W. R. Hagen. 1997. 'Direct electrochemistry of Megasphaera elsdenii iron hydrogenase. Definition of the enzyme's catalytic operating potential and quantitation of the catalytic behaviour over a continuous potential range', *Eur J Biochem*, 245: 116-22.

Calusinska, M., T. Happe, B. Joris, and A. Wilmotte. 2010. 'The surprising diversity of clostridial hydrogenases: a comparative genomic perspective', *Microbiology*, 156: 1575-88.

Calusinska, M., B. Joris, and A. Wilmotte. 2011. 'Genetic diversity and amplification of different clostridial [FeFe] hydrogenases by group-specific degenerate primers', *Lett Appl Microbiol*, 53: 473-80.

Casalot, Laurence, and Marc Rousset. 2001. 'Maturation of the [NiFe] hydrogenases', *Trends in Microbiology*, 9: 228-37.

Cendron, Laura, Paola Berto, Sarah D'Adamo, Francesca Vallese, Chiara Govoni, Matthew C. Posewitz, Giorgio M. Giacometti, Paola Costantini, and Giuseppe Zanotti. 2011. 'Crystal Structure of HydF Scaffold Protein Provides Insights into [FeFe]-Hydrogenase Maturation', *Journal of Biological Chemistry*, 286: 43944-50.

Chen, Jiann-Shin, and D. Kay Blanchard. 1978. 'Isolation and properties of a unidirectional H2-oxidizing hydrogenase from the strictly anaerobic N2-fixing bacterium Clostridium pasteurianum W5', *Biochem Biophys Res Commun*, 84: 1144-50.

Chen, Jiann-Shin, and Leonard E. Mortenson. 1974. 'Purification and properties of hydrogenase from Clostridium pasteurianum W5', *Biochimica et Biophysica Acta (BBA) - Protein Structure*, 371: 283-98.

Chen, V. B., W. B. Arendall, 3rd, J. J. Headd, D. A. Keedy, R. M. Immormino, G. J. Kapral, L. W. Murray, J. S. Richardson, and D. C. Richardson. 2010. 'MolProbity: all-atom structure validation for macromolecular crystallography', *Acta Crystallogr D Biol Crystallogr*, 66: 12-21.

Chen, Z., B. J. Lemon, S. Huang, D. J. Swartz, J. W. Peters, and K. A. Bagley. 2002. 'Infrared studies of the CO-inhibited form of the Fe-only hydrogenase from Clostridium pasteurianum I: examination of its light sensitivity at cryogenic temperatures', *Biochemistry*, 41: 2036-43.

Cohen, J., K. Kim, P. King, M. Seibert, and K. Schulten. 2005. 'Finding gas diffusion pathways in proteins: application to O2 and H2 transport in CpI [FeFe]-hydrogenase and the role of packing defects', *Structure*, 13: 1321-9.

Cohen, J., K. Kim, M. Posewitz, M. L. Ghirardi, K. Schulten, M. Seibert, and P. King. 2005. 'Molecular dynamics and experimental investigation of H(2) and O(2) diffusion in [Fe]-hydrogenase', *Biochem Soc Trans*, 33: 80-2.

Cornish, A. J., K. Gartner, H. Yang, J. W. Peters, and E. L. Hegg. 2011. 'Mechanism of proton transfer in [FeFe]-hydrogenase from Clostridium pasteurianum', *J Biol Chem*, 286: 38341-7.

Cowtan, K., P. Emsley, and K. S. Wilson. 2011. 'From crystal to structure with CCP4', *Acta Crystallogr D Biol Crystallogr*, 67: 233-4.

Czech, Ilka, Alexey Silakov, Wolfgang Lubitz, and Thomas Happe. 2010. 'The [FeFe]-hydrogenase maturase HydF from Clostridium acetobutylicum contains a CO and CN− ligated iron cofactor', *FEBS Letters*, 584: 638-42.

Czech, Ilka, Sven Stripp, Oliver Sanganas, Nils Leidel, Thomas Happe, and Michael Haumann. 2011. 'The [FeFe]-hydrogenase maturation protein HydF contains a H-cluster like [4Fe4S]–2Fe site', *FEBS Letters*, 585: 225-30.

Dalton, H., J. A. Morris, M. A. Ward, and L. E. Mortenson. 1971. 'Purification and some properties of molybdoferredoxin, a component of nitrogenase from Clostridium pasteurianum', *Biochemistry*, 10: 2066-72.

Delano, W. L. 2002. 'The PyMOL Molecular Graphics System'.

Dey, Subal, Atanu Rana, Danielle Crouthers, Biswajit Mondal, Pradip Kumar Das, Marcetta Y. Darensbourg, and Abhishek Dey. 2014. 'Electrocatalytic O2 Reduction by [Fe-Fe]-Hydrogenase Active Site Models', *Journal of the American Chemical Society*, 136: 8847-50.

Driesener, Rebecca C., Benjamin R. Duffus, Eric M. Shepard, Ian R. Bruzas, Kaitlin S. Duschene, Natalie J. R. Coleman, Alexander P. G. Marrison, Enrico Salvadori, Christopher W. M. Kay, John W. Peters, Joan B. Broderick, and Peter L. Roach. 2013. 'Biochemical and Kinetic Characterization of Radical S-Adenosyl-l-methionine Enzyme HydG', *Biochemistry*, 52: 8696-707.

Emsley, P., B. Lohkamp, W. G. Scott, and K. Cowtan. 2010. 'Features and development of Coot', *Acta Crystallographica Section D*, 66: 486-501.

English, C. M., C. Eckert, K. Brown, M. Seibert, and P. W. King. 2009. 'Recombinant and in vitro expression systems for hydrogenases: new frontiers in basic and applied studies for biological and synthetic H2 production', *Dalton Trans*: 9970-8.

Erbes, D. L., D. King, and M. Gibbs. 1979. 'Inactivation of Hydrogenase in Cell-free Extracts and Whole Cells of Chlamydomonas reinhardi by Oxygen', *Plant Physiol*, 63: 1138-42.

Evans, P. 2006. 'Scaling and assessment of data quality', *Acta Crystallogr D Biol Crystallogr*, 62: 72-82.

Evans, Rhiannon M., and Fraser A. Armstrong. 2014. 'Electrochemistry of Metalloproteins: Protein Film Electrochemistry for the Study of E. coli [NiFe]-Hydrogenase-1.' in Juan C. Fontecilla-Camps and Yvain Nicolet (eds.), *Metalloproteins: Methods and Protocols* (Humana Press: Totowa, NJ).

Finkelmann, A. R., M. T. Stiebritz, and M. Reiher. 2014. 'Activation barriers of oxygen transformation at the active site of [FeFe] hydrogenases', *Inorg Chem*, 53: 11890-902.

Forestier, M., P. King, L. Zhang, M. Posewitz, S. Schwarzer, T. Happe, M. L. Ghirardi, and M. Seibert. 2003. 'Expression of two [Fe]-hydrogenases in Chlamydomonas reinhardtii under anaerobic conditions', *Eur J Biochem*, 270: 2750-8.

Fourmond, Vincent, Claudio Greco, Kateryna Sybirna, Carole Baffert, Po-Hung Wang, Pierre Ezanno, Marco Montefiori, Maurizio Bruschi, Isabelle Meynial-Salles, Philippe Soucaille, Jochen Blumberger, Hervé Bottin, Luca De Gioia, and Christophe Léger. 2014. 'The oxidative inactivation of FeFe hydrogenase reveals the flexibility of the H-cluster', *Nat Chem*, 6: 336-42.

Fox, B, and C T Walsh. 1982. 'Mercuric reductase. Purification and characterization of a transposon-encoded flavoprotein containing an oxidation-reduction-active disulfide', *Journal of Biological Chemistry*, 257: 2498-503.

Gasteiger, Elisabeth, Christine Hoogland, Alexandre Gattiker, S'everine Duvaud, Marc R. Wilkins, Ron D. Appel, and Amos Bairoch. 2005. 'Protein Identification and Analysis Tools on the ExPASy Server.' in John M. Walker (ed.), *The Proteomics Protocols Handbook* (Humana Press: Totowa, NJ).

Ghirardi, M. L. 2015. 'Implementation of photobiological H2 production: the O 2 sensitivity of hydrogenases', *Photosynth Res*, 125: 383-93.

Ghirardi, M. L., M. C. Posewitz, P. C. Maness, A. Dubini, J. Yu, and M. Seibert. 2007. 'Hydrogenases and hydrogen photoproduction in oxygenic photosynthetic organisms', *Annu Rev Plant Biol*, 58: 71-91.

Ghirardi, Maria L., Jordi Cohen, Paul King, Klaus Schulten, Kwiseon Kim, and Michael Seibert. 2006. "[FeFe]-hydrogenases and photobiological hydrogen production." In, 63400X-00X-6.

Ghosh, S., P. C. Sadhukhan, J. Chaudhuri, D. K. Ghosh, and A. Mandal. 1999. 'Purification and properties of mercuric reductase from Azotobacter chroococcum', *Journal of Applied Microbiology*, 86: 7-12.

Ginovska-Pangovska, Bojana, Arnab Dutta, Matthew L. Reback, John C. Linehan, and Wendy J. Shaw. 2014. 'Beyond the Active Site: The Impact of the Outer Coordination Sphere on Electrocatalysts for Hydrogen Production and Oxidation', *Accounts of Chemical Research*, 47: 2621-30.

Goldet, G., C. Brandmayr, S. T. Stripp, T. Happe, C. Cavazza, J. C. Fontecilla-Camps, and F. A. Armstrong. 2009. 'Electrochemical kinetic investigations of the reactions of [FeFe]-hydrogenases with carbon monoxide and oxygen: comparing the importance of gas tunnels and active-site electronic/redox effects', *J Am Chem Soc*, 131: 14979-89.

Goris, J., K. T. Konstantinidis, J. A. Klappenbach, T. Coenye, P. Vandamme, and J. M. Tiedje. 2007. 'DNA-DNA hybridization values and their relationship to whole-genome sequence similarities', *Int J Syst Evol Microbiol*, 57: 81-91.

Greco, C; Fourmond, V; Baffert, C; Wang, P-H; Dementin, S; Bertrand, P; Bruschi, M. 2014. 'Combining experimental and theoretical methods to learn about the reactivity of gas-processing metalloenzymes', *ENERGY & ENVIRONMENTAL SCIENCE*, 7: 3543-73.

Guindon, S., J. F. Dufayard, V. Lefort, M. Anisimova, W. Hordijk, and O. Gascuel. 2010. 'New algorithms and methods to estimate maximum-likelihood phylogenies: assessing the performance of PhyML 3.0', *Syst Biol*, 59: 307-21.

Hamilton, T. L., M. Ludwig, R. Dixon, E. S. Boyd, P. C. Dos Santos, J. C. Setubal, D. A. Bryant, D. R. Dean, and J. W. Peters. 2011. 'Transcriptional profiling of nitrogen fixation in Azotobacter vinelandii', *J Bacteriol*, 193: 4477-86.

Han, Shubo, Min Zhu, Zhuobin Yuan, and Xin Li. 2001. 'A methylene blue-mediated enzyme electrode for the determination of trace mercury(II), mercury(I), methylmercury, and mercury–glutathione complex', *Biosensors and Bioelectronics*, 16: 9-16.

Happe, T., and A. Kaminski. 2002. 'Differential regulation of the Fe-hydrogenase during anaerobic adaptation in the green alga Chlamydomonas reinhardtii', *Eur J Biochem*, 269: 1022-32.

Happe, T., B. Mosler, and J. D. Naber. 1994. 'Induction, localization and metal content of hydrogenase in the green alga Chlamydomonas reinhardtii', *Eur J Biochem*, 222: 769-74.

Hardy, R. W. F., R. D. Holsten, E. K. Jackson, and R. C. Burns. 1968. 'The Acetylene-Ethylene Assay for N2 Fixation: Laboratory and Field Evaluation', *Plant Physiology*, 43: 1185-207.

Henry, J. T., and S. Crosson. 2011. 'Ligand-binding PAS domains in a genomic, cellular, and structural context', *Annu Rev Microbiol*, 65: 261-86.

Herrmann, Gloria, Elamparithi Jayamani, Galina Mai, and Wolfgang Buckel. 2008. 'Energy Conservation via Electron-Transferring Flavoprotein in Anaerobic Bacteria', *J Bacteriol*, 190: 784-91.

Hong, G., and R. Pachter. 2012. 'Inhibition of biocatalysis in [Fe-Fe] hydrogenase by oxygen: molecular dynamics and density functional theory calculations', *ACS Chem Biol*, 7: 1268-75.

Huang, H., S. Wang, J. Moll, and R. K. Thauer. 2012. 'Electron bifurcation involved in the energy metabolism of the acetogenic bacterium Moorella thermoacetica growing on glucose or H2 plus CO2', *J Bacteriol*, 194: 3689-99.

Huber, Gertrud, Carola Spinnler, Agata Gambacorta, and Karl O. Stetter. 1989. 'Metallosphaera sedula gen, and sp. nov. Represents a New Genus of Aerobic, Metal-Mobilizing, Thermoacidophilic Archaebacteria', *Systematic and Applied Microbiology*, 12: 38-47.

Huber, R., H. Huber, and K. O. Stetter. 2000. 'Towards the ecology of hyperthermophiles: biotopes, new isolation strategies and novel metabolic properties', *FEMS Microbiol Rev*, 24: 615-23.

Ikai, A. 1980. 'Thermostability and aliphatic index of globular proteins', *J Biochem*, 88: 1895-8.

Kabsch, W. 2010a. 'XDS', *Acta Crystallogr D Biol Crystallogr*, 66: 125-32.

Kabsch, Wolfgang. 2010b. 'Integration, scaling, space-group assignment and post-refinement', *Acta Crystallographica Section D: Biological Crystallography*, 66: 133-44.

Keita, Bineta, Ulrich Kortz, Luis Roberto Brudna Holzle, Spencer Brown, and Louis Nadjo. 2007. 'Efficient Hydrogen-Evolving Cathodes Based on Proton and Electron Reservoir Behaviors of the Phosphotungstate $[H_7P_8W_{48}O_{184}]_{33}$- and the Co(II)-Containing Silicotungstates $[Co_6(H_2O)_{30}\{Co_9Cl_2(OH)_3(H_2O)_9(\beta$-$SiW_8O_{31})_3\}]_5$- and $[\{Co_3(B$-β-$SiW_9O_{33}(OH))(B$-β-$SiW_8O_{29}OH)_2\}_2]_{22}$', *Langmuir*, 23: 9531-34.

Kembel, Steven. 2010. 'An introduction to the picante package'.

Kettenhofen, N. J., and M. J. Wood. 2010. 'Formation, reactivity, and detection of protein sulfenic acids', *Chem Res Toxicol*, 23: 1633-46.

King, Paul W. 2013. 'Designing interfaces of hydrogenase–nanomaterial hybrids for efficient solar conversion', *Biochimica et Biophysica Acta (BBA) - Bioenergetics*, 1827: 949-57.

King, Paul W., Matthew C. Posewitz, Maria L. Ghirardi, and Michael Seibert. 2006. 'Functional Studies of [FeFe] Hydrogenase Maturation in an Escherichia coli Biosynthetic System', *J Bacteriol*, 188: 2163-72.

King, Paul W., Drazenka Svedruzic, Jordi Cohen, Klaus Schulten, Michael Seibert, and Maria L. Ghirardi. 2006. "Structural and functional investigations of biological catalysts for optimization of solar-driven H2 production systems." In, 63400Y-00Y-9.

King, S. A., S. Behnke, K. Slack, D. P. Krabbenhoft, D. K. Nordstrom, M. D. Burr, and R. G. Striegl. 2006. 'Mercury in water and biomass of microbial communities in hot springs of Yellowstone National Park, USA', *Applied Geochemistry*, 21: 1868-79.

Knörzer, Philipp, Alexey Silakov, Carina E. Foster, Fraser A. Armstrong, Wolfgang Lubitz, and Thomas Happe. 2012. 'Importance of the Protein Framework for Catalytic Activity of [FeFe]-Hydrogenases', *Journal of Biological Chemistry*, 287: 1489-99.

Kolek, Jan, Karel Sedlář, Ivo Provazník, and Petra Patáková. 2014. 'Draft Genome Sequence of Clostridium pasteurianum NRRL B-598, a Potential Butanol or Hydrogen Producer', *Genome Announcements*, 2.

Kowal, A. T., M. W. Adams, and M. K. Johnson. 1989. 'Electron paramagnetic resonance studies of the low temperature photolytic behavior of oxidized hydrogenase I from Clostridium pasteurianum', *J Biol Chem*, 264: 4342-8.

Kriek, Marco, Filipa Martins, Martin R Challand, Anna Croft, and Peter L Roach. 2007. 'Thiamine Biosynthesis in Escherichia coli: Identification of the Intermediate and By-Product Derived from Tyrosine', *Angewandte Chemie International Edition*, 46: 9223-26.

Kubas, A., D. De Sancho, R. B. Best, and J. Blumberger. 2014. 'Aerobic damage to [FeFe]-hydrogenases: activation barriers for the chemical attachment of O2', *Angew Chem Int Ed Engl*, 53: 4081-4.

Kuchenreuther, Jon M., R. David Britt, and James R. Swartz. 2012. 'New Insights into [FeFe] Hydrogenase Activation and Maturase Function', *PLoS ONE*, 7: e45850.

Kuchenreuther, Jon M., Simon J. George, Celestine S. Grady-Smith, Stephen P. Cramer, and James R. Swartz. 2011. 'Cell-free H-cluster Synthesis and [FeFe] Hydrogenase Activation: All Five CO and CN$^-$ Ligands Derive from Tyrosine', *PLoS ONE*, 6: e20346.

Kuchenreuther, Jon M., William K. Myers, Daniel L. M. Suess, Troy A. Stich, Vladimir Pelmenschikov, Stacey A. Shiigi, Stephen P. Cramer, James R. Swartz, R. David Britt, and Simon J. George. 2014. 'The HydG Enzyme Generates an Fe(CO)^2(CN) Synthon in Assembly of the FeFe Hydrogenase H-Cluster', *Science*, 343: 424-27.

Laane, Colja, Huub Haaker, and Cees Veeger. 1979. 'On the Efficiency of Oxidative Phosphorylation in Membrane Vesicles of Azotobacter vinelandii and of Rhizobium leguminosarum Bacteroids', *European Journal of Biochemistry*, 97: 369-77.

Lambertz, Camilla, Nils Leidel, Kajsa G. V. Havelius, Jens Noth, Petko Chernev, Martin Winkler, Thomas Happe, and Michael Haumann. 2011. 'O(2) Reactions at the Six-iron Active Site (H-cluster) in [FeFe]-Hydrogenase', *J Biol Chem*, 286: 40614-23.

Larkin, M. A., G. Blackshields, N. P. Brown, R. Chenna, P. A. McGettigan, H. McWilliam, F. Valentin, I. M. Wallace, A. Wilm, R. Lopez, J. D. Thompson, T. J. Gibson, and D. G. Higgins. 2007. 'Clustal W and Clustal X version 2.0', *Bioinformatics*, 23: 2947-8.

Lautier, T., P. Ezanno, C. Baffert, V. Fourmond, L. Cournac, J. C. Fontecilla-Camps, P. Soucaille, P. Bertrand, I. Meynial-Salles, and C. Leger. 2011. 'The quest for a functional substrate access tunnel in FeFe hydrogenase', *Faraday Discuss*, 148: 385-407; discussion 21-41.

Ledwidge, R., B. Patel, A. Dong, D. Fiedler, M. Falkowski, J. Zelikova, A. O. Summers, E. F. Pai, and S. M. Miller. 2005. 'NmerA, the metal binding domain of mercuric ion reductase, removes Hg2+ from proteins, delivers it to the catalytic core, and protects cells under glutathione-depleted conditions', *Biochemistry*, 44: 11402-16.

Letunic, Ivica, and Peer Bork. 2007. 'Interactive Tree Of Life (iTOL): an online tool for phylogenetic tree display and annotation', *Bioinformatics*, 23: 127-28.

Li, Fuli, Julia Hinderberger, Henning Seedorf, Jin Zhang, Wolfgang Buckel, and Rudolf K. Thauer. 2008. 'Coupled Ferredoxin and Crotonyl Coenzyme A (CoA) Reduction with NADH Catalyzed by the Butyryl-CoA Dehydrogenase/Etf Complex from Clostridium kluyveri', *J Bacteriol*, 190: 843-50.

Lian, P., H. B. Guo, D. Riccardi, A. Dong, J. M. Parks, Q. Xu, E. F. Pai, S. M. Miller, D. Q. Wei, J. C. Smith, and H. Guo. 2014. 'X-ray structure of a Hg2+ complex of mercuric reductase (MerA) and quantum mechanical/molecular mechanical study of Hg2+ transfer between the C-terminal and buried catalytic site cysteine pairs', *Biochemistry*, 53: 7211-22.

Liebgott, Pierre-Pol, Antonio L. de Lacey, Bénédicte Burlat, Laurent Cournac, Pierre Richaud, Myriam Brugna, Victor M. Fernandez, Bruno Guigliarelli, Marc Rousset, Christophe Léger, and Sébastien Dementin. 2011. 'Original Design of an Oxygen-Tolerant [NiFe] Hydrogenase: Major Effect of a Valine-to-Cysteine Mutation near the Active Site', *Journal of the American Chemical Society*, 133: 986-97.

Liebgott, Pierre-Pol, Fanny Leroux, Bénédicte Burlat, Sébastien Dementin, Carole Baffert, Thomas Lautier, Vincent Fourmond, Pierre Ceccaldi, Christine Cavazza, Isabelle Meynial-Salles, Philippe Soucaille, Juan Carlos Fontecilla-Camps, Bruno Guigliarelli, Patrick Bertrand, Marc Rousset, and Christophe Léger. 2010. 'Relating diffusion along the substrate tunnel and oxygen sensitivity in hydrogenase', *Nat Chem Biol*, 6: 63-70.

Liu, Jing, Saumen Chakraborty, Parisa Hosseinzadeh, Yang Yu, Shiliang Tian, Igor Petrik, Ambika Bhagi, and Yi Lu. 2014. 'Metalloproteins Containing Cytochrome, Iron–Sulfur, or Copper Redox Centers', *Chem Rev*, 114: 4366-469.

Liu, T., B. Li, M. L. Singleton, M. B. Hall, and M. Y. Darensbourg. 2009. 'Sulfur oxygenates of biomimetics of the diiron subsite of the [FeFe]-hydrogenase active site: properties and oxygen damage repair possibilities', *J Am Chem Soc*, 131: 8296-307.

Liu R, Zhang G, Cao H, Zhang S, Xie Y, Haider A, Kortz U, Chen B, Dalal NS, Zhao Y. 2016. 'Enhanced proton and electron reservoir abilities of polyoxometalate grafted on graphene for high-performance hydrogen evolution' *Energy & Environmental Science,* 9: 1012-1023.

Lubitz, Wolfgang, Hideaki Ogata, Olaf Rüdiger, and Edward Reijerse. 2014. 'Hydrogenases', *Chem Rev*, 114: 4081-148.

Madden, Christopher, Michael D. Vaughn, Ismael Díez-Pérez, Katherine A. Brown, Paul W. King, Devens Gust, Ana L. Moore, and Thomas A. Moore. 2012. 'Catalytic Turnover of [FeFe]-Hydrogenase Based on Single-Molecule Imaging', *Journal of the American Chemical Society*, 134: 1577-82.

Mallette, M. F., Paul Reece, and E. A. Dawes. 1974. 'Culture of Clostridium pasteurianum in Defined Medium and Growth as a Function of Sulfate Concentration', *Applied Microbiology*, 28: 999-1003.

Marchler-Bauer, A., M. K. Derbyshire, N. R. Gonzales, S. Lu, F. Chitsaz, L. Y. Geer, R. C. Geer, J. He, M. Gwadz, D. I. Hurwitz, C. J. Lanczycki, F. Lu, G. H. Marchler, J. S. Song, N. Thanki, Z. Wang, R. A. Yamashita, D. Zhang, C. Zheng, and S. H. Bryant. 2015. 'CDD: NCBI's conserved domain database', *Nucleic Acids Res*, 43: D222-6.

Mardis, Elaine R. 2008. 'Next-Generation DNA Sequencing Methods', *Annual Review of Genomics and Human Genetics*, 9: 387-402.

Markowitz, Victor M., I-Min A. Chen, Krishna Palaniappan, Ken Chu, Ernest Szeto, Yuri Grechkin, Anna Ratner, Biju Jacob, Jinghua Huang, Peter Williams, Marcel Huntemann, Iain Anderson, Konstantinos Mavromatis, Natalia N. Ivanova, and Nikos C. Kyrpides. 2012. 'IMG: the integrated microbial genomes database and comparative analysis system', *Nucleic Acids Research*, 40: D115-D22.

McGlynn, Shawn E., Eric M. Shepard, Mark A. Winslow, Anatoli V. Naumov, Kaitlin S. Duschene, Matthew C. Posewitz, William E. Broderick, Joan B. Broderick, and John W. Peters. 2008. 'HydF as a scaffold protein in [FeFe] hydrogenase H-cluster biosynthesis', *FEBS Letters*, 582: 2183-87.

McKinlay, J. B., and C. S. Harwood. 2010. 'Photobiological production of hydrogen gas as a biofuel', *Curr Opin Biotechnol*, 21: 244-51.

McWilliam, H., W. Li, M. Uludag, S. Squizzato, Y. M. Park, N. Buso, A. P. Cowley, and R. Lopez. 2013. 'Analysis Tool Web Services from the EMBL-EBI', *Nucleic Acids Res*, 41: W597-600.

Melis, A., M. Seibert, and T. Happe. 2004. 'Genomics of green algal hydrogen research', *Photosynth Res*, 82: 277-88.

Meuser, J. E., E. S. Boyd, G. Ananyev, D. Karns, R. Radakovits, U. M. Narayana Murthy, M. L. Ghirardi, G. C. Dismukes, J. W. Peters, and M. C. Posewitz. 2011. 'Evolutionary significance of an algal gene encoding an [FeFe]-hydrogenase with F-domain homology and hydrogenase activity in Chlorella variabilis NC64A', *Planta*, 234: 829-43.

Meyer, J. 2007. '[FeFe] hydrogenases and their evolution: a genomic perspective', *Cellular and Molecular Life Sciences*, 64: 1063-84.

Misra, T. K., N. L. Brown, L. Haberstroh, A. Schmidt, D. Goddette, and S. Silver. 1985. 'Mercuric reductase structural genes from plasmid R100 and transposon Tn501: functional domains of the enzyme', *Gene*, 34: 253-62.

Morra, Simone, Sara Maurelli, Mario Chiesa, David W. Mulder, Michael W. Ratzloff, Elio Giamello, Paul W. King, Gianfranco Gilardi, and Francesca Valetti. 'The effect of a C298D mutation in CaHydA [FeFe]-hydrogenase: Insights into the protein-metal cluster interaction by EPR and FTIR spectroscopic investigation', *Biochimica et Biophysica Acta (BBA) - Bioenergetics*.

Morra, Simone, Francesca Valetti, Sheila J. Sadeghi, Paul W. King, Toby Meyer, and Gianfranco Gilardi. 2011. 'Direct electrochemistry of an [FeFe]-hydrogenase on a TiO2 Electrode', *Chemical Communications*, 47: 10566-68.

Mortenson, L. E., R. C. Valentine, and J. E. Carnahan. 1962. 'An electron transport factor from Clostridium pasteurianum', *Biochem Biophys Res Commun*, 7: 448-52.

Mulder, D. W., D. O. Ortillo, D. J. Gardenghi, A. V. Naumov, S. S. Ruebush, R. K. Szilagyi, B. Huynh, J. B. Broderick, and J. W. Peters. 2009. 'Activation of HydA(DeltaEFG) requires a preformed [4Fe-4S] cluster', *Biochemistry*, 48: 6240-8.

Mulder, D. W., M. W. Ratzloff, M. Bruschi, C. Greco, E. Koonce, J. W. Peters, and P. W. King. 2014. 'Investigations on the role of proton-coupled electron transfer in hydrogen activation by [FeFe]-hydrogenase', *J Am Chem Soc*, 136: 15394-402.

Mulder, D. W., M. W. Ratzloff, E. M. Shepard, A. S. Byer, S. M. Noone, J. W. Peters, J. B. Broderick, and P. W. King. 2013. 'EPR and FTIR analysis of the mechanism of H2 activation by [FeFe]-hydrogenase HydA1 from Chlamydomonas reinhardtii', *J Am Chem Soc*, 135: 6921-9.

Mulder, David W., Eric S. Boyd, Ranjana Sarma, Rachel K. Lange, James A. Endrizzi, Joan B. Broderick, and John W. Peters. 2010. 'StepwiseFeFe-hydrogenase H-cluster assembly revealed in the structure of HydA[Delta]EFG', *Nature*, 465: 248-51.

Mulder, David W., Eric M. Shepard, Jonathan E. Meuser, Neelambari Joshi, Paul W. King, Matthew C. Posewitz, Joan B. Broderick, and John W. Peters. 2011. 'Insights into FeFe -Hydrogenase Structure, Mechanism, and Maturation', *Structure*, 19: 1038-52.

Murshudov, G. N., A. A. Vagin, and E. J. Dodson. 1997. 'Refinement of Macromolecular Structures by the Maximum-Likelihood Method', *Acta Crystallographica Section D*, 53: 240-55.

Nakahara, H., J. L. Schottel, T. Yamada, Y. Miyakawa, M. Asakawa, J. Harville, and S. Silver. 1985. 'Mercuric reductase enzymes from Streptomyces species and group B Streptococcus', *J Gen Microbiol*, 131: 1053-9.

Nascimento, A. M., and E. Chartone-Souza. 2003. 'Operon mer: bacterial resistance to mercury and potential for bioremediation of contaminated environments', *Genet Mol Res*, 2: 92-101.

Nicolet, Y., B. J. Lemon, J. C. Fontecilla-Camps, and J. W. Peters. 2000. 'A novel FeS cluster in Fe-only hydrogenases', *Trends Biochem Sci*, 25: 138-43.

Nicolet, Yvain, Christine Cavazza, and J. C. Fontecilla-Camps. 2002. 'Fe-only hydrogenases: structure, function and evolution', *Journal of Inorganic Biochemistry*, 91: 1-8.

Nicolet, Yvain, Claudine Piras, Pierre Legrand, Claude E. Hatchikian, and Juan C. Fontecilla-Camps. 1999. 'Desulfovibrio desulfuricans iron hydrogenase: the structure shows unusual coordination to an active site Fe binuclear center', *Structure*, 7: 13-23.

Nicolet, Yvain, Roman Rohac, Lydie Martin, and Juan C. Fontecilla-Camps. 2013. 'X-ray snapshots of possible intermediates in the time course of synthesis and degradation of protein-bound Fe4S4 clusters', *Proceedings of the National Academy of Sciences*, 110: 7188-92.

Nicolet, Yvain, Jon K. Rubach, Matthew C. Posewitz, Patricia Amara, Carole Mathevon, Mohamed Atta, Marc Fontecave, and Juan C. Fontecilla-Camps. 2008. 'X-ray Structure of the [FeFe]-Hydrogenase Maturase HydE from Thermotoga maritima', *Journal of Biological Chemistry*, 283: 18861-72.

Nies, D. H. 2003. 'Efflux-mediated heavy metal resistance in prokaryotes', *FEMS Microbiol Rev*, 27: 313-39.

Niks, Dimitri, Jayant Duvvuru, Miguel Escalona, and Russ Hille. 2016. 'Spectroscopic and Kinetic Properties of the Molybdenum-containing, NAD+-dependent Formate Dehydrogenase from Ralstonia eutropha', *Journal of Biological Chemistry*, 291: 1162-74.

Nolling, J., G. Breton, M. V. Omelchenko, K. S. Makarova, Q. Zeng, R. Gibson, H. M. Lee, J. Dubois, D. Qiu, J. Hitti, Y. I. Wolf, R. L. Tatusov, F. Sabathe, L. Doucette-Stamm, P. Soucaille, M. J. Daly, G. N. Bennett, E. V. Koonin, and D. R. Smith. 2001. 'Genome sequence and comparative analysis of the solvent-producing bacterium Clostridium acetobutylicum', *J Bacteriol*, 183: 4823-38.

Ohnishi, T. 1998. 'Iron-sulfur clusters/semiquinones in complex I', *Biochim Biophys Acta*, 1364: 186-206.

Otwinowski, Zbyszek, and Wladek Minor. 1997. 'Processing of X-ray diffraction data collected in oscillation mode.' in (Elsevier).

Overbeek, Ross, Robert Olson, Gordon D. Pusch, Gary J. Olsen, James J. Davis, Terry Disz, Robert A. Edwards, Svetlana Gerdes, Bruce Parrello, Maulik Shukla, Veronika Vonstein, Alice R. Wattam, Fangfang Xia, and Rick Stevens. 2014. 'The SEED and the Rapid Annotation of microbial genomes using Subsystems Technology (RAST)', *Nucleic Acids Research*, 42: D206-D14.

Pandey, Arti S., Travis V. Harris, Logan J. Giles, John W. Peters, and Robert K. Szilagyi. 2008. 'Dithiomethylether as a Ligand in the Hydrogenase H-Cluster', *Journal of the American Chemical Society*, 130: 4533-40.

Parkin, A., C. Cavazza, J. C. Fontecilla-Camps, and F. A. Armstrong. 2006. 'Electrochemical investigations of the interconversions between catalytic and inhibited states of the [FeFe]-hydrogenase from Desulfovibrio desulfuricans', *J Am Chem Soc*, 128: 16808-15.

Patakova, P., M. Linhova, M. Rychtera, L. Paulova, and K. Melzoch. 2013. 'Novel and neglected issues of acetone-butanol-ethanol (ABE) fermentation by clostridia: Clostridium metabolic diversity, tools for process mapping and continuous fermentation systems', *Biotechnol Adv*, 31: 58-67.

Peters, J. W., W. N. Lanzilotta, B. J. Lemon, and L. C. Seefeldt. 1998. 'X-ray crystal structure of the Fe-only hydrogenase (CpI) from Clostridium pasteurianum to 1.8 angstrom resolution', *Science*, 282: 1853-8.

Peters, John W., Gerrit J. Schut, Eric S. Boyd, David W. Mulder, Eric M. Shepard, Joan B. Broderick, Paul W. King, and Michael W. W. Adams. 2015. '[FeFe]- and [NiFe]-hydrogenase diversity, mechanism, and maturation', *Biochimica et Biophysica Acta (BBA) - Molecular Cell Research*, 1853: 1350-69.

Pettersen, E. F., T. D. Goddard, C. C. Huang, G. S. Couch, D. M. Greenblatt, E. C. Meng, and T. E. Ferrin. 2004. 'UCSF Chimera--a visualization system for exploratory research and analysis', *J Comput Chem*, 25: 1605-12.

Pierik, A. J., M. Hulstein, W. R. Hagen, and S. P. Albracht. 1998. 'A low-spin iron with CN and CO as intrinsic ligands forms the core of the active site in [Fe]-hydrogenases', *Eur J Biochem*, 258: 572-8.

Poehlein, A., K. Riegel, S. M. Konig, A. Leimbach, R. Daniel, and P. Durre. 2015. 'Genome sequence of Clostridium sporogenes DSM 795(T), an amino acid-degrading, nontoxic surrogate of neurotoxin-producing Clostridium botulinum', *Stand Genomic Sci*, 10: 40.

Popescu, Codrina V., and Eckard Münck. 1999. 'Electronic Structure of the H Cluster in [Fe]-Hydrogenases', *Journal of the American Chemical Society*, 121: 7877-84.

Posewitz, Matthew C., Paul W. King, Sharon L. Smolinski, Liping Zhang, Michael Seibert, and Maria L. Ghirardi. 2004. 'Discovery of Two Novel Radical S-Adenosylmethionine Proteins Required for the Assembly of an Active [Fe] Hydrogenase', *Journal of Biological Chemistry*, 279: 25711-20.

Posewitz, Matthew C., David W. Mulder, and John W. Peters. 2008. 'New Frontiers in Hydrogenase Structure and Biosynthesis', *Current Chemical Biology*, 2: 178-99.

Poudel, S., M. Tokmina-Lukaszewska, D. R. Colman, M. Refai, G. J. Schut, P. W. King, P. C. Maness, M. W. Adams, J. W. Peters, B. Bothner, and E. S. Boyd. 2016. 'Unification of [FeFe]-hydrogenases into three structural and functional groups', *Biochim Biophys Acta*, 1860: 1910-21.

Pyne, Michael E., Sagar Utturkar, Steven D. Brown, Murray Moo-Young, Duane A. Chung, and C. Perry Chou. 2014. 'Improved Draft Genome Sequence of Clostridium pasteurianum Strain ATCC 6013 (DSM 525) Using a Hybrid Next-Generation Sequencing Approach', *Genome Announcements*, 2.

Quitterer, Felix, Anja List, Wolfgang Eisenreich, Adelbert Bacher, and Michael Groll. 2012. 'Crystal Structure of Methylornithine Synthase (PylB): Insights into the Pyrrolysine Biosynthesis', *Angewandte Chemie International Edition*, 51: 1339-42.

Rennex, Denise, Mark Pickett, and Mark Bradley. 1994. 'In vivo and in vitro effects of mutagenesis of active site tyrosine residues of mercuric reductase', *FEBS Letters*, 355: 220-22.

Rodriguez-R, L, and K Konstantinidis. 'Bypassing Cultivation To Identify Bacterial Species', *Microbe Magazine*.

Rodriguez-R LM, Konstantinidis KT. 2016. 'The enveomics collection: a toolbox for specialized analyses of microbial genomes and metagenomes', *PeerJ Preprints*, 4:e1900v1.

Roseboom, W., A. L. De Lacey, V. M. Fernandez, E. C. Hatchikian, and S. P. Albracht. 2006. 'The active site of the [FeFe]-hydrogenase from Desulfovibrio desulfuricans. II. Redox properties, light sensitivity and CO-ligand exchange as observed by infrared spectroscopy', *J Biol Inorg Chem*, 11: 102-18.

Rotta, Carlo, Anja Poehlein, Katrin Schwarz, Peter McClure, Rolf Daniel, and Nigel P. Minton. 2015. 'Closed Genome Sequence of Clostridium pasteurianum ATCC 6013', *Genome Announcements*, 3.

Sakaguchi, Yoshihiko, Tetsuya Hayashi, Ken Kurokawa, Keisuke Nakayama, Kenshiro Oshima, Yukako Fujinaga, Makoto Ohnishi, Eiichi Ohtsubo, Masahira Hattori, and Keiji Oguma. 2005. 'The genome sequence of Clostridium botulinum type C neurotoxin-converting phage and the molecular mechanisms of unstable lysogeny', *Proceedings of the National Academy of Sciences of the United States of America*, 102: 17472-77.

Sayed, Ahmed, Mohamed A. Ghazy, Ari J. S. Ferreira, Joao C. Setubal, Felipe S. Chambergo, Amged Ouf, Mustafa Adel, Adam S. Dawe, John A.C. Archer, Vladimir B. Bajic, Rania Siam, and Hamza El-Dorry. 2013. 'A novel mercuric reductase from the unique deep brine environment of Atlantis II in the Red Sea', *Journal of Biological Chemistry*.

Schelert, J., D. Rudrappa, T. Johnson, and P. Blum. 2013. 'Role of MerH in mercury resistance in the archaeon Sulfolobus solfataricus', *Microbiology*, 159: 1198-208.

Schelert, James, Vidula Dixit, Viet Hoang, Jessica Simbahan, Melissa Drozda, and Paul Blum. 2004. 'Occurrence and Characterization of Mercury Resistance in the Hyperthermophilic Archaeon Sulfolobus solfataricus by Use of Gene Disruption', *J Bacteriol*, 186: 427-37.

Schiering, N., W. Kabsch, M. J. Moore, M. D. Distefano, C. T. Walsh, and E. F. Pai. 1991. 'Structure of the detoxification catalyst mercuric ion reductase from Bacillus sp. strain RC607', *Nature*, 352: 168-72.

Schmidt, Oliver, Harold L. Drake, and Marcus A. Horn. 2010. 'Hitherto Unknown [Fe-Fe]-Hydrogenase Gene Diversity in Anaerobes and Anoxic Enrichments from a Moderately Acidic Fen', *Applied and Environmental Microbiology*, 76: 2027-31.

Schottel, J. L. 1978. 'The mercuric and organomercurial detoxifying enzymes from a plasmid-bearing strain of Escherichia coli', *J Biol Chem*, 253: 4341-9.

Schuchmann, K., and V. Muller. 2012. 'A bacterial electron-bifurcating hydrogenase', *J Biol Chem*, 287: 31165-71.

Schut, Gerrit J., and Michael W. W. Adams. 2009. 'The Iron-Hydrogenase of Thermotoga maritima Utilizes Ferredoxin and NADH Synergistically: a New Perspective on Anaerobic Hydrogen Production', *J Bacteriol*, 191: 4451-57.

Schwede, Torsten, Jürgen Kopp, Nicolas Guex, and Manuel C. Peitsch. 2003. 'SWISS-MODEL: an automated protein homology-modeling server', *Nucleic Acids Research*, 31: 3381-85.

Sebaihia, M., M. W. Peck, N. P. Minton, N. R. Thomson, M. T. Holden, W. J. Mitchell, A. T. Carter, S. D. Bentley, D. R. Mason, L. Crossman, C. J. Paul, A. Ivens, M. H. Wells-Bennik, I. J. Davis, A. M. Cerdeno-Tarraga, C. Churcher, M. A. Quail, T. Chillingworth, T. Feltwell, A. Fraser, I. Goodhead, Z. Hance, K. Jagels, N. Larke, M. Maddison, S. Moule, K. Mungall, H. Norbertczak, E. Rabbinowitsch, M. Sanders, M. Simmonds, B. White, S. Whithead, and J. Parkhill. 2007. 'Genome sequence of a proteolytic (Group I) Clostridium botulinum strain Hall A and comparative analysis of the clostridial genomes', *Genome Res*, 17: 1082-92.

Sedlar, K., J. Kolek, H. Skutkova, B. Branska, I. Provaznik, and P. Patakova. 2015. 'Complete genome sequence of Clostridium pasteurianum NRRL B-598, a non-type strain producing butanol', *J Biotechnol*, 214: 113-4.

Shannon, P., A. Markiel, O. Ozier, N. S. Baliga, J. T. Wang, D. Ramage, N. Amin, B. Schwikowski, and T. Ideker. 2003. 'Cytoscape: a software environment for integrated models of biomolecular interaction networks', *Genome Res*, 13: 2498-504.

Shepard, Eric M., Benjamin R. Duffus, Simon J. George, Shawn E. McGlynn, Martin R. Challand, Kevin D. Swanson, Peter L. Roach, Stephen P. Cramer, John W. Peters, and Joan B. Broderick. 2010. '[FeFe]-Hydrogenase Maturation: HydG-Catalyzed Synthesis of Carbon Monoxide', *Journal of the American Chemical Society*, 132: 9247-49.

Shepard, Eric M., Shawn E. McGlynn, Alexandra L. Bueling, Celestine S. Grady-Smith, Simon J. George, Mark A. Winslow, Stephen P. Cramer, John W. Peters, and Joan B. Broderick. 2010. 'Synthesis of the 2Fe subcluster of the [FeFe]-hydrogenase H cluster on the HydF scaffold', *Proceedings of the National Academy of Sciences*, 107: 10448-53.

Shepard, Eric M., Florence Mus, Jeremiah N. Betz, Amanda S. Byer, Benjamin R. Duffus, John W. Peters, and Joan B. Broderick. 2014. '[FeFe]-Hydrogenase Maturation', *Biochemistry*, 53: 4090-104.

Silakov, A., C. Kamp, E. Reijerse, T. Happe, and W. Lubitz. 2009. 'Spectroelectrochemical characterization of the active site of the [FeFe] hydrogenase HydA1 from Chlamydomonas reinhardtii', *Biochemistry*, 48: 7780-6.

Silakov, A., B. Wenk, E. Reijerse, and W. Lubitz. 2009. '(14)N HYSCORE investigation of the H-cluster of [FeFe] hydrogenase: evidence for a nitrogen in the dithiol bridge', *Phys Chem Chem Phys*, 11: 6592-9.

Silakov, Alexey, Eduard J. Reijerse, Simon P. J. Albracht, E. Claude Hatchikian, and Wolfgang Lubitz. 2007. 'The Electronic Structure of the H-Cluster in the [FeFe]-Hydrogenase from Desulfovibrio desulfuricans: A Q-band 57Fe-ENDOR and HYSCORE Study', *Journal of the American Chemical Society*, 129: 11447-58.

Simbahan, J., E. Kurth, J. Schelert, A. Dillman, E. Moriyama, S. Jovanovich, and P. Blum. 2005. 'Community analysis of a mercury hot spring supports occurrence of domain-specific forms of mercuric reductase', *Appl Environ Microbiol*, 71: 8836-45.

Smoot, M. E., K. Ono, J. Ruscheinski, P. L. Wang, and T. Ideker. 2011. 'Cytoscape 2.8: new features for data integration and network visualization', *Bioinformatics*, 27: 431-2.

Stamatakis, Alexandros. 2014. 'RAxML version 8: a tool for phylogenetic analysis and post-analysis of large phylogenies', *Bioinformatics*, 30: 1312-13.

Stiebritz, M. T., and M. Reiher. 2009. 'Theoretical study of dioxygen induced inhibition of [FeFe]-hydrogenase', *Inorg Chem*, 48: 7127-40.

Stiebritz, Martin T., Arndt R. Finkelmann, and Markus Reiher. 2011. 'Oxygen Coordination to the Active Site of Hmd in Relation to [FeFe] Hydrogenase', *European Journal of Inorganic Chemistry*, 2011: 1163-71.

Stiebritz, Martin Tillmann, and Markus Reiher. 2012. 'Hydrogenases and oxygen', *Chemical Science*, 3: 1739-51.

Stripp, Sven T., Gabrielle Goldet, Caterina Brandmayr, Oliver Sanganas, Kylie A. Vincent, Michael Haumann, Fraser A. Armstrong, and Thomas Happe. 2009. 'How oxygen attacks [FeFe] hydrogenases from photosynthetic organisms', *Proceedings of the National Academy of Sciences*, 106: 17331-36.

Szilagyi, A., and P. Zavodszky. 2000. 'Structural differences between mesophilic, moderately thermophilic and extremely thermophilic protein subunits: results of a comprehensive survey', *Structure*, 8: 493-504.

Tamura, Koichiro, Glen Stecher, Daniel Peterson, Alan Filipski, and Sudhir Kumar. 2013. 'MEGA6: Molecular Evolutionary Genetics Analysis version 6.0', *Molecular Biology and Evolution*.

Telser, J, M J Benecky, M W Adams, L E Mortenson, and B M Hoffman. 1987. 'EPR and electron nuclear double resonance investigation of oxidized hydrogenase II (uptake) from Clostridium pasteurianum W5. Effects of carbon monoxide binding', *Journal of Biological Chemistry*, 262: 6589-94.

Turner, John, George Sverdrup, Margaret K. Mann, Pin-Ching Maness, Ben Kroposki, Maria Ghirardi, Robert J. Evans, and Dan Blake. 2008. 'Renewable hydrogen production', *International Journal of Energy Research*, 32: 379-407.

Vagin, A. and Teplyakov, A. 1997. 'MOLREP: an automated program for Molecular Replacement', *Journal of Applied Crystallography*, 30: 1022-25.

Valentine, R. C., L. E. Mortenson, and J. E. Carnahan. 1963. 'The Hydrogenase System of Clostridium pasteurianum', *Journal of Biological Chemistry*, 238: 1141-44.

Vallese, Francesca, Paola Berto, Maria Ruzzene, Laura Cendron, Stefania Sarno, Edith De Rosa, Giorgio M. Giacometti, and Paola Costantini. 2012. 'Biochemical Analysis of the Interactions between the Proteins Involved in the [FeFe]-Hydrogenase Maturation Process', *Journal of Biological Chemistry*, 287: 36544-55.

Verhagen, M. F., T. W. O'Rourke, A. L. Menon, and M. W. Adams. 2001. 'Heterologous expression and properties of the gamma-subunit of the Fe-only hydrogenase from Thermotoga maritima', *Biochim Biophys Acta*, 1505: 209-19.

Vetriani, Costantino, Yein S. Chew, Susan M. Miller, Jane Yagi, Jonna Coombs, Richard A. Lutz, and Tamar Barkay. 2005. 'Mercury Adaptation among Bacteria from a Deep-Sea Hydrothermal Vent', *Applied and Environmental Microbiology*, 71: 220-26.

Vignais, P. M., and B. Billoud. 2007. 'Occurrence, classification, and biological function of hydrogenases: an overview', *Chem Rev*, 107: 4206-72.

Vignais, P. M., B. Billoud, and J. Meyer. 2001. 'Classification and phylogeny of hydrogenases', *FEMS Microbiol Rev*, 25: 455-501.

Vincent, Kylie A., Alison Parkin, Oliver Lenz, Simon P. J. Albracht, Juan C. Fontecilla-Camps, Richard Cammack, Bärbel Friedrich, and Fraser A. Armstrong. 2005. 'Electrochemical Definitions of O2 Sensitivity and Oxidative Inactivation in Hydrogenases', *Journal of the American Chemical Society*, 127: 18179-89.

Walker, C. C., C. D. P. Partridge, and M. G. Yates. 1981. 'The Effect of Nutrient Limitation on Hydrogen Production by Nitrogenase in Continuous Cultures of Azotobacter chroococcum', *Microbiology*, 124: 317-27.

Walker, C. C., and M. G. Yates. 1978. 'The hydrogen cycle in nitrogen-fixing Azotobacter chroococcum', *Biochimie*, 60: 225-31.

Wang, S., H. Huang, J. Kahnt, A. P. Mueller, M. Kopke, and R. K. Thauer. 2013. 'NADP-specific electron-bifurcating [FeFe]-hydrogenase in a functional complex with formate dehydrogenase in Clostridium autoethanogenum grown on CO', *J Bacteriol*, 195: 4373-86.

Wang, Shuning, Haiyan Huang, Jörg Kahnt, and Rudolf K. Thauer. 2013. 'A Reversible Electron-Bifurcating Ferredoxin- and NAD-Dependent [FeFe]-Hydrogenase (HydABC) in Moorella thermoacetica', *J Bacteriol*, 195: 1267-75.

Wang, Y., E. Boyd, S. Crane, P. Lu-Irving, D. Krabbenhoft, S. King, J. Dighton, G. Geesey, and T. Barkay. 2011. 'Environmental conditions constrain the distribution and diversity of archaeal merA in Yellowstone National Park, Wyoming, U.S.A', *Microb Ecol*, 62: 739-52.

Willard, L., A. Ranjan, H. Zhang, H. Monzavi, R. F. Boyko, B. D. Sykes, and D. S. Wishart. 2003. 'VADAR: a web server for quantitative evaluation of protein structure quality', *Nucleic Acids Res*, 31: 3316-9.

Winogradsky, S. 1895. 'Recherches sure l'assimilation de l'azote libre de l'atmosphere par les microbes', *Archives des science biologique*, 3: 297-352.

Wright, J. J., E. Salvadori, H. R. Bridges, J. Hirst, and M. M. Roessler. 2016. 'Small-volume potentiometric titrations: EPR investigations of Fe-S cluster N2 in mitochondrial complex I', *J Inorg Biochem*.

Y. Zeroual, A. Moutaouakkil, F.Z. Dzairi, M. Talbi,P.U. Chung, K. Lee, M. Blaghen. 2003. 'Purification and characterization of cytosolic mercuricreductase from Klebsiella pneumoniae', *Annals of Microbiology*, 53: 149-60.

Yacoby, Iftach, Lotta Tollstoy Tegler, Sergii Pochekailov, Shuguang Zhang, and Paul W. King. 2012. 'Optimized Expression and Purification for High-Activity Preparations of Algal [FeFe]-Hydrogenase', *PLoS ONE*, 7: e35886.

Yutin, Natalya, and Michael Y. Galperin. 2013. 'A genomic update on clostridial phylogeny: Gram-negative spore formers and other misplaced clostridia', *Environmental Microbiology*, 15: 2631-41.

Zhang, Ziping, Aman Tang, Shuzhen Liao, Pengfei Chen, Zhaoyang Wu, Guoli Shen, and Ruqin Yu. 2011. 'Oligonucleotide probes applied for sensitive enzyme-amplified electrochemical assay of mercury(II) ions', *Biosensors and Bioelectronics*, 26: 3320-24.

Zheng, Yanning, Jörg Kahnt, In Hyuk Kwon, Roderick I. Mackie, and Rudolf K. Thauer. 2014. 'Hydrogen Formation and Its Regulation in Ruminococcus albus: Involvement of an Electron-Bifurcating [FeFe]-Hydrogenase, of a Non-Electron-Bifurcating [FeFe]-Hydrogenase, and of a Putative Hydrogen-Sensing [FeFe]-Hydrogenase', *J Bacteriol*, 196: 3840-52.